Langley Grant

IN-27-??

302468

P-169

DEPARTMENT OF PHYSICS
COLLEGE OF SCIENCES
OLD DOMINION UNIVERSITY
NORFOLK, VIRGINIA   23529-0116

Technical Report No. PTR-90-3

STUDIES OF MOLECULAR PROPERTIES OF POLYMERIC MATERIALS

By

W.L. Harries, Principal Investigator
Department of Physics, Old Dominion University,
Norfolk, Virginia   23529-0116

and

S.A.T. Long and E.R. Long Jr.
National Aeronautics and Space Administration
Langley Research Center
Hampton, Virginia   23665-5225

Final Report
For the period ending August 31, 1990

May 1990

DEPARTMENT OF PHYSICS
COLLEGE OF SCIENCES
OLD DOMINION UNIVERSITY
NORFOLK, VIRGINIA 23529-0116

Technical Report No. PTR-90-3

**STUDIES OF MOLECULAR PROPERTIES
OF POLYMERIC MATERIALS**

By

W.L. Harries, Principal Investigator
Department of Physics, Old Dominion University,
Norfolk, Virginia 23529-0116

and

S.A.T. Long and E.R. Long Jr.
National Aeronautics and Space Administration
Langley Research Center
Hampton, Virginia 23665-5225

Final Report
For the period ending August 31, 1990

May 1990

TABLE OF CONTENTS

TABLE OF CONTENTS (Concluded)

GLOSSARY

α-transition - the glass transition

aromatic ether linkage - ether linkage connected to a
                         benzene ring

backbone of a polymer - the primary chain of the polymer,
                        does not include pendant groups

benzene ring - C_6H_6 -
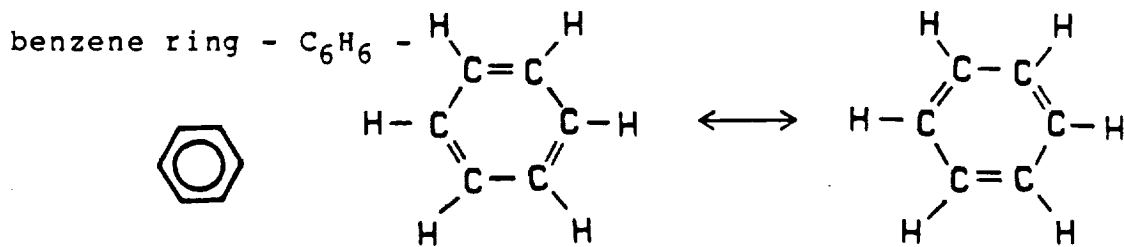
carbonyl group -
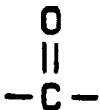
chain scissioning - the permanent division of a molecular
                    chain into pieces of lower molecular
                    weight

coupling constant - hyperfine splitting constant

crosslinking - the formation of bonds between neighboring
               molecular chains

cyclohexadienyl - a benzene ring with an additional
                  hydrogen
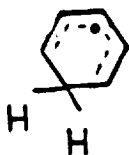
dissipation factor - the tangent of the phase angle between the applied electric field and the dielectric displacement in a material; a larger dissipation factor corresponds to a larger dissipation of energy

disubstituted - having two substitutions on the molecular group

EPR - electron paramagnetic resonance

equivalent nuclei - see magnetically equivalent nuclei

ether linkage - an oxygen atom link with single bonds between portions of a molecular chain

$$R - O - R$$

free volume (v_f) - voids present in a material which are not attributable to the molecular vibrations; the amount of free volume is constant below the glass transition temperature (see eq. (3.2))

g-factor - a dimensionless constant of proportionality relating the electronic spin to the magnetic moment (see eq. (4.1), eq. (4.17))

g-value - g-factor

glass transition temperature (T_g) - as the temperature of a viscous liquid is decreased, the glass transition temperature is the temperature at which the viscosity becomes so large that the molecules are rigidly fixed in place

hopping distance - the distance between two nearest-neighbor hopping sites

hopping parameter (d_Q) - a parameter dependent upon the molecules involved, which is an indication of the extent of the localized electronic wavefunction (see eq. (6.2), eq. (6.10))

hopping sites - locations in the material where appropriate localized electronic wavefunctions exist, such that some transfer of electrons between sites ("hopping") may occur

hyperfine coupling constant - hyperfine splitting constant

hyperfine lines - resonant absorption lines in an EPR spectrum which have been separated due to hyperfine splitting

hyperfine splitting constant - a constant of
      proportionality indicating the strength of the
      interaction between the electron spin and the
      nuclear spin (see eq. (4.18)); measured in units
      of gauss from the separation between hyperfine
      lines of the EPR spectrum (see Fig. 16)

imide ring -

$$\begin{array}{c} R-C \\ \quad\quad\ \ \diagdown \\ R \quad\quad\quad N- \\ \quad\quad\ \ \diagup \\ R-C \end{array}$$
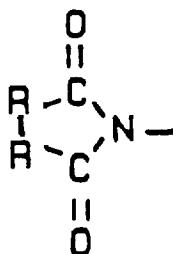
jump distance - hopping distance

Kapton® - a polyimide manufactured by du Pont de Nemours,
      Inc.
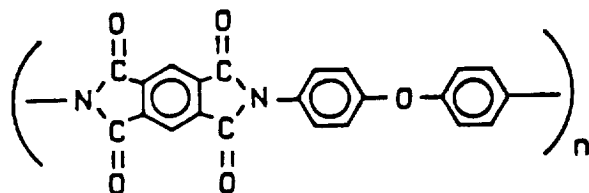
magnetically equivalent nuclei - nuclei in a radical which
      all have the same value of the hyperfine
      splitting constant

meta - (see phenyl radical)

methyl - radical derived from CH_4 by removal of one
      hydrogen atom

molecular doping - the addition of smaller molecules to a
      polymer matrix

monosubstituted - having one substitution on the molecular
      group

morphology - the structure of the polymeric material

Mylar* - a polyethylene terephthalate (PET) manufactured by du Pont de Nemours, Inc.
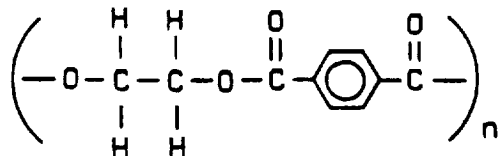
nvt - $\dfrac{\text{neutrons}}{\text{cm}^2\text{-sec}}$ *(exposure time in seconds)

organic radicals - radicals containing carbon atoms

ortho - (see phenyl radical)

para - (see phenyl radical)

pendant groups - molecular groups which are attached to the polymer molecule but which are not included in the backbone chain

peroxy radical - radical of the form $- O - \overset{\bullet}{O}$

PET - polyethylene terephthalate

phenoxyl - a benzene ring with the substitution of one oxygen atom for a hydrogen atom

phenyl radical - a benzene ring with one hydrogen atom removed. Substitutions on the remaining hydrogen atom positions would be labelled ortho- (o), meta- (m), and para- (p) as shown:
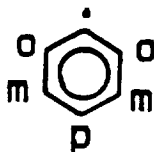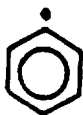
phonon - a quantum of vibrational energy

polyetherimide - a polymer containing ether linkages and
          imide groups (see Ultem)

polyethylene - a polymer composed of ethylene groups:

$$\left(\begin{array}{cc} H & H \\ | & | \\ -C- & C- \\ | & | \\ H & H \end{array}\right)_n$$
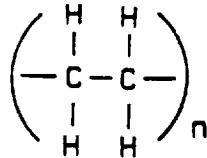
polyethylene terephthalate (PET) - generic chemical name
          for polymers with the repeat unit shown for
          Mylar

polyimide - polymer containing imide rings

polymer - a long molecular chain consisting of many
          identical molecular segments bonded together

quartet - a set of four hyperfine lines due to one radical

rad - a unit of absorbed dose of ionizing radiation equal
          to 100 ergs of energy absorbed per gram of
          irradiated material

rad, water equivalent - the dose in rad which would be
          absorbed by a mass of water equal to the mass of
          the irradiated material

radical - an atom or group of atoms containing an unpaired
          electron

radical decay - the elimination of radicals through the
          formation of chemical bonds

radical density - number of radicals present in a material
          per unit volume

repeat unit - structural unit of polymer chain; many
          identical repeat units are bonded together to
          form the complete polymer molecule

self-mending - original bonds of a molecule are reformed
          after having been broken due to irradiation

side groups - pendant groups

splitting constant - hyperfine splitting constant

substitution – the replacement of an atom or group from a
             site on the molecule by another atom or
             group (the hydrogen atoms are frequently
             replaced on benzene rings)

T_g – glass transition temperature

trisubstituted – having three substitutions on a
             molecular group

Ultem* – a polyetherimide manufactured by General Electric
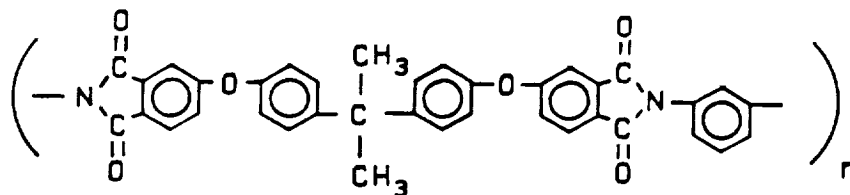
unpaired electron spin – an electron spin which is not
             coupled to any other electron spin, therefore
             having S = 1/2

wing structure – weak lines in an EPR spectrum somewhat
             removed from the primary lines of the
             spectrum

STUDIES OF MOLECULAR PROPERTIES OF POLYMERIC MATERIALS

By

W.L. Harries[1], S.A.T. Long[2], and E.R. Long Jr.[2]

1. INTRODUCTION

The report describes the experimental effort carried out at NASA Langley Research Center in a cooperative agreement between Old Dominion University and the Materials Division of NASA. The period covered is from 1 November 1984 to 31 October 1989. The personnel from Old Dominion include the author, four graduate research assistants namely Heidi R. Ries, Cynthia A. Bradbury, Kristen T. Kern and Philip C. Stancil, and three research assistants, namely Stephanie L. Gray, William D. Collins and Nicole K. Vogelsang.

The purpose of the work was to study aerospace environmental effects on polymeric and composite materials considered for structural use in spacecraft and advanced aircraft. In addition to providing information on the behavior of the materials, attemps would be made to relate the measurements to the molecular processes occurring in the material.

The report is organized as follows. A summary and overview of the technical aspects is given in Section 2. The work has resulted in a series of papers, theses and talks which are listed in Section 3 under Accomplishments. The titles of the nine papers of which six are refereed are given in Section 3.1 and the actual papers are included in Appendices A through I. In addition, the Appendices J and K show work written up during

---

[1]Professor, Department of Physics, Old Dominion University, Norfolk, Virginia 23529.
[2]Materials Division, NASA Langley Research Center, Hampton, Virginia 23665-5225

the period, but which was not published until April 1990. Appendix L describes preliminary work started on an Adhesive Program which continues. Section 3.1 is then chronological. Section 3.2 shows the two theses and degrees conferred together with summaries of the theses. The work in the theses has been incorporated into the papers mentioned previously. Section 3.3 lists the fifteen presentations and their literature references.

Section 4 includes a technical discussion and summarizes the results enumerated in Section 3. Overall conclusions are given in Section 5.

A glossary of technical terms and definitions compiled by H.R. Ries is included in the front matter.

2. OVERVIEW OF THE PROGRAM

2.1 The Aerospace Environment

The aerospace environmental effects considered are:

(1) Electron radiation; here the experiments utilize 0.1 and 1 MeV electrons at various doses and dose rates.

(2) Effect of thermal cycling.

(3) Effect of aircraft fluids.

(4) Effect of atomic oxygen.

2.2 Aerospace Materials Investigated

The program can be divided into three different categories according to the type of materials investigated and the effects of the aerospace environment:

(1) Studies of the properties of various polymers (before irradiation) either neat or metal doped which would be useful for aerospace applications.

(2) The effect of the aerospace environment on certain polymers (Mylar, Kapton, Ultem) and/or composite materials.

(3) The study of polymer matrices and carbon fibers in composite materials, and the behavior of adhesives--essentially an interface study

The work done under these subheadings is discussed in Section 4 in the above order.

2.3 Experimental Apparatus and Techniques Used

The following experimental techniques were used:

(1) Electrical D.C. and A.C. measurements--yield information on electrical resistivity, losses, capacitance etc.

3

(2) Multiple internal reflection infrared spectroscopy--information on chemical bonds.

(3) Diffuse reflection Fourier-Transform infrared spectroscopy--chemical bonds (preliminary work only).

(4) Electron paramagnetic resonance--measures density of free radicals which are created when molecular bonds are broken by radiation.

(5) Mechanical testing--ultimate stress, modulus, total elongation to failure.

(6) Dynamical mechanical analysis--dynamic loss modulus, storage modulus, loss tangent, and variations with temperature to give T_g glass transition temperature.

(7) Solubility measurements--indicate differences in number of cross-links before and after radiation.

(8) Spectroscopic techniques--indicate which materials are given off from surfaces under influence of atomic oxygen.

(9) Mass loss measurements--used in atomic oxygen studies

3. ACCOMPLISHMENTS

3.1 Papers (Refereed *)

*"Studies of Molecular Properties of Polymeric Materials--Aerospace Environmental Effects on Three Linear Polymers," Wynford L. Harries, Heidi R. Ries, Cynthia A. Bradbury, Stephanie L. Gray, William D. Collins, Sheila Ann T. Long and Edward R. Long Jr., NASA-TM-87532, Final Report for the period 1 November 1984 through 31 October 1985. (Appendix A)

"Electron-Radiation Induced Molecular Changes in a Polyetherimide Film," Stephanie L. Gray, Proceedings of the Virginia Junior Academy of Science 23, 313, (May 1985). (Appendix B)

"Radio-Frequency Electrical Properties of Some Neat and Metal-doped Polyimides," Edward R. Long Jr., Sheila Ann T. Long, Heidi R. Ries and Wynford L. Harries, Conference Record 1986 International Symposium on Electrical Insulation, Washington D.C., June 9-11, 1986. (Appendix C)

*"Electron-radiation Effects on the A.C. and D.C. Electrical Properties and Unpaired Electron Densities of Three Aerospace Polymers," Sheila Ann T. Long, Edward R. Long Jr., Heidi R. Ries and Wynford L. Harries, IEEE Transactions on Nuclear Science Vol. NS-33, No. 6, 1390 (December 1986). (Appendix D)

*"The Effects of Fluids in the Aircraft Environment on a Polyetherimide," Edward R. Long Jr., and William D. Collins, Polymer Engineering and Science, Vol. 28, No. 12, 823 (June 1988). (Appendix E)

*"Effects of Postcuring on Mechanical Properties of Pultruded Fiber-Reinforced Epoxy Composites and the Neat Resin," Edward R. Long Jr., Sheila Ann T. Long, William D. Collins, Stephanie L. Gray and Joan G. Funk. Society for the Advancement of Material and Process Engineering Quarterly Journal, Vol. 20, No. 3, 9, (April 1989). (Appendix F)

*"Absorbed Dose Thresholds and Absorbed Dose Rate Limitations for Studies of Electron Radiation Effects on Polyetherimides," Edward R. Long Jr., Sheila Ann T. Long, Stephanie L. Gray and William D. Collins, NASA Technical Paper 2928, July 1989. (Appendix G)

*"Mechanism of Electrical conductivity in an Irradiated Polyimide," H.R. Ries, W.L. Harries, S.A.T. Long and E.R. Long Jr., J. Phys. Chem. Solids, Vol. 50, No. 7, 735 (1989). (Appendix H)

"Dynamic Mechanical Analysis of Polymeric Materials," Kristen T. Kern, Wynford L. Harries and Sheila Ann T. Long, National Educators Workshop, New: Update 1989--Standard Experiments in Engineering Materials Science and Technology. NASA Langley Research Center, Hampton Virginia 17-19 October 1989. (Appendix I)

3.2 Theses and Degrees Conferred

H.R. Ries, "Studies of Radiation Effects in Three High Polymers,"
Ph.D. Thesis, Old Dominion University, 13 February 1987.

Ms. Ries received the degree of Ph.D. May 1987.

Cynthia Anne Bradbury, "The Effects of Low Doses (1 to 500 kilograys)
of 100-keV Electrons on Four Polymers." Masters Thesis, Old Dominion
University, Norfolk, Virginia, August 1988.

Ms. Bradbury received the degree of M.S. August 1988.

3.3 Abstracts of Theses

STUDIES OF RADIATION EFFECTS IN THREE HIGH POLYMERS

Heidi Rene-Mitchell Ries
Old Dominion University, 1987
Director: Dr. Wynford L. Harries

Three high polymers, Mylar®, Ultem®, and Kapton®, were
irradiated to total doses of 1, 5, and 9.5 gigarad using 1-MeV electrons.
The glass transition temperatures (T_g) of the materials before and after
irradiation were measured using an AC electrical dissipation factor
technique. From the T_g data, it was found that the electron radiation at
these total doses results in net chain scissioning in Mylar and net
crosslinking in Ultem, while self-mending is predominant in Kapton. The
dielectric constant was measured before and after irradiation, but no
significant changes due to irradiation were observed. Electron

paramagnetic resonance (EPR) was used to determine the total organic radical densities in the materials 0.5 hr after irradiation. Total organic radical densities of approximately 10^{18} spins/g were recorded in all threee materials. Additional postirradiation EPR radical density measurements were made at later times to determine the radical decay rates. The radical decay rates were highly varied and did not conform to first-order or second-order decay kinetics, due to the simultaneous presence of several different radical species. Utilizing the EPR spectra, postirradiation radical identifications were made for all three materials. The predominant radicals in Mylar were a phenyl radical and a carbonyl radical, both resulting from a main chain C-C bond scission. In Ultem, an ethylene radical due to a C-C bond scission in the crosslinked material is observed. In Kapton, phenyl and phenoxyl radicals are present resulting from the scission of an ether linkage. Ketone radicals due to the opening of imide rings are also present in Kapton. At long postirradiation times, peroxy radicals are present in all three materials. DC conductivity was measured before and 0.5 hr after irradiation, as well as at longer postirradiation times. Kapton exhibited a 5-order of magnitude increase in conductivity following irradiation, whereas Mylar and Ultem showed no significant change. A hopping model of conductivity, with radicals as hopping sites, is proposed to relate the postirradiation DC conductivity and total postirradiation organic radical density in Kapton.

THE EFFECTS OF LOW DOSES (1 TO 500 KILOGRAYS)
OF 100-KEV ELECTRONS ON FOUR POLYMERS

Cynthia Anne Bradbury
Old Dominion University, 1988
Director: W.L. Harries

Commercial films of polyetherimide (PEI), polyethereretherimide
(PEEI), polyethylene terephthalate (PET), and polycarbonate (PC) were
exposed in vacuum to 100-keV electron radiation to total absorbed doses of
1, 10, 100, 300, and 500 kilograys. The concentration of radiation-
generated radicals, as measured by electron paramagnetic resonance (EPR),
increased by over an order of magnitude in all four polymers.
Correspondingly, the intensity of the infrared absorption peaks increased
uniformly for all doses. Solubility tests resulted in decreased
solubility in all polymers. IR, EPR, and solubility suggest
dehydrogenation of the aliphatic C-H and phenyl C-H sites. The data
indicated that cross linking is occurring in all polymers tested.

3.4 Talks and Abstracts

1. Stephanie L. Gray: "Electron-Radiation Induced Molecular Changes in a Polyetherimide Film." Virginia Junior Academy of Science, 44th Annual Meeting, College of William and Mary, Williamsburg, Virginia, May 14-18, 1985.

   Proceedings of the Virginia Academy of Science, Vol. 23 pp 313-323, May 1985.

2. William D. Collins: "A Study of the Effects of Fluid Environments on the Physical and Mechanical Properties of ULTEM Resin." Virginia Junior Academy of Science, 44th Annual Meeting, College of William and Mary, Willimasburg, Virginia, May 14-18, 1985.

   Proceedings of the Virginia Academy of Science, Vol 23, 324-327, May 1985.

3. H.R. Ries, W.L. Harries, S.A.T. Long, and E.R. Long Jr., "Electrical Property Study of Radiation-Generated Homolytic Bond Cleavage in Three High Polymers." Presented at the Division of High Polymer Physics Meeting of the American Physical society, March 31 - April 4, 1986, Las Vegas, Nevada.

   Bull. Am. Phys. Soc., Vol. 31, No. 3, 464, March 1986.

4. S.A.T. Long, E.R. Long Jr., H.R. Ries and W.L. Harries, "Electron-Radiation Effects on the Electrical Conductivities and Unpaired Electron Densities of Three Aerospace Polymers." Presented at the 1986 IEEE Nuclear, Space, and Radiation Effects Conference, July 20-23, 1986, Providence, Rhode Island.

   (See paper, Appendix D). IEEE Transactions of Nuclear Science, Vol. NS-33, No. 6, 1390, December 1986.

5. E.R. Long Jr., S.A.T. Long, H.R. Ries and W.L. Harries, "Radio-frequency Electrical Properties of Some Neat and Metal-Doped Polyimides." Presented at the 1986 IEEE International Symposium on Electrical Insulation, June 9-11, 1986, Washington, D.C.
See paper, Conference Record of the 1986 International Symposium on Electrical Insulation, Appendix C.

6. S.A.T. Long, E.R. Long Jr., S.L. Gray and W.D. Collins, "Total Dose and Dose Rate Effects in Electron-Irradiated Polyetherimide." Presented at 1987 Regular Meeting of the Division of High Polymer Physics of the American Physical Society, March 16-20, 1986, New York, New York.
Bull. Am. Phys. Soc. 32, No. 3, 705, March 1987.

7. H.R. Ries, C.A. Bradbury, W.L. Harries, S.A.T. Long and E.R. Long Jr., "Electron paramagnetic Resonance and Infrared Spectroscopic Analyses of Electron-Irradiated Polyethylene Terephthalate." Presented at the 1986 Annual Meeting of the Southeastern Section of the American Physical Society, November 20-22, 1986, Williamsburg, Virginia.
Bull. Am. Phys. Soc. 31, 1771, (1986).

8. C.A. Bradbury, W.L. Harries, E.R. Long Jr. and S.A.T. Long, "Improvement of ATR IR Spectroscopy for Use with Solid Samples." Presented at the 1986 Annual Meeting of the Southeastern Section of the American Physical Society, November 20-22, 1986, Williamsburg, Virginia.
Bull. Am. Phys. Soc. 31, 1771 (1986).

9. H.R. Ries, S.A.T. Long, E.R. Long Jr. and W.L. Harries, "EPR and DC Conductivity Analysis of an Electron-Irradiated Polymide." 1987

Spring General Meeting of the American Physical Society, Crystal City, Virginia, April 20-23, 1987.

Bull. Am. Phys. Soc. 32. 1021 (1987).

10. C.A. Bradbury, W.L. Harries, S.A.T. Long and E.R. Long Jr., "Damage Effects of Threshold Doses of Electron Radiation on PEI, PEEI, PET and PC." 1987 Annual Meeting of the Division of Atomic, Molecular and Optical Physics Division of the American Physical Society, Cambridge, Massachusettes, May 18-20, 1987.

Bull. Am. Phys. Soc. 32, 1272 (1987).

11. S.A.T. Long, E.R. Long Jr., L.M. Parks, S.L. Gray, "Effects of Low Absorbed Doses of Electron Radiation on Five Thermoplastics." 1988 Annual Meeting of the Southeastern Section of the American Physical Society, Raleigh, North Carolina, November 10-12, 1988.

Bull. Am. Phys. Soc. 33, No. 10, 2211, November 1988.

12. S.A.T. Long, E.R. Long Jr., S.L. Gray, W.D. Collins and L.M. Parks, "Effects of Postcuring on Moisture Absorption in Epoxy, Carbon-Epoxy, and Glass-Epoxy." 1988 Annual Meeting of the Southeastern Section of the American Physical Society, Raleigh, North Carolina, November 10-12, 1988.

Bull. Am. Phys. Soc. 33, No. 10, 2211, November 1988.

13. K.T. Kern, K.M. Brown, Craig A. Hoogstraten, S.A.T. Long and W.L. Harries, "Space Environmental Effects on Aerospace Adhesives." 1989 Annual Joint Meeting of the American Physical Society and the American Association of Physics Teachers, San Francisco, California, January 15-19, 1989.

Bull. Am. Phys. Soc. 34, No. 1, 83, January 1989.

14. P.C. Stancil, S.A.T. Long, E.R. Long Jr. and W.L. Harries, "Low-Earth Orbit Atomic Oxygen Environment Simulation by Radio-Frequency Discharge." Presented at the Seventh American Physical Society Topical Conference on Atomic Processes in Plasmas, Gaithersburg, Maryland, October 2-5, 1989.

15. K.T. Kern, W.L. Harries and S.A.T. Long, "Dynamic Mechanical Analysis of Polymeric Materials." Presented at the National Educators' Workshop: Update 1989. October 17-19, 1989 at NASA Langley Research Center, Hampton, Virginia. See paper, Appendix I.

4. TECHNICAL DISCUSSION

The technical discussion will follow the format of Section 2.2. The substance of the report is contained in the papers in the appendices which have been recorded chronologically, and the purpose of this section is to provide guideposts to the relevant materials. It will be found that Appendix A will be useful in defining the purpose and describing the experimental tests in some detail. The papers are self-contained, each with its own list of references.

4.1 Studies of the Properties of Various Polymers Either Neat or Metal Doped and of Epoxy-Carbon Fiber Composites

To see whether certain polymers could be used for aerospace applications, study of the electrical properties of Mylar®, Kapton®, and Ultem® are reported in Appendices A and C. The latter reports results on the resistivity, capacitance, inductance and dissipation factors for these materials, as well as the effects of changes of temperature. The materials were studied both in their pure form and also with metal dopants.

The effects of postcuring on the mechanical properties of pultruded fiber-reinforced epoxy composites and the neat resin is relevant to the manufacturing processes for these materials and is discussed in Appendix F.

4.2 Effect of the Aerospace Environment on Various Polymers and Composites

The polymers studied were Mylar®, Kapton® and Ultem®. The studies are now subdivided according to the type of environmental effect.

4.2.1 Electron Radiation

Electron radiation at 0.1 and 1 MeV was available at NASA. The effect of electrons is described in Appendix B. Electron paramagnetic resonance measurements were made of the radical densities and their decay measured versus time. The decay was possibly due to cross-linking, a suggestion supported by a decrease in solubility with time.

The effects of electron radiation at 1 MeV on the polymers Mylar®, Ultem® and Kapton® are reported in Appendix D, and the unpaired electron densities (from EPR) and d.c. electrical properties were monitored versus time after exposures. A preliminary model relating the d.c. conductivity to the unpaired electron density in Kapton was proposed. The model was later published under the title "Mechanism of Electrical Conductivity in an Irradiated Polyimide," and is shown in Appendix H. Further studies of absorbed dose thresholds and absorbed dose rates of electron radiation on Ultem are described in Appendix G. Here, EPR measurements and tensile tests were made, and a model based on homolytic scissioning of the linear molecular structure, followed by subsequent cross linking was discussed to explain the changes in the tensile strength.

The effects of electron radiation and thermal cycling on sized and unsized carbon fiber-polyetherimide composites are studied in Appendix J. This study is essentially of the interface between fibers and the matrix, a matter of importance in aerospace materials. Further interface studies are given in Appendix L--The Adhesives Program. Appendix J was written up during the period of the cooperative agreement and the paper shown is the version submitted for "Polymer Preprints" for the American Chemical Society Spring Meeting, 1990, in which it was published April 1990.

15

One of the experimental techniques used in Appendix K was Dynamical Mechanical Analysis, and a paper on the method is shown in Appendix I, which was presented in the National Educators Workshop at Langley October 17-19, 1989. It must be emphasized that this is a simplified version of the actual system where torsion, not extension, was applied, but it is useful for outlining the basic principles.

4.2.2 <u>Thermal Cycling</u>

Throughout the work, whenever the effect of electron radiation was studied, the effect of thermal cycling was also investigated. The results for polymers and composites under the four conditions--no exposure, exposed to electron radiation, exposed to thermal cycling and exposed to electron radiation plus thermal cycling usually appears in the same appendices. The results of thermal cycling therefore appear in Appendices A, B, I, J and L.

4.2.3 <u>Effects of Fluids in the Aircraft Environment</u>

Materials used in aerospace vehicles will be subjected to the effects of various fluids, namely water, JP4 jet fuel, ethylene glycol and hydraulic fluid. Studies of an Ultem and Ultem-fiber composite showed only hydraulic fluid caused erosion, but water and hydraulic fluid affected the flexural properties of the composite, due to capillary absorption along the resin-fiber interface. Details are given in Appendix E.

4.2.4 <u>Effects of Atomic Oxygen</u>

An important consideration for vehicles in Low Earth Orbit (LEO) is the effect of atomic oxygen (AO) which is highly reactive with many materials currently used and intended for future use in space applications. Shuttle flight experiments have shown dramatic deterioration of many

polymers, and as a result, the development of Earth-based AO simulation facilities has become a major research endeavor.

An extensive survey of the literature relating to AO was conducted. Focus points included: atmospheric characteristics at LEO, Shuttle flight experiments, developments of AO simulators, and mechanisms of AO interactions.

The method of AO production for LEO simulation is a hotly debated subject and several oxygen beam apparati are being developed elsewhere. The use of an oxygen plasma created by a radio-frequency (RF) discharge (commonly called an Asher) has been shown to produce material degradation comparable to Shuttle flight experiments and such an apparatus was used at Langley. Determination of the plasma constituents was the first step in the investigation.

Analysis of atomic/molecular spectra has yielded information on the atomic species present, whether ionized or neutral, whether excited or ground states, as well as trace contaminants and molecular species. The results are given in detail in Appendix K which shows the write-up submitted for publication in the American Chemical Society Spring Meeting (published April 1990). Unfortunately, it has been decided that the work on oxygen will be discontinued at NASA Langley.

5. CONCLUSIONS

The work reported relates how the aerospace environment (high energy electrons, thermal cycling, atomic oxygen, aircraft fluids) affects certain polymers used in the aerospace industry (Mylar, Ultem, Kapton) and outlines the experimental techniques used. The work on atomic oxygen is to be discontinued at Langley, but work on the other aspects continues under a

17

new Cooperative Agreement NCCI-139. The appendices give the macroscopic effects useful for designers of space vehicles and also in several instances relate these results to the molecular parameters of the materials (crosslinking, scissioning, type of chemical erosion). An explanation of electrical conductivity in irradiated polymers is also given.

6. ACKNOWLEDGEMENTS

APPENDIX A

STUDIES OF MOLECULAR PROPERTIES OF POLYMERIC MATERIALS
Aerospace Environmental Effects on Three Linear Polymers

Wynford L. Harries (Principal Investigator),
Heidi R. Ries, Cynthia A. Bradbury,
Stephanie L. Gray, and William D. Collins

Department of Physics
School of Sciences and Health Professions
Old Dominion University
Norfolk, Virginia 23508-0369

and

Sheila Ann T. Long and Edward R. Long Jr.

National Aeronautics and Space Administration
Langley Research Center
Hampton, Virginia 23665-5225

(NASA-TM-87532) STUDIES OF MOLECULAR
PROPERTIES OF POLYMERIC MATERIALS:
AEROSPACE ENVIRONMENTAL EFFECTS ON THREE
LINEAR POLYMERS Final Technical Report, 1
Nov. 1984 - 31 Oct. 1985 (NASA) 42 p

N86-15391
THRU
N86-15393
Unclas
G3/27 03170

Old Dominion University Research Foundation

STUDIES OF MOLECULAR PROPERTIES OF POLYMERIC MATERIALS
Aerospace Environmental Effects on Three Linear Polymers

Wynford L. Harries (Principal Investigator),
Heidi R. Ries, Cynthia A. Bradbury,
Stephanie L. Gray, and William D. Collins

Department of Physics
School of Sciences and Health Professions
Old Dominion University
Norfolk, Virginia 23508-0369

and

Sheila Ann T. Long and Edward R. Long, Jr.

National Aeronautics and Space Administration
Langley Research Center
Hampton, Virginia 23665-5225

Final Technical Report
For the period November 1, 1984, through October 31, 1985

Submitted by the
Old Dominion University Research Foundation
P.O. Box 6369
Norfolk, Virginia 23508

December 1985

-ii-

STUDIES OF MOLECULAR PROPERTIES OF POLYMERIC MATERIALS
Aerospace Environmental Effects on Three Linear Polymers

Wynford L. Harries, Heidi R. Ries, Cynthia A. Bradbury,
Stephanie L. Gray[1], and William D. Collins[2]
Department of Physics
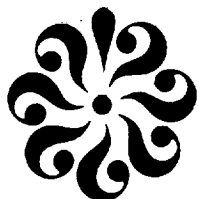Old Dominion University
Norfolk, Virginia 23508-0369

and

Sheila Ann T. Long and Edward R. Long, Jr.
National Aeronautics and Space Administration
Langley Research Center
Hampton, Virginia 23665-5225

ABSTRACT

The development of crystal handling techniques for reflection infrared spectroscopy and methods for the fabrication and testing of tensile specimens are discussed.

Data from mechanical, AC and DC electrical, and electron paramagnetic resonance studies conducted to determine the effects of 0.1-MeV and 1.0-MeV electron radiation on Mylar®, Kapton®, Ultem®, and metal-doped Ultem are presented. Total doses ranging from 1×10^8 rads to 1×10^{10} rads and dose rates from 5×10^7 rads/hr to 1×10^9 rads/hr were employed.

The results of a study on the effects of aircraft service-environment fluids on Ultem are also reported. The weights and mechanical properties of Ultem were evaluated before and after exposure to water, JP4, Skydrol®, an antifreeze, and a paint stripper.

---

[1]Presently attending the School of Engineering and Applied Science, University of Virginia, Charlottesville, Virginia.

[2]Presently attending the School of Engineering, Virginia Polytechnic Institute and State University, Blacksburg, Virginia.

-iii-

Acknowledgement

TABLE OF CONTENTS

LIST OF TABLES

-v-

LIST OF FIGURES

-vi-

STUDIES OF MOLECULAR PROPERTIES OF POLYMERIC MATERIALS

Aerospace Environmental Effects on Three Linear Polymers

I.   INTRODUCTION AND PURPOSE

The purpose of this work is to study aerospace environmental effects on polymeric materials. The polymers under study are being considered for use as structural materials for spacecraft and advanced aircraft. It is necessary to understand the durability of these polymers to the environment in which they are to be used.

In the geosynchronous space environment, materials are constantly being bombarded by electron radiation. The interaction between the material and the radiation causes changes in the molecular structure. These changes may alter the functional properties of the material. Electron beams with energies of 0.1-MeV and 1.0-MeV are used to irradiate the polymeric specimens. After the irradiation, mechanical tests, electron paramagnetic resonance spectroscopy, AC and DC electrical measurements, and internal reflection infrared spectroscopy are employed in order to relate the changes in the molecular properties to the changes in the functional properties.

In the aircraft service environment, the structural components will be exposed to many fluids that may cause a degradation of the polymeric component of the fiber/polymer composite. A study of the degradation effects of aircraft fluids on a polyetherimide has been conducted. After exposure, tensile, weight, and dimensional property measurements

are performed and comparisons are made to the baseline data.

In this report, the results achieved to date under the ongoing NASA Cooperative Agreement NCC1-90 are presented.

II. DEVELOPMENT OF EXPERIMENTAL APPARATUS AND TECHNIQUES

A. DC Resistivity Measurements

Equipment and techniques for making DC resistivity measurements on thin polymer samples were developed, as reported in detail in the Progress Report[1] for the period November 1, 1984, through May 1, 1985. The DC resistivity measurements are made in accordance with ASTM D 257. Palladium/chromium, 2.75-inch diameter electrodes are sputtered onto the specimens, with a guard ring provided on the low voltage side. A Keithley 247 High Voltage Supply delivers the 500V voltage required, and a Keithley 619 Electrometer/Multimeter controlled by a Hewlett Packard 9816 computer is used for the current measurements (Figure 1).

B. Multiple Internal Reflection Infrared Spectroscopy

Multiple internal reflection infrared spectroscopy (MIRIR) is a technique to analyze materials too thick to produce suitable transmission spectra. It utilizes a MIR accessory and a regular IR instrument. This accessory includes a mirror assembly that directs the radiant energy through a crystal (Figure 2). The crystal produces multiple internal reflections, the number being dependent upon the angle of entry of the electromagnetic wave. Even in the case of total reflection, electromagnetic fields exist on the external face of the

crystal. If a sample is placed against the crystal face, it can interact with this field, absorbing energy at characteristic frequencies. A reflection spectrum that is almost identical to a transmission spectrum of the same sample is obtained (Figure 3).

The crystal used is a KRS5 (thallium bromoiodide, ionic coordination lattice) 45° trapezoid. To be compatible with the materials currently being studied, its index of refraction must be higher. The crystal does, however, mar readily with handling. To increase its usable life, a holder was developed to eliminate the movement of the mount pieces against the crystal when mounting a specimen. This reduces the scratching of the crystal surface. A proposed NASA Tech Brief that fully describes this holder is being prepared.

A key parameter in the reproducibility of the spectra is the contact between the sample and the crystal. Contact is accomplished by pressure supplied by three screws. To insure that this pressure is the same each time, a torque screwdriver with one inch-pound resolution was used.

Studies were conducted to compare reflection versus transmission spectra. They are being analyzed using a ratio of peak intensities. This technique eliminates the effect of any changes in peak intensity due to the sample handling procedure and, therefore, enhances the sensitivity with which changes occurring due to radiation damage are detected.

C. Mechanical Testing Techniques

Methods for the fabrication of tensile specimens from neat-resin sheet stock with thicknesses from 10 to 20 mils were evaluated. The method for evaluation was visual inspection followed by tensile testing and comparison of the data to those previously determined from 3-mil specimens. Two methods were investigated: slicing and shearing. Slicing was not found to be practical for the hand-powered method previously used for the 3-mil sheet stock. Power methods, such as motor-driven and ultrasonics, were considered, but have not been evaluated. The shearing method was found to be acceptable, unless the shearing blades are nicked. The consequence of nicked blades was jagged-edged specimens that failed prematurily.

A fixture for machining compression shear specimens from pultruded constant-cross-section stock was designed and fabricated. This fixture was designed to be used with a small table saw. A fixture was also fabricated for holding shear specimens while they were tested for shear properties in the compression mode. The support fixture was evaluated using shear specimens fabricated from pultruded stock. This also yielded preliminary information about the shear properties of pultruded composites. The data from the study will be a part of a larger evaluation of the mechanical properties of pultruded graphite/epoxy and Kevlar®/epoxy materials to be conducted in the near future.

-5-

III. SPACE ENVIRONMENTAL EFFECTS

The effects of electron radiation on various properties of Mylar®, Kapton®, Ultem®, and metal-doped Ultem were studied. The Mylar, Kapton, and Ultem data will be included in a presentation that is currently being proposed for the 1986 Regular Meeting of the Division of High Polymer Physics of the American Physical Society.

A. Mylar

Castings of 10-mil Mylar, a poly(ethylene terephthalate) manufactured by Dupont, were exposed to 1.0-MeV electrons for total doses of 1×10^9 rads and 5×10^9 rads. The dose rate was 5×10^7 rads/hr.

In each case, mechanical measurements were made. Decreases in the ultimate stress, modulus, and total elongation-to-failure were observed (Table I).

TABLE I. MECHANICAL DATA FOR 10-MIL MYLAR WITH 1.0-MEV ELECTRON RADIATION
(Dose Rate = 5×10^7 rads/hr)

Dose, rads	Ultimate stress, psi	Modulus, psi	Elongation, %
0	27135	458578	182
1×10^9	14824	226295	71
5×10^9	7139	234561	2.2

-6-

The DC resistivity was observed to decrease from 2.1 X 10^{17} ohm-cm to 1.5 X 10^{17} ohm-cm for a total dose of 5 X 10^9 rads. The measurements at 1 X 10^9 rads were inconclusive.

EPR measurements indicated over two orders of magnitude increase in the organic radical density after the irradiation (Figures 4 and 5). There is little difference between the results for 1 X 10^9 rads and 5 X 10^9 rads. However, this is probably due to an unexpected shutdown of the electron accelerator that resulted in a 72-hour interruption in the 5 X 10^9 rad exposure, during which time radical decay took place. Post-irradiation decay in air at room temperature of the radical density occurred (Figures 6 and 7).

Measurements of the glass transition temperature (Tg) were made using an AC electrical technique. In this technique, the dissipation factor is measured as a function of the temperature. By convention, the Tg is the temperature at the intersection of the tangent lines to the dissipation factor curve in the first region of major increase in the dissipation factor. The Tg was observed to decrease with increased radiation dose (Figures 8 and 9). The dissipation factor also changed with dose.

B. Kapton

Films of 3-mil research-grade Kapton, a polyimide manufactured by Dupont, were exposed to 1.0-MeV electrons at a dose rate of 5 X 10^7 rads/hr for a total dose of 9.5 X 10^9 rads. The glass transition temperature decreased upon irradiation from 388 $^{\circ}$C to 366 $^{\circ}$C (Figure 10). No significant changes in the magnitudes of the

dissipation factor, the capacitance, or the impedance were observed at 10 kHz from room temperature up to 500 °C.

Films of 3-mil standard-stock Kapton were exposed to 1.0-MeV electrons at a dose rate of 5×10^7 rads/hr for a total dose of 5×10^9 rads. After the irradiation the radical density increased by more than an order of magnitude (Figure 11). The EPR signal was observed to decay upon exposure to air at room temperature (Figure 12). The DC conductivity was observed to increase by nearly five orders of magnitude (Figure 13). Both the EPR radical density and the DC conductivity increases were observed to decay in time with two distinct decay rates (Figures 14 and 15). These decay studies were conducted in air at room temperature. A theory that relates the DC and the EPR results for decay is currently being developed.

C. Ultem

Exposures of 3-mil and 20-mil Ultem, a polyetherimide manufactured by General Electric, were made using 1.0-Mev electrons at a dose rate of 5×10^7 rads/hr. No significant changes in the Tg, the dissipation factor, the capacitance, or the impedance were observed using 3-mil Ultem for a total dose of 5×10^9 rads.

A slight increase in the DC conductivity was found for both thicknesses of Ultem for a total dose of 5×10^9 rads (Figure 13). No significant change in the DC conductivity was observed for the 3-mil Ultem for a total dose of 1×10^9 rads. Possible explanations for the vastly different responses of the DC conductivity to irradiation for Ultem and Kapton are being considered.

The EPR radical density increased by over three orders of magnitude for each thickness of Ultem (Figure 11). This induced radical density increase in Ultem was observed to decay much more rapidly (Figure 16) than that in Kapton.

Films of 3-mil Ultem were exposed to 100-keV electrons at a dose rate of 1×10^9 rads/hr for a total dose of 5×10^9 rads. No significant change in the T_g was observed.

As discussed in detail in Appendix A of the Progress Report[1], EPR radical decay studies at room temperature in vacuum of 3-mil Ultem exposed to 100-keV electrons for a total dose of 2.5×10^8 rads were conducted (Figures 17 and 18). The total EPR radical signal was stored on a computer; and the portion of the signal attributable to the phenoxyl radical was separated from the total, using the known characteristics of the phenoxyl radical. The phenoxyl decay curve thus obtained is shown (Figure 19).

The EPR radical density in 3-mil Ultem was determined as a function of total dose over the range from 1×10^8 to 1×10^{10} rads (Figure 20). The dose rate was 1×10^9 rads/hr using 100-keV electrons.

A preliminary dose rate study was conducted using 3-mil Ultem film irradiated with 100-keV electrons for a total dose of 1×10^8 rads (Figure 21). Little difference was observed between the EPR radical density produced using 1×10^8 rads/hr and that produced using 1×10^9 rads/hr.

D. Metal-Doped Ultem

The effects of 100-keV electron irradiation on Ultem doped with cerium trifluoride were also considered. This material is currently under development by the Virginia Commonwealth University. No organic radical signal was distinguishable from the metal signal background before the irradiation. The EPR organic radical density after the irradiation with a total dose of 1×10^9 rads is shown (Figure 22). The infrared and UV-Vis spectra before and after radiation were also taken. These data are currently being analyzed.

IV. AERONAUTICAL ENVIRONMENTAL EFFECTS

A series of three-month-soak exposures and tests to evaluate the effects of aircraft fluids on the tensile, weight, and dimensional properties of 3-mil specimens of Ultem were performed. The fluids were water, JP4 (a jet fuel), and Skydrol® (a hydraulic fluid manufactured by Monsanto). The data from this experiment indicated that the hydraulic fluid had the most significant effect, in that it caused extensive embrittlement of the Ultem. The JP4 also caused embrittlement, but not to the same extent. Each of these two fluids caused a weight gain of approximately three percent and an approximate two percent increase in thickness. As expected, there was little or no weight gain caused by the water. On the other hand, there was an embrittlement which, although small compared to that caused by the other two fluids, was completely unexpected.

-10-

Two additional fluids, as well as the preceding three, were included in a second fluid-effects study: ethylene glycol (an antifreeze) and methylene chloride (a paint stripper). Thicker, 20-mil, film specimens of Ultem, as well as specimens of the original 3-mil thickness, were used for this study. In addition to these specimens for measuring changes in weight, thickness, and mechanical properties, ultra-thin, 0.25-mil, specimens of Ultem were used to record the effects of these fluids on the infrared spectra of Ultem. The mechanical and physical data showed repeatability for the fluids studied previously and similar effects for the two additional fluids. The infrared data have not yet been analyzed.

The data from this fluid-effects study will be analyzed and prepared for a proposed report.

-11-

V. PAPERS

Stephanie L. Gray: "Electron-Radiation Induced Molecular Changes in a Polyetherimide Film." Virginia Junior Academy of Science, Spring 1985.

William D. Collins: "A Study of the Effects of Fluid Environments on the Physical and Mechanical Properties of ULTEM Resin." Virginia Junior Academy of Science, Spring 1985.

E. R. Long, Jr., S. A. T. Long, H. R. Ries, and W. L. Harries: "Radio-Frequency Electrical Properties of Some Neat and Metal-Doped Polyimides." Abstract submitted to the 1986 IEEE International Symposium on Electrical Insulation.

REFERENCES

[1]W. L. Harries, H. R. Ries, S. L. Gray, and W. L. Collins: "Studies of Molecular Properties of Polymeric Materials." Progress Report for the period November 1, 1984, through May 1, 1985, prepared for the National Aeronautics and Space Administration, Langley Research Center under NASA NCC1-90.
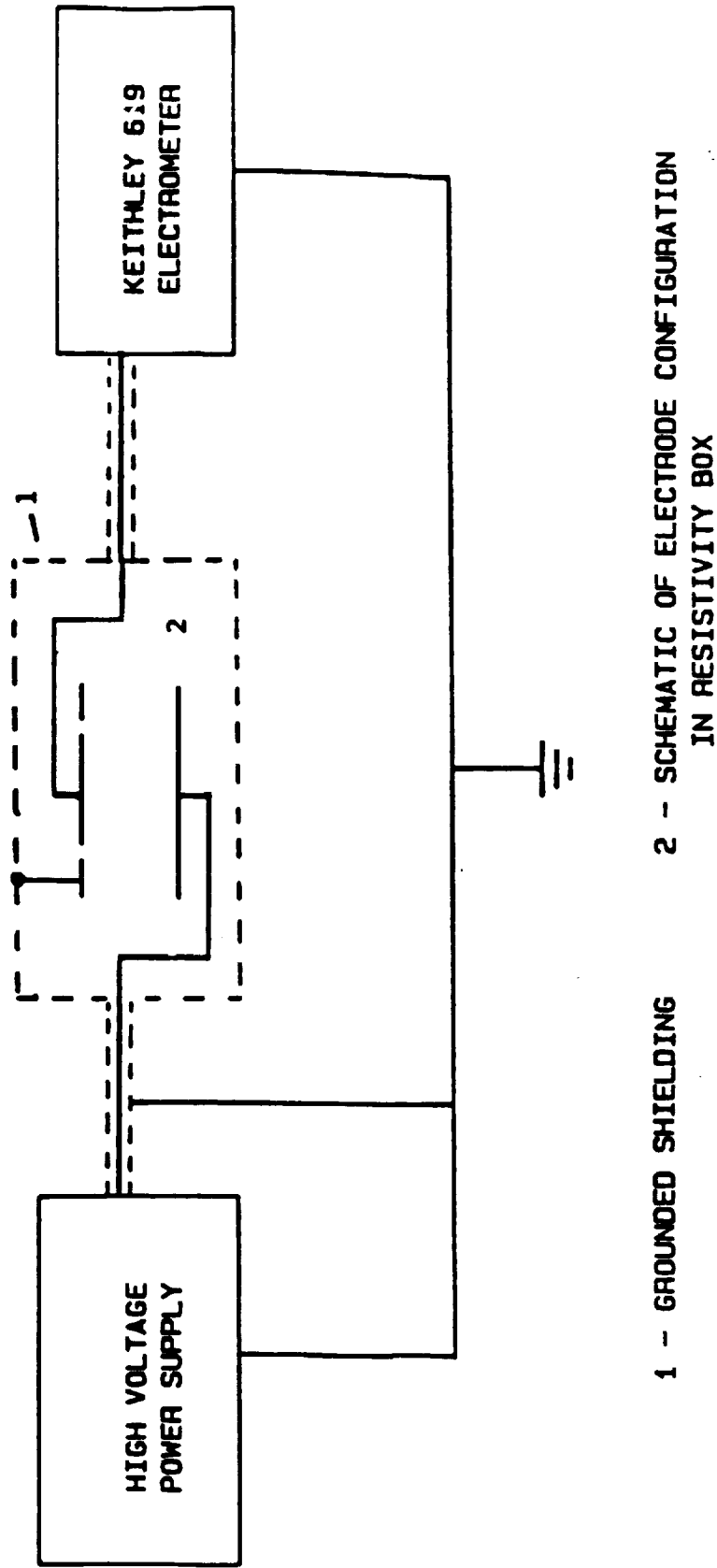
1 – GROUNDED SHIELDING   2 – SCHEMATIC OF ELECTRODE CONFIGURATION
                              IN RESISTIVITY BOX

Figure 1.- Experimental arrangement for direct-current resistivity measurements.
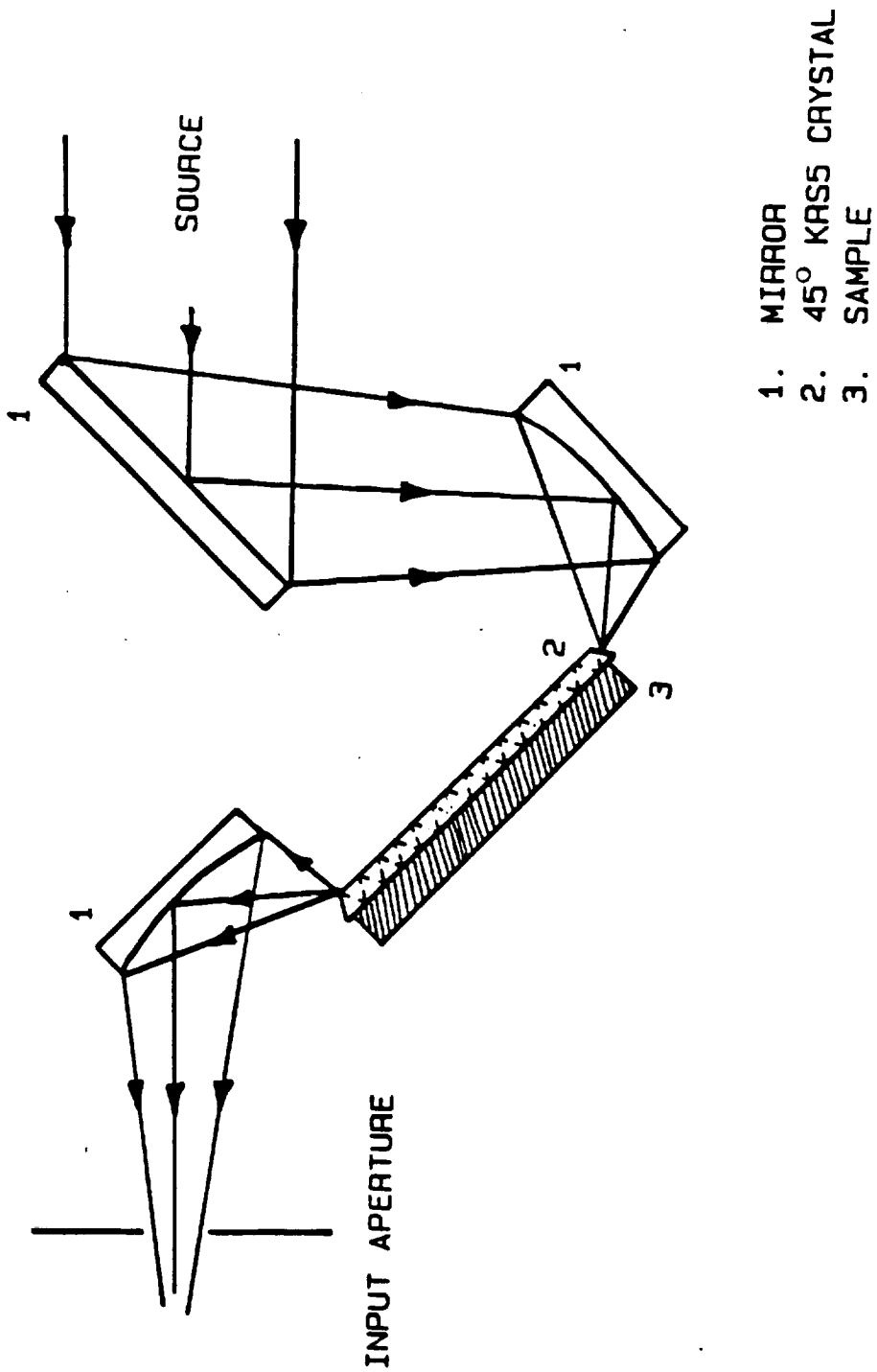
Figure 2.- Schematic of multiple internal reflection accessory for surface IR measurements.
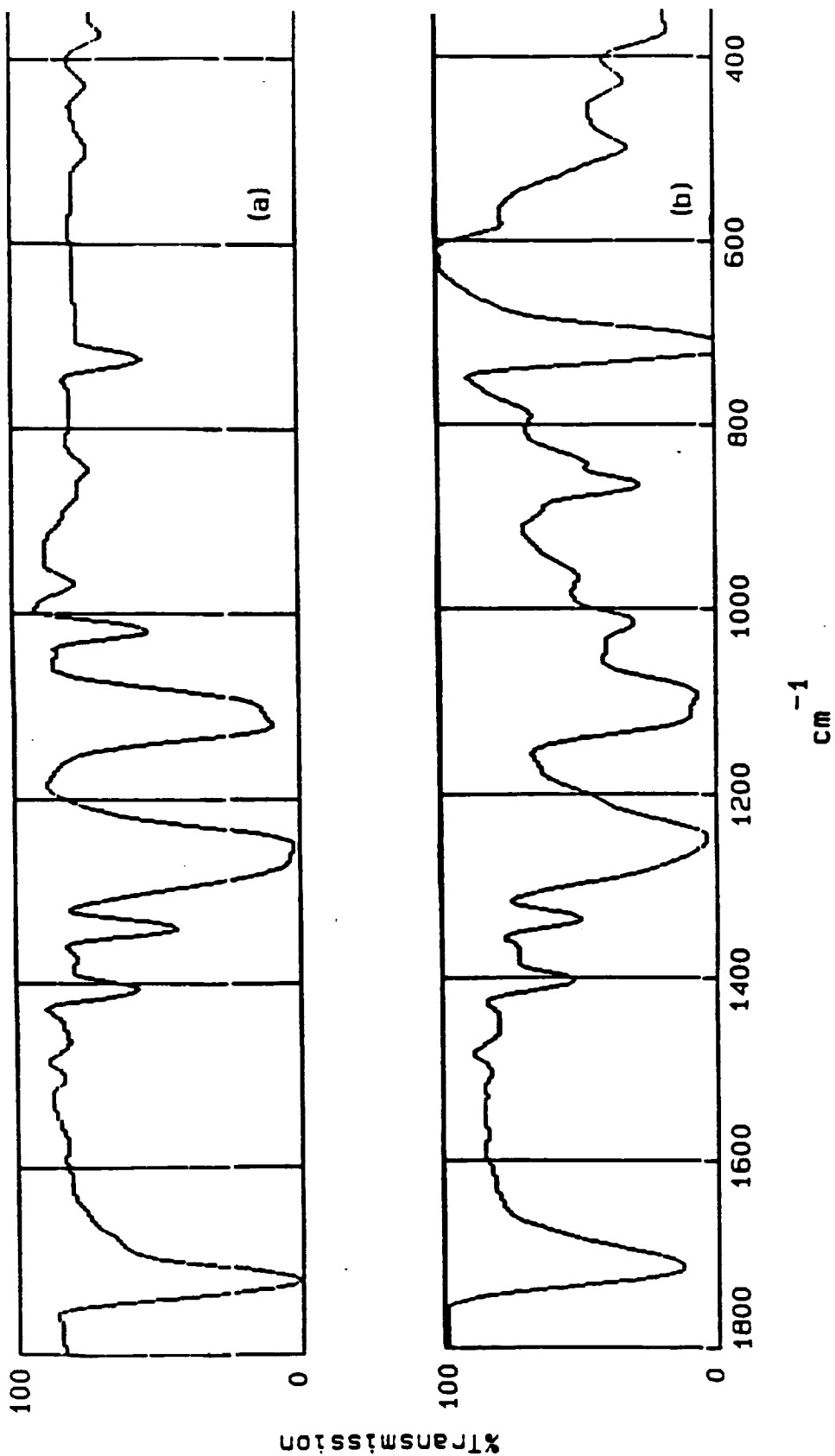
Figure 3.- Infrared spectra of Mylar: (a) transmission and (b) reflection.

4000 GAUSS

MEASUREMENT PARAMETERS:
MICROWAVE POWER = 100 mW
RECEIVER GAIN = 2500
TEMPERATURE = -190 °C
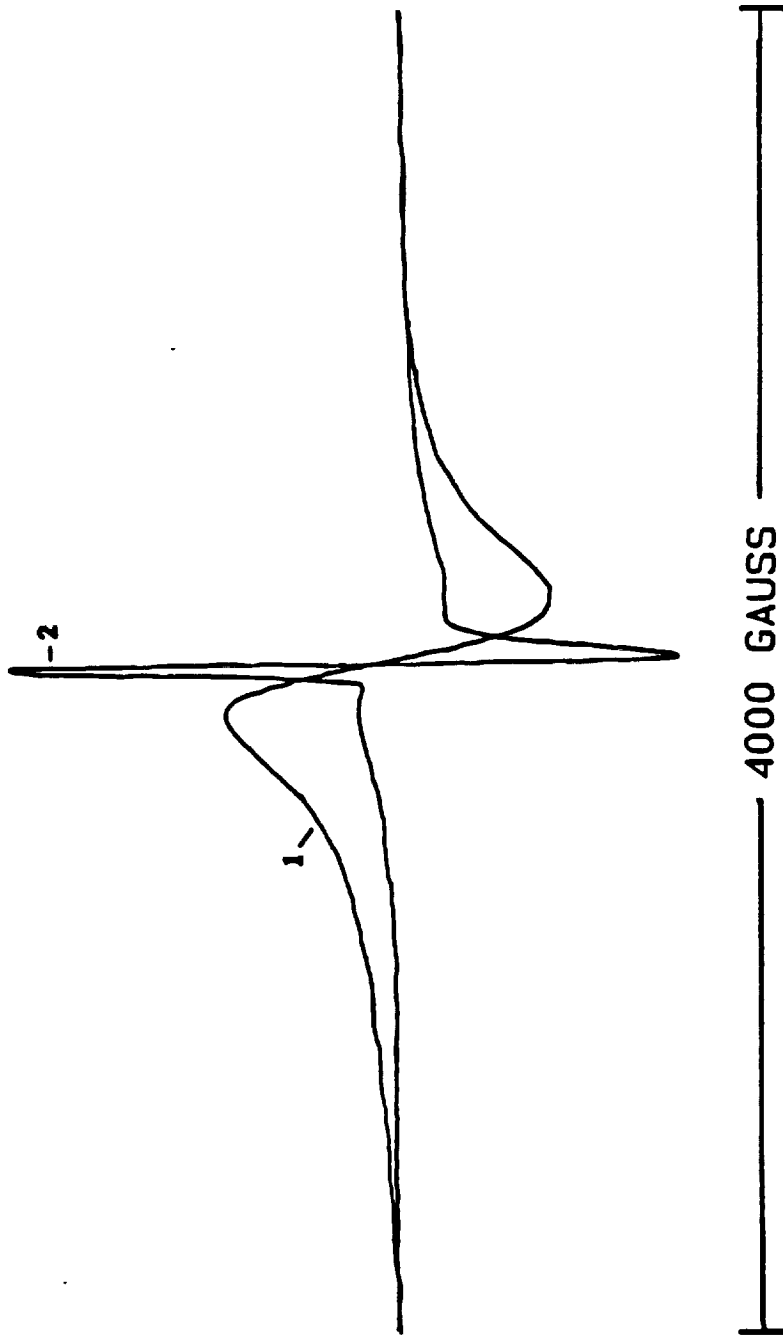
1. NONIRRADIATED CONTROL SPECIMEN
   (MASS = .0533g)

2. SPECIMEN EXPOSED TO 1.0-MEV ELECTRONS
   (MASS = .0126g)
   TOTAL DOSE = 1 X 10^9 RADS
   DOSE RATE = 5 X 10^7 RADS/HR

Figure 4.- EPR spectra of Mylar before and 30 min. after exposure to 1.0-MeV electron radiation.
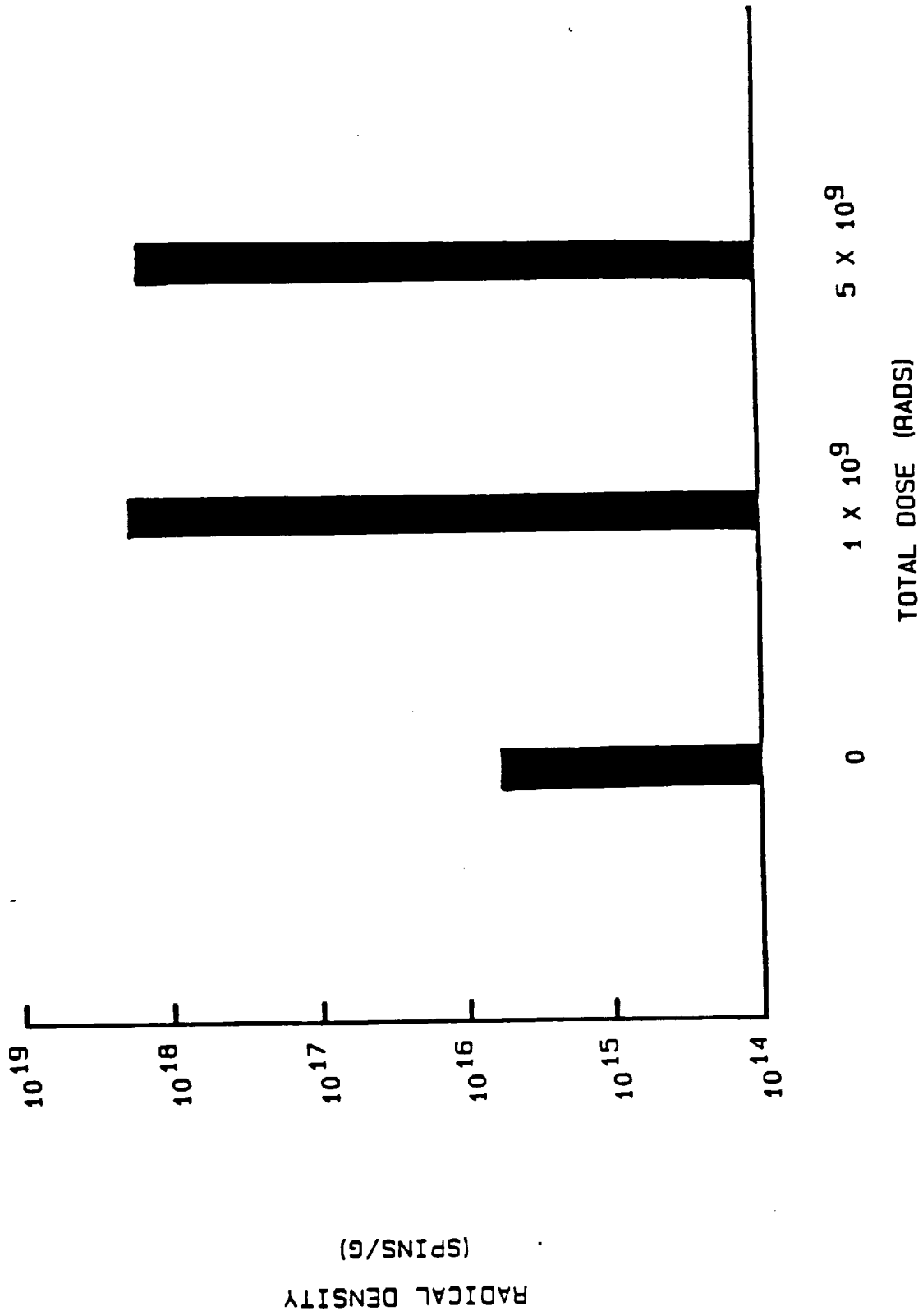
Figure 5.- EPR radical density in Mylar before and 30 min. after exposure to 1.0-MeV electron radiation, dose rate = 5 X 10^7 rads/hr.

MEASUREMENT PARAMETERS:
MICROWAVE POWER = 12.5 mW
RECEIVER GAIN = 400
TEMPERATURE = -190 °C

160 GAUSS
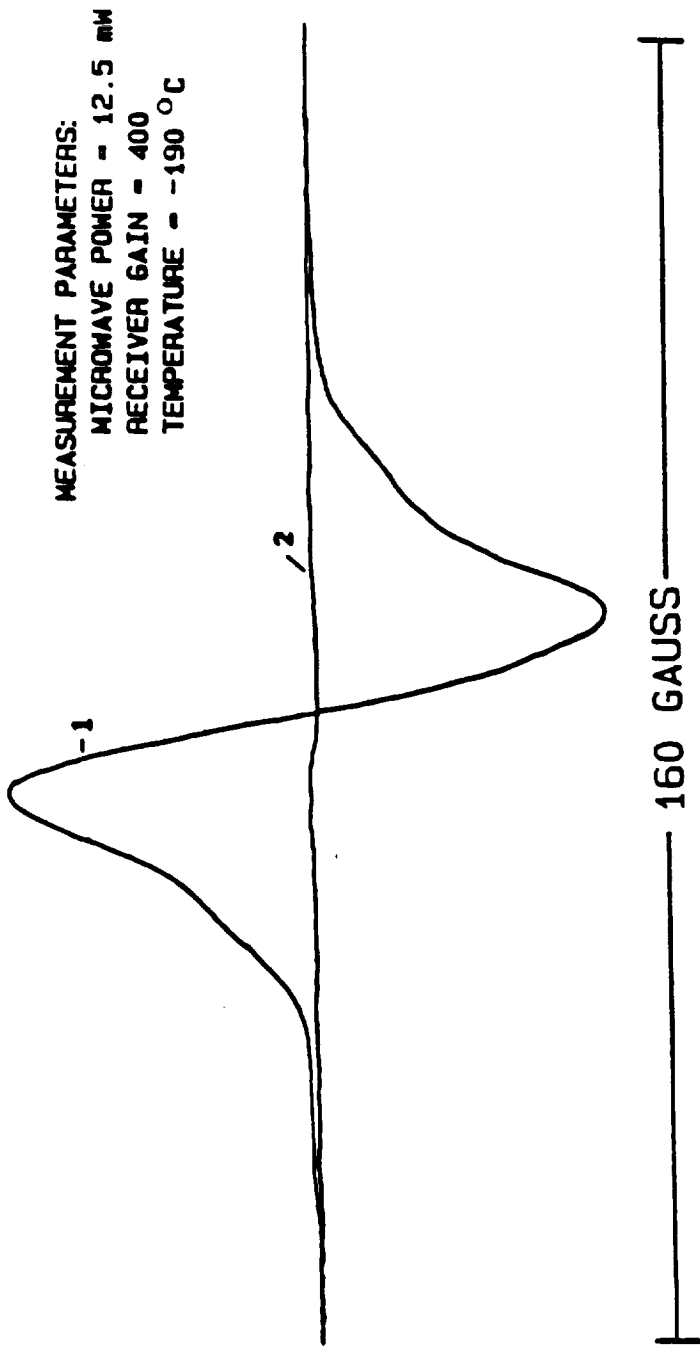
1. SPECIMEN SHORTLY AFTER COMPLETION OF THE 1 X 10⁹ RAD EXPOSURE
   (APPROX. 35 MIN AT ROOM TEMPERATURE IN AIR)

2. IRRADIATED SPECIMEN AFTER 20 DAYS AT ROOM TEMPERATURE IN AIR

Figure 6.- Decay of EPR signal from Mylar after exposure to 1.0-MeV electron radiation, dose rate = 5 X 10⁷ rads/hr.
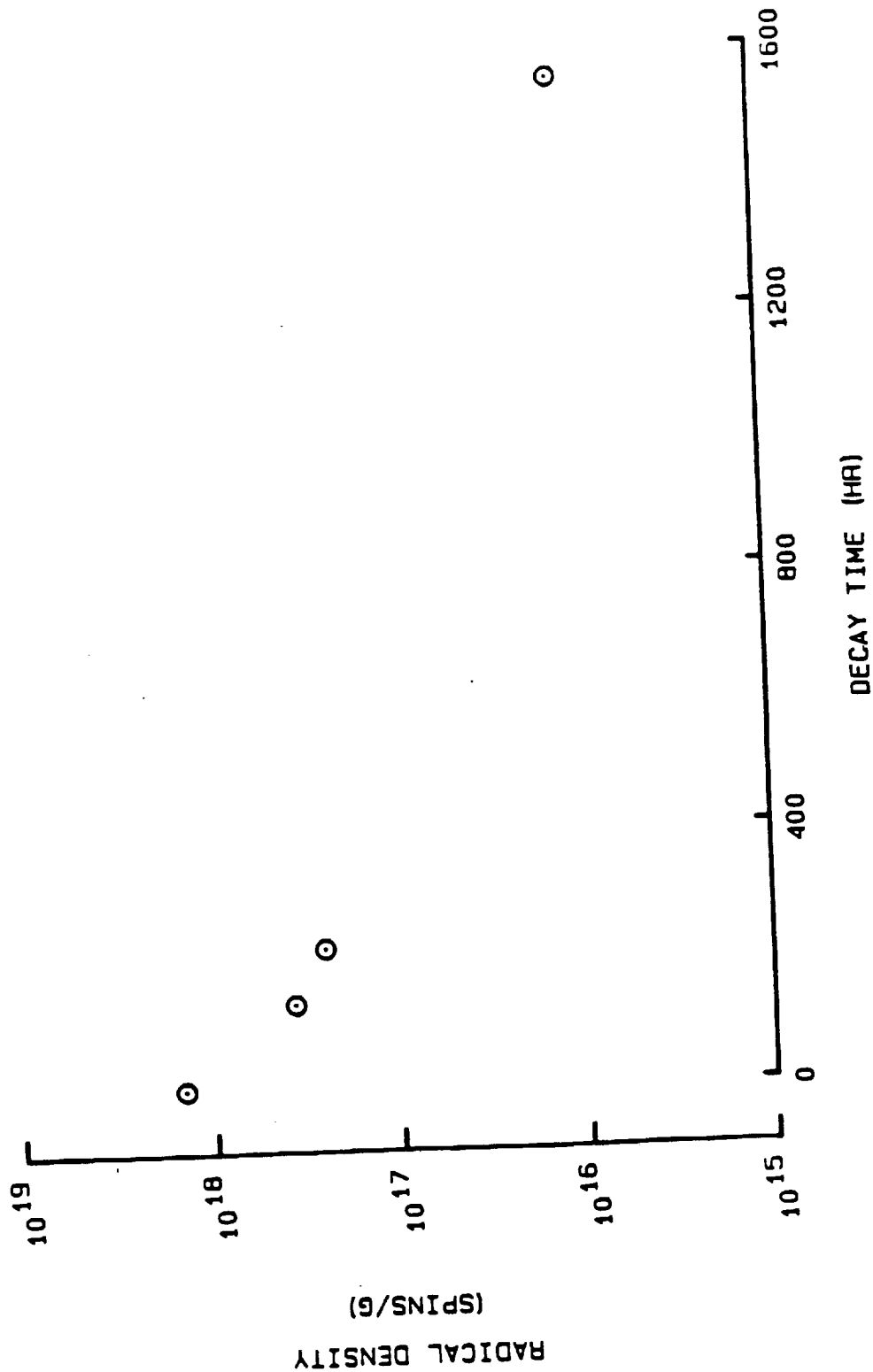
Figure 7.- Decay of EPR organic radical density in Mylar after exposure to 1.0-MeV electron radiation, total dose = 5 X 10^9 rads and dose rate = 5 X 10^7 rads/hr.

Figure 8.- Dissipation factor curves and glass transition temperatures for Mylar before and after exposure to 1.0-MeV electron radiation, dose rate = 5 X 10^7 rads/hr.

1. 5 X 10^9 RADS, Tg = 31 °C
2. 1 X 10^9 RADS, Tg = 38 °C
3. NONIRRADIATED, Tg = 69 °C

DISSIPATION FACTOR
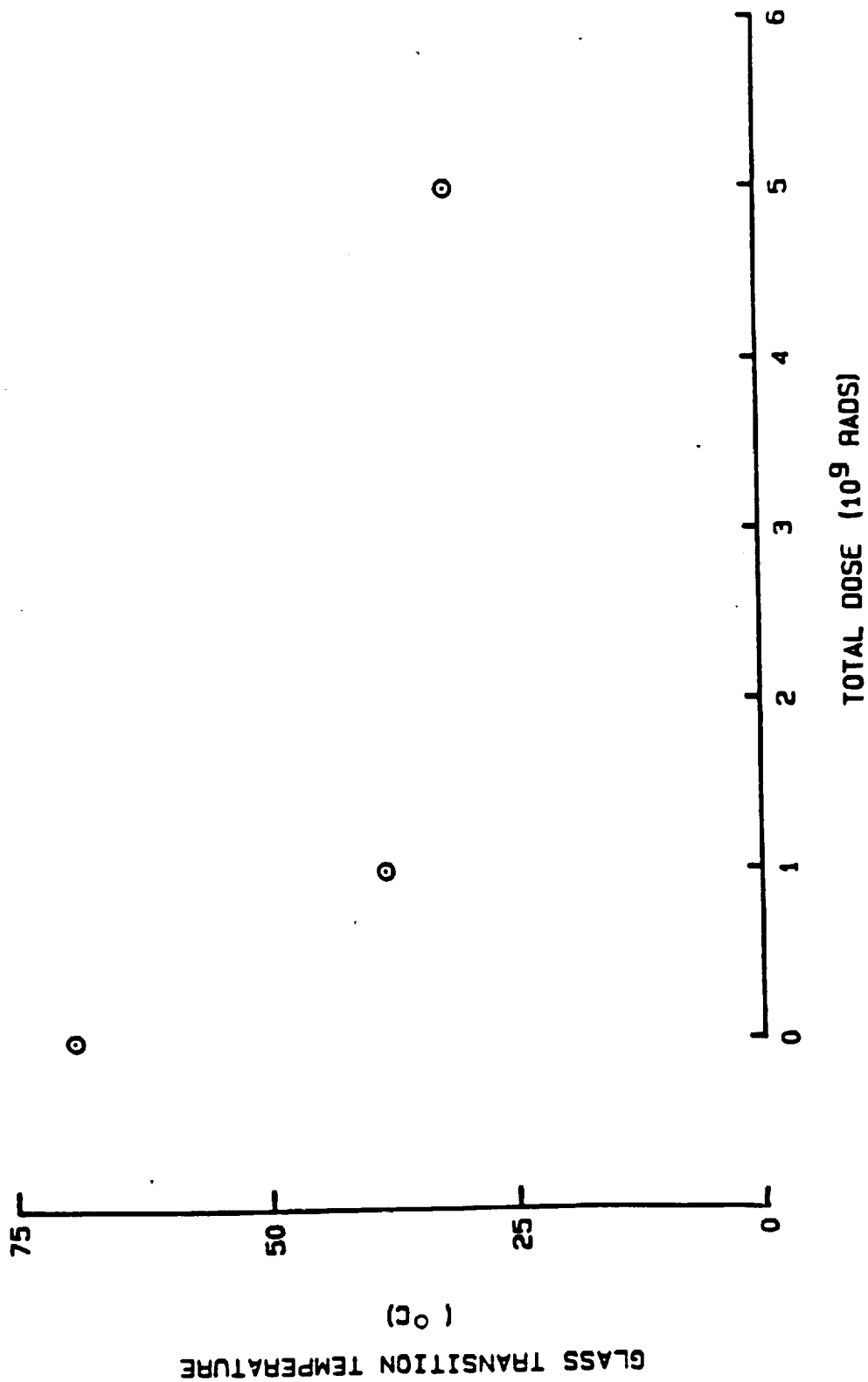
TEMPERATURE (°C)

Figure 9.- Glass transition temperature for Mylar vs. exposure to 1.0-MeV electron radiation, dose rate = 5 X 10^7 rads/hr.
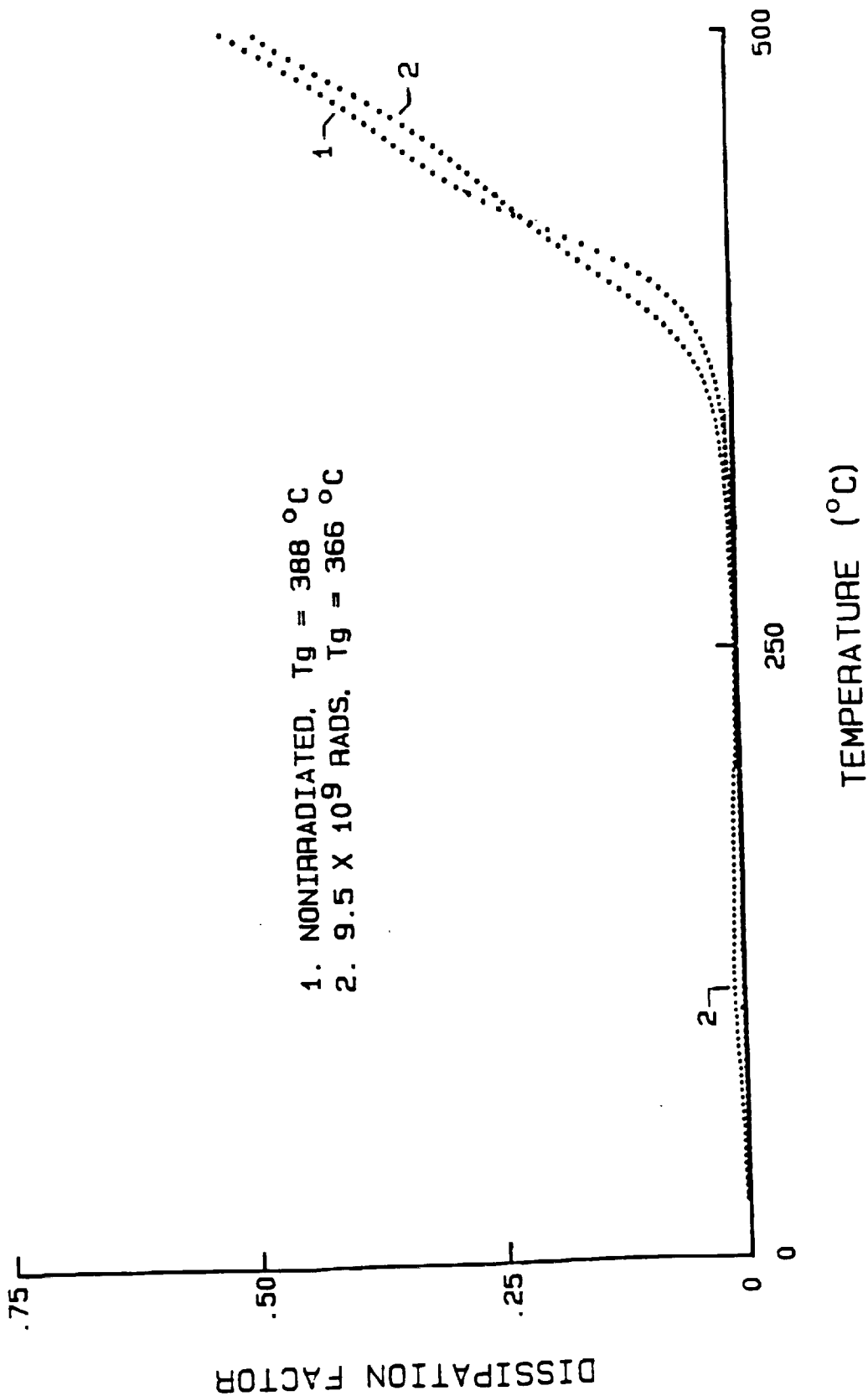
Figure 10.- Dissipation factor curves and glass transition temperatures for research-grade Kapton before and after exposure to 1.0-MeV electron radiation, dose rate = 5 X 10^7 rads/hr.
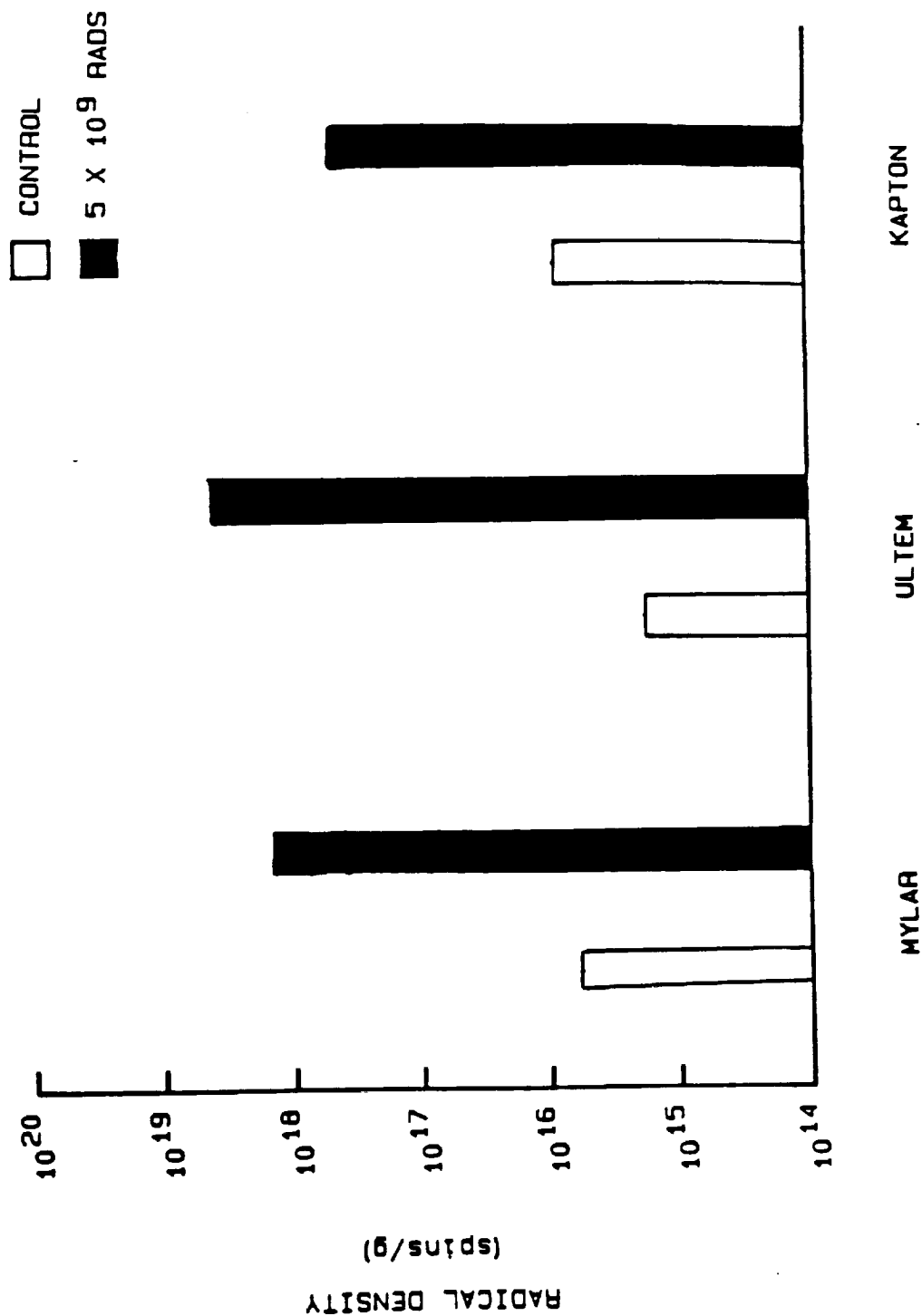
Figure 11.- EPR radical densities in Mylar, Ultem, and Kapton, before and 30 min. after exposure to 1.0-MeV electron radiation, dose rate = 5×10^7 rads/hr.

-23-
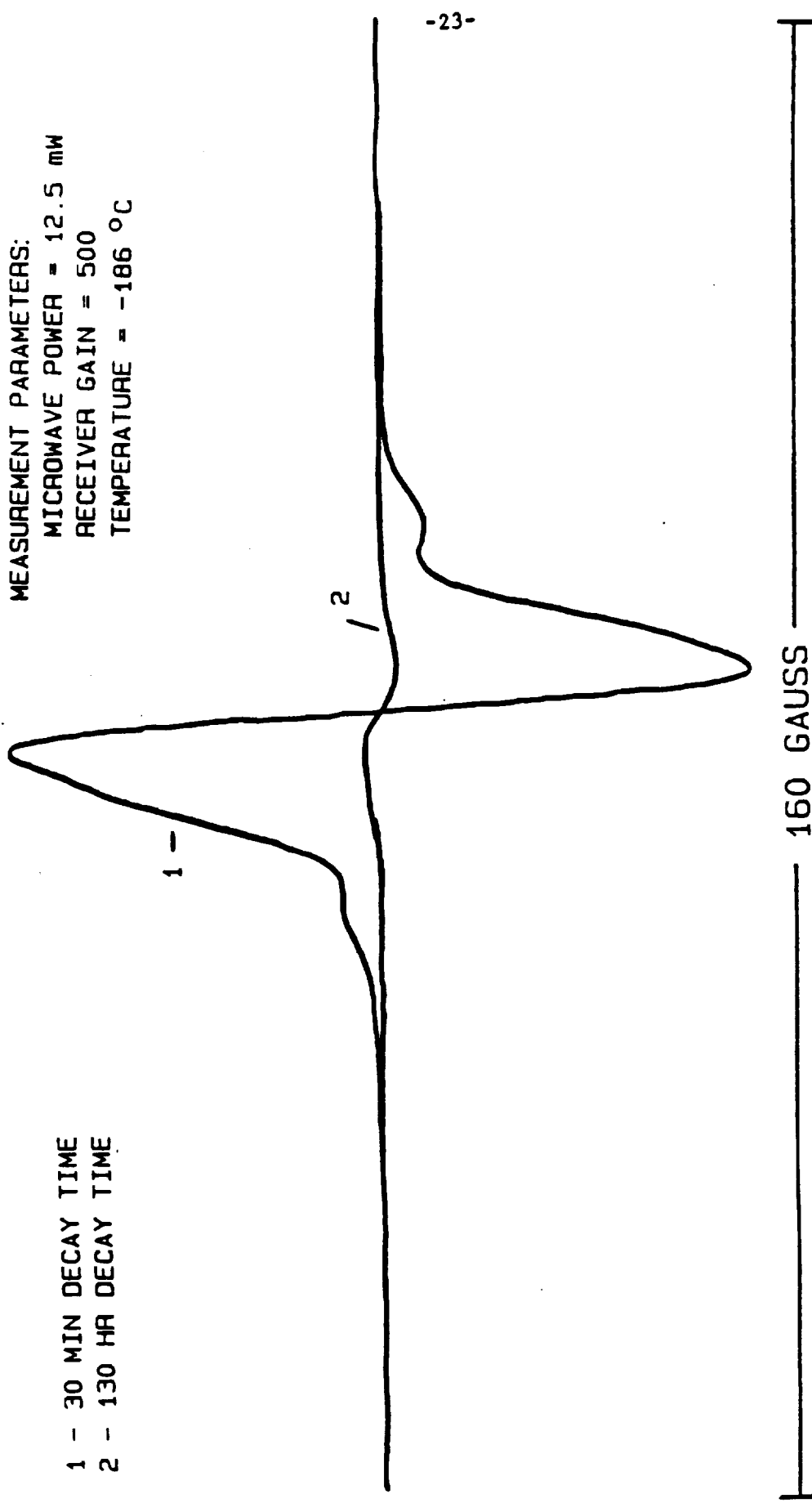
MEASUREMENT PARAMETERS:
MICROWAVE POWER = 12.5 mW
RECEIVER GAIN = 500
TEMPERATURE = -186 °C

2

1

1 - 30 MIN DECAY TIME
2 - 130 HR DECAY TIME

— 160 GAUSS

Figure 12.- Decay of EPR signal from Kapton after exposure to 1.0-MeV electron radiation, total dose = 5 X 10^9 rads and dose rate = 5 X 10^7 rads/hr.

Figure 13.- Electrical conductivities of Mylar, Ultem, and Kapton, before and 30 min. after exposure to 1.0-MeV electron radiation, dose rate = 5×10^7 rads/hr.
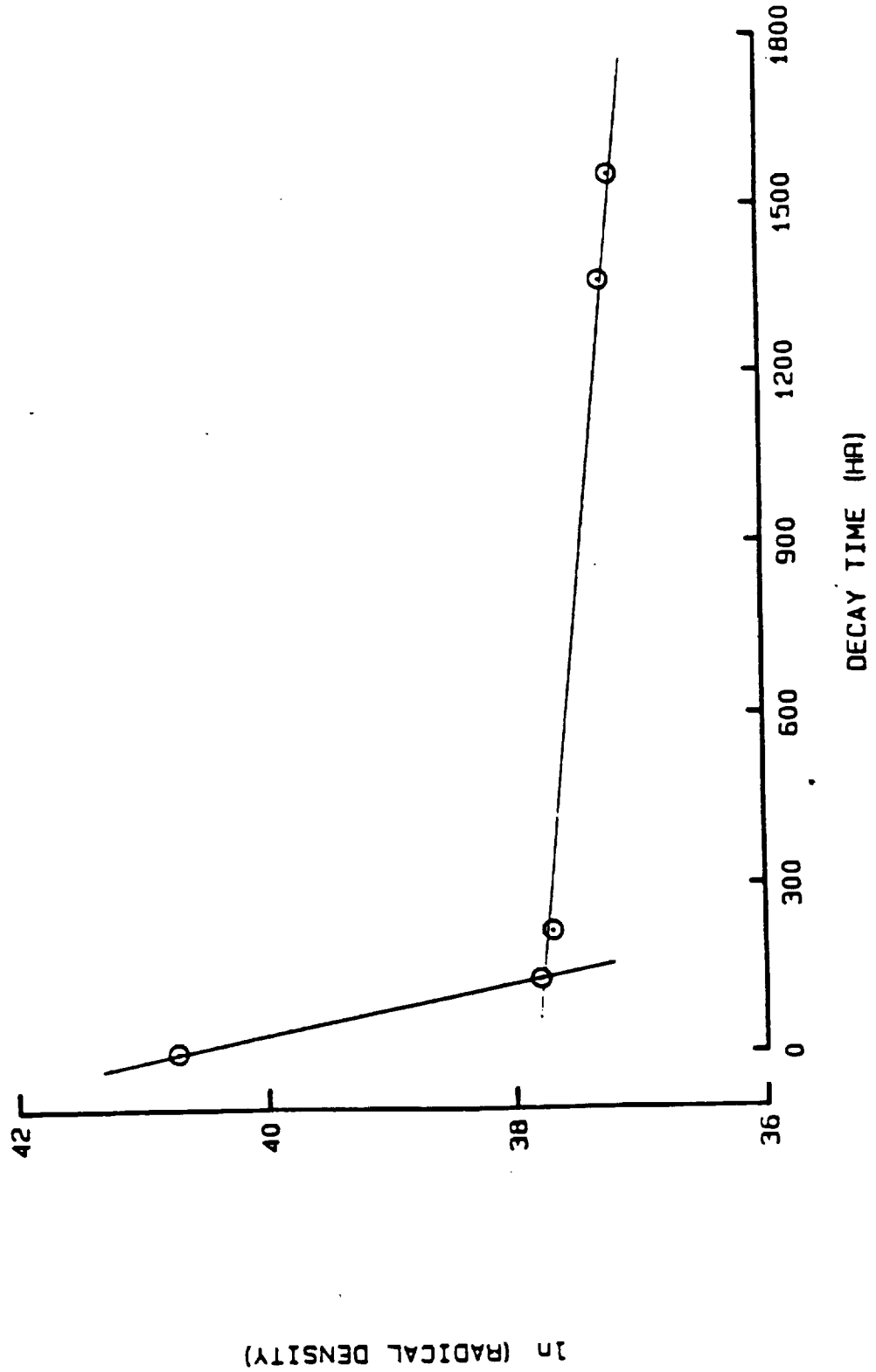
Figure 14.- Decay of EPR radical density in Kapton after exposure to 1.0-MeV electron radiation, total dose = 5 X 10^9 rads and dose rate = 5 X 10^7 rads/hr.

Figure 15.- Electrical conductivity of Kapton as a function of time after exposure to 1.0-MeV electron radiation, total dose = 5×10^9 rads and dose rate = 5×10^7 rads/hr.

A-35

MEASUREMENT PARAMETERS:
MICROWAVE POWER = 12.5 mW
RECEIVER GAIN = 125
TEMPERATURE = -186 °C

1 - 30 MIN DECAY TIME
2 - 130 HR DECAY TIME

160 GAUSS
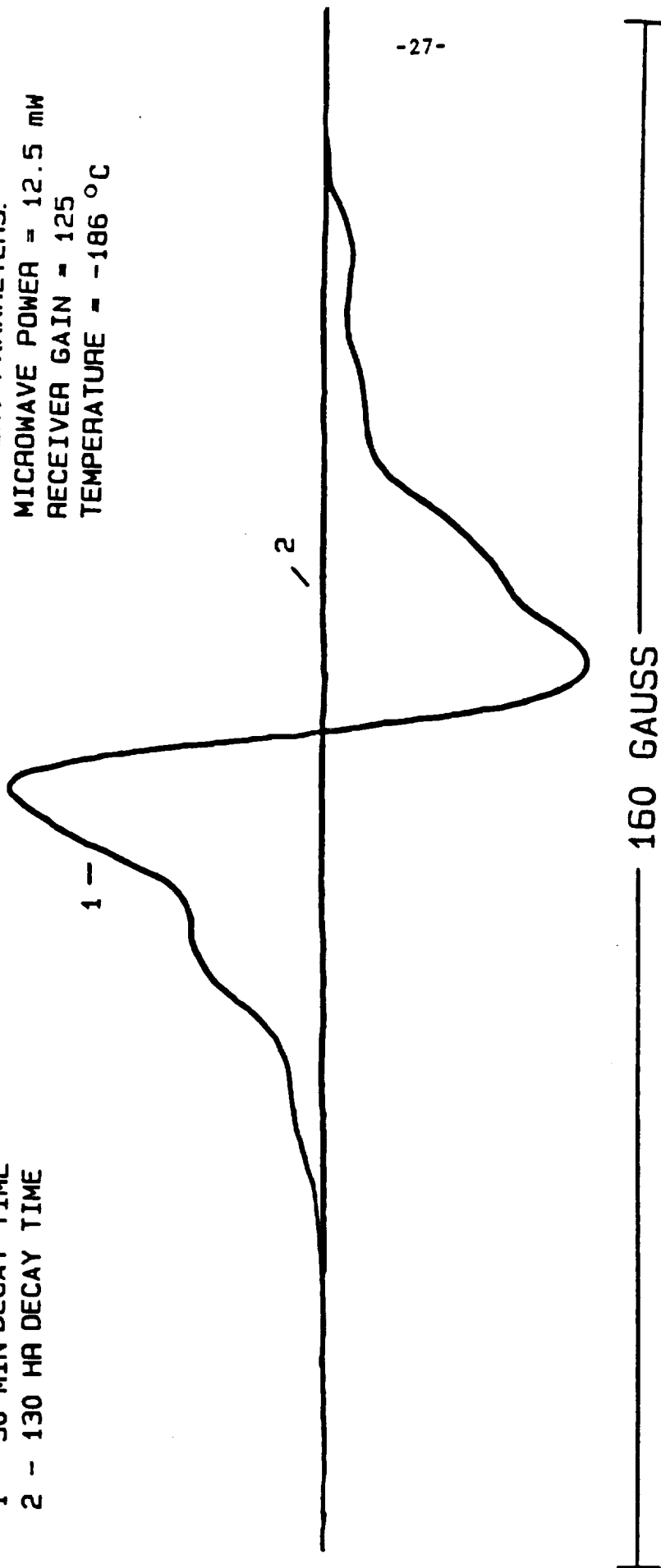
Figure 16.- Decay of EPR signal from Ultem after exposure to 1.0-MeV electron radiation, total dose = 5 X 10^9 rads and dose rate = 5 X 10^7 rads/hr.

-28-
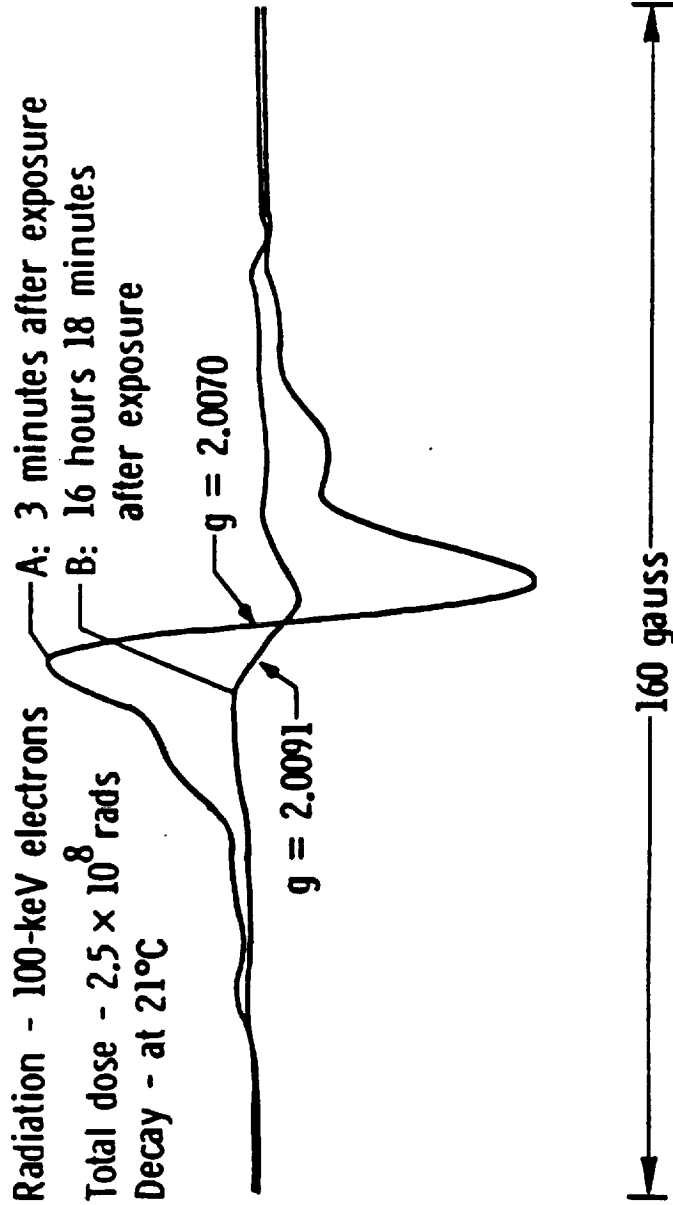
Figure 17.- Decay of EPR signal from Ultem, dose rate = 1 X 10⁹ rads/hr.
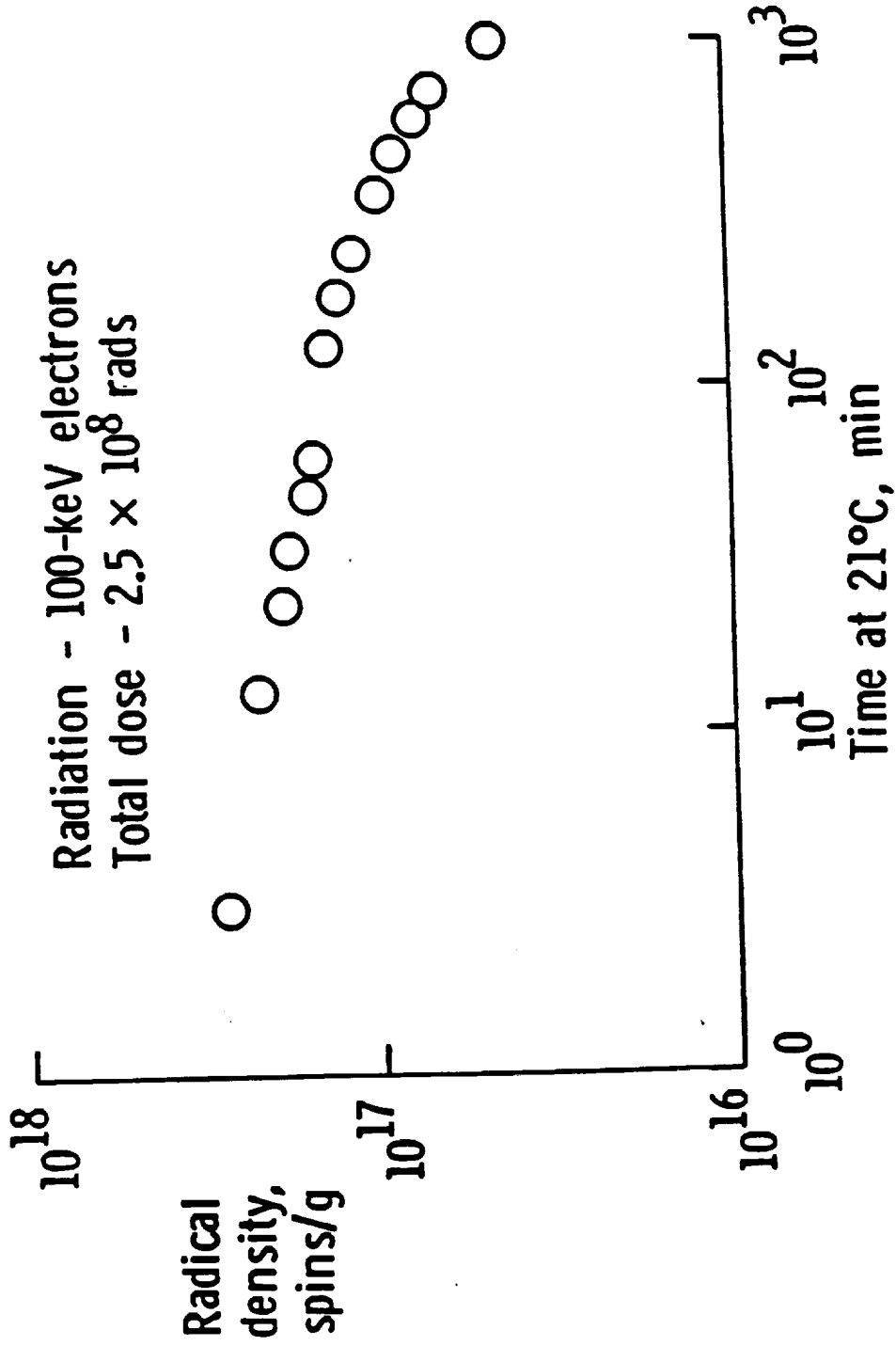
Figure 18.- Decay of EPR radical density in Ultem, dose rate = 1 X 10⁹ rads/hr.
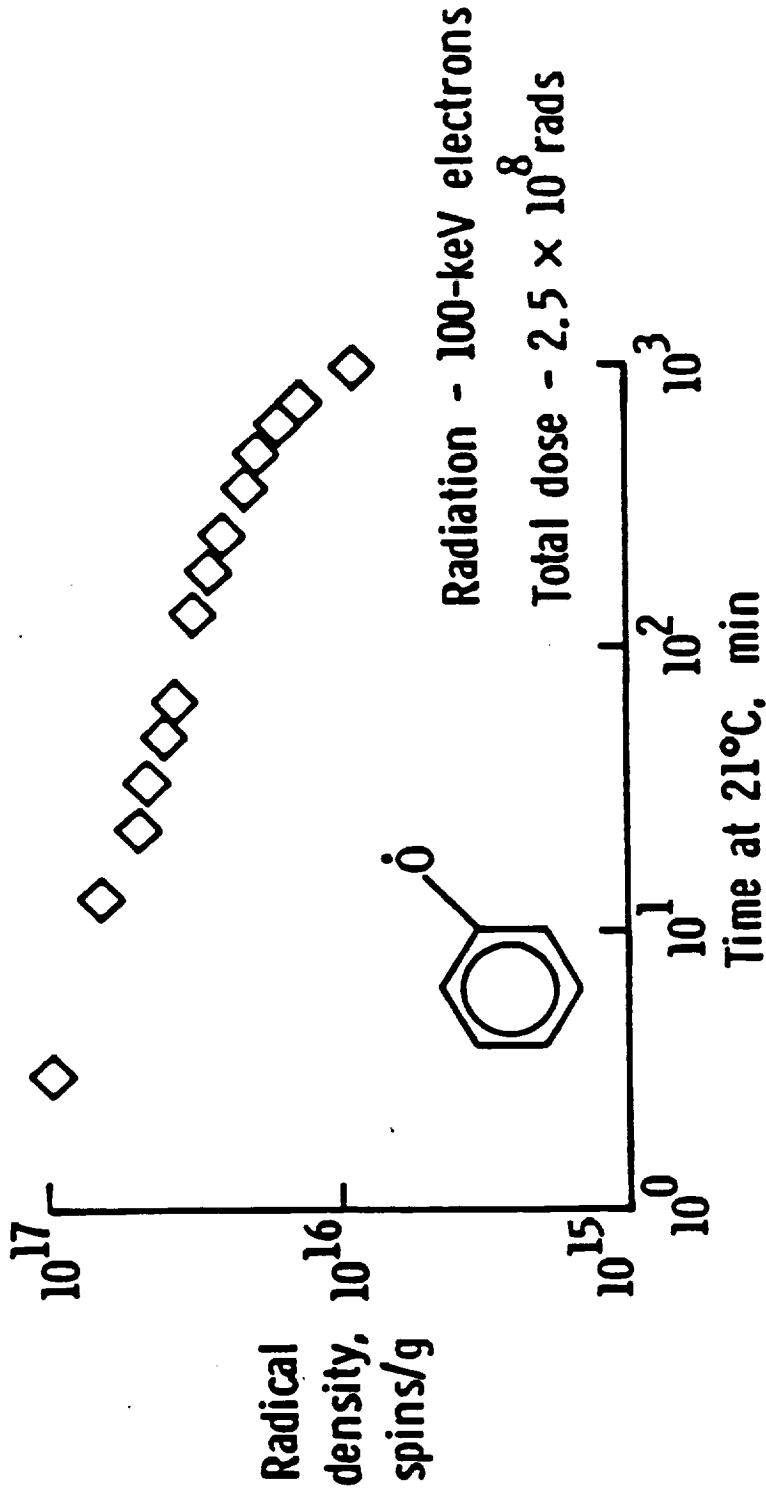
Figure 19.- Decay of EPR phenoxyl radical density in Ultem, dose rate = 1 X 10⁹ rads/hr.
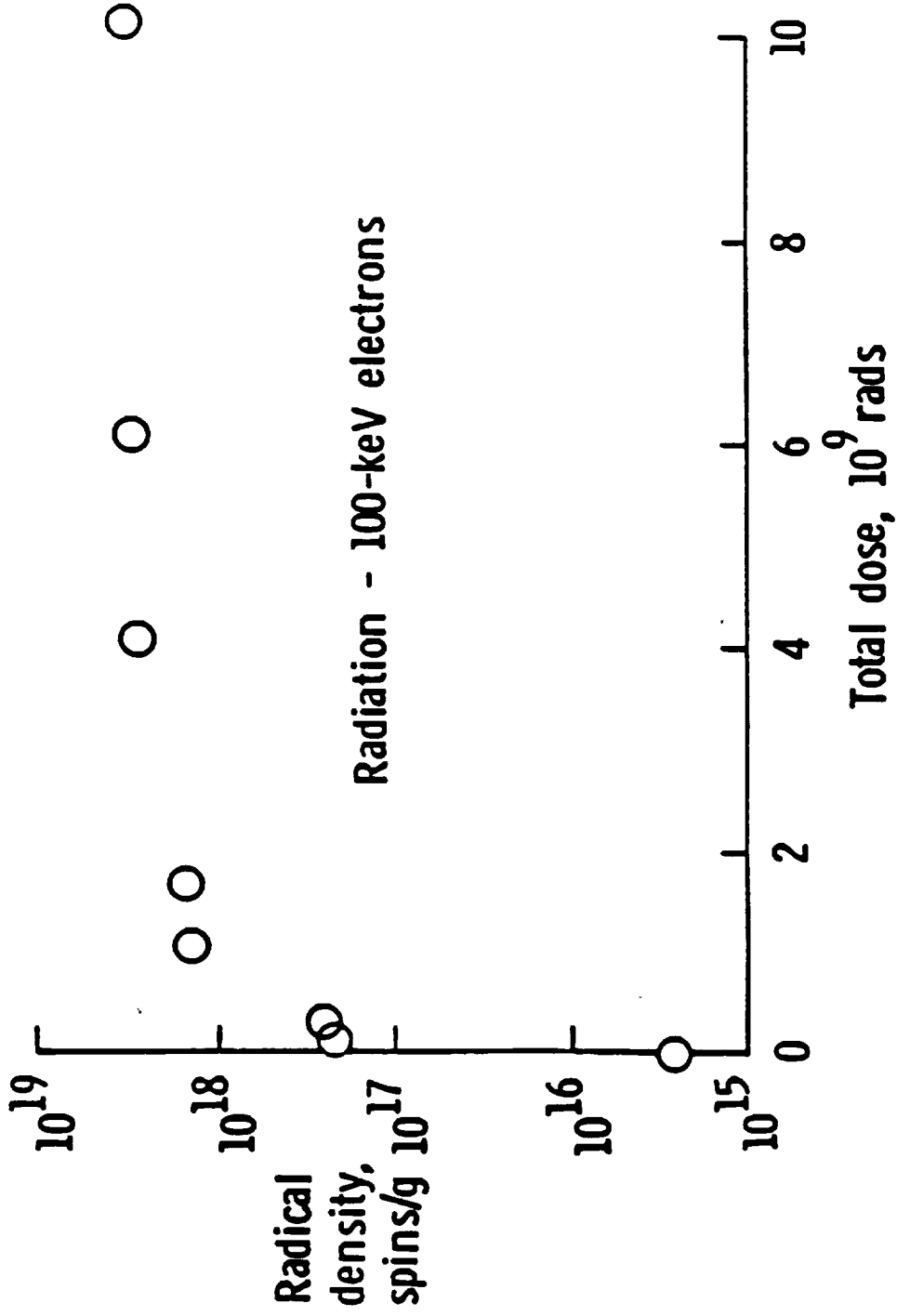
Figure 20.- EPR radical density in Ultem, 3 minutes after exposure for various total doses, dose rate = 1 X 10^9 rads/hr.
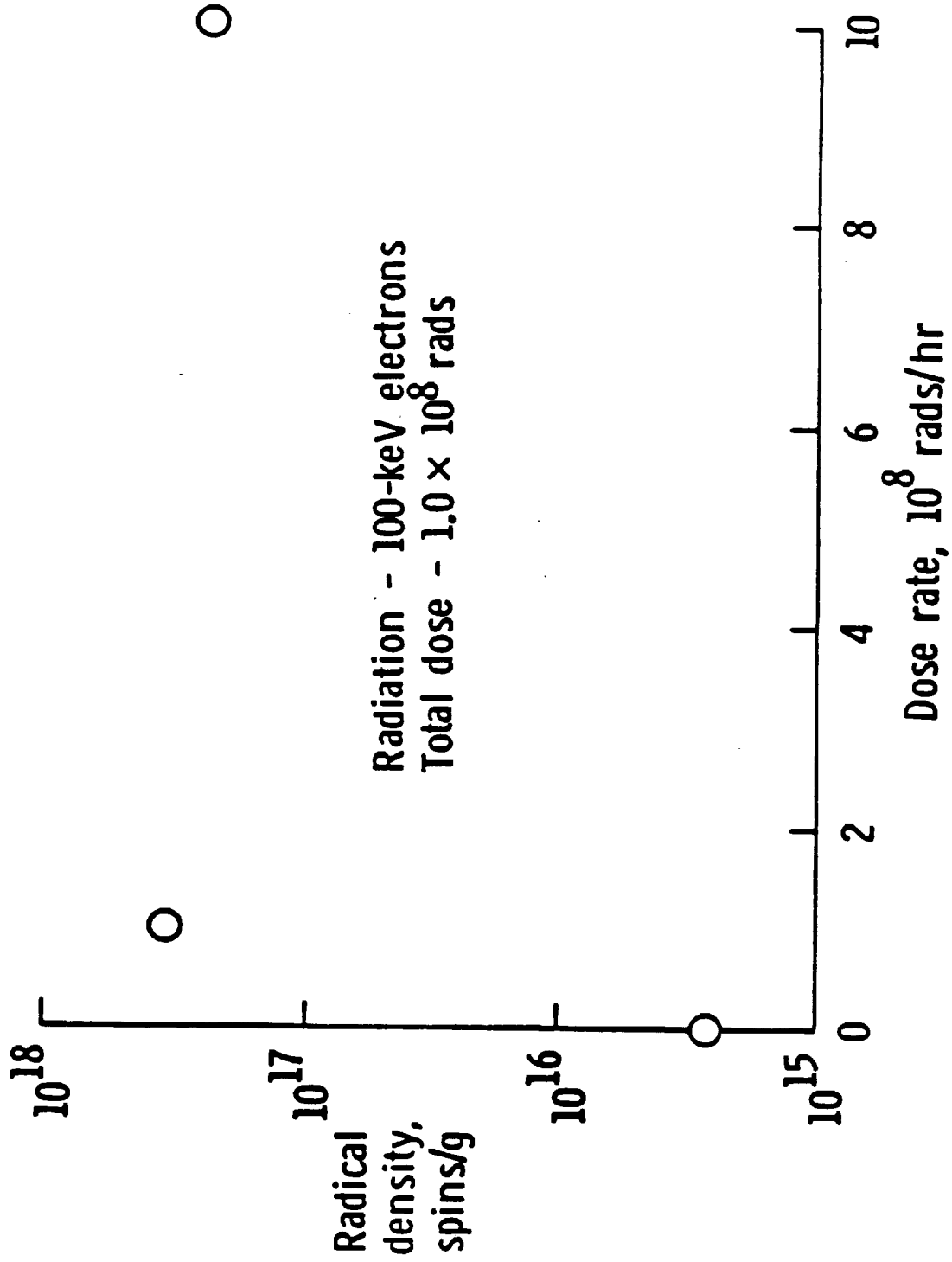
Figure 21.- EPR radical density in Ultem, 3 minutes after exposure for two different dose rates.

The plot shows Radical density, spins/g (vertical axis, from 10^{15} to 10^{18}) versus Dose rate, 10^8 rads/hr (horizontal axis, from 0 to 10).

Radiation - 100-keV electrons
Total dose - 1.0×10^8 rads

RADICAL DENSITY.

10^{16} spins/g

20.0

15.0

10.0

5.0

0.0

0

5

10

15

CeF_3 CONTENT, percent
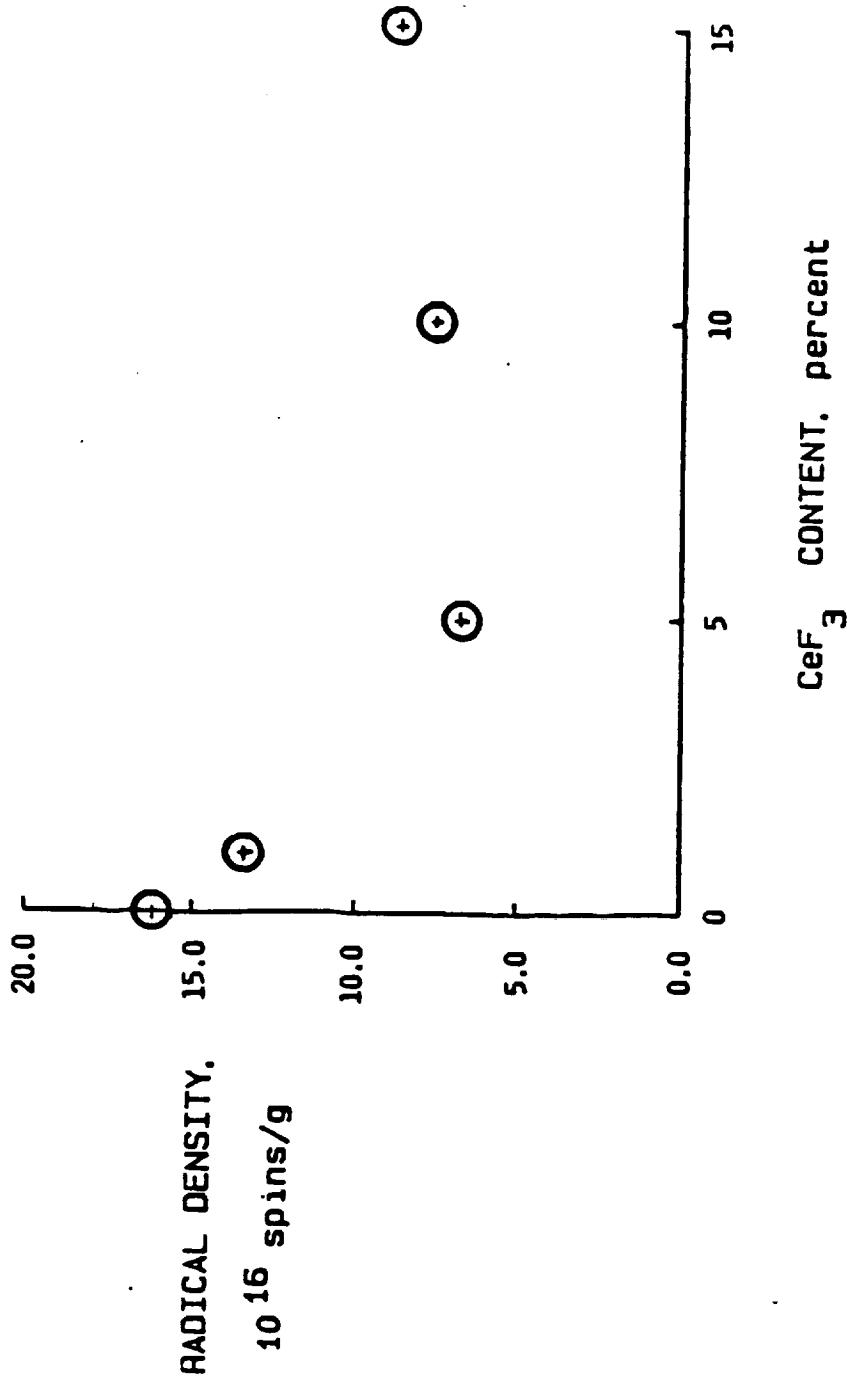
Figure 22.- EPR organic radical densities in metal-doped Ultem after exposure to 100-keV electron radiation, total dose = 1 X 10^9 rads and dose rate = 1 X 10^9 rads/hr.

APPENDIX AA

RADIO-FREQUENCY ELECTRICAL PROPERTIES OF
SOME NEAT AND METAL-DOPED POLYIMIDES

Edward R. Long, Jr. and Sheila Ann T. Long
National Aeronautics and Space Administration
Langley Research Center
Hampton, Virginia 23665-5225

and

Heidi R. Ries and Wynford L. Harries
Department of Physics
Old Dominion University
Norfolk, Virginia 23508-0369

ABSTRACT

As the size and complexity of aerospace systems increase, the uses of polymers are also expected to increase. Polyimides constitute one promising generic class of polymeric materials. They retain good mechanical and physical properties at higher temperatures and absorb less moisture than do the epoxies, which are the polymers most frequently used in present aerospace systems. The properties of these polyimide materials are, therefore, of considerable interest to the aerospace community. Of particular importance are the electrical properties because these properties relate to both electrical and structural applications.

This paper presents data on the radio-frequency electrical properties of two thermoset polyimides, pyromellitic dianhydride - oxydianiline (PMDA-ODA) and benzophenone tetracarboxylic acid dianhydride - oxydianiline (BTDA-ODA), and one thermoplastic, a polyetherimide. Two commercial grades of the PMDA-ODA were investigated and neat and metal-doped forms of the BTDA-ODA were studied.

Capacitance, inductance, and impedance properties are reported for a frequency range from 10 kilohertz to 10 megahertz. In addition, the effects of temperature on some of these properties are reported for 10 and 100 kilohertz.

The research-grade of the PMDA-ODA displayed approximately 20 percent higher capacitance and 20 percent lower inductance and impedance than did the stock-grade at room temperature. The thermal variation of the dissipations of these two grades indicated that the second-order glass-transition temperature was 388 $^{\circ}$C for the research-grade and 400 $^{\circ}$C for the stock-grade. The room temperature electrical properties for the BTDA-ODA were similar to those for the PMDA-ODA. The second-order thermal transition for the BTDA-ODA occurred at 319 $^{\circ}$C. The polyetherimide displayed a much lower value for capacitance, a much higher value for inductance, and a similar value for impedance, compared with the PMDA-ODA. The second-order thermal transition for the polyetherimide occurred at 213 $^{\circ}$C.

The volume resistivity was approximately 10^{17} ohm-cm for all four neat polymers. This is a typical value for the volume resistivity of dielectrics; it represents a potential problem for charge buildup in a charged-particle environment, such as that which exists for geosynchronous orbit applications. Metal doping is one method proposed for preventing charge buildup. The effects of metal doping on the values of the radio-frequency electrical parameters were studied for the BTDA-ODA doped with three different metals. Silver and tin were studied for one concentration each, and palladium was studied for two concentrations. Only palladium significantly reduced the resistivity, and then only for the high-concentration formulation (1:2 mole ratio of metal complex to polymer). The dissipation for the high-concentration palladium-doped BTDA-ODA was an order of magnitude larger than that for the neat BTDA-ODA, from 10 to 100 kilohertz. The other dopants did not alter the dissipation. The capacitance values for the silver-doped and the low-concentration palladium-doped BTDA-ODA were lower than that for the neat BTDA-ODA at all frequencies. None of the dopants affected the impedance and inductance properties.

APPENDIX B

PHYSICS 'A'

FIRST PLACE

ELECTRON-RADIATION INDUCED MOLECULAR CHANGES
IN A POLYETHERIMIDE FILM

Stephanie L. Gray
4 Alexander Drive, Hampton, Virginia 23664
Phoebus High School, Hampton, Virginia 23663

Introduction: Ultem polyetherimide is a plastic, or polymer, manufactured by General Electric.[1] It is currently being studied at the National Aeronautics and Space Administration (NASA) Langley Research Center in Hampton, Virginia. The purpose of this research is to determine Ultem's durability to the space environment. The molecular changes Ultem undergoes as a result of exposure to radiation will be determining factors of the future use of Ultem in Space.

Polymers are chemical compounds linked together in chains consisting of repeating structural units; cellulose, proteins, natural and synthetic rubbers, and plastics all consist of polymer chains. The Ultem polyetherimide chain is made up of imide rings, benzene rings (C_6H_6), and methyl (CH_3) groups (fig.1).[2] The advantages of using Ultem in a composite form are low thermal expansion, strength, and stiffness. However, one of the disadvantages may be the possible degradation of the material after irradiation.

Energy is a means of breaking molecular bonds; and because radiation is a form of energy, it also can break bonds. The breaking of molecular bonds results in the presence of radicals, which have unpaired electrons. In Ultem, four different kinds of radicals are formed as a result of irradiation. They have been identified in earlier research as the phenoxyl, gem-dimethyl, carbonyl, and cyclohexadienyl radicals (figs. 2-6).[3] Each radical may have a different decay behavior. Radical decay occurs when the unpaired electrons combine with other unpaired electrons. One of the more predominant forms of radical decay in polymers is crosslinking. Crosslinking is the formation of new bonds, or links, between adjacent polymer chains. This experiment was conducted in order to examine the decay behavior of Ultem and the phenoxyl radical.

Purpose: I became interested in the study of radiation effects as a result of the opportunity I was given from NASA last summer. I was employed in the 1984 Summer High School Apprenticeship Research Program (SHARP). I worked at the NASA Langley Research Center for eight weeks as a research assistant with Mrs. Sheila Ann T. Long, a physicist at the center. During my eight-week stay at NASA, I was given a project, the effects of electron beam radiation on the molecular structure of Ultem. The program was soon over; however, my interest in the subject never dies. As a result, I was offered a position at NASA as a

research assistant with Mrs. Long for a year. A grant was given to me from NASA through the Old Dominion University Physics Department. This opportunity has enabled me to further my research on Ultem for the benefit of NASA and myself. My research on Ultem is far from complete; however, the data and research presented in this paper will explain the decay behavior of Ultem and one of its radicals after exposure to electron beam radiation.

Materials: The materials and equipment used in this experiment were supplied by NASA. The complexity of the equipment used ranges from a simple cutting bar to a state-of-the-art Electron Paramagnetic Resonance (EPR) Spectroscopy System. The materials and equipment necessary for this experiment were: Ultem film specimens (.6" x .081"), freon, acetone, .110" diameter test tubes, cutting bars, a specimen mount, an electron gun, Electron Paramagnetic Resonance Spectroscopy System, a Hewlett Packard 9836 computer and software, liquid nitrogen, dry nitrogen, a vacuum pump, and an acetylene blow torch.

The Ultem specimen mount used in the exposure chamber was a new mount I designed last summer (fig. 7). I was given the task of designing a specimen mount that would increase the efficiency of the experiment. The mount I designed made the process of removing the specimens from the mount and placing them into the test tubes quicker and easier. This decrease in time after the exposure led to an increase in the accuracy of the EPR data.

The radiation source used in this experiment was an electron gun. The electron gun was a modified transmission electron microscope. The changes made in the electron microscope were the removal of the objective lens so that the electron beam current would be increased in the exposure chamber, the addition of a Faraday cup which monitored the current of the electron beam, and a modification in the lead viewing window that would allow one to remove the specimens quickly and easily.[4] The electron gun operated at 100-keV electrons with a dose of 2.5×10^8 rads. Dr. Edward R. Long, Jr., a materials engineer at NASA, made the electron microscope modifications and ran the radiation exposure.

Electron Paramagnetic Resonance (EPR) is defined as the absorption of electromagnetic waves by paramagnetic substances in a constant magnetic field. EPR is used to reveal and measure the presence of unpaired electrons. The EPR system mainly consists of a power source, which is a microwave bridge, and a magnet. The test tube is placed in the specimen cavity, which is situated between the poles of the magnet. An unpaired electron spins about its own axis creating a magnetic moment, or field. When this electron is placed in the cavity, the electron begins to feel the magnetic force pulling on it. The electron then tries to align itself with the magnetic field; the precession about the field is very similar to the movement of a spinning top. When the microwave frequency is equal to the precessional frequency of the unpaired electron, resonance occurs and a first derivative curve is produced as the EPR signal. The signal is shown on the screen of the Hewlett Packard 9836 computer. The Hewlett Packard 9836 and the EPR system work together using the software written in Hewlett Packard Language (HPL).

Procedure: The preparation of the Ultem specimens was the first and most important step in the experiment. Any kind of impurity could alter the results of the experiment. Thus, it was important to be as clean and accurate as possible. Clean gloves were worn when the specimens were being handled.

The specimens were first cut to specific widths and lengths using the cutting boards. The films were cut to a 0.081" width and a 0.6" length with a 0.003" thickness. The specimens were then checked and rechecked for any impurities or knicks along the edges, and to make sure that the length was exact and the width constant throughout each specimen. The film specimens were cleaned with acetone first and then freon. The next step was to mount the specimens onto the cleaned mount with cleaned tweezers. The specimens were made to lie flat so that the radiation absorption would remain constant throughout the material.

After the specimens were prepared, they were placed in the exposure chamber for a period of twenty-four hours before the radiation exposure. During this time, a vacuum was pulled to at least 10^{-4} torr inside the chamber; the vacuum was pulled in order to have conditions similar to those of space. After, the vacuum was pulled, the radiation exposure was run. The exposure lasted approximately fifteen minutes and produced a total dose of 2.5×10^8 rads.

Speed was an important factor in the next step of the experiment. The specimens had to be removed from the mount, placed in the test tubes (four films per tube), and emersed in liquid nitrogen all in a matter of minutes. This step was a three-man operation. The time between the exposure and the emersion into liquid nitrogen was three minutes. The specimens were placed in liquid nitrogen in order to freeze their molecular activity; the temperature of the liquid nitrogen was -196°C.

The one specimen used for decay studies had a vacuum pulled on the test tube. This was done while the test tube was still in liquid nitrogen. The vacuum was pulled to 10^{-8} torr. After the vacuum was pulled, the test tube was sealed off at the open end with an acetylene blow torch; the sealing of one end was also done while the specimen was in liquid nitrogen. Keeping the specimen at liquid nitrogen temperature was necessary in order to get an accurate account of the radicals present in Ultem.

The specimen was placed in the cavity, which was kept between -186°C and -188°C. Dry nitrogen gas was run through a hose into the liquid nitrogen dewar where the gas was cooled to near liquid nitrogen temperature. The dry nitrogen then continued through the hose to the specimen cavity; the cooled, dry nitrogen gas kept the specimen cavity also near liquid nitrogen temperature. Liquid nitrogen could not be pumped directly into the cavity because it would form ice inside the cavity which would interfere with the signal received from the material. The EPR system was then ready to run.

After a signal was found, it was recorded onto the EPR 1024 data points disk. The first specimen stored on file was Ultem #1 – 3 minutes at room temperature (fig. 8). The specimen was placed back into the liquid nitrogen. The second EPR run was done on Ultem #1 – 13 minutes at room temperature. The specimen was removed from the dewar and thawed to room temperature. Once the specimen was thought to have reached room temperature, it was left out of the dewar for a set length of time to decay. The specimen was then placed back into the dewar, and later the specimen cavity for another EPR run. There were fourteen decay specimen observations and one control. The control was non-irradiated Ultem.

Results: Certain characteristics of the EPR first derivative curves are pertinent in describing the decay behavior of the specimen. The g-value, which was found by using the Epr software, is used to identify the radical. The g-value is where the derivative curve physically crosses the x-axis and is found by using the formula

$$g = \frac{h\nu_o}{BH},$$

where g is the g-value, h is Planck's constant (6.2×10^{-34} joule-sec), ν_o is the microwave frequency, B is Bohr's magneton ($.9273 \times 10^{-23}$ joule/(weber/m²)), and H is the magnetic field.[5]

The following g-values were generated by the computer for the Ultem decay specimen:

3 min = 2.007043	183 min = 2.007521
13 min = 2.007194	243 min = 2.007652
23 min = *	363 min = 2.007543
33 min = 2.007652	483 min = 2.007652
48 min = 2.007717	603 min = 2.007826
63 min = 2.007782	725 min = 2.008392
130 min = 2.007521	978 min = 2.009112

control = 2.006629

*A g-value was not found for Ultem #1 - 23 minutes at room temperature because there was a malfunction in the computer.

The radical densities were also calculated. The radical density is the number of spins, or radicals, per gram of material. In order to find the radical density, the values of the second integrals and spin concentrations, which is the number of spins per material specimens, had to be generated. The values of the second integrals of the EPR curves were generated by the Hewlett Packard computer using the EPR software. The spin concentrations were calculated using the formula

$$\text{spin concentration (unknown)} = \frac{\text{second integral (unknown)}}{\text{second integral (standard)}}$$

$$\times \text{ spin concentration (standard)} \times \frac{\text{gain (standard)}}{\text{gain (unknown)}} \times \frac{\sqrt{\text{power (standard)}}}{\sqrt{\text{power (unknown)}}}.$$ [6]

The standard used in the experiment was strong pitch. The power used for all EPR runs was 12.5 milliwatts (mW). The gain used on strong pitch was 1.25 x 10², and 2.5 x 10³ for all the Ultem specimens. The second integrals, spin concentrations, and radical densities (spin concentration/mass) were calculated for the control and each observation of the decay experiment. The same process was done for the phenoxyl radical as well. Using the software, it was possible to isolate the phenoxyl radical on the first derivative curve and to find the values for the second integrals, spin concentrations, and radical densities for all fourteen observations of the phenoxyl decay.

Decay plots were made by graphing the radical density as a function of the log of the time in minutes (figs. 9 and 10). Statistical analyses of these plots were made by using a program written in BASIC. The program fit a line to the decay plot, printed out the residuals between the observed and predicted y-values, and found an equation for the decay line (figs. 11-16). The equation of the radical decay of Ultem is

$$y = (-.86122) (\log_{10} t) + 3.11060,$$

where t is the time in minutes and where y is the radical density in units of 10^{17} spins/g. The equation of the radical decay of the phenoxyl radical is

$$y = (-3.01738)(\log_{10} t) + 9.69118,$$

where t is the time in minutes and where y is the radical density in units of 10^{16} spins/g.

Conclusions: The data produced through experimentation shows that Ultem and the phenoxyl radical both decay linearly as a result of irradiation. One explanation for this decay is the possible existence of crosslinking. A darkening in color of the specimen is a determining factor of the existence of crosslinking. The Ultem films changed from a clear, pale yellow to a clear, orange-yellow. The darkening in color is caused by an increase in the molecular weight of the polymer, which is in turn caused by crosslinking. Solubility is also a factor in determining whether a substance has undergone massive crosslinking. In previous research conducted by Mrs. Sheila Ann T. Long, solubility experiments were conducted on Ultem. The experiment showed that non-irradiated Ultem dissolved quickly in the solvent, while the irradiated specimen did not dissolve at all. The decrease in solubility supports the crosslinking theory of Ultem. One possible example of crosslinking can be seen between the phenoxyl and gem-dimethyl radicals (fig 17). Because of the results presented, it is possible to conclude that Ultem polyetherimide should not be used for long-term space missions without an extensive study of its durability to space-like conditions.

ENDNOTES

[1] Edward R. Long Jr., and Sheila Ann T. Long, "Effects of Intermediate-Energy Electrons on Mechanical and Molecular Properties of a Polyetherimide," EEE Transactions on Nuclear Science, Dec. 1984, p. 1293.

[2] Edward R. Long Jr., and Sheila Ann T. Long, Spectroscopic Analysis of Radiation-Generated Changes in Tensile Properties of a Polyetherimide Film, (NASA TP), p. 8.

[3] Edward R. Long Jr., and Sheila Ann T. Long, p. 18.

[4] Edward R. Long Jr., and Sheila Ann T. Long, "Effects of Intermediate-Energy Electrons on Mechanical and Molecular Properties of a Polyetherimide," EEE Transactions on Nuclear Science, Dec. 1984, p. 1293.

[5] Raymond S. Alger, Electron Paramagnetic Resonance: Techniques and Applications, (New York: Interscience Publishers, 1968), p. 13.

[6]Varian Associates, Inc.

BIBLIOGRAPHY

1. Alger, Raymond S. Electron Paramagnetic Resonance: Techniques and Applications. New York: Interscience Publishers, 1968.

2. Bowmer, Trever N., and James H. O'Donnell. "Post-Irradiation Thermal Degradation of Poly (Olefin-Sulfones)," Journal of Polymer Science, 1981, pp. 71-74.

3. Bowmer, T. N., S. Y. Ho, J. H. O'Donnell, G. S. Park, and M. Saleem. "Characterizations of the Short-Chain Branches in Poly(Vinyl Chlorides) by -Irradiation of the Reduced Polymers," European Polymer Journal, 1982, pp. 61-66.

4. Box, Harold C. Radiation Effects: ESR and ENDOR Analysis. New York: Academic Press, 1977.

5. Davidson, Arthur W., Harry H. Sisler, and Calvin A. VanderWerf. College Chemistry: A Systematic Approach. New York: The Macmillan Company, 1961.

6. DePuy, Charles H., and Kenneth L. Rinehart Jr. Introduction to Organic Chemistry. New York: John Wiley and Sons, Inc., 1967.

7. Kent, George Michael. X-Ray and ESR Characterizations of the Effects of High Energy Radiation on Graphite Fiber Reinforced Composite Materials. North Carolina: North Carolina State University (thesis paper), 1982.

8. Long, Edward R., Jr., and Sheila Ann T. Long. Spectroscopic Analysis of Radiation-Generated Changes in Tensile Properties of a Polyetherimide Film. NASA TP

9. Long, Edward R., Jr., and Sheila Ann T. Long. "Effects of Intermediate-Energy Electrons on Mechanical and Molecular Properties of a Polyetherimide," IEEE Transaction on Nuclear Science, Dec. 1984, pp. 1293-98.

10. Nebergall, William H., and Frederic C. Schmidt. General Chemistry. D. C. Health and Company, 1959.

11. O'Donnell, James H., and P. J. Pomery. "ESR Studies of Degradation in Polymers. I. -Irradiation of Poly (Styrene-CO-Methyl Methacrylate) at $77^{\circ}K$," Polymer Science, 1967, pp. 269-278.

12. O'Donnell, James H., and David F. Sangster. Principles of Radiation Chemistry. New York: American Elsevier Publishing Company, Inc., 1970.

13. Poole, Charles P., Jr. Electron Spin Resonance: A Comprehensive Feature on Experimental Techniques. New York: John Wiley and Sons, 1983.

14. Rabek, J. F., and B. Ranby. ESR Spectroscopy in Polymer Research. Germany: Springer-Verlag Berline Heidelberg, 1977.

15. Shelnitz, P., trans. EPR of Free Radicals in Radiation Chemistry. New York:

John Wiley and Sons, 1974.

16. Wilmhurst, T. H. ESR Spectrometers. New York: Plenum Press, 1967.

17. E-Line Century Series EPR: Spectrometer System Operator's Manual.
    California: Varian Instrument Division.

ACKNOWLEDGEMENTS

Ultem

Time	Second integral	Spin concentration	Radical density
(min)		$\times 10^{15}$ spins	$\times 10^{17}$ spins/g
3	162858.46	3.8987	2.7761
13	137047.78	3.1024	2.2091
23	109307.92	2.6167	1.8632
33	106127.54	2.4294	1.7298
48	95692.58	2.1905	1.5597
63	90693.61	2.0761	1.4783
130	82360.55	1.8854	1.3425
183	75605.80	1.7307	1.2323
243	67499.29	1.5452	1.1003
363	57936.97	1.3263	.94439
483	52736.63	1.2072	.85958
603	44784.26	1.0252	.72999
725	40218.25	.92066	.65555
978	27468.80	.62880	.44774
Control	4326.69	.099044	.029062

Phenoxyl

Time	Second integral	Spin concentration	Radical density
(min)		$\times 10^{14}$ spins	$\times 10^{16}$ spins/g
3	57959.91	13.268	9.4474
13	40227.05	9.2086	6.5569
23	30029.86	6.8743	4.8948
33	27739.97	6.3501	4.5216
48	24620.00	5.6359	4.0130
63	22317.58	5.1088	3.6377
130	19358.50	4.4314	3.1554
183	17228.10	3.9438	2.8082
243	15400.16	3.5253	2.5102
363	12938.20	2.9617	2.1089
483	11700.61	2.6784	1.9072
603	9928.34	2.2727	1.6183
725	8278.56	1.8951	1.3494
978	5457.89	1.2494	.88963

1. ULTEM POLYETHERIMIDE

n
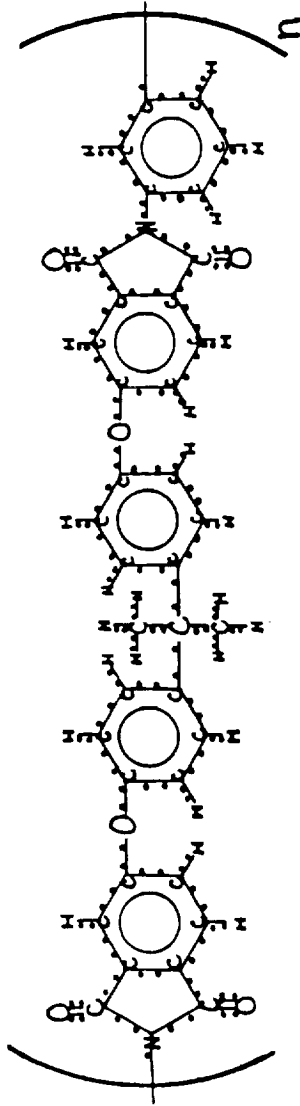
2. PHENOXYL RADICAL
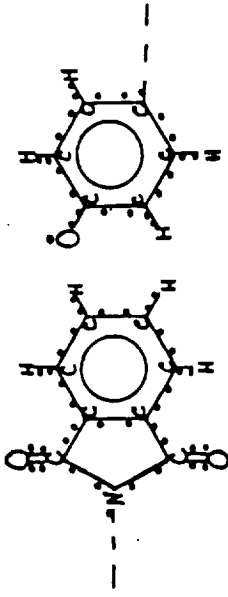
3. GEM-DIMETHYL RADICAL
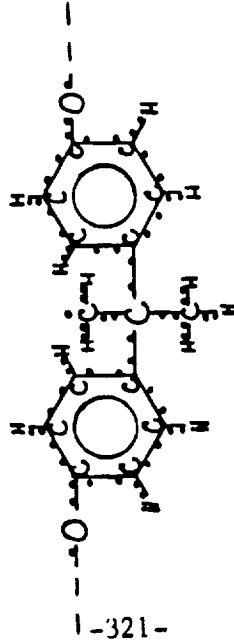
4. CARBONYL RADICAL

5. CYCLOHEXADIENYL RADICAL

6.

Dose - 6.0 x 10^9 rad
Time - 4 min after exposure

g = 2.0067

160 G
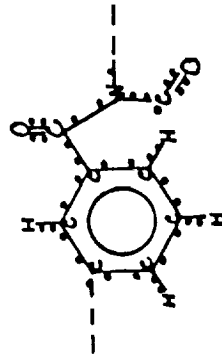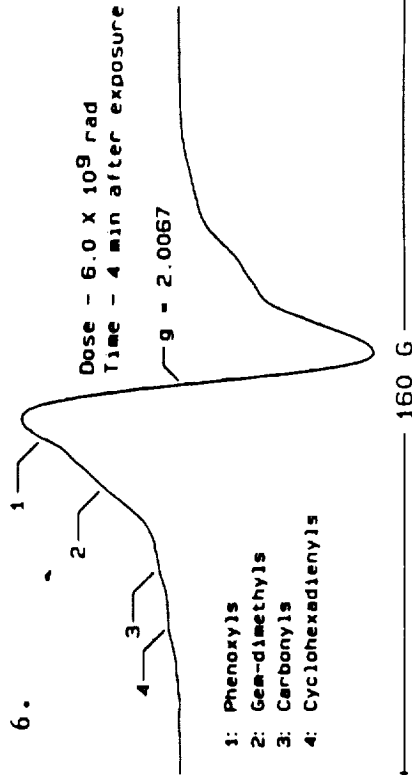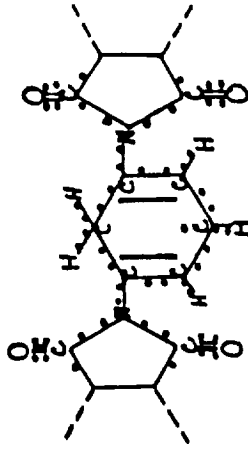
1: Phenoxyls
2: Gem-dimethyls
3: Carbonyls
4: Cyclohexadienyls

7. SPECIMEN MOUNT FOR RADIATION EXPOSURES
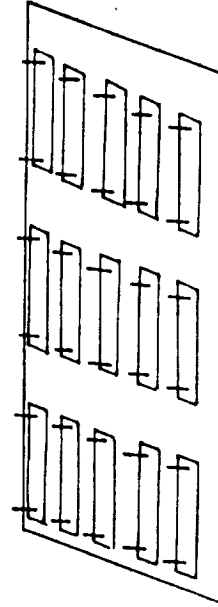
FIGURES

-321-

8. RADICAL DECAY AFTER RADIATION EXPOSURE
Ultem Polyetherimide

Radiation - 100-keV electrons
Total dose - 2.5×10^8 rads
Decay - at 21°C

A: 3 minutes after exposure
B: 16 hours 18 minutes after exposure

g = 2.0070

g = 2.0091

C = A-B

160 gauss

9. RADICAL DECAY AFTER RADIATION EXPOSURE
Ultem Polyetherimide

Radiation - 100-keV electrons
Total dose - 2.5×10^8 rads

Radical density, 10^{17} spins/g

Time at 21°C, min
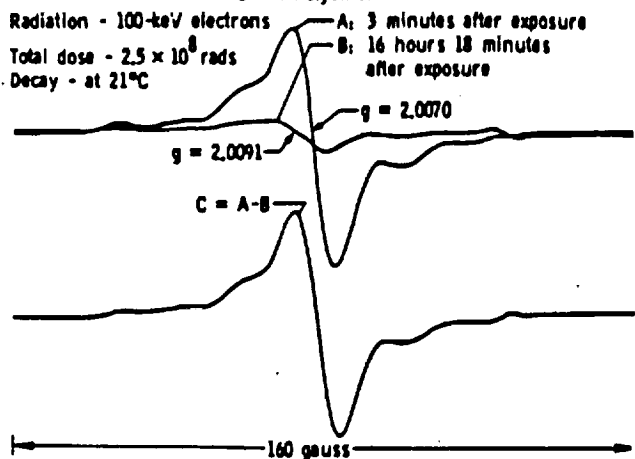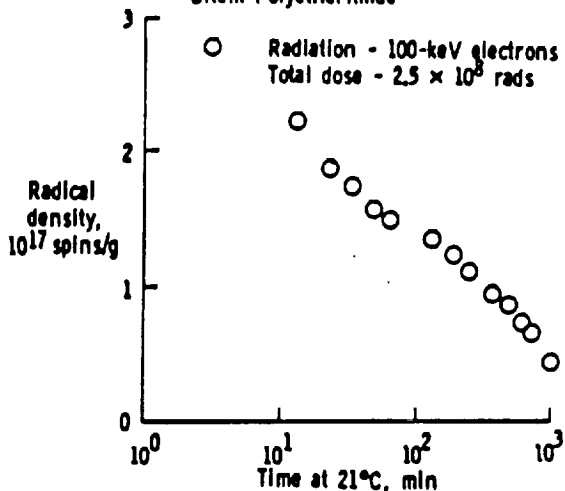
0. PHENOXYL DECAY AFTER RADIATION EXPOSURE
Ultem polyetherimide

Radiation - 100-keV electrons
Total dose - 2.5×10^8 rads

Radical density, 10^{16} spins/g

Time at 21°C, min
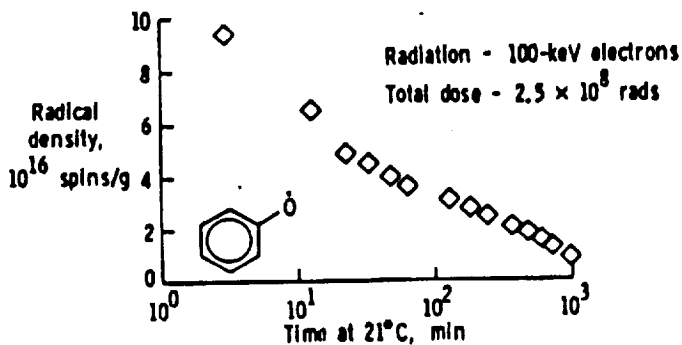
11.

POLYNOMIAL REGRESSION ON DATA SET:

DECAY RATE OF ULTEM

ANALYSIS OF VARIANCE TABLE

SOURCE	DF	SUM OF SQUARES	MEAN SQUARE
TOTAL	13	5.40185	
REGRESSION	1	5.34149	5.34149
X^1	1	5.34149	5.34149
RESIDUAL	12	.06036	.00503

VARIABLE	REGRESSION COEFFICIENTS		STANDARD ERROR
	STD FORMAT	E FORMAT	REG COEFFICIENT
CONSTANT	3.11060	3.11059564098E+01	.05726
X^1	.86122	-.86132325630E+00	.02643

		95 % CONFIDENCE INTERVAL	
	COEFFICIENT	LOWER LIMIT	UPPER LIMIT
CONSTANT	3.11060	2.98574	3.23525
X^1	.86122	.91002	.80363

12. DECAY RATE OF ULTEM

RAD. DENS. $(10^{17}$ spins/g)

3.0
2.5
2.0
1.5
1.0
.5

LOG(T) (M)
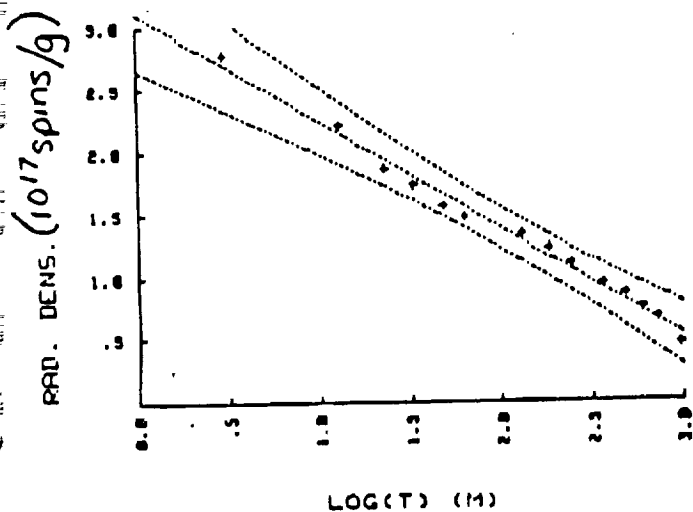
13. TABLE OF RESIDUALS

OBS	OBSERVED Y	PREDICTED Y	RESIDUAL
1	2.77610	2.69979	.07631
2	2.30918	2.15117	.15771
3	1.86330	1.93761	.07441
4	1.72700	1.80326	.07346
5	1.55970	1.66208	.10310
6	1.47630	1.54120	.06496
7	1.34250	1.20997	.05253
8	1.23230	1.16251	.06979
9	1.10030	1.05572	.04458
10	.94432	.90586	.03853
11	.85958	.79907	.06051
12	.72999	.71640	.01359
13	.65555	.64750	.00805
14	.44774	.53054	.08708

Durbin-Watson Statistic .834486040337

15. DECAY RATE OF THE PHENOXYL RADICAL

RAD. DENS. $(10^{16}$ Spins/g$)$

LOG(T) (M)
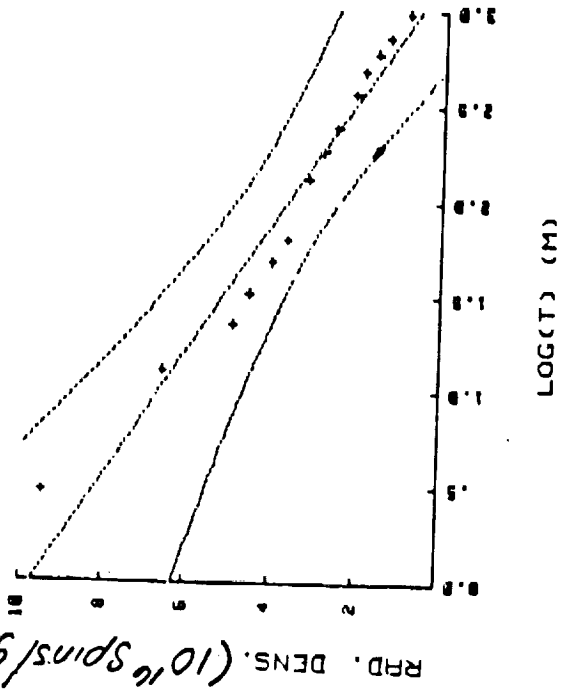
14. POLYNOMIAL REGRESSION ON DATA SET.

DECAY RATE OF THE PHENOXYL RADICAL

ANALYSIS OF VARIANCE TABLE

16. TABLE OF RESIDUALS

17. CROSSLINKING BETWEEN TWO MOLECULAR CHAINS
Gem-Dimethyl and Phenoxyl Linkage

FIGURES

-323-

APPENDIX C

RADIO-FREQUENCY ELECTRICAL PROPERTIES OF SOME
NEAT AND METAL-DOPED POLYIMIDES

Edward R. Long, Jr., and Sheila Ann T. Long
National Aeronautics and Space Administration
Langley Research Center
Hampton, VA 23665-5225

and

Heidi R. Ries and Wynford L. Harries
Department of Physics
Old Dominion University
Norfolk, VA 23508-0369

ABSTRACT - Radio-frequency electrical properties of films of two polyimides (Kapton® and BTDA-ODA), one polyetherimide (Ultem®), and one polyethylene terephthalate (Mylar®) have been investigated at room temperature for the frequency range from 10 KHz to 1 MHz. The electrical properties were the dissipation, capacitance, inductance, and impedance. One of the polyimides was studied for two grades of production. The other polyimide was studied in its neat (no additives) form and also with metal dopants. The polyetherimide was studied for two thicknesses. In addition to the room-temperature studies, these materials were investigated at elevated temperatures, to above each polymer's glass transition temperature.

INTRODUCTION

Polymeric materials are increasingly used in aerospace systems for a wide variety of structural and electrical applications. The electrical properties of these polymers are important for both applications.

A recent publication [1] has discussed the electrical conductivities of some of the polymers that are currently used in space. Among the polymers discussed were the polyimide Kapton and the polyethylene terephthalate Mylar. But, as recently cited in a trade journal [2], there are advanced polymers, primarily thermoplastics, which are candidates for a much wider range of applications because of their processability and improved toughness. Among these are the polyetherimide Ultem. Both reports [1,2] discussed altering the electrical conductivities of polymers by doping them with impurities.

In this paper we report the room-temperature alternating-current (ac) electrical properties - dissipation, capacitance, inductance, and impedance - of several polymers for frequencies from 10 KHz to 1 MHz. The polyimides Kapton and neat BTDA-ODA (benzophenone tetracarboxylic acid dianhydride - oxydianiline) and the polyethylene terephthalate Mylar were selected to represent polymers that are used currently. BTDA-ODA was also studied with metal dopants. The polyetherimide Ultem was selected to represent a new, advanced polymer. The dissipations of these polymers at 10 KHz were investigated at elevated temperatures.

MATERIALS

Ultem, a polyetherimide manufactured by the General Electric Company*, was studied for two thicknesses, 71 microns (nominally 3 mils) and 538 microns (nominally 20 mils). The 71-micron thickness was studied for two different production batches, both

from the same supplier. One batch of film had a shiny surface that contained micron-size dimples, while the film from the other batch had a frosted surface and no dimples.

The Kapton, a polyimide, and the Mylar, a polyethylene terephthalate, were manufactured by the E. I. du Pont de Nemours and Company, Inc. The Kapton (H film) was investigated for two grades, a stock grade and a research grade. Both grades were 71 microns thick. The Mylar was 269 microns (nominally 10 mils) thick and was a stock grade.

The BTDA-p,p'-ODA (benzophenone tetracarboxylic acid dianhydride - oxydianiline) was fabricated at the NASA Langley Research Center and was approximately 25 microns (nominally 1 mil) thick. The dopants for the BTDA-p,p'-ODA were salts of tin, silver, and palladium. The mole-ratios of the tin salt ($SnCl_2 \cdot 2H_2O$) and the silver salt ($AgNO_3$) to the BTDA-ODA were both 1 to 4, [3]. The palladium salt (H_2PdCl_4) was used at a high mole-ratio of 1 to 2 and also at a low mole-ratio of 1 to 17, [4].

EXPERIMENTAL ARRANGEMENT

The experimental arrangement is shown in figure 1. The specimen of polymer film was placed between 5.0-cm diameter aluminum electrodes. This capacitor-like configuration rested between glass disks that provided flat surfaces. The stack was pressed together by a 669-g brass weight. The top disk was twice as thick as the bottom disk, so that a thermocouple at the midpoint of the top disk would be nearly at the same temperature as the capacitor. The entire stack rested on a low-heat capacity base and was placed in a muffle furnace. The measurements were computer controlled.
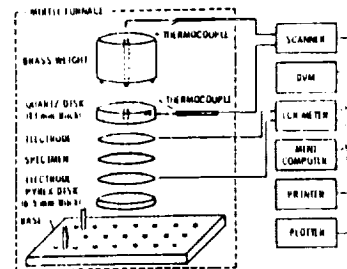
Figure 1.- Experimental arrangement.

ROOM-TEMPERATURE PROPERTIES

The room-temperature electrical properties of the polymers at three frequencies are shown in table 1. No corrections have been made to the data for the specimens' thicknesses. The electrical properties of the two production batches of the 71-micron thick Ultem were nearly identical, so only the properties of the dimpled version are being reported. The electrical properties of the two grades of Kapton were also essentially the same, so only the properties of the stock grade are being included.

Table 1.- Room-temperature ac electrical properties of five polymers.

POLYMER	THICKNESS, 10^{-6} m	DISSIPATION	CAPACITANCE, 10^{-12} F	INDUCTANCE, 10^{-3} H	SERIES RESISTANCE, ohm	IMPEDANCE, 10^3 ohm
			——— 10 KHz ———			
ULTEM	71.0	0.00080	319.7	793.5	27.00	49.77
ULTEM	538.0	0.00147	91.3	778.8	260.00	174.20
KAPTON	72.9	0.00150	358.0	707.0	64.00	44.40
BTDA-ODA	23.8	0.00084	590.3	429.1	24.00	29.98
MYLAR	244.0	0.00880	188.8	518.2	867.00	95.53
			——— 100 KHz ———			
ULTEM	71.0	0.00200	319.0	7.94	9.40	4.99
ULTEM	538.0	0.00380	91.0	27.88	87.00	17.49
KAPTON	72.9	0.00320	377.0	7.09	14.10	4.46
BTDA-ODA	23.8	0.00210	588.1	4.30	5.60	2.70
MYLAR	244.0	0.01100	184.5	15.38	107.70	9.88
			——— 1000 KHz ———			
ULTEM	71.0	0.00370	320.1	0.078	1.58	0.50
ULTEM	538.0	0.00510	90.5	0.280	8.90	1.78
KAPTON	72.9	0.00560	357.8	0.071	2.46	0.44
BTDA-ODA	23.8	0.00380	594.0	0.043	0.97	0.27
MYLAR	244.0	0.01300	162.0	0.156	12.87	0.98

The values shown for the dissipation (D) are at the lower end of the range of typical values for polymeric materials [5]. In general, aromatic materials appear to have a smaller dissipation than do aliphatic materials. This may explain why the Mylar, which has more aliphatic character, had the largest dissipation for the materials in this study. The differences in the values for the dissipation suggest that materials can be tailored to obtain the desired dissipation.

The dissipation was frequency (ω) sensitive, as may be expected, since dissipation losses can be due to electronic, atomic, orientation, and/or space charge polarizations. The dissipation also followed the series-resistance-capacitance (R_sC_s) circuit expression

$$D = \omega R_s C_s. \qquad (1)$$

The inductance-capacitance-resistance (LCR) meter (figure 1) that was used for these measurements determined an equivalent-series R_sC_s-circuit representation for the material under test. Therefore, D is directly related to the capacitance and resistance values in the table through expression (1).

The capacitance did not change with frequency, because the dielectric constant of an organic solid is a constant in this frequency range [5]. An unexpected result from these data is that the capacitance did not have an inverse linear relationship to the specimen thickness. One possible explanation is that the brass weight did not sufficiently compress the stack to eliminate all air spaces. For the thinner specimens,

air spaces would significantly reduce the measured capacitance values.

The series inductance (L_s), measured in the configuration shown in figure 1, varied as

$$L_s = 1/ \omega^2 C_s. \qquad (2)$$

This relation is ordinarily associated with a resonance condition. However, no resonance exists in this case. The data fit may well be a reflection of how the LCR meter interprets the data. The capacitance was frequency independent, and the reactance of the device was the same whether it was represented as an equivalent-series inductance-resistance circuit or as an equivalent-series capacitance-resistance circuit.

To verify that resonance was not taking place, inductance measurements were also made with and without a cast rod of Ultem as the core of a coil. A comparison of the two sets of measurements indicated a near-zero contribution by the Ultem to the coil's inductance. This appears reasonable, since the Ultem's relative permeability is 1.0.

The series resistance, as noted previously, was the resistance of an equivalent R_sC_s-circuit representation of the material specimen. It is clear from the values for the series resistance and for the series capacitance that the impedance followed the expression

$$|Z| = \sqrt{R_s^2 + 1/ \omega^2 c_s^2}. \qquad (3)$$

Table 2.- Room-temperature ac electrical properties of neat and doped BTDA-p,p'-ODA.

POLYMER	THICKNESS, 10^{-6} m	DISSIPATION	CAPACITANCE, 10^{-12} F	INDUCTANCE, 10^{-3} H	SERIES RESISTANCE, ohm	IMPEDANCE, 10^3 ohm
			——— 10 KHz ———			
BTDA-ODA	23.0	0.00084	590.3	429.1	24.00	29.98
BTDA-ODA: Sn	22.8	0.00410	846.8	373.1	93.00	23.37
BTDA-ODA: Ag	35.0	0.00146	577.8	439.8	37.00	27.52
BTDA-ODA: Pd (1o)	27.7	0.00270	814.8	413.3	70.00	25.66
BTDA-ODA: Pd (hi)	19.1	0.00426	821.1	366.8	82.00	18.38
			——— 100 KHz ———			
BTDA-ODA	23.0	0.00210	588.1	4.30	5.60	2.70
BTDA-ODA: Sn	22.8	0.00300	877.8	3.74	7.10	2.35
BTDA-ODA: Ag	35.0	0.00250	578.1	4.41	8.90	2.70
BTDA-ODA: Pd (1o)	27.7	0.00720	810.9	4.15	18.00	2.60
BTDA-ODA: Pd (hi)	19.1	0.00410	810.5	3.10	8.00	1.85
			——— 1000 KHz ———			
BTDA-ODA	23.0	0.00380	594.0	0.043	0.97	0.27
BTDA-ODA: Sn	22.8	0.00430	883.5	0.037	1.00	0.23
BTDA-ODA: Ag	35.0	0.00380	578.8	0.044	1.08	0.27
BTDA-ODA: Pd (1o)	27.7	0.01500	808.8	0.042	4.03	0.26
BTDA-ODA: Pd (hi)	19.1	0.00810	825.6	0.031	1.17	0.19

The effects of the metal dopants on the room-temperature properties of the BTDA-ODA are shown in table 2. The previous discussions pertaining to the relationships of the electrical properties to each other and to the frequency also apply to the data in table 2.

All the dopants increased the BTDA-ODA's dissipation values, most significantly at the lower frequencies. The silver had the least effect. Except for the tin dopant at 10 KHz, the palladium dopant caused the larger changes. The lower mole-ratio concentration of the palladium appears to have caused the largest changes.

The capacitance, though constant with frequency, was altered by all four dopants. The tin dopant caused a fifteen-percent increase, the silver dopant caused a two-percent decrease, the low-mole palladium concentration caused a four-percent increase, and the high-mole palladium concentration caused a fourty-percent increase in capacitance. While the changes in the capacitance increased or decreased depending on the dopant, the direct-current (dc) resistivity was reduced for all four dopants. The dc electrical resistivity was measured using a computer-controlled electrometer. The tin-doped BTDA-ODA had a dc resistivity of 10^{14} ohm-cm, the silver-doped BTDA-ODA had 10^{16} ohm-cm, the low-mole palladium-doped BTDA-ODA had 10^{16} ohm-cm, and the high-mole palladium-doped BTDA-ODA had 10^{8} ohm-cm, while the resistivity of the neat BTDA-ODA was 10^{17} ohm-cm. So, there does not appear to be an immediately recognizable relationship between the capacitance and the dc resistivity. A detailed understanding of doping effects would require a more fundamental examination.

The series resistance and the impedance (table 2) both increased with the addition of the metal dopants. These changes are opposite in direction to those given for the dc resistivity in the preceding paragraph, which suggests that the series resistance and the impedance values pertain to the equivalent-series $R_s C_s$-circuit representation of the material measurement and not to free charge carriers.

ELEVATED-TEMPERATURE PROPERTIES

The glass transition temperature (T_g) of a polymer may be determined from the elevated-temperature properties of the dissipation curve, as shown in figure 2. Tangents are taken to the curve at temperatures above and below the local minimum. The point of intersection of the tangents is termed the glass transition temperature [6].
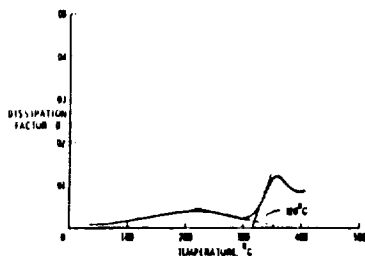
Figure 2.- Use of dissipation data to determine glass transitions.

The T_g is the temperature at which the polymer changes from a glassy, low-loss state to a rubbery, high-loss state. The values for the T_g determined in the manner just described are shown in table 3. A T_g of 286 °C has been previously reported for BTDA-ODA, [4]. However, the specimens were from a different fabrication batch of the material. This may account for the different value, 319 °C, found in this study.

The dissipation curves are shown in figure 3. Close inspection shows that their features are very similar. As previously explained, tangents for each curve above and below the first change in slope have a point of intersection that is called the T_g. The change in slope usually occurs over a relatively small temperature interval. The broader the interval, the broader the molecular-weight distribution. Changes

Table 3.- Glass transition temperatures from electrical dissipation data.

POLYMER	THICKNESS, 10^{-6} m	GLASS TRANSITION TEMPERATURE, °C
ULTEM	71.0	213
ULTEM	538.0	221
KAPTON (Research Grade)	72.9	388
KAPTON (Stock Grade)	72.4	399
BTDA-ODA	23.0	319
MYLAR	244.0	69

such as the low-temperature broad bump for the BTDA-ODA are usually associated with glass-glass transitions. This bump is too broad for the molecular-weight distribution of BTDA-ODA in order to be interpreted as its glass-rubber transition.

For Ultem, the glass transition temperatures, determined by the intersection of the tangent lines, were different for the two thicknesses. In contrast, the peak (relative maximum) that followed the change in slope occurred at the same temperature (246 °C) for both thicknesses. This peak, whose equivalent occurs in dynamic mechanical analysis data, has also been described as the T_g, [7].

The different values of the T_g, as determined by the line-intersection method, for the two Ultem thicknesses may be accounted for by the following argument. There was probably a thermal lag for the thick specimen, causing the temperature in this specimen to lag the temperature of the thermocouple. A thermal lag would be particularly evident at the onset of the glass transition, because at this temperature
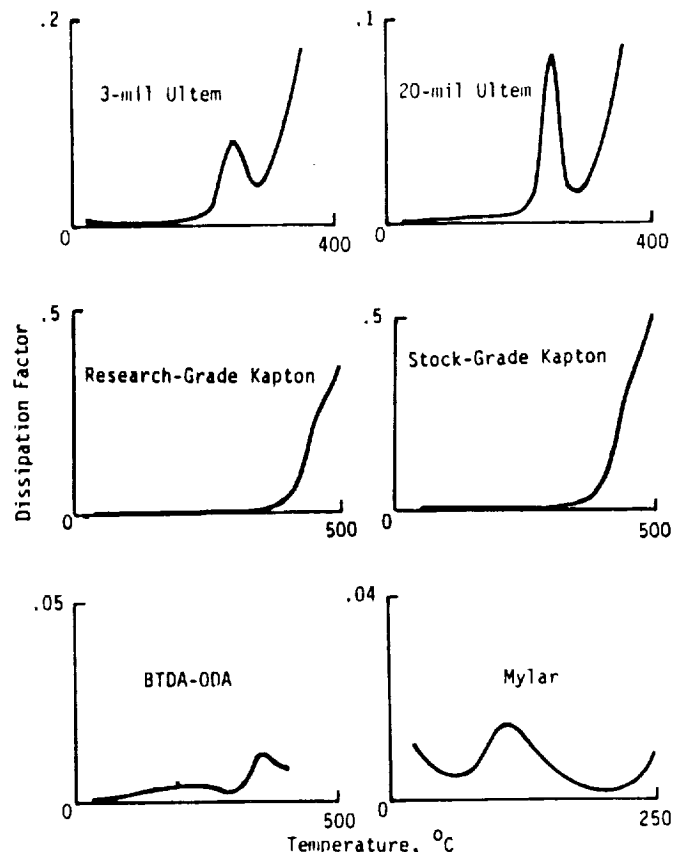
Figure 3.- Curve shapes for variation of polymers' electrical dissipations with temperature.

the heat capacity of the material begins to change. At the peak that follows the onset of the transition, the transition is essentially complete; the specimen has had time to come completely to its new heat capacity and to equilibrate in temperature throughout its mass.

The Kapton's dissipation curves indicated that there was a small difference between the stock and the research grades. The value of the T_g defined by the change in slope was 388 °C for the research grade and 399 °C for the stock grade. This T_g difference cannot be attributed to thickness, since the two grades were of the same thickness. In contrast to the Ultem, there is no peak following the change in slope. However, there is an inflection in each of the curves and, for both, this inflection occurs at 450 °C. The inflection could be easily interpreted as the equivalent of the maximum that occurred for the Ultem, with the difference that some additional change began at the maximum transition. If the positive slope of the onset of the additional change was slightly greater than the negative slope following the glass transition, then an inflection point, instead of a maximum, would occur in the curve.

The curve for the BTDA-ODA, as pointed out earlier, had a low-temperature broad bump that was caused by a glass-glass transition. For glass-glass transitions, the material remains in its glassy state, while either short segments or branches of the polymer, whose molecular weights are small compared with the polymer's molecular weight, acquire additional degrees of freedom. The broadness indicates that the segments or branches have a wide distribution of molecular weights, even though their individual molecular weights are comparatively small. The BTDA-ODA's T_g as measured by the onset was 319 °C, while the temperature at the peak that followed was 359 °C.

For Mylar, there was a general decrease in the dissipation as the onset of the transition at 69 °C was approached. This was probably part of a glass-glass transition similar to the one just discussed for the BTDA-ODA; but, since all the tests began at room temperature, the lower temperature portion of the curve was not recorded. The peak maximum transition for the Mylar was at 114 °C.

For either definition of the T_g, the useful temperature range for each of the materials is somewhat lower than the value at which the onset of the glass-rubber transition occurs. Indeed, for amorphous materials such as the ones in this report, the T_g is more properly termed as a softening temperature. For

Figure 4.- Curve shapes for polymers' capacitances.

acceptable mechanical and electrical properties, the use temperature has to be lower than either value.

The capacitance versus temperature curves for Ultem, Kapton, and Mylar are shown in figure 4. If, for a particular application such as a temperature-independent capacitor, the capacitance is required to be independent of the temperature, then Kapton and Mylar are not good selections. The capacitance of Ultem, on the other hand, appears to be constant with temperature, up to the onset of the glass transition.

CONCLUSIONS

The ac electrical properties of all the polymers in this study changed at their glass-rubber transition temperatures (T_g). Two values of the T_g were determined, one at the onset of transition and one at the peak of transition. The latter was independent of the specimen thickness and the grade-quality of the material.

The molecular glass-glass and glass-rubber transitions had a major influence on the dissipation and capacitance properties of the polymeric dielectric materials, in that they defined the maximum use temperature and the temperature dependence of the properties within the useful range. These transitions also affected the dissipation and capacitance properties differently, in that the temperature independence of one property did not assure the temperature independence of the other.

The dissipation of a polymer appeared to vary with its mixture of aliphatic and aromatic character, and therefore, these two molecular structural characteristics can probably be used, within some limits, to tailor the dissipation of a polymer.

The addition of dopant metal salts to a polymer also altered the dissipation and, in addition, the capacitance. The relationships between the effects of dopants on these two electrical properties were not immediately obvious and would require a more detailed molecular examination than the one conducted for this study.

REFERENCES

[1] Cotts, D. B.; and Reyes, Z., "New Polymeric Materials Expected to Have Superior Properties for Space-Based Uses", RADC-TR-85-129, July 1985.

[2] Friedman, M.; Leonard, L.; and Galli, F., "Materials of Tomorrow", Plastics Design Forum, Vol 11, No 1, January/February 1986.

[3] Taylor, L. T.; Carver, V. C.; Furtsch, T. A.; and St. Clair, A. K., "Incorporation of Metal Ions into Polyimides", ACS Symposium Series, No 121, Modification of Polymers, ACS, 1980.

[4] Wohlford, T. L.; Schaff, J.; Taylor, L. T.; Furtsch, T. A.; Khor, E.; and St. Clair, A. K., "Synthesis and Characterization of Conductive Palladium Containing Polyimide Films", Conductive Polymers, Plenum Publishing Corp., New York, NY, 1981.

[5] Von Hippel, A. R., Dielectric Materials and Application, M.I.T. Press, Cambridge, MA, January 1961.

[6] Hedvig, P., Dielectric Spectroscopy of Polymers, p. 84, John Wiley and Sons, New York, NY, 1977.

[7] Wilson, T.; Memory, J. D.; Gilbert, R. D.; and Fornes, R. E., "Effects of 0.5 MeV Electron Radiation on Dynamic Mechanical Properties of TGDDM/DDS Epoxy", Bull. Am. Phys. Soc., Vol 29, p. 410, February 1984.
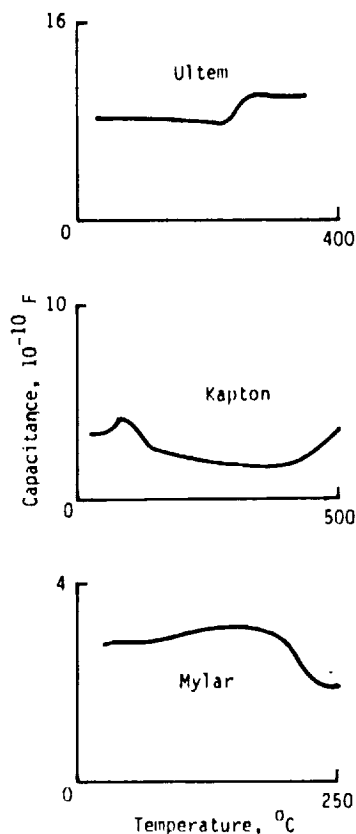
APPENDIX D

ELECTRON-RADIATION EFFECTS ON THE AC AND DC
ELECTRICAL PROPERTIES AND UNPAIRED ELECTRON DENSITIES
OF THREE AEROSPACE POLYMERS

Sheila Ann T. Long[*] and Edward R. Long, Jr.[*]

and

Heidi R. Ries[**] and Wynford L. Harries[**]

ABSTRACT

The effects of gigarad-level total absorbed doses from 1-MeV electrons on the post-irradiation alternating-current (ac) and direct-current (dc) electrical properties and the unpaired electron densities have been studied for Kapton,® Ultem,® and Mylar.® The unpaired electron densities (determined from electron paramagnetic resonance spectroscopy) and the dc electrical conductivities of the irradiated materials were monitored as functions of time following the exposures to determine their decay characteristics at room temperature.

The elevated-temperature ac electrical dissipations of the Ultem and Mylar were affected by the radiation. The dc conductivity of the Kapton increased by five orders of magnitude, while the dc conductivities of the Ultem and Mylar increased by less than an order of magnitude, due to the radiation.

The observed radiation-generated changes in the ac electrical dissipations are explained in terms of known radiation-generated changes in the molecular structures of the three materials. A preliminary model relating the dc electrical conductivity and the unpaired electron density in the Kapton is proposed.

INTRODUCTION

Kapton, a polypyromellitimide, is used extensively in space for passive thermal control of spacecraft, substrates for solar cell arrays, and electrical insulation. The effects of electron radiation on the molecular[1-3] and mechanical[2,3] properties of Kapton have been reported. Although Kapton has generally performed satisfactorily in the radiation environment of geosynchronous orbit, its applications are limited because it is available only in the form of film.

The need for materials that are also processable as castings or as fiber-reinforced composites and the need for tougher (impact-resistant) materials have been recognized. One such material is Ultem, a polyetherimide. The effects of electron radiation on the mechanical and molecular properties of Ultem have been reported.[3-5]

Mylar, a polyethylene terephthalate, is widely used for electrical insulation. It is also frequently employed as a model polymer for the study of more complex polymer structures. The effects of gamma radiation on the molecular[6-10] and mechanical[10] properties of Mylar have been studied.

The primary research emphasis, to date, on studying the effects of radiation on the electrical properties of polymers has been to measure the electric currents and electrical conduction induced in the polymers during the irradiation process. Such studies have been presented for polystyrene,[11] polyethylene,[12-15] polypyromellitimide,[15] and polyethylene terephthalate.[15,16]

The purpose of the present research study is to determine the post-irradiation ac and dc electrical properties of the polymers Kapton, Ultem, and Mylar. The goal is to correlate the radiation-generated changes in the electrical properties with known radiation-generated changes in the molecular structures of these three dielectric materials.

MATERIALS

Kapton is a polypyromellitimide manufactured by the E. I. du Pont de Nemours and Company, Inc.[***] The Kapton studied was Type H film. Both the stock grade and the aerospace grade of the Type H film were investigated. Both grades were 3 mils thick. (One mil is equal to 25.4 micrometers.)

Ultem, a polyetherimide, is a product of the General Electric Company. Two thicknesses, 3 mils and 20 mils, of 1000 Ultem film were investigated.

Mylar, a polyethylene terephthalate, is also produced by the E. I. du Pont de Nemours and Company, Inc. The Mylar for this study was a stock grade and was 10 mils thick.

The chemical structures of the repeat units for Kapton, Ultem, and Mylar are shown in figure 1. All three materials have six-membered-ring phenyl groups.
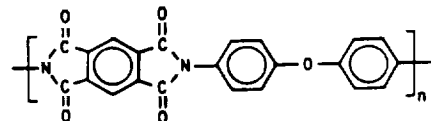
a.- Kapton.
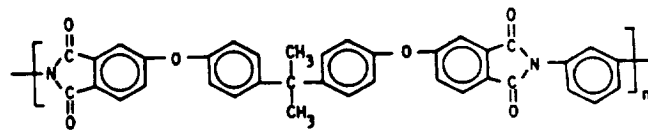
b.- Ultem.
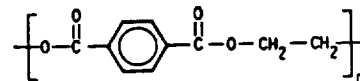
c.- Mylar.

Figure 1.- Chemical structures of repeat units for Kapton, Ultem, and Mylar.

[*] National Aeronautics and Space Administration, Langley Research Center, Hampton, VA 23665-5225.
[**] Department of Physics, Old Dominion University, Norfolk, VA 23508-0369.

The Kapton and Ultem, in addition, have five-membered-ring imide groups and aromatic ether linkages. The Ultem has more aromatic ether structure than the Kapton and, also, has gem-dimethyl groups. These additional structures, plus the existence of meta- as well as para-substitution on the phenyl rings, all contribute to the Ultem's thermoplastic properties. The proportion of ring (phenyl plus imide) structure in the repeat unit (figure 1) decreases in the order of Kapton, Ultem, and Mylar. The glass transition temperatures (T_g) also decrease in this same order. The T_g values[17] are 388 °C, 213 °C, and 69 °C for the aerospace-grade Kapton, the 3-mil thick Ultem, and the Mylar, respectively.

EXPERIMENTAL PROCEDURE

The polymer specimens were all exposed in vacuum to 1-MeV electrons from a Dynamatron source at an absorbed dose rate of 5×10^7 rads/hr.[18] The specimens were maintained between 20 °C and 35 °C during the radiation exposures.[18] The Mylar was irradiated to two different total absorbed doses - 1×10^9 rads and 5×10^9 rads. Attempts to irradiate the Mylar to higher total doses resulted in such highly degraded specimens that no property measurements could be made on them. The Kapton and Ultem materials were each irradiated to four different total absorbed doses - 1×10^9 rads, 5×10^9 rads, 9.5×10^9 rads, and 9.75×10^9 rads. This range of total absorbed doses is equivalent to the range of doses anticipated for the external portion of a space structure in service for 30 years in geosynchronous orbit.

The ac properties studied included the capacitance, dissipation, impedance, and series resistance. The measurements were made at a frequency of 10 KHz with a computer-controlled multifrequency inductance-resistance-capacitance (LRC) meter. The equivalent circuit was resistance in series with capacitance. The experimental arrangement has been described previously.[17] The dielectric constants, as determined from the measured capacitance values, and the measured dissipation factors for the nonirradiated materials were in agreement with the manufacturers' values. The glass transition temperatures (T_g) were determined from the ac electrical dissipation data and dielectric spectroscopic techniques.[17] The accuracy of the glass transition temperature values was to within ± 1 °C. The glass transition temperatures of the nonirradiated polymers were also in agreement with the manufacturers' specifications.

The dc electrical conductivity was determined from measurements of the current through the film or cast polymer specimens, at an applied voltage of 500 V, using a computer-controlled electrometer/multimeter. The resulting electric fields were 10-66 KV/cm. The procedure that was followed is the one prescribed in ASTM Standard D-257.[19] The dc conductivity measurement was a bulk (volume) measurement. The chromium-palladium electrodes[19] were vacuum-deposited directly onto the front and back surfaces of the specimens prior to the electron radiation exposures, in order to ensure good electrode-specimen contact. All dc measurements were made at room temperature. The electrification period was 60 sec for each measurement. The measured dc resistivities for the nonirradiated polymers were in agreement with the manufacturers' values. Two different thicknesses of the Ultem were measured, and the results were thickness independent.

The unpaired electron densities were computed from the second integrals of the electron paramagnetic resonance (EPR) first-derivative signals.[20] The EPR system included a Varian E-Line Century-Series Model E-109E spectrometer, a variable temperature accessory for controlling the temperature of the specimens during the magnetic scans, a precision microwave frequency counter, a gaussmeter, and a Hewlett-Packard Model

9836A computer. The EPR instrumentation and measurement procedures used in this study have been previously discussed in detail.[3,5] Also, reference 20 is a standard text for EPR theory and techniques. The EPR spectrometer parameters used for the experiments in this study were as follows: field set = 3280 gauss, scan range = 160 gauss, modulation amplitude = .5-8 gauss, scan time = 4 min, time constant = .250 sec, microwave power = 12.5 mW, microwave frequency = 9.0-9.5 GHz, and modulation frequency = 100 KHz. The specimens for the EPR measurements were all rectangular strips, .09 in X .6 in. The EPR system was calibrated using calibrated weak pitch and strong pitch standards furnished by Varian Associates, Inc. The electronic g-values were accurate to at least three significant figures.

The ac, dc, and EPR specimens were all irradiated simultaneously for a given material and total dose. All property measurements on the irradiated materials were commenced 30 min after the completion of the radiation exposures.

RESULTS AND DISCUSSION

Alternating-Current Properties

A summary of the room-temperature alternating-current electrical properties of the three polymers is presented in table I for the nonirradiated and irradiated conditions. For the Kapton and Ultem, each value listed is the average for five specimens. The Kapton had the smallest changes of the three materials. The standard deviations for the Kapton values and the Ultem values imply that the changes (even those for the series resistance and dissipation of the Ultem) were not statistically significant. For the Mylar, only one or two specimens were used to obtain each value given in the table. The changes for the Mylar were, for the most part, small.

TABLE I.- ROOM-TEMPERATURE ALTERNATING-CURRENT DATA AT 10 KHz FOR THREE POLYMERS

Polymer	Kapton* (3-mil film)		Ultem* (20-mil film)		Mylar** (10-mil film)	
Radiation dose, gigarads	0	9.75	0	9.75	0	5.00
Capacitance, nF	.38 ± .06	.37 ± .03	.094 ± .006	.094 ± .004	.279	.254
Impedance, kohm	43 ± 7	41 ± 1	171 ± 10	190 ± 10	57	63
Series resistance, ohm	100 ± 64	95 ± 36	411 ± 439	608 ± 400	647	539
Dissipation	.0024 ± .0009	.0022 ± .0006	.0024 ± .0023	.0036 ± .0021	.0108	.0086

* Each datum (for both nonirradiated and irradiated conditions) is the average ± the standard deviation for five specimens.

** Each datum for the nonirradiated condition is the average for two specimens, and for the irradiated condition is the value for one specimen.

The 10-KHz electrical dissipation curve for the Kapton at elevated temperatures, up to approximately 400 °C, showed little or no change due to the radiation. Figures 2 and 3 present the 10-KHz dissipation data at elevated temperatures for nonirradiated and irradiated specimens of the Ultem and Mylar, respectively. The temperature at which the ac electrical dissipation begins to increase rapidly with temperature is the onset of the material's glass-rubber transition (i.e., the transition from a glassy to a rubbery state). This is called the glass transition temperature (T_g). The value for the T_g is determined by fitting local tangents to the dissipation curve,

above and below the onset of the rapid increase, and locating their point of intersection. The method for fitting has been discussed in an earlier report.[17] For the Ultem (figure 2), the T_g from the dissipation curve for the nonirradiated specimen was 215 °C and for the irradiated specimen was 235 °C, which is a significant increase. For the Mylar (figure 3), the T_g for the nonirradiated specimen was 69 °C and for the irradiated specimen was 48 °C, which is a significant decrease. The magnitude of the Mylar's dissipation at elevated temperatures was three times greater for the irradiated specimen than for the nonirradiated specimen. In addition, the dissipation curve for the irradiated Mylar has a bimodal character, in contrast to the original single-mode character. The Kapton's T_g value for the nonirradiated condition was 381 °C and for the irradiated condition was 377 °C. This one-percent change for the Kapton is a further indication that the radiation had little effect on the Kapton's elevated-temperature ac electrical dissipation properties.
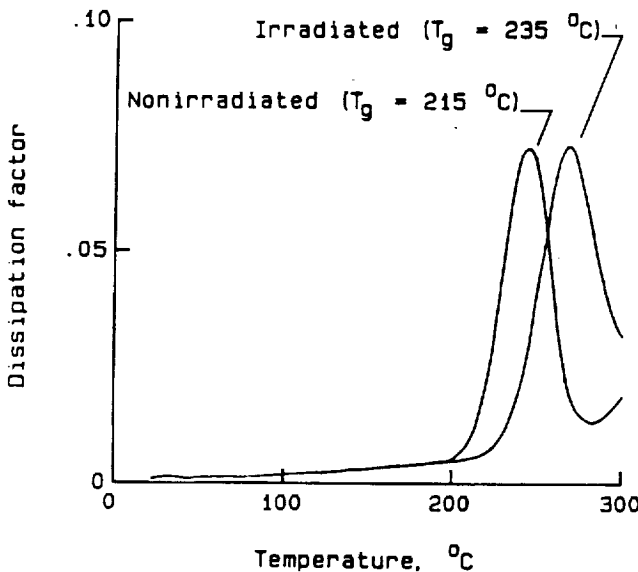

Figure 2.- Ultem's dissipation factor (for 10 KHz) at elevated temperatures before and after absorbing 9.5 gigarads from electron radiation.
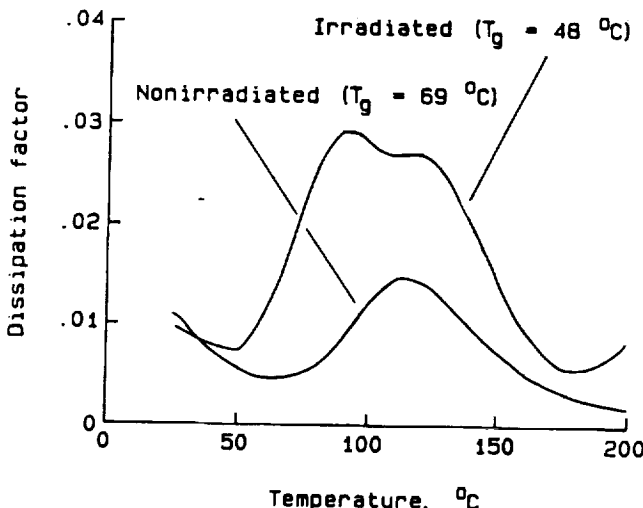

Figure 3.- Mylar's dissipation factor (for 10 KHz) at elevated temperatures before and after absorbing 5.0 gigarads from electron radiation.

Earlier work has shown that radiation causes crosslinking in Ultem,[3-5] chain scissioning in Mylar,[10] and essentially no change in Kapton because self-mending takes place.[3] Reference 21, a classic text on radiation chemistry, discusses crosslinking and chain scissioning as the dominant effects of radiation on a number of different polymers. Examples[21] of other polymers that predominantly crosslink due to radiation are polystyrene and polyethylene; examples[21] of others that predominantly scission are polymethylmethacrylate and polytetrafluoroethylene.

The crosslinking in the Ultem accounts for the observed increase in the Ultem's T_g after the radiation because crosslinking reduces the free volume of a polymer. Less free volume in a polymer causes the glass transition temperature to be increased.[22]

For the Mylar, the chain scissioning increases the free volume. This, in turn, causes the temperature at which the glass transition occurs to be decreased.[22] Also, for the Mylar, the chain scissioning causes shorter chains and more dangling groups, many of which have an electric dipole moment. A larger number of molecular structural components with dipole moments are, hence, free to vibrate with the applied ac signal. The increased vibration means an increased absorption of the energy from the radio-frequency field. A portion of this absorbed energy is lost, so the electrical dissipation factor for the Mylar increases. The bimodal character (figure 3) is due to the coexistence of the scissioned and nonscissioned portions of the irradiated Mylar.

Because of self-mending in the Kapton, the ac electrical dissipation of the Kapton was not appreciably changed. The Kapton's self-mending occurs because radiation-generated phenyl radicals in the Kapton are long-lived (minutes to hours) and recombine with radiation-generated phenoxyl and ketone radicals to form the same molecular bonds that existed prior to the radiation exposure.[3] In contrast, the radiation-generated phenyl radicals in the Ultem and Mylar, for the most part, are short-lived (fractions of seconds to seconds) and combine with hydrogen atoms (which are radicals), thereby blocking self-mending. In the following section, the phenyl radicals are postulated to be a cause of the changes observed in the Kapton's dc electrical properties after the radiation.

DC Electrical Conductivities and Unpaired Electron Densities

Table II presents the values of the dc electrical conductivities and the unpaired electron densities in the nonirradiated and irradiated polymers. The values

TABLE II.- DC ELECTRICAL CONDUCTIVITIES AND UNPAIRED ELECTRON DENSITIES IN IRRADIATED POLYMERS

Polymer	Total absorbed dose, gigarads	DC electrical conductivity, $ohm^{-1}-cm^{-1}$	Unpaired electron density, spins/g
Kapton (stock-grade)	0	2.0×10^{-17}	8.40×10^{15}
	1.00	6.0×10^{-12}	2.25×10^{17}
	5.00	3.9×10^{-12}	4.90×10^{17}
	9.50	2.0×10^{-12}	6.29×10^{17}
	9.75	1.7×10^{-12}	7.39×10^{17}
Ultem (20-mil thick)	0	2.0×10^{-17}	2.95×10^{15}
	1.00	3.0×10^{-17}	8.12×10^{17}
	5.00	3.8×10^{-17}	4.08×10^{18}
	9.50	1.0×10^{-17}	4.19×10^{18}
	9.75	3.8×10^{-17}	7.48×10^{18}
Mylar	0	6.3×10^{-18}	5.71×10^{15}
	1.00	2.0×10^{-17}	2.37×10^{18}
	5.00	---	1.46×10^{18}

listed in the table for the irradiated polymers are the
values for the initial measurements, 30 min after the
completion of the radiation exposures. The dc
electrical conductivity of the Kapton increased by five
orders of magnitude, whereas the dc conductivities of
the Ultem and the Mylar increased by less than an order
of magnitude, after the radiation exposures. The
unpaired electron densities, however, increased by
several orders of magnitude - for all three polymers -
due to the radiation. This suggests that the dc
electrical conductivity and the density of unpaired
electrons, or the density of a particular radical
species such as the phenyl radicals, might be related
in the Kapton.

The monotonic increase of the unpaired electron
density with total absorbed doses from 1-MeV electrons
for the Kapton and Ultem (table II) is consistent with
earlier experiments[3-5] with 100-KeV electrons. The
Mylar irradiated to a total absorbed dose of 5×10^9
rads was so embrittled that the dc conductivity
measurements could not be made. This extreme
embrittlement of the Mylar probably accounts for the
decrease (table II) of the unpaired electron density
between the total absorbed doses of 1×10^9 rads and
5×10^9 rads. An explanation is that a number of the
radicals produced by the extreme scissioning were, most
likely, able to combine to form gaseous by-products.

In addition, the unpaired electron density is
increased more by the radiation in the Ultem than in
the Kapton (table II). This is also consistent with
earlier findings[3] using 100-KeV electrons. This result
is attributed to the self-mending[3] in the Kapton, as
opposed to the crosslinking[3-5] in the Ultem. Because
self-mending has a higher probability of occurring than
does crosslinking because of the immediate proximity of
radicals formed by homolytic bond cleavage during the
irradiation process, the net effect at the end of the
exposure is less of an increase in the total radical
density for the Kapton.

Figures 4-7 are for the irradiated Kapton at the
highest total absorbed dose, 9.75×10^9 rads. Figures
4 and 5 give the dc electrical conductivities and the
unpaired electron densities, respectively, measured at
various times after the completion of the radiation
exposure. Both the dc and EPR specimens were stored in
a desiccator to prevent them from absorbing moisture
during the time intervals between the measurements. As
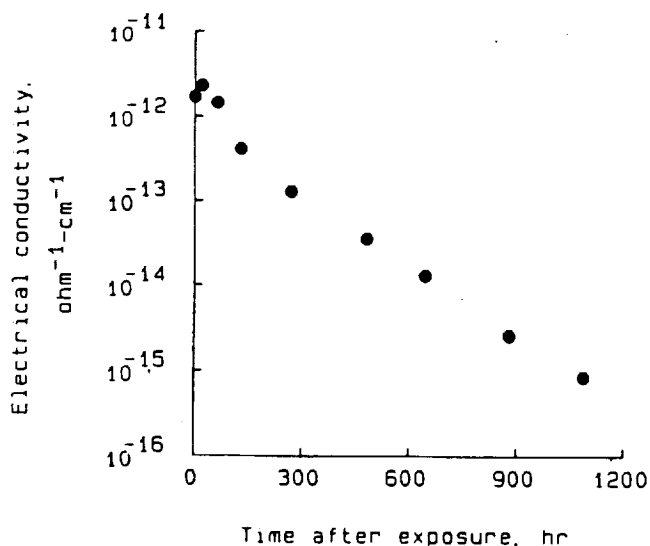can be seen from figures 4 and 5, the post-irradiation

Figure 5.- Unpaired electron density in irradiated
Kapton, measured at various times after the
exposure.

room-temperature decay curves for the dc electrical
conductivity and the density of unpaired electrons
again suggest that these two properties might be
related, in some manner, in the Kapton. Both
quantities decrease by orders of magnitude during the
1200-hr time period of the decay study. To
recapitulate, the dc electrical conductivity and the
radical density of Kapton both increase by orders of
magnitude with radiation exposure at room temperature
and then both decrease by orders of magnitude with time
at room temperature after the radiation exposure.

Figure 6 is a plot of the dc electrical
conductivity versus the unpaired electron density, for
the different measurement times after the completion of
the radiation exposure. The dc electrical conductivity
of the dielectric initially increases rapidly with the
radiation-generated unpaired electron density and then
reaches a saturation level between 10^{-12} ohm^{-1}-cm^{-1} and
10^{-11} ohm^{-1}-cm^{-1}.

Figure 4.- DC electrical conductivity of irradiated
Kapton, measured at various times after the
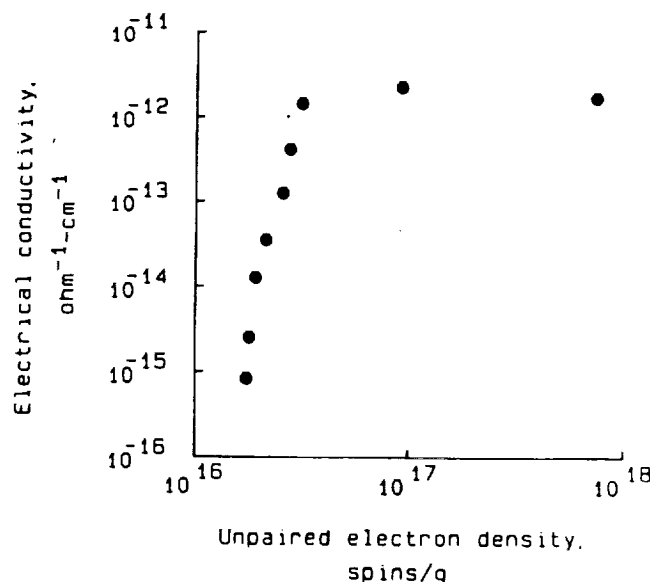exposure.

Figure 6.- DC electrical conductivity versus unpaired
electron density in irradiated Kapton.

1394

The radiation-generated radicals (the molecular groups containing the unpaired electrons) have been previously identified for the three polymers under investigation. The predominant long-lived radical species are as follows: phenyl, phenoxyl, and ketone in the Kapton;[3] phenoxyl, ketone, and gem-dimethyl in the Ultem;[3-5] and ethylene in the Mylar.[6-8] Free electron signals have not been observed in the EPR spectra[3-8] of irradiated Kapton, Ultem, or Mylar.

For an unpaired electron in a polymer to have a high probability of hopping from site to site under the influence of an electric force produced by a moderate applied voltage, the unpaired electron should be in a localized state. It should be mechanically constrained (possess few translational and rotational degrees of freedom) and should be chemically nonresonant (possess few resonant modes within its molecular group). Of the aforementioned five radical species, the unpaired electron in the phenyl is the only one that is both highly constrained and nonresonant. Specifically, the unpaired electron in the phenyl radical is located in the sp^2 molecular orbital of the carbon atom from which the hydrogen atom has been abstracted. For the three polymers in this study, the phenyl radicals are longer lived and more abundant in the Kapton than in the Ultem or in the Mylar. The previously reported molecular model[3] of the basic radiation damage mechanisms in Kapton proposed that half the total radical density in the irradiated Kapton consists of phenyl radicals. One can, therefore, postulate that the radiation-generated phenyl radicals in the Kapton might be responsible, at least in part, for the large increase in the dc electrical conductivity of the Kapton after the radiation.

Assuming that the phenyl radicals are uniformly distributed throughout the irradiated Kapton, one can calculate (from figure 6) the average separation distances of the unpaired electrons associated with these particular radicals. The post-irradiation separation, or hopping, distances corresponding to the dc electrical conductivity values of 10^{-12}-10^{-11} ohm^{-1}-cm^{-1} are determined to be 12-36 nm for the phenyl radical population (figure 7).

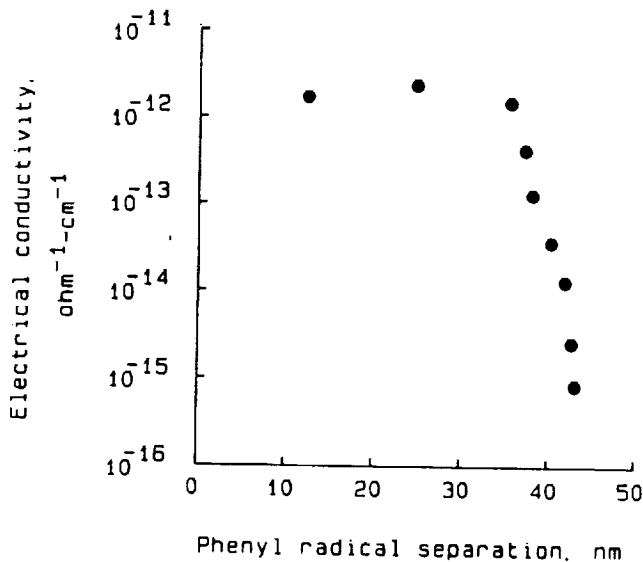A completely different study[23] exposed 3-mil thick Kapton Type H film to elevated temperatures (100-200 °C) in high electric fields (50-450 KV/cm) and found that the resulting in-situ hopping distances of the charge carriers responsible for the dc electrical conduction were approximately 5-6 nm. Considering that the hopping distance of 12 nm in the present study corresponds to a post-irradiation time of 30 min, whereas the distances of 5-6 nm correspond to in-situ conditions, one notes that the two studies are in agreement.

The molecular model[3] reported earlier for irradiated Kapton proposed that the Kapton undergoes a self-mending process due to the radical-radical recombination of the phenyl radicals with the phenoxyl and the ketone radicals. This self-mending process is believed to account for the observed post-irradiation decay of the dc electrical conductivity in the Kapton, as seen in figure 4.

CONCLUDING REMARKS

Radiation exposures to 1-MeV electrons, up to a total absorbed dose of 9.75 X 10^9 rads, produced no statistically significant effects on the room-temperature ac electrical properties of Kapton, Ultem, or Mylar. The elevated-temperature ac electrical dissipations of the Ultem and Mylar, but not of the Kapton, were changed by the radiation. The irradiated Ultem required a higher elevated temperature before its dissipation began to change, even though the magnitude of the increase was the same as for the nonirradiated Ultem. In contrast, the dissipation of the irradiated Mylar began to change at a lower elevated temperature, and the magnitude of the increase was three times greater than that of the nonirradiated Mylar.

The glass transition temperature, determined from the elevated-temperature ac electrical dissipation data, increased for the Ultem, decreased for the Mylar, and remained unchanged for the Kapton. The explanations for the T_g and, hence, dissipation results were found in earlier molecular modeling. These earlier studies showed that radiation causes Ultem to crosslink and Mylar to scission, while causing no appreciable change in the molecular structure of the Kapton.

The dc electrical conductivity of the Kapton increased by five orders of magnitude as a result of the radiation. In contrast, the dc electrical conductivities of the Ultem and Mylar increased by less than an order of magnitude after the radiation exposures.

The unpaired electron densities in all three polymers - Kapton, Ultem, and Mylar - increased by several orders of magnitude due to the radiation. For the irradiated Kapton, the dc electrical conductivity and the unpaired electron density both decayed with time at room temperature.

The differences in the effects of the electron radiation on the ac and dc electrical properties of the Ultem and Mylar, compared with those of the Kapton, are attributed to the differences in the kinetics of the radiation-generated phenyl radicals in these polymers. In the Kapton, the phenyl radicals are long-lived and recombine with the phenoxyl and ketone radicals to produce self-mending. In the Ultem and Mylar, the phenyl radicals are short-lived and combine with atomic hydrogen, thereby blocking self-mending and, thus, allowing crosslinking and chain scissioning to take place in the Ultem and Mylar, respectively.

Figure 7.- DC electrical conductivity versus phenyl radical separation distance in irradiated Kapton.

The unpaired electron in the phenyl radical is in
a highly localized state and is, therefore, available
as a charge carrier for dc electrical conduction. The
mechanism for the dc electrical conduction in the
irradiated Kapton is proposed to be the hopping of the
unpaired electrons from phenyl site to phenyl site.
The post-irradiation (30 min after the completion of
the radiation exposure) hopping distance between the
phenyl radicals in the Kapton is determined to be
12 nm.

The large percentage (50 percent) of phenyl
radicals in the irradiated Kapton is thought to
account, at least in part, for the large increase (five
orders of magnitude) in the dc electrical conductivity
of the Kapton due to the radiation. The post-
irradiation decay of the Kapton's dc electrical
conductivity is attributed to the self-mending process
that is due to the radical-radical recombination of the
phenyl radicals with the phenoxyl and ketone radicals.

ACKNOWLEDGMENT

The authors wish to thank Wayne S. Slemp, Senior
Research Scientist in the Materials Division of the
NASA Langley Research Center, for providing the 1-MeV
electron-radiation exposures for this study.

REFERENCES

1. J. E. Ferl and E. R. Long, Jr., "Infrared
Spectroscopic Analysis of the Effects of Simulated
Space Radiation on a Polyimide," IEEE Transactions on
Nuclear Science, Vol. NS-28, No. 6, p. 4119-4124,
December 1981.
2. J. E. Ferl and E. R. Long, Jr., "Low-Energy
Electron Effects on Tensile Modulus and Infrared
Transmission Properties of a Polypyromellitimide
Film," NASA TM 81977, 16 p., June 1981.
3. E. R. Long, Jr., and S. A. T. Long, "Spectroscopic
Comparison of the Effects of Electron Radiation on the
Mechanical Properties of Two Polyimides," NASA TP,
Performing Organization Report No. L-16200, November
1986.
4. S. A. T. Long and E. R. Long, Jr., "Effects of
Intermediate-Energy Electrons on Mechanical and
Molecular Properties of a Polyetherimide," IEEE
Transactions on Nuclear Science, Vol. NS-31, No. 6,
p. 1293-1298, December 1984.
5. E. R. Long, Jr., and S. A. T. Long, "Spectroscopic
Analysis of Radiation-Generated Changes in Tensile
Properties of a Polyetherimide Film," NASA TP 2429,
Performing Organization Report No. L-15873, 36 p., May
1985.

6. K. Araki, D. Campbell, and D. T. Turner, "ESR
Study of Free Radicals Formed by Gamma-Irradiation of
Poly(ethylene Terephthalate)," Polymer Letters, Vol. 3,
p. 993-996, 1965.
7. D. Campbell, K. Araki, and D. T. Turner, "ESR
Study of Free Radicals Formed by Gamma-Irradiation of
Poly(ethylene Terephthalate)," Journal of Polymer
Science: Part A-1, Vol. 4, p. 2597-2606, 1966.
8. D. Campbell and D. T. Turner, "ESR Study of
Radicals Trapped in Amorphous and Crystalline Samples
of Poly(ethylene Terephthalate) After
Gamma-Irradiation," Journal of Polymer Science: Part
A-1, Vol. 5, p. 2199-2201, 1967.
9. R. S. Rogowski, "Concentration of Radicals in
Gamma-Irradiated Poly(ethylene Terephthalate)," Journal
of Polymer Science: Part A-2, Vol. 9, No. 10,
p. 1911-1914, October 1971.
10. V. L. Bell and G. F. Pezdirtz, "Effects of
Ionizing Radiation on Linear Aromatic
Polyesters," Journal of Polymer Science: Polymer
Chemistry Edition, Vol. 21, p. 3083-3092, 1983.
11. J. Kyokane, S. Harada, K. Yoshino, and Y. Inuishi,
"Electron-Beam-Induced Conduction in
Polystyrene," Japanese Journal of Applied Physics, Vol.
18, No. 8, p. 1479-1483, August 1979.
12. Y. Inuishi, K. Yoshino, S. Harada, and J. Kyokane,
"Conduction and Breakdown in Polymers," Conference
Record of the 1978 IEEE International Symposium on
Electrical Insulation, The Institute of Electrical and
Electronics Engineers, Inc., p. 205-208, c. 1978.
13. F. Nakashima and K. Yahagi, "Electrical Current
Decay in Polyethylene After Irradiation with
Monoenergetic Electron Beam," Proceedings of the 1978
Conference on Electrical Insulation and Dielectric
Phenomena, National Academic Press, Inc., p. 33-38, c.
1978.
14. K. Yoshino, J. Kyokane, T. Nishitani, and Y.
Inuishi, "Electron-Beam-Induced Conduction in
Polyethylene," Journal of Applied Physics, Vol. 49, No.
9, p. 4849-4853, September 1978.
15. D. B. Cotts and Z. Reyes, "New Polymeric Materials
Expected to Have Superior Properties for Space-Based
Uses," RADC TR 85-129, 224 p., July 1985.
16. L. K. Monteith, D. T. Turner, and L. F. Ballard,
"Correlation of Electrical Conductivity and
Radiation-Induced Free Radical Concentration in
Poly(ethylene Terephthalate) and Related
Compounds," NASA CR 66743, 68 p., 1969.
17. E. R. Long, Jr., S. A. T. Long, H. R. Ries, and W.
L. Harries, "Radio-Frequency Electrical Properties of
Some Neat and Metal-Doped Polyimides," Conference
Record of the 1986 IEEE International Symposium on
Electrical Insulation, The Institute of Electrical and
Electronics Engineers, Inc., p. 331-334, c. 1986.
18. A. K. St. Clair and W. S. Slemp, "Evaluation of
Colorless Polyimide Film for Thermal Control Coating
Applications," NASA TM 86341, 20 p., January 1985.
19. Anonymous, "ASTM Standard D-257: Test Methods for
D-C Resistance or Conductance of Insulating
Materials," 1984 Annual Book of ASTM Standards, Vol.
08.01, American Society for Testing and Materials,
Inc., p. 121-142, c. 1984.
20. J. E. Wertz and J. R. Bolton, Electron Spin
Resonance - Elementary Theory and Practical
Applications, McGraw-Hill Book Company, Inc., p. 21-37,
p. 164-191, p. 450-467, c. 1972.
21. R. O. Bolt and J. G. Carroll (Editors), Radiation
Effects on Organic Materials, Academic Press, Inc.,
p. 127-244, c. 1963.
22. F. W. Billmeyer, Jr., Textbook of Polymer Science
- Second Edition, John Wiley and Sons, Inc.,
p. 207-211, p. 228-231, c. 1971.
23. B. L. Sharma and P. K. C. Pillai, "Electrical
Conduction in Kapton Polyimide Film at High Electrical
Fields," Polymer, Vol. 23, p. 17-20, January 1982.

APPENDIX E

The Effects of Fluids in the Aircraft Environment on a Polyetherimide

EDWARD R. LONG, JR.

*National Aeronautics and Space Administration
Langley Research Center
Hampton, Virginia 23665-5225*

and

WILLIAM D. COLLINS*

*Department of Physics
Old Dominion University
Norfolk, Virginia 23508-0369*

Fluid absorption studies have been made for a polyetherimide thermoplastic film and a unidirectional composite of the thermoplastic with graphite fibers immersed in water, JP4 jet fuel, ethylene glycol, and hydraulic fluid. The changes in the weight, thickness, and tensile properties were measured for the film. The changes in the flexural properties of the composite were measured for specimens whose fiber orientation was transverse to their length. Only the hydraulic fluid, which caused an erosion or dissolving of the resin at the specimen surface, affected the film's properties. Both the water and the hydraulic fluid affected the flexural properties of the composite, due to capillary absorption along the fiber-resin interface.

INTRODUCTION

The applications of carbon-fiber reinforced polymer matrix composites for aircraft structures have increased significantly in recent years. Tests of carbon-fiber/epoxy composites have shown that moisture and aircraft fluids, such as fuel and hydraulic fluids, in the service environment can cause a degradation of mechanical properties (1–4), especially at elevated temperatures (5–6). These problems have been reduced by the use of 177°C-cured epoxies which are more resistive to degradation than are lower cure-temperature epoxies. However, the 177°C-cure epoxies are rather brittle and their composites may exhibit poor resistance to impact (i.e., toughness). The toughness of composites has been determined to be of considerable importance to their performance in aircraft structures. A composite's toughness can be increased by using additives, such as elastomers, in the epoxy-based matrix systems. Toughness can also be increased by using thermoplastic matrices which are inherently tougher than thermoset polymers.

This paper reports a study of the effects of some of the fluids found in aircraft environments, water, antifreeze, jet fuel, and hydraulic fluid, on a polyetherimide thermoplastic which is representative of the types of thermoplastics being evaluated for aerospace composite matrix applications. Specimens made from Ultem polyetherimide film were used to evaluate the changes in weight, thickness, tensile properties, and infrared (IR) transmission spectra of the neat resin. Specimens of composite made from unidirectional layups with fiber direction perpendicular to the specimen's length were used to evaluate the changes in the flexural properties of graphite/polyetherimide composite material.

EXPERIMENTAL DESCRIPTION

Materials and Specimens

Ultem polyetherimide thermoplastic is a product of the General Electric Company. The thicknesses of the films used for the measurements of changes of both weight and thickness were 7.6 by 10^{-5} and 5.1 by 10^{-4} meters. The thick-

ness of the film for the tensile property measurements was 7.6 by 10^{-5} meters. The thickness of the film for the infrared spectroscopy was 7.6 by 10^{-6} meters. The 7.6 by 10^{-5}-meter- and 5.1 by 10^{-4}-meter-thick specimens for weight and thickness measurements were 0.04 m by 0.04 m and 0.064 m by 0.01 m, respectively. The tensile specimens were 0.005 by 0.15 m. A description of the fabrication of the tensile specimens is given in *Ref. 7.* Four specimens were used for the weight measurements and four specimens were used for the thickness measurements, for each of the exposure conditions. A minimum of six specimens at each exposure condition were used for the tensile property tests of the film. The IR specimens were 0.01 m by 0.025 m.

The carbon-fiber/Ultem composite was a 4-ply, unidirectional layup molded from 0.10-meter wide, single plies of nonsized C6000 fiber tows coated with Ultem. The C6000 fiber is a product of Celanese Corporation. The molding was accomplished in a dam-type steel mold at 399°C and 3.45×10^6 Pa.

The composite flexural specimens were 0.01 m by 0.025 m. The fiber orientation was transverse to the specimen length so that the properties were dominated by the resin and/or the fiber-resin interface. At least six specimens were used for the flexural property tests of the composite, for each of the exposure conditions.

Exposure and Testing Facilities

The specimens were immersed in closed, individual containers of the fluids which were placed in an oven and exposed to a temperature of 82 ± 2°C. The fluids were water, ethylene glycol (antifreeze), JP4 (jet fuel), and Skydrol (a hydraulic fluid manufactured by Monsanto Corporation). The exposure durations were up to 82 days.

The weights were measured with a Sartorius model 2600 semimicrobalance and the thicknesses were measured with Starrett no. 673 bench-top comparator. The flexural and tensile tests were conducted with a model 1130 Instron testing machine. The tensile test and the flexural test are described in *Refs.* 7 and 8, respectively. The IR spectra were recorded with a model 599B Perkin Elmer spectrometer which was controlled by a model 3600 Perkin Elmer data station. All of the measurements were made at room temperature.

The fluids were washed from the surfaces of the specimens before measurements were made. The method consisted of a room-temperature, liquid freon wash using a laboratory dispensing bottle and cotton swabs. The method was evaluated, using IR spectroscopy, for both NaCl single crystals and the 7.6 by 10^{-6}-meter film. No detectable amount of fluid remained after washing the surface of either a NaCl crystal or a polymer film specimen which had been immersed in the fluid for several seconds.

RESULTS AND DISCUSSION

Physical Properties and Infrared Spectra

The weight change data for the 5.1 by 10^{-4}-meter Ultem film specimens are shown in *Fig. 1.* At the end of 82 days, the specimens immersed in water had gained approximately one percent weight, the specimens immersed in hydraulic fluid had lost approximately 0.7-percent weight, and there was no appreciable weight change for the specimens immersed in ethylene glycol and JP4. The 7.6 by 10^{-5}-meter specimens immersed in water, ethylene glycol, and JP4 underwent percentage weight changes similar to those for the 5.1 by 10^{-4}-meter specimens. However, these thinner specimens broke into small pieces before the first weighing when immersed in the hydraulic fluid.

The thickness data for 5.1 by 10^{-4}-meter specimens are shown in *Fig. 2.* At the end of 82 days, the specimen thickness increased approximately 0.6 percent for immersion in water, decreased approximately 2.4 percent for immersion in hydraulic fluid, and showed no
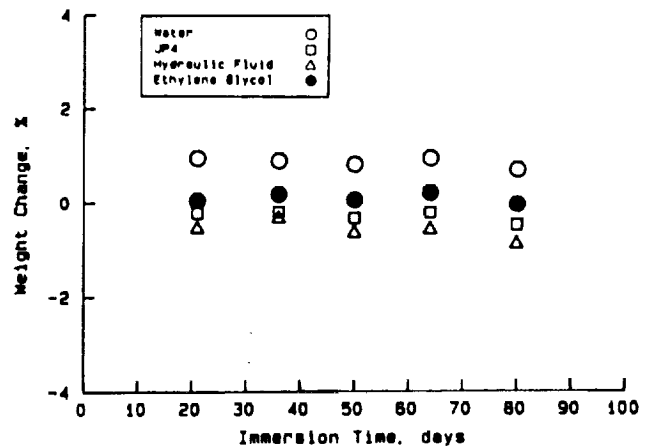
Fig. 1. Percent weights changes of neat-resin Ultem specimens for immersions in four fluids at 82°C for selected time periods.
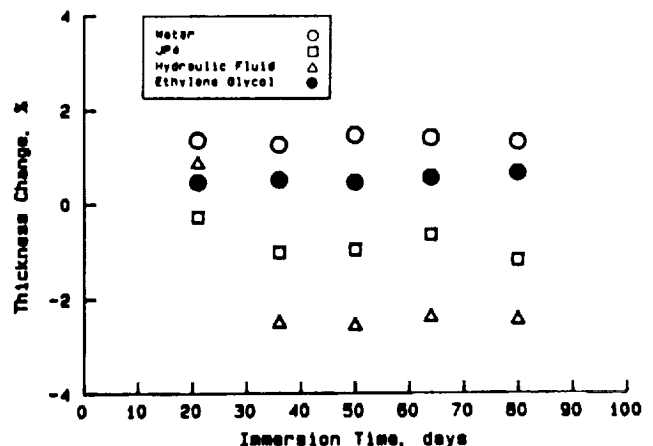
Fig. 2. Percent thickness changes of neat-resin Ultem specimens for immersions in four fluids at 82°C for selected time periods.

measurable changes for immersions in ethylene glycol and JP4. As in the case of the weight changes, the magnitudes of these changes were small. The thinner, 7.6 by 10^{-5}-meter, specimens immersed in water, ethylene glycol, and JP4 had percent changes in thickness similar to those for the 5.1 by 10^{-4}-meter specimens. The 7.6 by 10^{-5}-meter specimens, immersed in hydraulic fluid, broke into small pieces before the first thickness measurement, which was at ten days of immersion.

The IR spectra, from 4000 to 2000 cm^{-1}, of the 7.6 by 10^{-6}-meter film specimens, before and after immersions, are shown in *Fig. 3*. The reference spectrum for Ultem is shown in *Fig. 3a*. The IR spectrum of a specimen which had been immersed in water for 50 hours is shown in *Fig. 3b*. The spectrum did not have O-H stretching or rocking absorption bands which are associated with the water molecule. Therefore, a detectable amount of moisture was not absorbed. The IR spectrum of a specimen which had been immersed in ethylene glycol for fifty hours is shown in *Fig. 3c*. The spectrum had a band at 3370 cm^{-1}, due to O-H stretching, and bands at 2931 and 2870 cm^{-1}, due to antisymmetric and symmetric stretching of CH_2 structure. These bands are respectively indicated by the three arrows, from left to right, in *Fig. 3c*. The magnitude of these bands were small, which indicated that only small amounts of these structures were present, i.e. only a small amount of ethylene glycol was present.
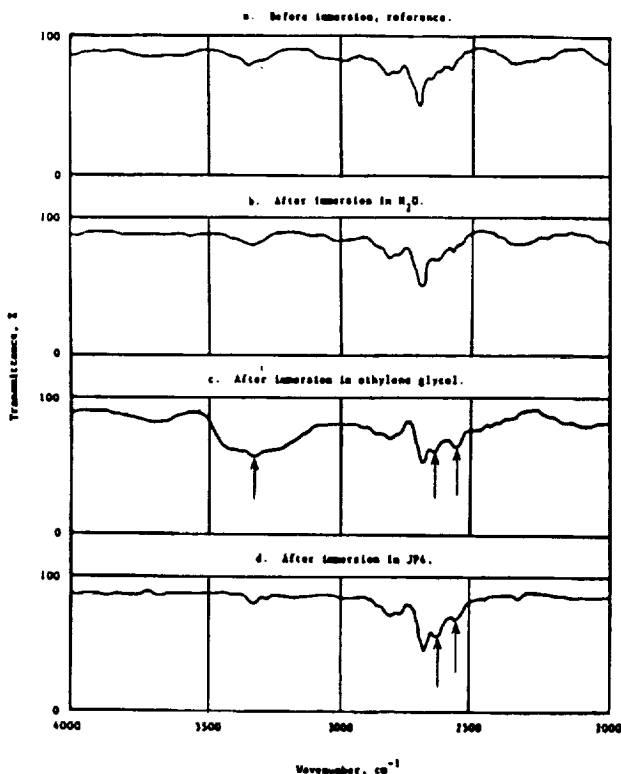
The IR spectrum of a specimen which had been immersed in JP4 for fifty hours is shown in *Fig. 3d*. The spectrum had bands at 2925 and 2868 cm^{-1}, indicated by the two arrows, which were due to CH_2 stretching. Again, the small magnitude of these bands indicated only a small amount of JP4 was present.

The spectrum of a specimen after immersion in hydraulic fluid showed no new bands, hence no evidence of absorption. However, the immersions were less than one minute because longer exposures caused the IR specimen to crumble into small pieces. These short exposures may have not been sufficient for any absorption to have occurred.

Both the physical property data and the crumbling of the IR specimens suggest that the hydraulic fluid had a degrading effect upon the film. The losses in weight and thickness suggest that the hydraulic fluid dissolved resin from the specimens. The crumbling of the IR specimens, for exposures longer than one minute, suggests embrittlement or some form of stress. Since there was no spectral evidence of the hydraulic fluid having been absorbed, any dissolving of the resin probably occurred at the surface (that is, an erosion process). After immersion in hydraulic fluid, the surfaces of the specimens appeared stressed or eroded. The erosion could have been due to chain scissioning. Several attempts were made to isolate and concentrate dissolved residue, within the container of hydraulic fluid, for identification of fragmented species using infrared spectroscopy. The attempts were not successful.

Tensile Properties of Films

The tensile properties of 7.6 by 10^{-5}-meter specimens after 15-day and 30-day immersions in the four fluids are shown in *Figs. 4 through 6*. The term "reference" means the specimens were not exposed to either fluids or elevated temperature and the term "control" means exposure at 82°C in air only. The other data in each figure refers to the properties after exposure to the fluids at 82°C.

The elongation-to-failure, *Fig. 4*, changed more than did the other tensile properties. The change appeared primarily due to the elevated temperature. Degradation at elevated temperatures which are much lower than the glass transition temperature (211°C for Ultem) is possible in an oxidative environment. The immersion in the hydraulic fluid caused additional reduction in elongation. There were no significant additional changes caused by the other fluids. These results are consistent with the weight and thickness data which indicated that those fluids were not absorbed.

The ultimate tensile strength data, *Fig. 5*, showed changes less than 17 percent. For the immersions in JP4 and in hydraulic fluid, an increase in the ultimate strength occurred. However, the 2σ bands overlap with those of

Fig. 3. Transmission infrared spectra for neat-resin Ultem film specimens before and after immersions in three fluids.
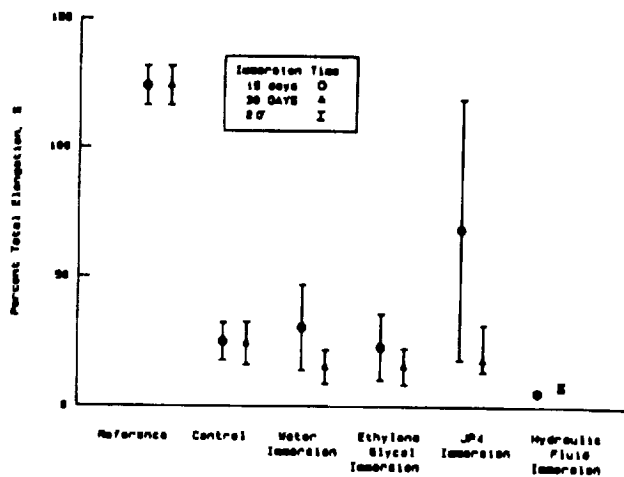
Fig. 4. Percent elongation-to-failure for neat-resin Ultem specimens before exposure (reference) and after 82°C exposures to air (control) and immersions in four fluids.

Fig. 6. Tensile modulus for neat-resin Ultem specimens before exposure (reference) and after 82°C exposures to air (control) and immersions in four fluids.
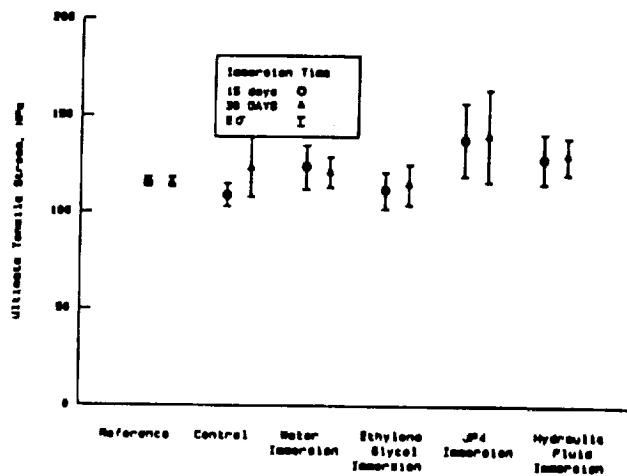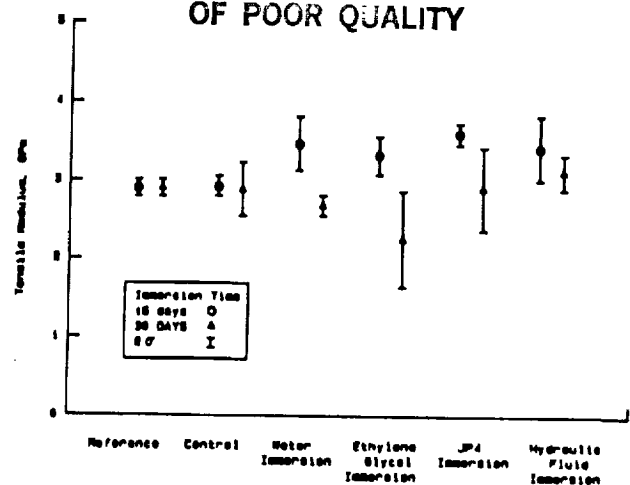

Fig. 5. Ultimate tensile strength for neat-resin Ultem specimens before exposure (reference) and after 82°C exposures to air (control) and immersions in four fluids.

the reference values. Therefore, the increases are not statistically significant.

The tensile modulus data, Fig. 6, suggest that some changes occurred. The modulus increased for the immersions in hydraulic fluid. The results were mixed for the two durations of immersion in the other fluids.

Ultem is a linear polymer. Therefore the mechanical properties of the reference specimens may be attributed to van der Waal, dipole-dipole, and other weak interactions between adjacent molecules. These interactions between the relatively long-molecule chains provide strength and allow large plastic deformations. If chain scissioning is caused by an immersion, which was implied by the weight and thickness data, then the molecular chains are shortened and therefore the elongation-to-failure is reduced. However, the chain scissioning would have reduced the ultimate strength. Instead, there was an increase in ultimate strength which indicates that crosslinking may have oc-

curred within the portion of the specimen not eroded. (Crosslinking also reduces the elongation to failure.)

The modulus properties are measured in the elastic region and are primarily due to straightening of a polymer's molecular structure followed by an onset of slippage between adjacent molecules. For immersions in water, in ethylene glycol, and in JP4 the modulus had a net increase for 15-day durations and a net decrease for 30-day durations. The increase for the fifteen day immersions could have been caused by crosslinking. Crosslinking can introduce bonding which reduces the amount of possible straightening at each site where straightening occurs. For the 30-day immersion duration a significant amount of plasticization may have taken place in addition to any crosslinking, therefore the modulus would decrease.

The hydraulic fluid caused a net increase of the modulus value for both immersion durations. Again, the longer immersion caused less increase than did the 15-day immersion. So a combination of effects could have occurred for the hydraulic fluid similar to what occurred for the other fluids. However there is almost complete overlap of the 2σ bands in the case of the hydraulic fluid. So, statistically, the changes in the modulus values are the same for both immersion durations.

Therefore, the combination of the physical and mechanical data for specimens of the neat resin suggests that both chain scissioning and crosslinking may have occurred during the immersion in hydraulic fluid. The changes in physical properties and appearances suggest surface erosion occurred, perhaps due to chain scissioning. However, the mechanical data suggests that crosslinking occurred in the portion of the specimen which remained after immersion.

To determine whether crosslinking or chain scissioning occurred in the portion of a speci-

men which remained after immersion in hydraulic fluid, five specimens for each of four immersion durations, 0 days, 15 days, 30 days, and 60 days, were dissolved in chloroform. The weights of the specimens were measured after dissolving times of 5 minutes, 10 minutes, 20 minutes, 40 minutes, and 80 minutes. As shown in *Fig. 7*, the specimens dissolved less for longer immersions in the hydraulic fluid. This indicates that immersion in the hydraulic fluid caused crosslinking of the molecules within the originally linear thermoplastic.

Flexural Properties of Composites

For no exposure, the flexural properties of transverse-fiber specimens of graphite/Ultem composite are shown in Figs. 8 through 10 as control values. For comparison, transverse-fiber specimens of unidirectional T300/5208 have a flexural modulus of approximately 8.27 by 10^8 Pa and an ultimate flexural stress of approximately 8.62 by 10^7 Pa (9). (T300 is a graphite fiber manufactured by Hercules Cor-

Fig. 9. Flexural modulus for transverse unidirectional carbon/Ultem composite specimens before and after 97 day immersions in four fluids at 82°C.

Fig. 10. Ultimate flexural strain for transverse unidirectional carbon/Ultem composite specimens before and after 97 day immersions in four fluids at 82°C.
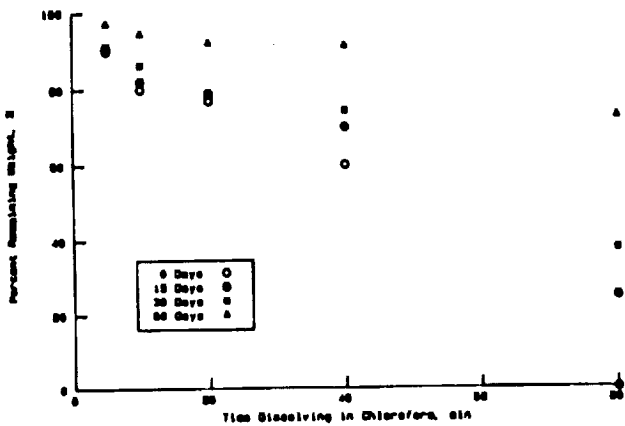

Fig. 7. Percent remaining weight after selected dissolving times in chloroform for specimens presoaked in hydraulic fluid for 0 days, 15 days, 30 days, and 60 days.

poration and 5208 is an epoxy manufactured by Celanese Corporation.)

The flexural data shown in Figs. 8 through 10 indicate that both hydraulic fluid and water affected the flexural properties of the composite specimens. Both fluids reduced the ultimate flexural stress, but had no significant effects on the flexural modulus. The water also reduced the composite specimens' ultimate flexural strain. In contrast, these fluids did not significantly alter the film specimens' tensile stress.

These differences of effects on the composite and on the film could have occurred if the fiber-resin interface of the composite were involved, perhaps because of capillary absorption along the interface. Once the fluids were present, they would provide a lubrication which could contribute to a reduction in the strength of the mechanical locking of the resin around the fiber.

Figures 11a through 11f are photomicrographs at magnification factors of 1000 and
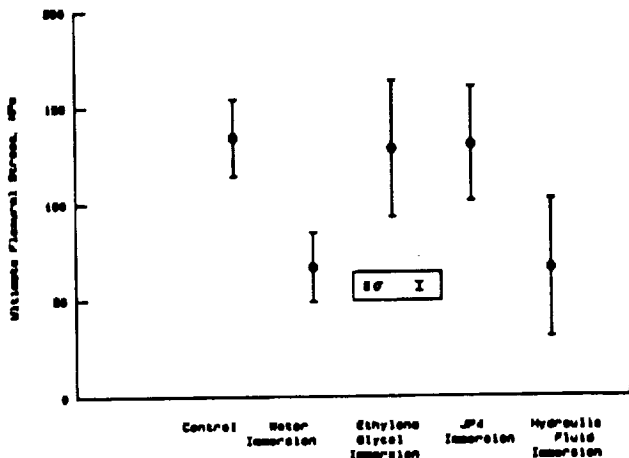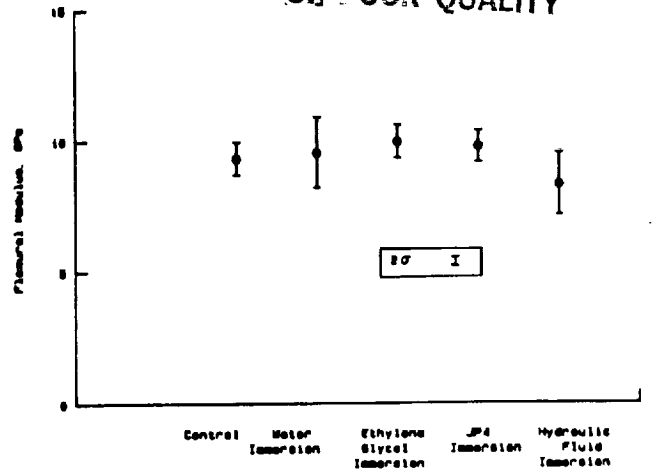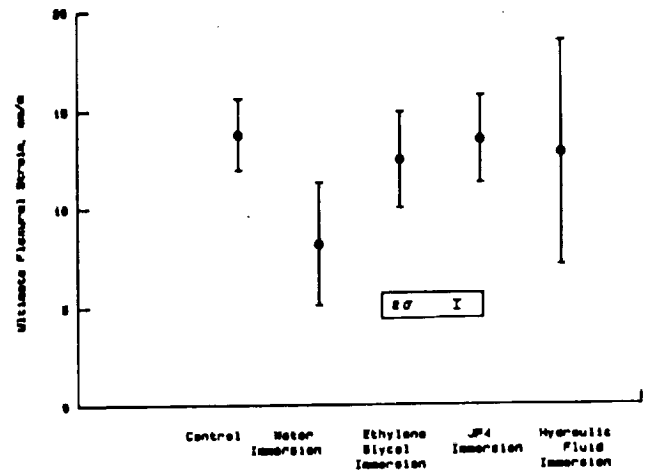

Fig. 8. Ultimate flexural stress for transverse unidirectional carbon/Ultem composite specimens before and after 97 day immersions in four fluids at 82°C.
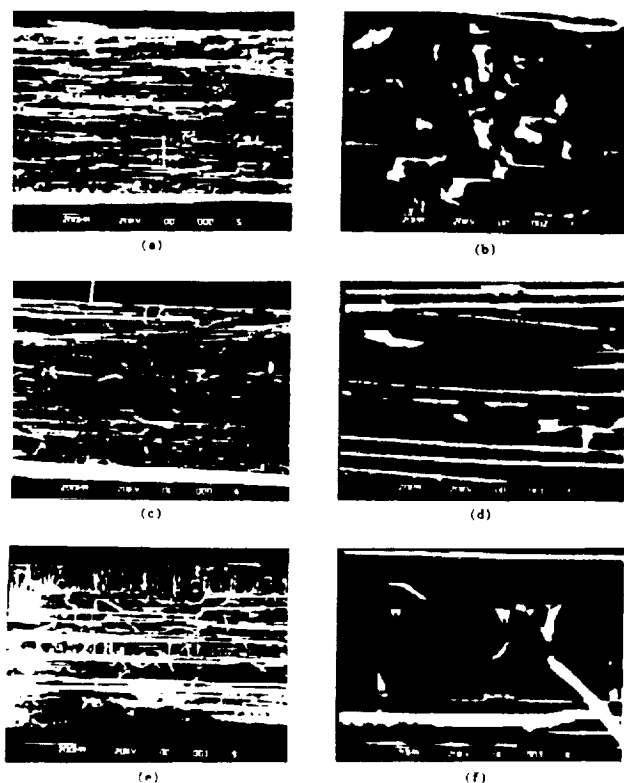
Fig. 11. Photomicrographs of the failure edges of composite flexural specimens for no exposure (a and b) and after 97 days immersions at 82°C to water (c and d) and to hydraulic fluid (e and f).

10000 of the failure surfaces of composite specimens after no immersion (*Figs. 11a* and *11b*), water immersion (*Figs. 11c* and *11d*), and hydraulic fluid immersion (*Figs. 11e* and *11f*), all at 82°C. The specimen, having no immersion, appears to have undergone predominantly cohesive failure in the matrix. In contrast, the specimen immersed in water appears to have undergone a significant amount of adhesive failure. The adhesive failure may be due to a significant decrease in the mechanical locking of the resin around the fiber caused by capillary absorption of the water. The specimen immersed in hydraulic fluid shows distinct embrittlement at the surface and along the mid-thickness line. This also is an indication that capillary absorption may have occurred. The failure mode appears to be adhesive. Adhesive failures, for the specimens immersed in water and hydraulic fluid, are in agreement with the

preceding interpretation of the mechanical data.

SUMMARY

A study has been made of the effects of 82°C immersions in water, ethylene glycol, JP4, and hydraulic fluid on the tensile properties of Ultem film and flexural properties of carbon/Ultem composite. The film was also studied for changes in weight and thickness.

The largest effect on the film's tensile properties was a large reduction in the elongation-to-failure after immersions in all of the fluids. The reduction appeared related to the elevated temperature; however, the hydraulic fluid did cause an additional reduction in elongation. Except for water, none of the fluids were absorbed. The tensile data suggested that the hydraulic fluid, caused crosslinking within the specimen while the weight and thickness data indicated that the hydraulic fluid, caused chain scissioning at the surface of a specimen. Solubility tests showed that crosslinking did occur. The presence of chain scissioning at the surface could not be confirmed. The other fluids did not have significant effects on weight, thickness, or tensile properties.

Both water and hydraulic fluid immersions caused changes in the flexural properties of the composite. The changes were not the same as the changes caused in the Ultem film's tensile properties. The interface between the fibers and the Ultem resin provided a partial explanation for the difference. The effects of the fluids, on the composite, suggest that screening studies, such as this one, can reveal important limitations of the aerospace environmental durability, of new polymeric materials, and polymer matrix composites.

REFERENCES

1. R. L. Levy, AFML-TR-77-41, April (1977).
2. G. S. Springer and C. H. Shen, AFML-TR-76-102, June (1976).
3. E. R. Long, Jr., NASA TP 1474, August (1979).
4. E. R. Long, Jr., and N. D. Danieley, *J. Polym. Sci.*, 19, 2443 (1981).
5. C. W. Browning, AFML-TR-76-153, March (1977).
6. R. L. Levy, AFML-TR-76-190, December (1976).
7. E. R. Long, Jr., and S. A. T. Long, NASA TP 2429, May (1985).
8. H. R. Phelps and E. R. Long, Jr., *J. Compos. Mater.*, 14, 334 (1980).
9. R. W. Wolf, J. D. Memory, R. D. Gilbert, and R. E. Fornes, *J. Appl. Phys.*, 54, 5558 (1983).

APPENDIX F

Effects of Postcuring on Mechanical Properties of Pultruded Fiber-Reinforced Epoxy Composites and the Neat Resin

Edward R. Long, Jr., Sheila Ann T. Long, William D. Collins†,
Stephanie L. Gray‡ and Joan G. Funk

National Aeronautics and Space Administration
Langley Research Center
Hampton, VA 23665-5225

Introduction

Pultrusion has been used as a method for fabricating composite materials for the past 30 years. Until recently, the fabrication materials have been primarily fiberglass and polyester resin. However, if pultrusion is to be used as a method for the mass production of high-strength, high-stiffness fiber-reinforced composites for aerospace structures, then advanced fibers, such as carbon and aramid, and resins such as epoxies will have to be used.

An epoxy that has a relatively short gel time, 2 to 4 minutes, at processing temperatures of 350°F to 400°F has been recently developed[1,3]. Studies have shown that this particular epoxy can be used for the pultrusion of high-performance, close-tolerance fiber-reinforced epoxy composite components[1,3]. Kershaw[2] found that the mechanical properties of the pultruded composite were improved by postcuring in a conventional oven at a temperature that was slightly higher than the maximum temperature used during the pultrusion.

Postcuring is done for a variety of purposes, including cure completion, moisture or solvent removal, and relief of internal stress. However, the use of a conventional oven for the postcure is probably appropriate only for short length composites parts. A more advanced concept for postcuring, such as postcuring in line with the pultrusion process, must be used if the full capacity of pultrusion for mass production of composites is to be attained.

This paper presents an evaluation of postcuring pultruded fiber-reinforced epoxy materials within the time period (minutes) that would be required if the postcuring were done in line with the pultrusion process. Measurements were made of the effects of the postcures on the flexural, shear, and interlaminar fracture toughness properties of the

materials for a range of postcure temperatures. The epoxy used was the same as that discussed by Kershaw[2]. Three different types of fibers - carbon, glass, and aramid - were investigated.

Materials

The epoxy and curing agents for this study were developed especially for pultrusion by the Shell Chemical Company[1,4]: Epon Resin 9310 and Epon Curing Agents CA 9360 and CA 537*. The combination of the two curing agents provided a rate of activation much higher than for epoxies used for autoclaved fiber-epoxy composites because of the short time in the pultrusion die. These were mixed with additional ingredients using the formulation in Table 1.

Abstract

The effects of postcuring on mechanical properties of pultruded fiber-reinforced epoxy-resin composites have been investigated for a simulation of postcuring in line with the pultrusion fabrication process. Composites of carbon, glass, and aramid reinforcement fibers were individually studied. The epoxy was a commercially-available resin that was especially developed for pultrusion fabrication. The pultrusions were conducted at 400°F with postcures at 400, 450, 500, and 550°F. Measurements of the flexural, shear, and interlaminar fracture toughness properties showed that significant postcuring can occur within the time frame available during the pultrusion process. All three mechanical properties were degraded by the higher (500°F and 550°F) temperature postcures; photomicrographs suggest that the degradation was caused at the fiber-resin interface for all three fiber types.

Ingredient	Units by Weight
9310	100.00
CA 537	0.65
CA 9360	33.00
ASP-400	13.00
Axel 1846	0.50
butyl-glycidylether	3.68

Table 1. Formulation for epoxy resin

Axel 1846, also called Mold Whiz, is a mold release compound manufactured by Axel Plastics Research Laboratories, Inc.; and ASP-400 is alumina silicate powder manufactured by the Engelhard Minerals and Chemicals Corporation. The butyl-glycidylether is used to control the crosslinking density which affects the formulation's coefficient of thermal expansion, viscosity, and capacity to wet the fiber.

The epoxy mixture was molded into neat resin specimens and also used as the matrix resin for pultruding the composites, which had a fiber volume fraction of 70 percent. Three fiber types were separately used for the composites: sized AS4W, 12K carbon, manufactured by Hercules, Inc.; Kevlar 49, 22720 denier aramid, manufactured by the E. I. duPont de Nemours and Company; and E-glass type 712 roving, 12.5 yards per pound of glass, manufactured by Pittsburg Plate Glass Industries.
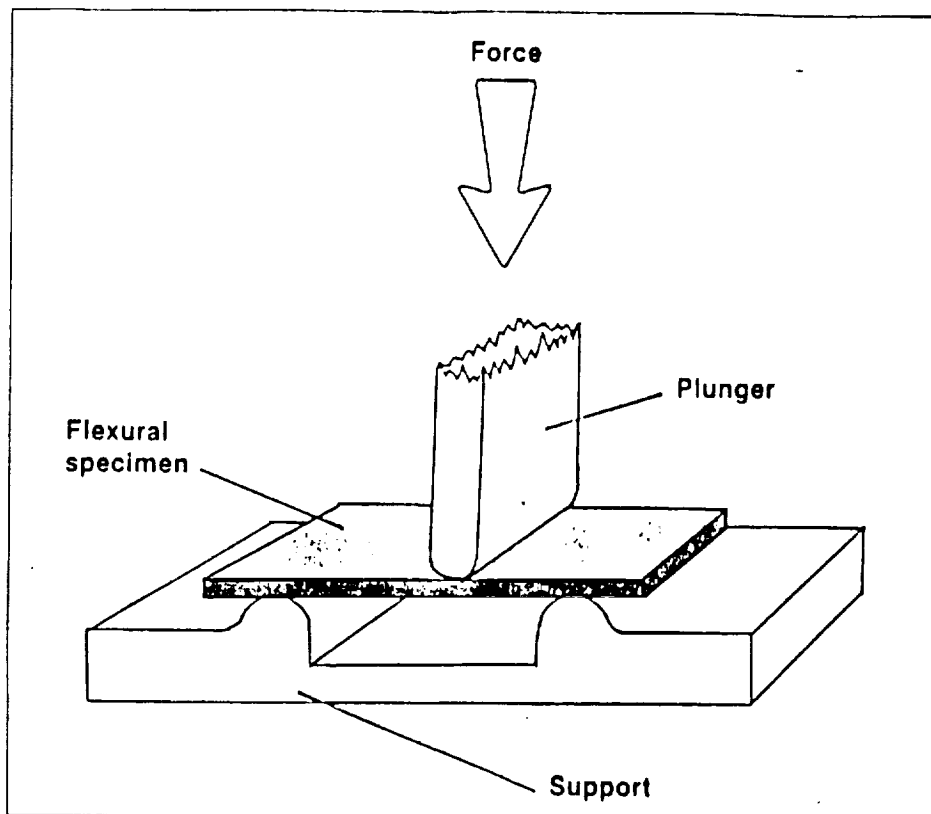
Figure 1. Schematic of flexural specimen and three-point flexural test fixture in test configuration.
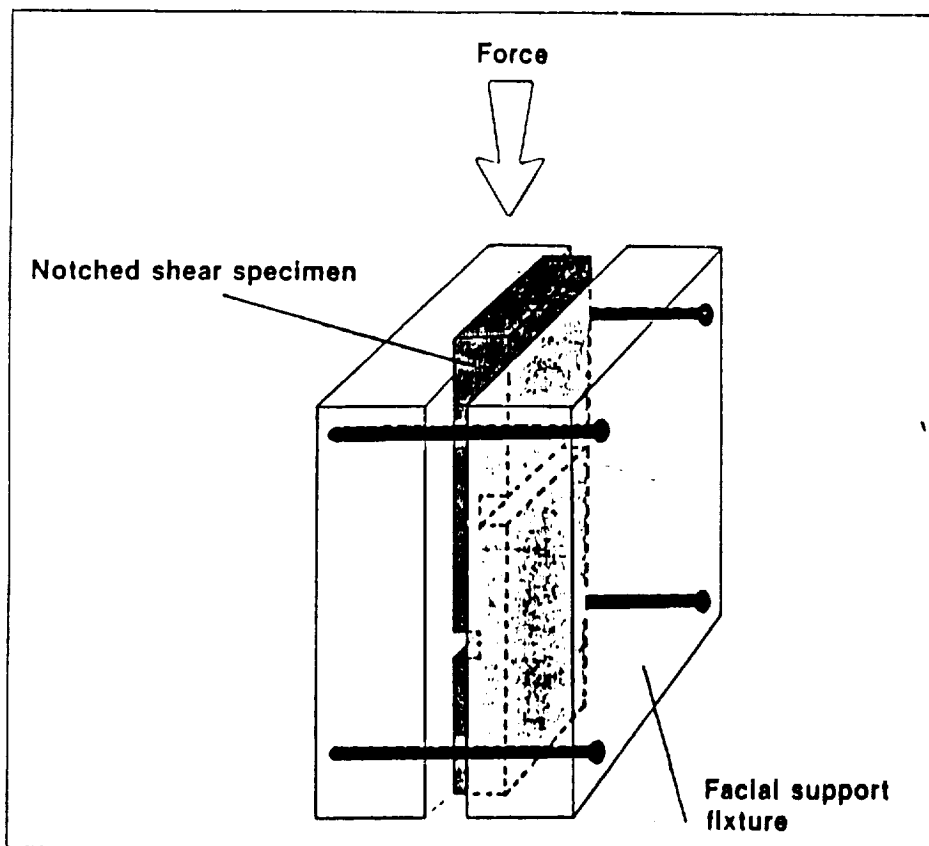

Figure 2. Schematic of notched shear specimen and facial support fixture in compressive shear test configuration.

The neat resin castings were made in open-faced molds; the epoxy mixture was degassed under vacuum at room temperature before it was poured into the molds. The castings were allowed to harden in the molds overnight at room temperature; they were then cured at 400°F for 2 minutes. The initial hardening was at room temperature because the "just-mixed" resin tended to foam at 400°F, even after extensive vacuum degassing.

Mechanical Specimens and Testing

Flexural, shear, and interlaminar fracture toughness tests were used to evaluate the effects of postcuring on the pultruded composite materials; only the flexural test was used to evaluate the molded neat resin material. The flexural tests and strength and modulus determinations were performed according to the specifications and equations prescribed in Method I of ASTM Standard D790; a drawing of the specimen under test is given in Figure 1. The specimens were 3 inches long, 1 inch wide, and 1/8 inch thick; and the support span of the test fixture was 2 inches.

The shear tests were conducted following ASTM Standard D3846, with a modification of the specimen size; the specimens were 3.1 inches long, 1 inch wide, and 1/8 inch thick. A sketch of a shear specimen under test is given in Figure 2; the two halves of the facial support fixture were 3 inches long and 1.5 inches wide and were clamped together by screws at the four corners, each at a torque setting of 1 lb-in.

The interlaminar fracture toughness was determined by a double-cantilevered beam (DCB) test. Figure 3 is a drawing of a DCB specimen under test; the specimens were 1 inch wide, 7 inches long, and 1/8 inch thick, with a 1-inch starter crack.

A minimum of seven flexural, seven shear, and three double-cantilevered beam composite specimens and a minimum of five flexural neat resin specimens were tested at room temperature for each postcure temperature evaluated.

Pultrusion System

The pultrusion machine used was a Glastruder, Model PM-12-14-8, manufactured by Goldsworthy Corporation; a profile schematic of the pultrusion system is shown in Figure 4. The tows of fiber were fed from a creel into a bath containing the epoxy resin mixture. In-
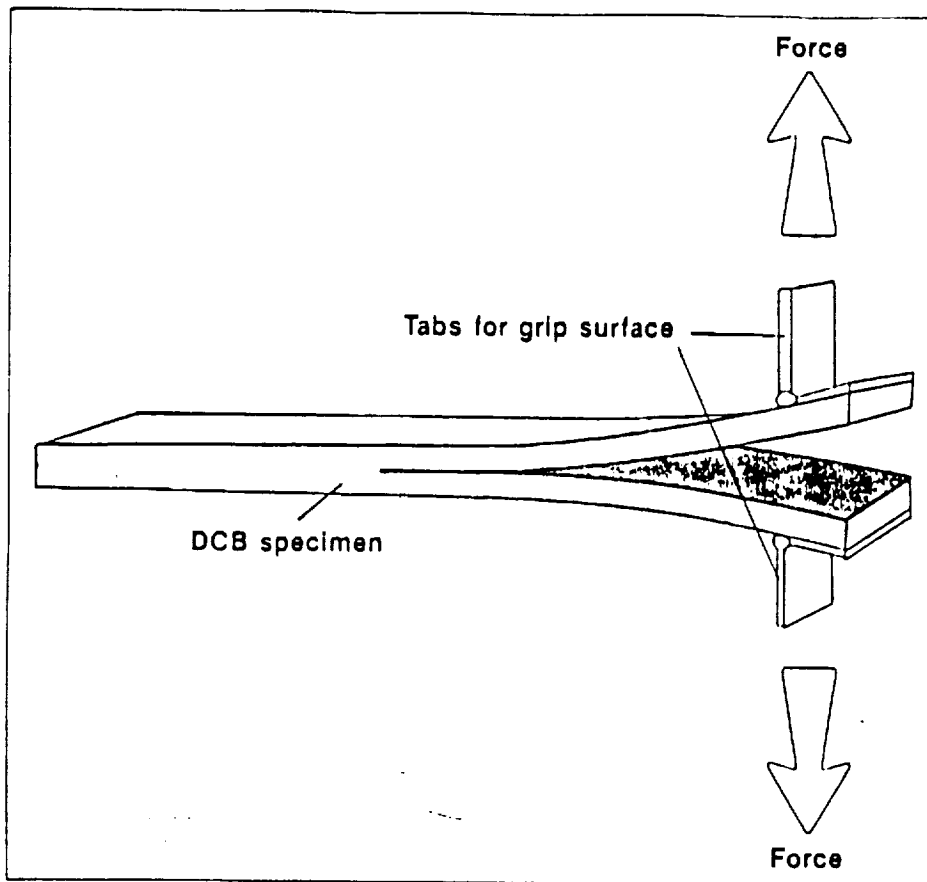
Figure 3. Schematic of Double-Cantilevered Beam (DCB) Composite Specimen with Tabs in Mode 1 (Peel) Interlaminar Fracture Toughness Test.

still within the curing die. This requires an in-line postcuring station or a curing die with additional heating stages. Post-cure temperatures higher than those used in reference 2 may be required, even for fairly long postcuring stations.

Simulation of In-Line Postcuring

In-line postcuring was simulated by exposing the specimens to elevated temperatures for 4 minutes, which represents the length of time to traverse through a 4-foot in-line curing station at a pultrusion rate of 1 foot per minute.

The carbon-epoxy and glass-epoxy composite specimens were postcured at temperatures of 400, 450, 500, and 550°F for all three mechanical tests. The aramid-epoxy specimens were postcured at 300°F for the shear and toughness tests and postcured at 500°F for the flexural test. The neat resin castings were post-cured at temperatures of 450, 500, and 550°F.

Results and Discussion

Neat Resin
FLEXURAL DATA

The ultimate flexural strength of the neat epoxy resin at room temperature, with and without postcuring, is shown in Figure 5. For no postcure, the average stress was 11.4 ksi; the average stresses were 14.2, 12.8, and 13.1 ksi for the post-cures at 450, 500, and 550°F, respectively. The largest stress value, which was achieved for the 450°F postcure, was due to the additional crosslinking caused by the postcure, while at the higher-temperature postcures, degradation effects, such as chain scissioning, also occurred[10].

The ultimate flexural strain data in Figure 6 show that, for postcuring temperatures higher than 450°F, the strain decreases monotonically with increasing postcure temperature. Crosslinking accounts for the decreased strain for the 450°F postcure, while the additional decreases in the strain for the postcure temperatures above 450°F may be attributed to chain scissioning.

Stress-strain curves for the postcured neat-resin epoxy specimens are given in Figure 7; each curve is for a typical specimen for the postcure it represents. These curves show, as was seen in Figures 5 and 6 that strain decreased monotonically with increasing postcure temperature and that gains in strength by postcuring are lost if the postcure tem-

side the bath the tows passed over and under the rungs of vertical "ladders" to spread the tows for improving the resin impregnation; the impregnated fibers then passed through the cure die. The two-part 30-inch die had a cavity entrance that was 1 inch wide and 0.65 inch high. The height of the cavity tapered to 0.125 inch in the first 3 inches of length, forming 5-degree taper; the cavity for the remaining length of the die had a constant cross section of 0.125 inch high by 1 inch wide. The die was between platens that contained heaters for controlling the temperature profile along the die; cooling water was passed through ports located in the last 4 inches of the platens. The pultrusion feed-through rate was 1 foot per minute. The maximum temperature of the material within the die was 400 °F.

Curing and Postcuring of Epoxy

An epoxy resin is cured by chemically bonding the epoxy molecules to a curing agent. After bonding, the epoxide moiety no longer exists; in its place is an hydroxide structure. The cured epoxy

gelates because the bonding is accompanied by crosslinking, the rate and the extent of which depend on the temperature and the time.

As the crosslinking becomes more extensive, the curing and/or crosslinking of remaining unreacted sites on the epoxy molecules and on the curing agent become less probable; the sites are less mobile and, hence, unable to reach each other. A method for providing the energy required for increasing the mobility of the unreacted sites in the molecular structure, and thereby increasing the amount of crosslinking, is to expose the cured epoxy resin to a temperature higher than that used during the curing; this is known as postcuring.

In reference 2 the effects of postcuring on the shear properties of a pultruded glass-reinforced epoxy composite are discussed. The postcuring was performed for several hours in an oven, after the pultrusion had been completed. However, in order to incorporate the automated, mass-production aspect of pultrusion, the pultruded composite should be postcured in line with the pultrusion, after it exits the curing die or while it is
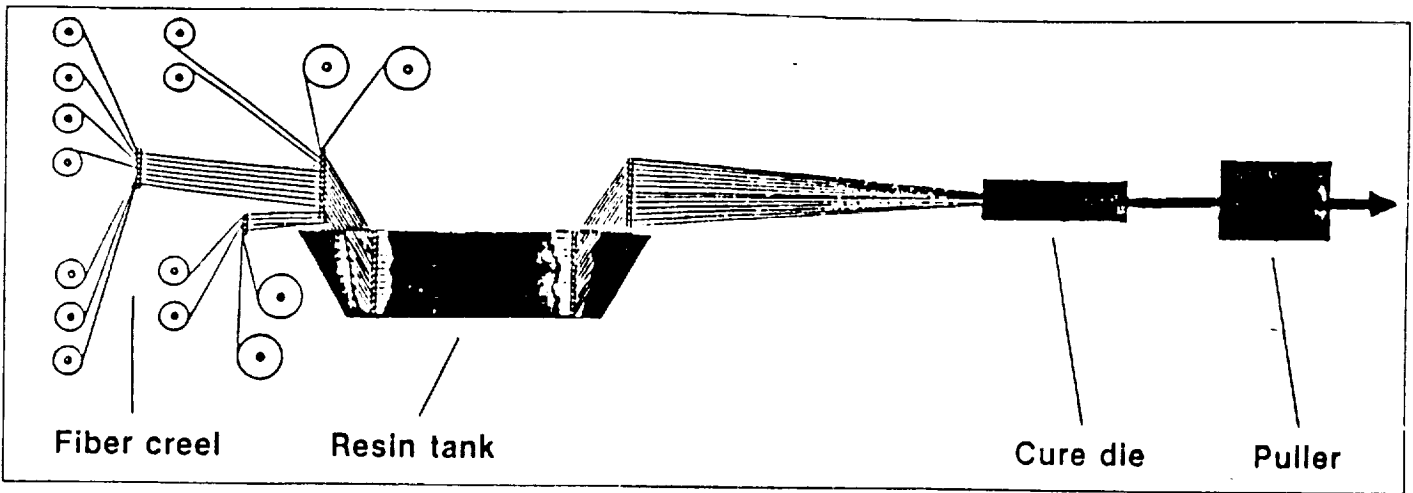
Figure 4. Profile Schematic of Pultrusion System.

perature is too high. The combination of lower strength and higher stiffness is embrittlement due to the excessive temperature during postcure.

The effect of the postcuring on the flexural modulus of the neat epoxy resin is shown in Figure 8. The modulus increases as the postcure temperature is increased. Both crosslinking and chain scissioning are candidates for the observed increase in the modulus as the postcure temperature was increased. Crosslinking causes stiffer material, and the chain scissioning of a highly crosslinked structure renders small clusters of highly crosslinked structure. The resulting chain scissioned material may be less strong but more stiff. This is the description of an embrittled material, which is probably the consequence of the exposures at the higher postcure temperatures.

The variability in the data for the neat resin flexural specimens after postcuring is generally larger than it is for no postcure. An explanation for this difference is that the specimens were machined to the test thickness after the postcures, resulting in different residual internal stress patterns among the specimens.

Composites
FLEXURAL DATA

Figure 9 shows that for no postcure the ultimate flexural strengths of the pultruded specimens were similar to those of unidirectional autoclaved specimens. The reference points for carbon-epoxy and aramid-epoxy autoclaved composites were taken from chapter 11 of reference 11, and the reference point for the glass-epoxy composite was taken from reference 12. Note

Figure 5. Ultimate Flexural Stress at Room Temperature of Neat Epoxy Resin for Different Postcure Temperatures. (Average Values With + One Standard Deviation Error Bands.)
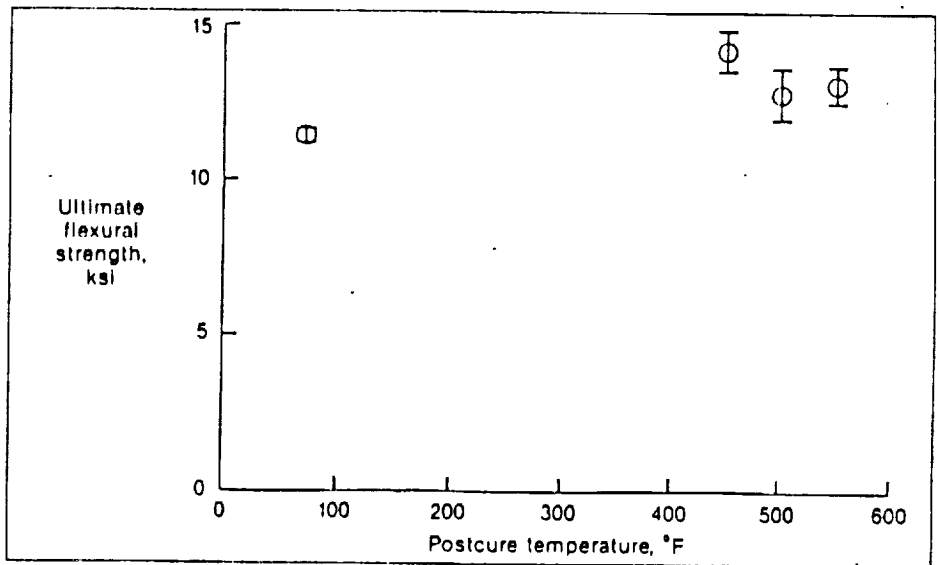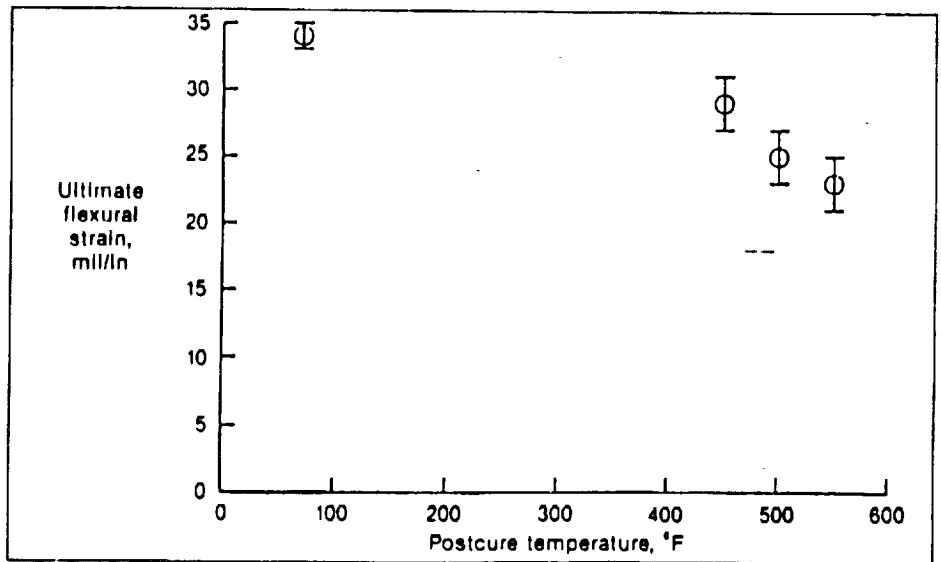

Figure 6. Ultimate Flexural Strain at Room Temperature of Neat Epoxy Resin for Different Postcure Temperatures. (Average Values With + One Standard Deviation Error Bands.)
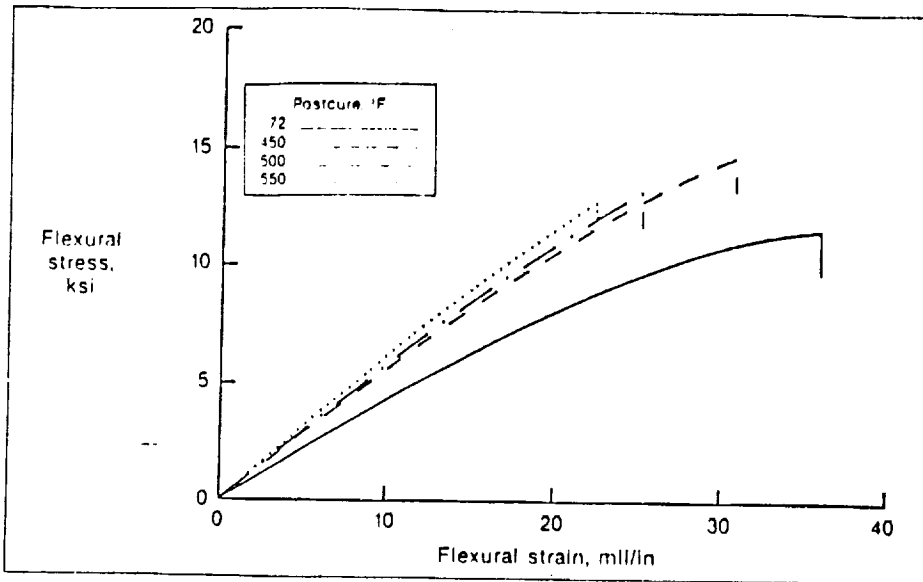
Figure 7. Flexural Stress-Strain Curves at Room Temperature of Neat-Resin Specimens of the Epoxy Used for Pultrusion for Different Postcure Temperatures.
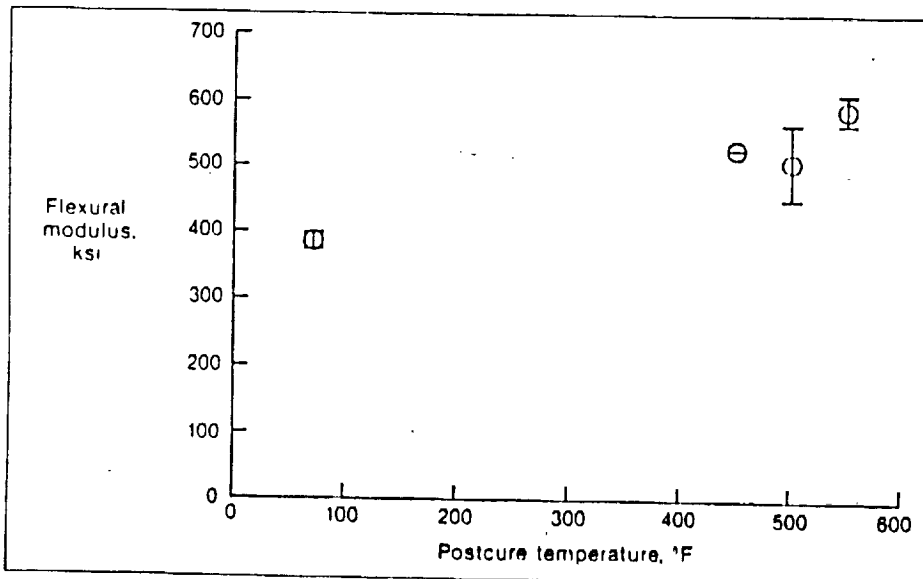

Figure 8. Flexural Elastic Modulus at Room Temperature of Neat Epoxy Resin for Different Postcure Temperatures. (Average Values With + One Standard Deviation Error Bands.)

that the variability in the data for the composites is similar for no postcure and for the postcures at all temperatures. The composite specimens were completely fabricated to the test dimensions before the postcuring was conducted; hence, any residual stresses introduced by the machining were probably relaxed by the postcuring.

For the pultruded carbon-fiber composite, the 450°F and higher postcures decreased the average ultimate flexural strength. Visual inspection after testing indicated that, for no postcure and for the postcures at 400 and 450°F, tensile failure occurred on the tension side of

the specimens while a small amount of interlaminar shear failure occurred on the compression side. For the higher temperature postcures interlaminar shear was the dominant mode of failure.

Flexural stress-strain curves for the postcured carbon-epoxy specimens are given in Figure 10; each curve is for a typical specimen for the postcure it represents. These curves also show, as was seen in Figure 8, that higher postcure temperatures caused decreases in the ultimate flexural strength. The curves indicate that the failures occurred in steps, as was suggested by the occurrence of the shear failure mode mentioned previously.

The pultruded glass-fiber composite's ultimate flexural strength, shown in Figure 8, also decreased for postcures at 500 and 550°F, but the decrease was less than for the carbon-fiber composite. A visual inspection of the tested specimens indicated that the flexural specimens failed in tension for all the postcure temperatures; there was no indication of shear failure. Representative stress-strain curves for the glass-fiber composite shown in Figure 11 indicate that the ultimate flexural strength decreased for the two highest postcure temperatures and that there was little or no shear failure.

The pultruded aramid-fiber composite's ultimate flexural strength was not significantly altered by the postcuring (Figure 8). The failure was predominantly in tension.

The ultimate flexural strains for the three different fiber systems are shown in Figure 12. In general, postcuring caused a small decrease in the ultimate strain, which was expected because of the additional crosslinking produced by the postcures. No flexural strain reference data was found for specimens made from composites fabricated by either high-pressure/high-temperature or autoclaved methods.

As shown in Figure 13, the postcuring caused small decreases in the flexural moduli for all three fiber systems. Since the postcuring produced additional crosslinking within the resin, the opposite, an increase in stiffness, would have been expected. However this apparent discrepancy is explained in the following discussion of the shear data and the changes which occurred at the fiber-resin interface.

Shear data

The ultimate shear strengths from compression in-plane shear tests of double-notched composite specimens are shown in Figure 14. The postcuring significantly reduced the shear strength of the pultruded carbon-fiber composite, but had little or no effect on the shear strength of either the pultruded glass-fiber or aramid-fiber composite. Figure 14 also shows that the pultruded materials' shear strengths are lower than the values for autoclaved composite materials of the same fiber type.

Figure 15 shows scanning electron microscopy (SEM) photomicrographs of the shear failure surfaces of carbon-fiber specimens with no postcure and for after
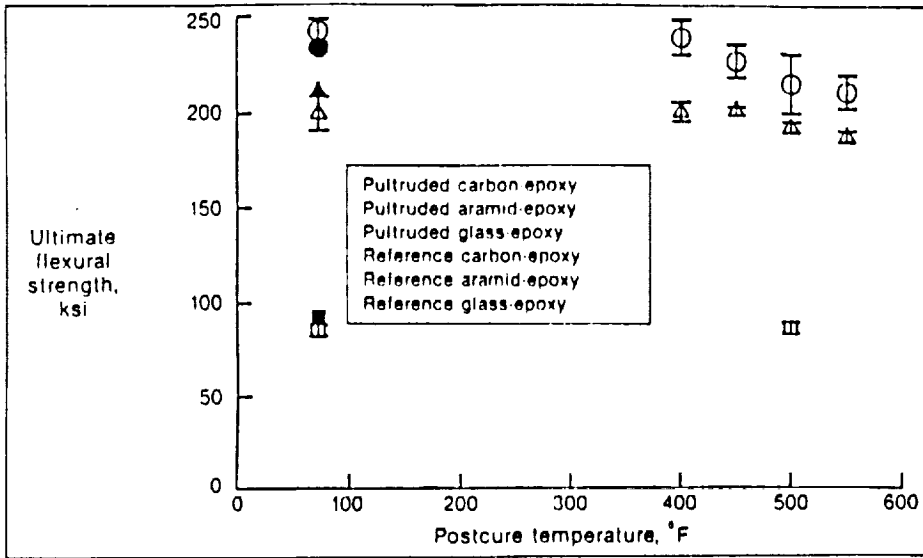
Figure 9. Ultimate Flexural Stress at Room Temperature of Pultruded Fiber-Reinforced-Epoxy Composites for Different Postcure Temperatures. (Average Values With + One Standard Deviation Error Bands; Reference 10 for Carbon-Epoxy and Aramid-Epoxy and Reference 11 for Glass-Epoxy.)
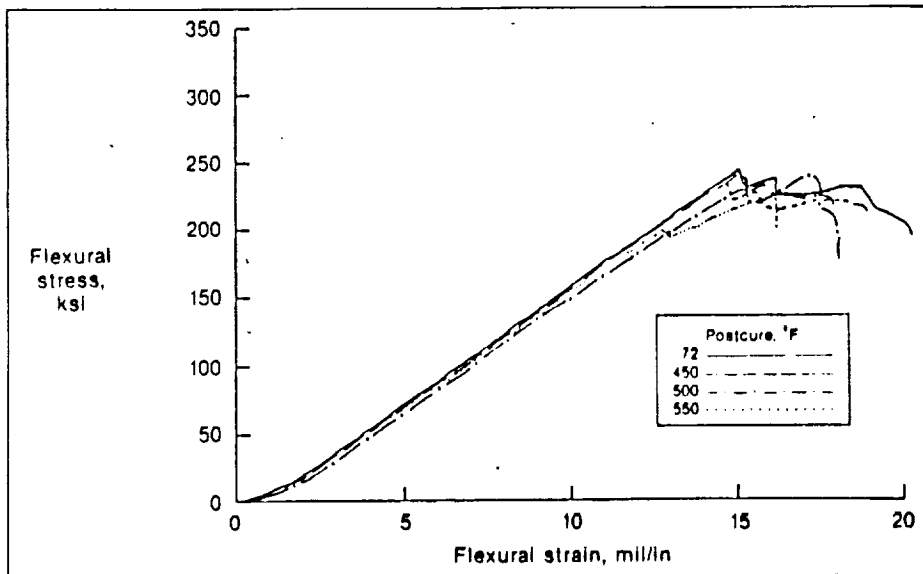

Figure 10. Flexural Stress-Strain Curves at Room Temperature of Pultruded Carbon-Fiber-Reinforced Epoxy Composites for Different Postcure Temperatures.

pultrusion fabrication process, the fiber tows are subjected to longitudinal loads that cause them to be in tight bundles as they pass through the resin bath. Even with the "ladder rungs" in the bath, the tows tend to bundle between sets of rungs. The bundling prevents adequate resin penetration into each tow and, hence, insufficient wetting of the fibers inside each tow. The actual penetration and wetting of the fibers within each tow takes place under the pressure generated within the die before the resin gels. The Epon 9310 resin, however, is formulated to have a very short gel time at higher temperatures.

Carbon fiber is a much better thermal conductor than are the glass and aramid fibers; so, the resin throughout the cross section of a carbon-fiber epoxy-resin combination would experience a higher temperature. This could cause the epoxy to gel more quickly with an excess of resin as a coating around each tow and with dry fibers inside each tow; that is, inadequate consolidation.

As stated earlier, the gelation of the epoxy is due to the crosslinking; but, the crosslinking also causes shrinkage of the epoxy volume. Any pockets of gelled epoxy would cause excessive local shrinkage, which would tend to degrade an already-poor fiber-resin interface. The higher the temperature, the greater the crosslinking and, hence, the greater the shrinkage. Unlike the autoclave process that externally applies and maintains pressure, the pultrusion process relies on internal pressure generated by passing a slightly excessive volume of fiber and resin through a die. The shrinkage of the epoxy during curing (gelation) therefore causes a drop in pressure which is not compensated. Thus, the quality of the interface and, therefore, the value of shear strength can be lower for higher temperature postcures.

This line of thought would also suggest that, even without any postcure, the fiber-resin interface properties of the carbon fibers with the epoxy designed for pultrusion could be worse than with the epoxies which gel more slowly, such as those used in the autoclave processes. This may, therefore, provide an explanation for the lower shear strength of the pultruded carbon-epoxy composite compared with the autoclaved composites that used the slower gelling epoxies.

Toughness

A major advantage of pultruded com-

postcure at 550°F. Cohesive failure occurred in the matrix in the no-postcure specimen, while adhesive failure between fiber and matrix occurred for the 550°F postcure. In contrast, for the other two fiber types, there was cohesive failure for no postcure and primarily cohesive failure for the higher temperature postcures. In addition, a small amount of adhesive failure occurred for the higher temperature postcures for the glass- and aramid-fiber composites; however, the amount of adhesive failure was less than for the carbon-fiber composite.

The presence of adhesive failure after the highest temperature postcure, of

which there was a particularly significant amount for the carbon-fiber composite, was probably due to degradation of the fiber-resin interface. The degradation of the carbon-resin interface is also an explanation for the large amount of shear failure in the flexural tests and the large decrease in the ultimate shear strength after the higher temperature postcures for the carbon-fiber composite.

There is no definitive explanation from these data for the degradation of the fiber-resin interface in the pultruded carbon fiber reinforced composite; however, several degradation mechanisms can be postulated: During the

'Standard Test Method for In-Plane Shear Strength of Reinforced Plastics. ASTM Standard D3846, 1982 Book of ASTM Standards, Part 35, (1982).
'Standard Tests for Toughened Resin Composites. NASA Reference Publication 1092, July, (1983).
'°*An Introduction to Radiation Chemistry*, J. W. T. Spinks and R. J. Woods, John Wiley and Sons, p. 160, (1964).
''*Handbook of Composites*, ed. by George Lubin, Van Nostrand Reingold Company, p. 256, (1982).
'²*Handbook of Plastics and Elastomers*, ed. by Charles A. Harper, McGraw-Hill Publishing Company, p. 5.12, (1975).
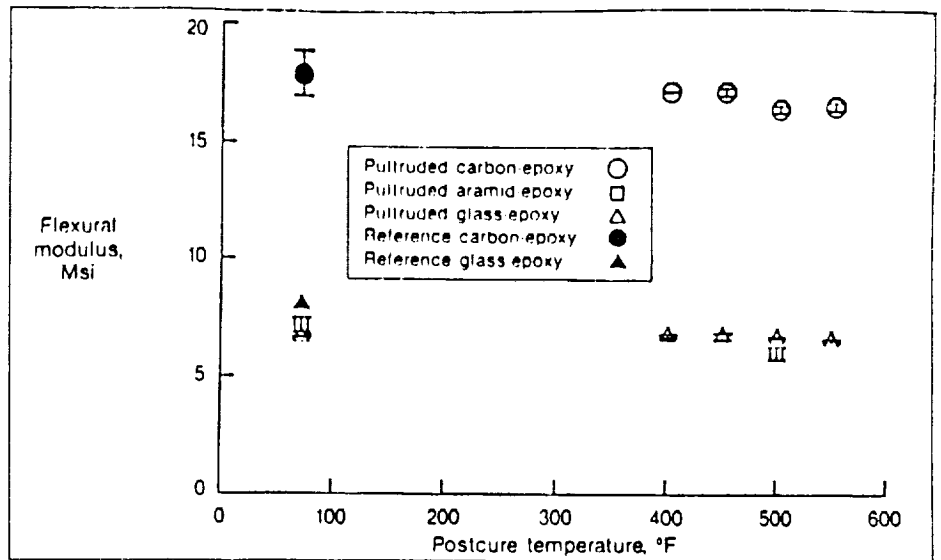
Figure 13. Flexural Elastic Modulus at Room Temperature of Pultruded Fiber-Reinforced Epoxy Composites for Different Postcure Temperatures. (Average Values With + One Standard Deviation Error Bands; Reference 10 For Carbon-Epoxy and Reference 11 for Glass-Epoxy.)

Figure 14. Ultimate Shear Stress at Room Temperature of Pultruded Fiber-Reinforced Epoxy Composites for Different Postcure Temperatures. (Average Values With + One Standard Deviation Error Bands; Reference 10 for Carbon-Epoxy and Aramid-Epoxy and Reference 11 For Glass-Epoxy.)

Figure 16. Interlaminar Fracture Toughness at Room Temperature of Pultruded Fiber-Reinforced Epoxy Composites for Different Postcure Temperatures.

(a) No postcure.

(b) 550 °F postcure.
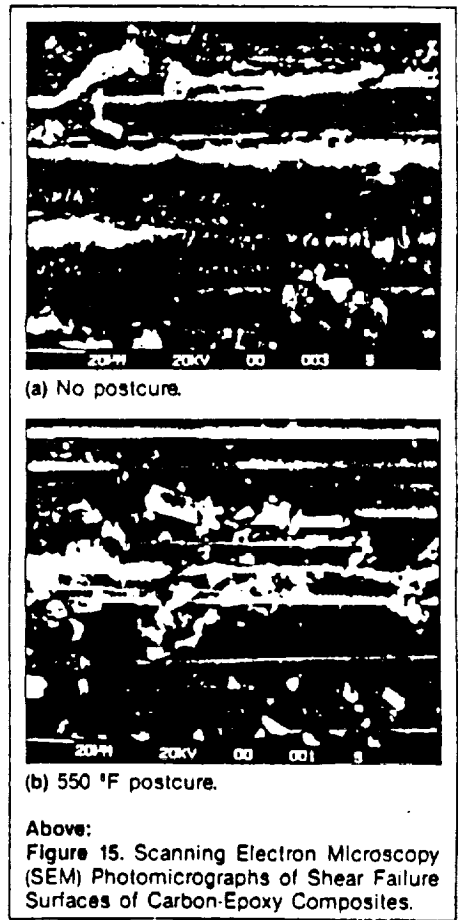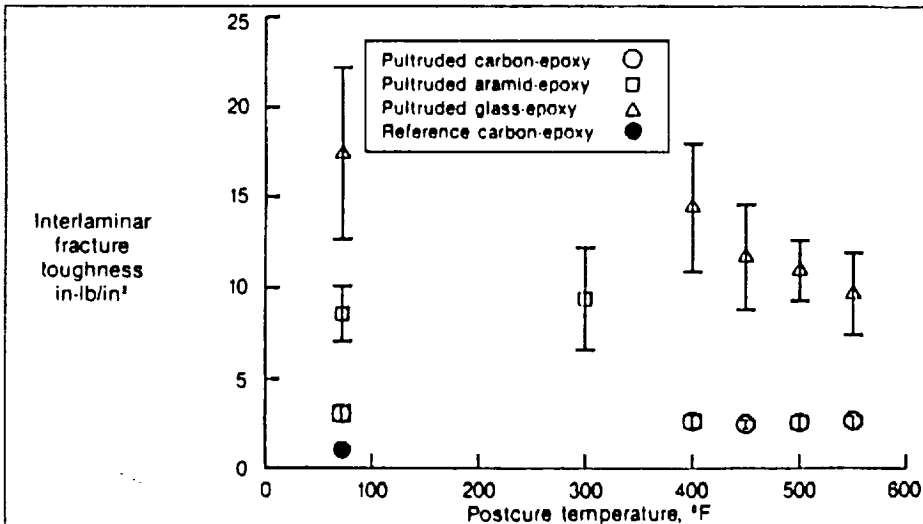
Above:
Figure 15. Scanning Electron Microscopy (SEM) Photomicrographs of Shear Failure Surfaces of Carbon-Epoxy Composites.

Left:
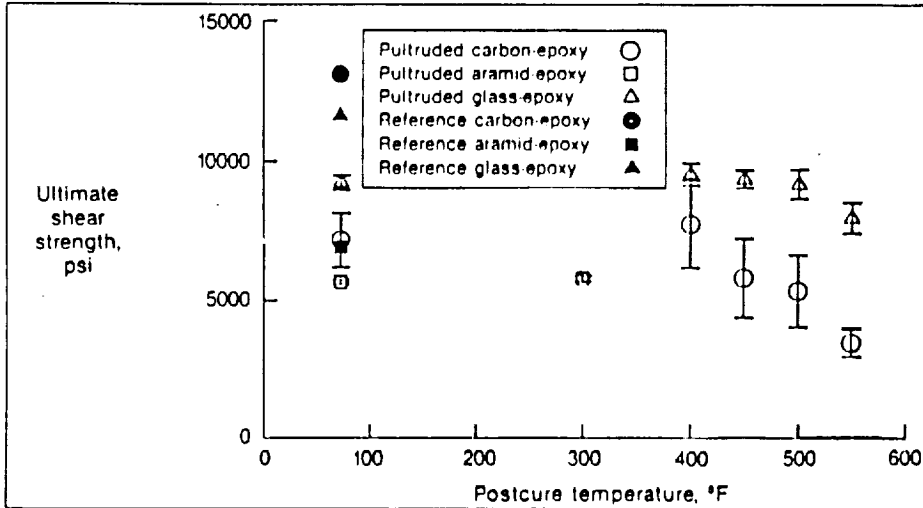Figure 16. Interlaminar Fracture Toughness at Room Temperature of Pultruded Fiber-Reinforced Epoxy Composites for Different Postcure Temperatures. (Average Values With + One Standard Deviation Error Bands; Reference 10 for Carbon-Epoxy.)

APPENDIX G

**NASA
Technical
Paper
2928**

1989

Absorbed Dose Thresholds and Absorbed Dose Rate Limitations for Studies of Electron Radiation Effects on Polyetherimides

Edward R. Long, Jr.,
and Sheila Ann T. Long
*Langley Research Center
Hampton, Virginia*

Stephanie L. Gray
and William D. Collins
*Old Dominion University
Norfolk, Virginia*

Summary

The effects of electron radiation on Ultem, a polyetherimide manufactured by General Electric Company, were studied for total absorbed doses from 1.0 kGY to 100 MGy at absorbed dose rates from 0.01 to 100 MGy/hr. Tensile property tests and electron paramagnetic resonance (EPR) spectroscopic measurements were conducted on Ultem film. (The EPR spectroscopy provides the density of radicals which are created when molecular bonds are homolytically broken by the radiation.)

There was an effect of total absorbed dose on the tensile properties and the radical densities of Ultem. For a 1.0-kGy total absorbed dose, the elastic modulus, the ultimate tensile strength, and the elongation-to-failure all decreased slightly. These changes in the tensile properties were maintained for all total absorbed doses up to 1.0 MGy. Above 1.0 MGy for the elastic modulus and above 2.5 MGy for the ultimate strength, there were additional changes. For a 100-MGy total absorbed dose, the modulus and the strength were, respectively, ten percent and twenty percent less than the nonexposed values. A pronounced decrease in elongation-to-failure occurred at approximately 2.5 MGy. Above this total absorbed dose the elongation-to-failure was four percent of the nonexposed value. In contrast to the tensile data, the radical densities increased monotonically with total absorbed dose.

There was no significant absorbed dose rate effect observed for either the tensile properties or radical densities.

A molecular model for the radiation effects has been reported earlier (NASA TP-2663, 1987). The model showed that the radical formation was due to homolytic scissioning of primary bonds within the linear molecular structure and that the radicals were the source of subsequent crosslinking. The chain scissioning and crosslinking cause the changes the the tensile properties. This published model of radiation effects and the radical densities and their rates of change presented in this report are used to explain the effects of total absorbed dose and absorbed dose rate on the tensile properties of Ultem. The onset of changes in the tensile properties at 1.0 to 2.5 MGy occurred because 25 or more percent of the polymer molecules were crosslinked. An absorbed dose rate effect was not found because the rate of radical creation significantly exceeded the rate of radical decay for all the exposures conducted.

Introduction

Polymer resins are useful in space as low density insulations, solar-cell substrates, and composite matrices. Long-term stability in ionizing space radiation environments, as in geosynchronous orbit, is an important consideration for these applications.

Polyetherimides (PEI) are among the high-temperature thermoplastic polymers being considered for future space applications. They maintain desirable mechanical properties at temperatures of 300°C or above. They can be used as foams, films, castings, and matrices for fiber-reinforced composites. However, a recent study, reference 1, has shown that the tensile properties of a PEI are significantly affected by the total absorbed doses anticipated for approximately 30-year service in geosynchronous orbit.

The research reported in references 1–3 used total absorbed doses from 20 to 60 MGy at an absorbed dose rate of 10 MGy/hr exposures to assess the changes in the tensile properties of polyimides for total absorbed doses equivalent to approximately 30-year exposure to the ionizing radiation in geosychronous orbit (GEO). Smaller total absorbed doses were not studied to determine the doses at which changes are first observed nor to determine how the changes vary with total dose. The earlier work used an absorbed dose rate of 10 MGy/hr, for which the specimen temperature was found not to exceed 38°C. An assumption was made that there would not be thermal artifacts at or below this temperature. Additional absorbed dose rates were not studied.

In reference 2, the effects of the ionizing radiation on the molecular structure of the PEI were determined to be both chain scissioning and crosslinking. In brief, the radiation cleaved the main-chain bonds at two sites and dehydrogenated the pendant group as shown in figure 1. These cleavages, or chain scissions, and dehydrogenations were homolytic; therefore, several types of radicals were generated. (Homolytic bond cleavage means that the atoms sharing the bond each retained an electron from the pair shared during bonding; therefore each has an unpaired electron.) The chemical structures of the radicals are shown in figure 2. In all, six different radicals were created. Two of these radicals, the hydrogen and the phenyl, were not observed because they immediately combined with one another. The other four radicals, as shown in figure 3, generated crosslinked structures as shown in figure 4. (The two radicals not observed were known to have initially existed because of the detection of the other four.)

The objectives of this study were (1) to determine the effects of ionizing radiation on the tensile and molecular properties of the polyetherimide for total absorbed doses which are expected in GEO for lengths of time from hours to years, (2) to determine the effects of absorbed dose rate, and (3) to

correlate the radical density and tensile property data to understand total absorbed dose and absorbed dose rate effects. In this report, data are presented and compared for total absorbed doses from 1.0 kGy to 100 MGy and for absorbed dose rates from 0.01 MGy/hr to 100 MGy/hr. The total absorbed doses are equivalent to exposure times from 2.5 hr to 30 years in GEO. The absorbed dose rates are accelerations of the absorbed dose rate in GEO by factors from 26 to 2.6×10^5.

Materials and Specimens

The polyetherimide material was Ultem, a product of General Electric Company. The Ultem was type 1000, the density for which is 1.27 g/cm^3, and was in the form of 0.0075-cm film for both the EPR and the tensile specimens. The tensile specimens were 0.5 ± 0.0025 cm wide and 15 ± 0.25 cm long, with a gage length of 5 cm. The EPR specimens were 0.25 ± 0.0025 cm wide and 0.15 ± 0.0075 cm long. The specimens were fabricated from larger pieces of film, using dual razor blade cutters. Details of the specimen preparation are in reference 2. At least six tensile and four EPR specimens were tested for each exposure condition.

Experimental Procedures

Tensile and EPR specimens in this study were simultaneously exposed to 100-keV electron radiation for total absorbed doses from 1.0 kGy to 100 MGy at absorbed dose rates from 0.01 to 100 MGy/hr. A 1-kGy total absorbed dose is equivalent to a 2.5-hr exposure in GEO. A 100-MGy total absorbed dose is equivalent to the largest absorbed dose estimated for a 30-year exposure in GEO.

Both the tensile and the EPR specimens were placed in liquid nitrogen within 3 min of the completion of an exposure to "freeze" the molecular structural components present at the end of the exposure. For the EPR tests, this meant that all the unpaired electrons (radicals) caused by breaking molecular bonds (except those with half-lives of seconds or less) were trapped and therefore their spectra could be observed. The testing began immediately thereafter.

The tensile specimens were brought to room temperature, one at a time, and tested by using a model 1130 tabletop Instron universal mechanical test machine. The faces of the specimen grips were rubber surfaced. The grip displacement during each test was monitored with a direct displacement transducer (DCDT). The outputs of the DCDT and the load cell were recorded on an X-Y recorder. The crosshead rate was 0.2 in/min. A minimum of six specimens were tested per exposure condition.

For recording spectra, the EPR specimens were placed in quartz glass tubes. The tubes were sealed with rubber caps, and the end of the tubes containing the specimens were kept in liquid nitrogen until the first EPR scan, during which they were maintained in a thermal environment of $-188°$C. The EPR spectrometer was a Varian E-Line Century Series Model E-109E. The spectrometer system included a variable temperature accessory for controlling the temperature during the scans, a precision microwave frequency counter, and a gaussmeter. Following the first scan, the sealed tubes were brought to room temperature for 10 min and immediately afterwards stored in the liquid nitrogen. Then, another cycle of EPR scanning was conducted, followed by another 10 min at room temperature. In this manner, the postirradiation radical decay at room temperature was measured for accumulated exposure at room temperature up to 10 hr.

More complete descriptions of the radiation facility, the testing equipment, the specimens, and the manner in which they were prepared and handled are given in reference 2. The methods used for monitoring the dose rate and the specimen temperature and other experimental details are also described in reference 2.

Results and Discussion

Tensile Properties

Load-elongation behavior. With no radiation exposure, Ultem film elongates under tensile loading in a manner shown in figure 5. The load increases with elongation through the elastic region and into the yield or plastic region (region 1 in fig. 5). Further loading causes a local necking in the specimen, during which the load drops because of the sudden additional yielding (region 2). The necking then extends and the load gradually increases (region 3) until the specimen breaks, at which point the load is nearly back to the value it was at the onset of the initial local necking. For specimens exposed to electron radiation, the extent of the local necking is reduced, with increasing total absorbed dose, until there is none; that is, the elongation is uniform along the entire gage length. Further increases of the total absorbed dose reduce the extent of this uniform elongation.

Elastic modulus. In figure 6, the room temperature elastic modulus is plotted as a function of the total absorbed dose. The band shown for each group of data is the envelope for 1 σ (one standard deviation) of the data. The tensile modulus decreased

2

slightly for the smallest total absorbed dose. The average nonirradiated value was 427 ksi, and the average value for a 1-kGy total absorbed dose was 409 ksi, a 4-percent decrease which was within the 1 σ of the data. At the largest total absorbed dose, 100 MGy, the average modulus was 384 ksi, a 10-percent decrease from the nonirradiated value.

A determination of absorbed dose rate effects on the modulus can be made by plotting a portion of the modulus data as a function of absorbed dose rate. The data at 0.1, 1.0, and 10, 100 MGy in figure 6 (the total absorbed doses for which there was more than one dose rate) are plotted in figure 7 as a function of absorbed dose rate. There is no trend with respect to absorbed dose rate. There is overlap of the 1 σ bands, and therefore there is no statistical difference between absorbed dose rates.

Ultimate strength. The ultimate strength data for Ultem film at room temperature are shown as a function of total absorbed dose in figure 8. The ultimate strength was 15.9 ksi for 1-kGy total absorbed dose, a 7-percent decrease from the nonirradiated value of 17.0 ksi. The change was approximately the same for total absorbed doses up to approximately 2.5 MGy, but above this total absorbed dose the ultimate strength decreased further until, at 100 MGy, it was 13.4 ksi, a 21-percent decrease from the nonirradiated value. The onset of additional change at the higher total absorbed doses appears to be a total absorbed dose effect and not an absorbed dose rate effect. Although the ultimate strength data point for 100 MGy/hr suggests an absorbed dose rate effect, it is not interpreted as such because the modulus data and the elongation-to-failure data for that absorbed dose rate do not suggest an absorbed dose rate effect. No explanation can be offered for why the ultimate tensile strength is the value it is for 100 MGy/hr.

The lack of a significant effect of absorbed dose rate on the ultimate strength may be seen by replotting a portion of the ultimate strength data as a function of absorbed dose rate. In figure 9, data for 0.1-, 1-, and 10-MGy total absorbed doses have been plotted as a function of absorbed dose rate. There is no significant change with absorbed dose rate and the 1 σ bands overlap each other.

Elongation to failure. Elongation-to-failure (ETF) data are shown as a function of total absorbed dose in figure 10. For total absorbed doses less than 2.5 MGy, the effect was small. At the smallest total absorbed dose, 1 kGy, the ETF was 116 percent, a 9-percent decrease from the nonirradiated value of 126-percent elongation. For total doses of 2.5 MGy or larger, the ETF reduced to 28 percent or less. The

ETF was 7.2 percent at 100 MGy, a 94-percent decrease from the nonirradiated value. Clearly there is a total absorbed dose threshold at approximately 2.5 MGy. In earlier studies, references 1-3, the large decreases in ETF at the higher total absorbed doses were shown to be due to crosslinking. The threshold at 2.5 MGy suggests either a sharp transition from little or no crosslinking to extensive crosslinking, or that a threshold amount of crosslinking was required for the large change in ETF. Solubility tests, which have been described in reference 2, were also conducted for these exposures; they indicated that crosslinking occurred for all the total absorbed doses and that the extent of crosslinking increased with the total dose. Hence, the change in ETF at approximately 2.5 MGy is an indication that a threshold amount of crosslinking is responsible, as opposed to a transition from no crosslinking to extensive crosslinking.

Figure 11 is a plot of the portion of ETF data in figure 10 for which there was more than one absorbed dose rate per total dose. The three lines, each of which connect data points for a total absorbed dose, are practically horizontal. Thus different absorbed dose rates did not significantly alter the effect of a given total absorbed dose.

Absorbed Dose Rate Effects

The unpaired electron densities 3 min after completion of the electron exposures are shown in figure 12. (In this study the unpaired electrons were radicals. Each electron has a spin value of 0.5.) As seen from the figure, there is no absorbed dose rate effect. Obviously the electron densities shown result from a combination of both radical creation and decay. The creation and decay rates must be studied separately to understand why there is no absorbed dose rate effect.

The decay of the radiation-generated radical density, starting 3 minutes after the completion of a 2.5-MGy absorbed dose exposure, is shown in figure 13. The decay curve has two parts, an initial portion, defined as the first six data points, and a long-time linear portion, represented by the last six data points.

The long-time portion is a straight line and fits first-order kinetics as discussed in reference 4:

$$-d(R_d)/dt = kR_d$$

The radical density R_d and the rate constant k are determined to be

$$R_d = 7.471 \times (10)^{16} e^{-0.086t}$$

and

$$k = .086s^{-1}$$

The rate of decay may be evaluated from this expression for any time; for example, at $t = 5$ hr,

$$d(R_d)/dt = -4.179 \times (10)^{15} \text{ spins/g-hr}$$

The data from the initial portion of the decay curve fit the expression for second-order kinetics

$$-d(R_d)/dt = 2k_1(R_d)^2$$

which integrates to

$$1/R_d - 1/R_{do} = 2k_1 t$$

where R_{do} is the radical density at time $t = 0$, with

$$R_{do} = 1.5 \times (10)^{17} \text{ spins/g}$$

$$d(R_d)/dt = -4.697 \times (10)^{17} \text{ spins/g-hr at } t = 0$$

and

$$k_1 = 5.17 \times (10)^{-18} \text{ (hr-spins/g)}^{-1}$$

In comparison to the decay rates at $t = 0$ hr and $t = 5$ hr, the rate of radical creation for the 2.5-MGy exposure was much higher. The dose was absorbed at a rate of 10 MGy/hr. Therefore, 1.56×10^{22} eV/g were absorbed at a rate of 6.25×10^{22} eV/g-hr. If each ion pair caused by this exposure resulted in a pair of radicals, then approximately 32 eV were required for every two radicals, according to reference 5. Thus, the total number of radicals created during the exposure was 9.7×10^{20} per gram at a rate of 3.9×10^{21} per gram per hour. This rate is four orders of magnitude greater than the decay rate at $t = 0$ hr. Using the same set of assumptions, the lowest absorbed dose rate in this study created radicals at a rate of 3.9×10^{19} per gram per hour, which is two orders of magnitude higher than the initial rate of radical decay. In other words, the rate at which radicals were created by the irradiations exceeded the rate at which these radicals decayed for all of the absorbed dose rates investigated and, therefore, there was no absorbed dose rate effect for the tensile properties.

Total Absorbed Dose and Broken Bond Thresholds for Crosslinking

In the preceding discussion of elongation-to-failure data the large change in ETF for total absorbed doses of 2.5 MGy and higher was attributed to a threshold amount of crosslinking where the

crosslinking monotonically increases with total absorbed dose. But crosslinking requires that bonds are broken in the original linear molecular structure. Therefore, there should also be a threshold of broken bond density for the large change in ETF to occur. The ETF is plotted as a function of broken bond density (one-half the radical density) in figure 14. Indeed, there appears to be a value for the broken bond density below which there is little or no change and above which there is a very extensive decrease. The threshold value, from figure 14, is approximately 7×10^{16} broken bonds per gram of material.

In the preceding discussion of absorbed dose rate effects, the total number of radicals created per gram of material during the exposure at 10 Mg/hr was estimated to be 9.7×10^{20}, which is twice the total number of broken bonds per gram of material. Not every broken bond will result in a crosslink but, as reference 6 indicates, significant changes in the properties of a polymer will occur if 0.1 percent of the changes, such as crosslinking, are permanent. If 0.1 percent of the broken bonds were to result in crosslinking, then 4.9×10^{17} crosslinks per gram of material would occur. The average molecular weight of Ultem 1000 is 42 000 g/mole (verbal communication with Paul M. Hergenrother, Polymeric Materials Branch, Materials Division, NASA Langley Research Center) so there are 1.48×10^{19} molecules per gram of material. Therefore, at least approximately 3 percent of the polymer molecules must be crosslinked in order for a large change in elongation to failure to occur.

Concluding Remarks

The threshold values of total absorbed dose for causing changes in tensile properties of a polyetherimide film and the limitations of the absorbed dose rate for accelerated-exposure evaluation of the effects of electron radiation in geosynchronous orbit have been studied. Total absorbed doses from 1.0 kGy to 100 MGy and absorbed dose rates from .01 to 100 MGy/hr were investigated.

Total absorbed doses less than 2.5 MGy did not significantly change the tensile properties of the film, whereas absorbed doses 2.5 MGy or larger significantly reduced the elongation to failure. From electron paramagnetic resonance spectroscopic measurements, at least 3 percent of the molecules of the originally linear polymer were crosslinked by the 2.5 MGy absorbed dose.

There was no measurable effect of the absorbed dose rate on the tensile properties. The rate at which radicals were created by the irradiations exceeded the rate at which these radicals decayed, for all of the absorbed dose rates investigated.

NASA Langley Research Center
Hampton, VA 23665-5225
June 28, 1989

References

1. Long, Edward R., Jr.; and Long, Sheila Ann T.: *Spectroscopic Comparison of Effects of Electron Radiation on Mechanical Properties of Two Polyimides.* NASA TP-2663, 1987.

2. Long, Edward R., Jr.; and Long, Sheila Ann T.: *Spectroscopic Analysis of Radiation-Generated Changes in Tensile Properties of a Polyetherimide Film.* NASA TP-2429, 1985.

3. Long, Sheila Ann T.; Long, Edward R., Jr.; Ries, Heidi R.; and Harries, Wynford L.: Electron-Radiation Effects on the AC and DC Electrical Properties and Unpaired Electron Densities of Three Aerospace Polymers. *IEEE Trans. Nucl. Sci.*, vol. NS-33, no. 6, Dec. 1986, pp. 1390–1395.

4. Matheson, Max S.; and Dorfman, Leon M.: *Pulse Radiolysis.* M.I.T. Press, c.1969.

5. Bolt, Robert O.; and Carroll, James G., eds.: *Radiation Effects on Organic Materials.* Academic Press, Inc., 1963.

6. Spinks, J. W. T.; and Woods, R. J.: *An Introduction to Radiation Chemistry.* John Wiley & Sons, Inc., c.1964.
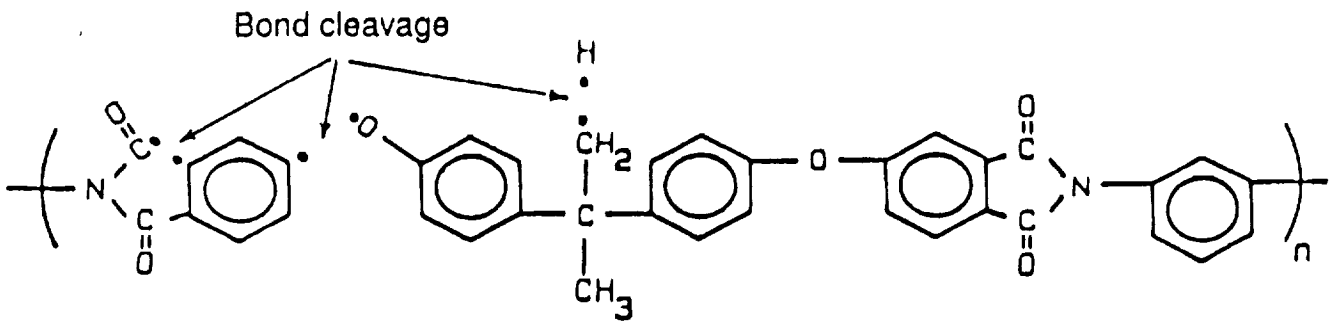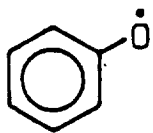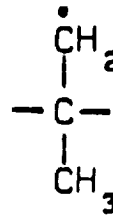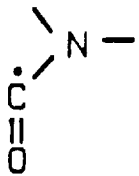
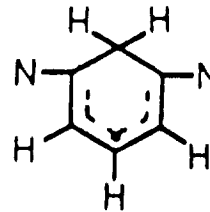Figure 1. Homolytic bond breakage in polyetherimide caused by electron radiation.

Figure 2. Radical species in polyetherimide generated by electron radiation.
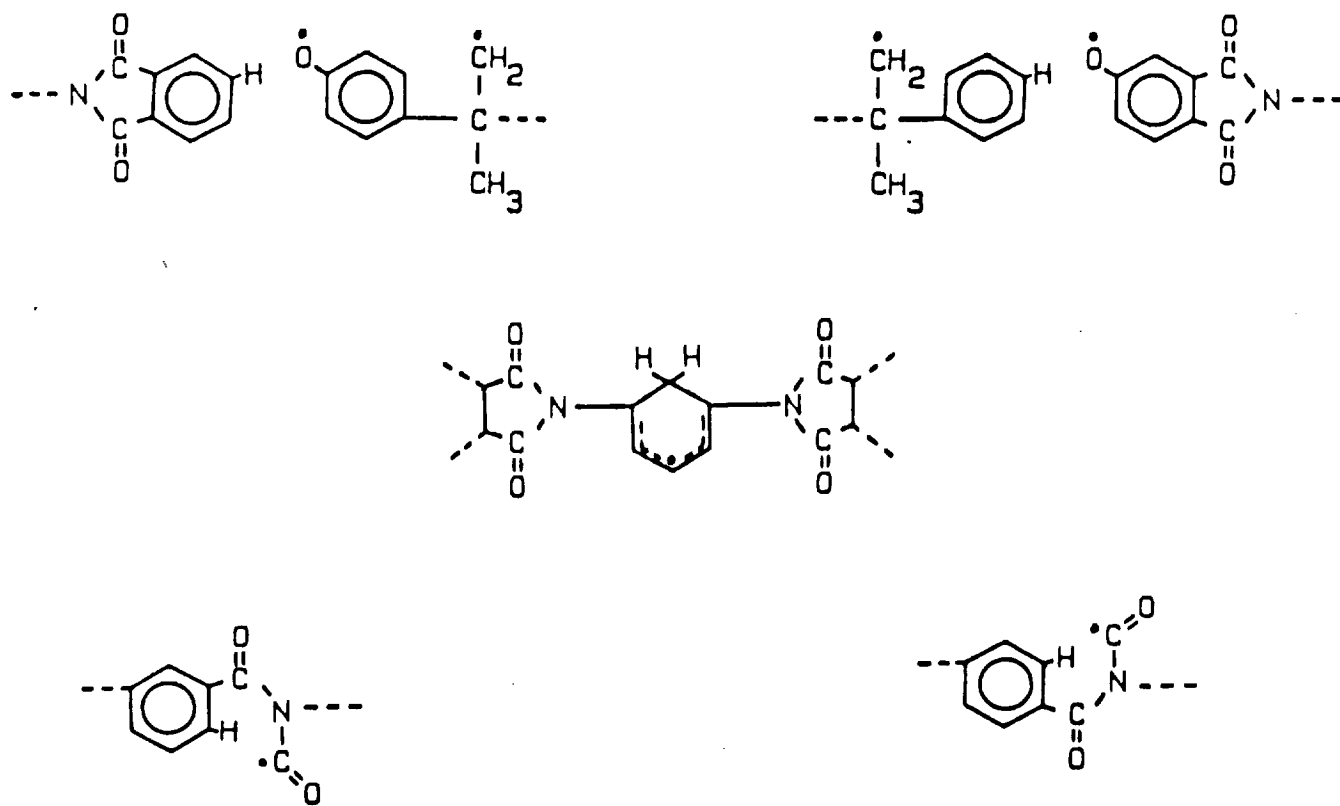
Figure 3. Radicals in electron-irradiated polyetherimide.

(a) Ethylene.

(b) Amide.

(c) Ether.

(d) Urethane.

(e) Peroxide.
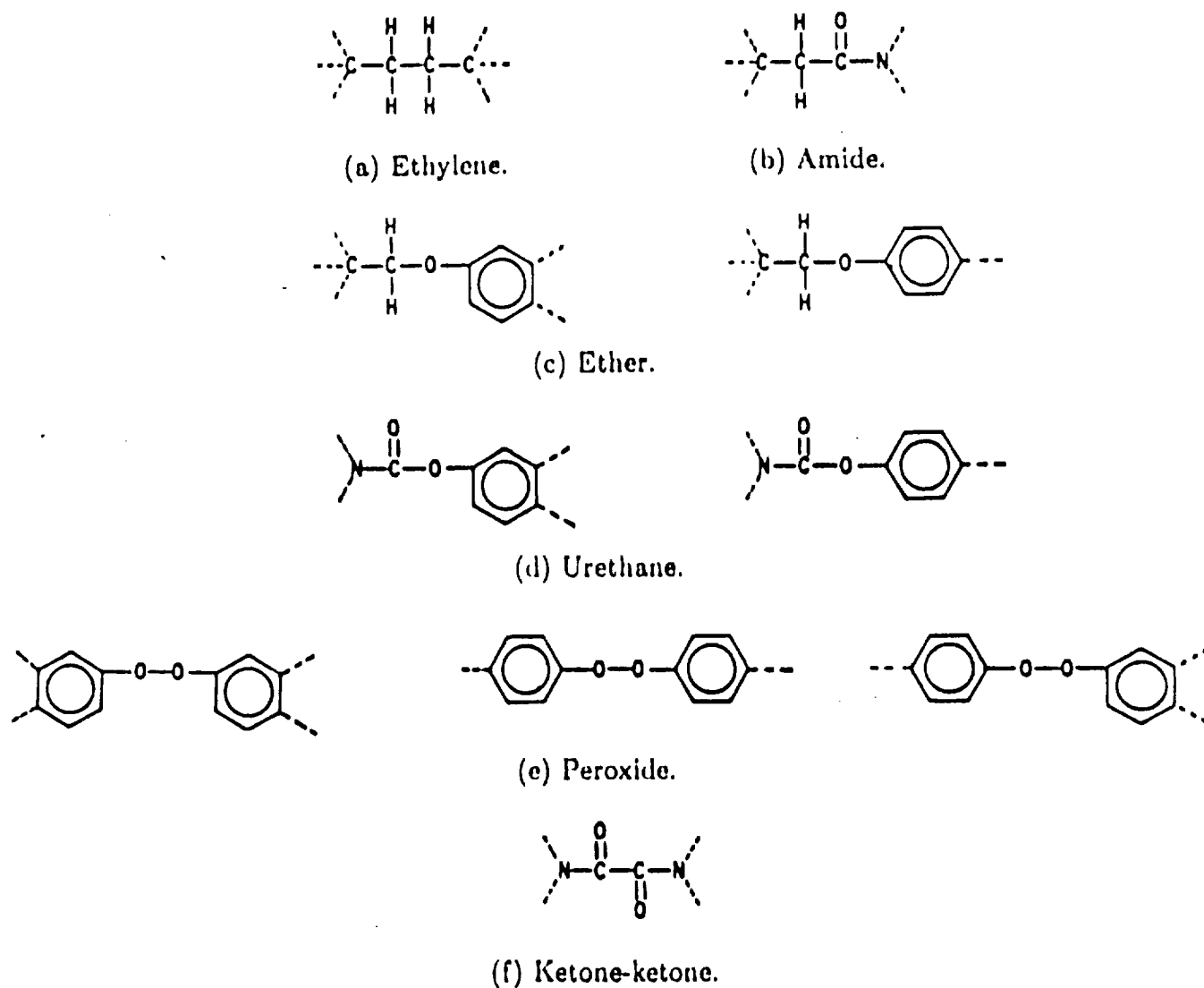
(f) Ketone-ketone.

Figure 4. Crosslinked structures in electron-irradiated polyetherimide formed by combinations of radicals.
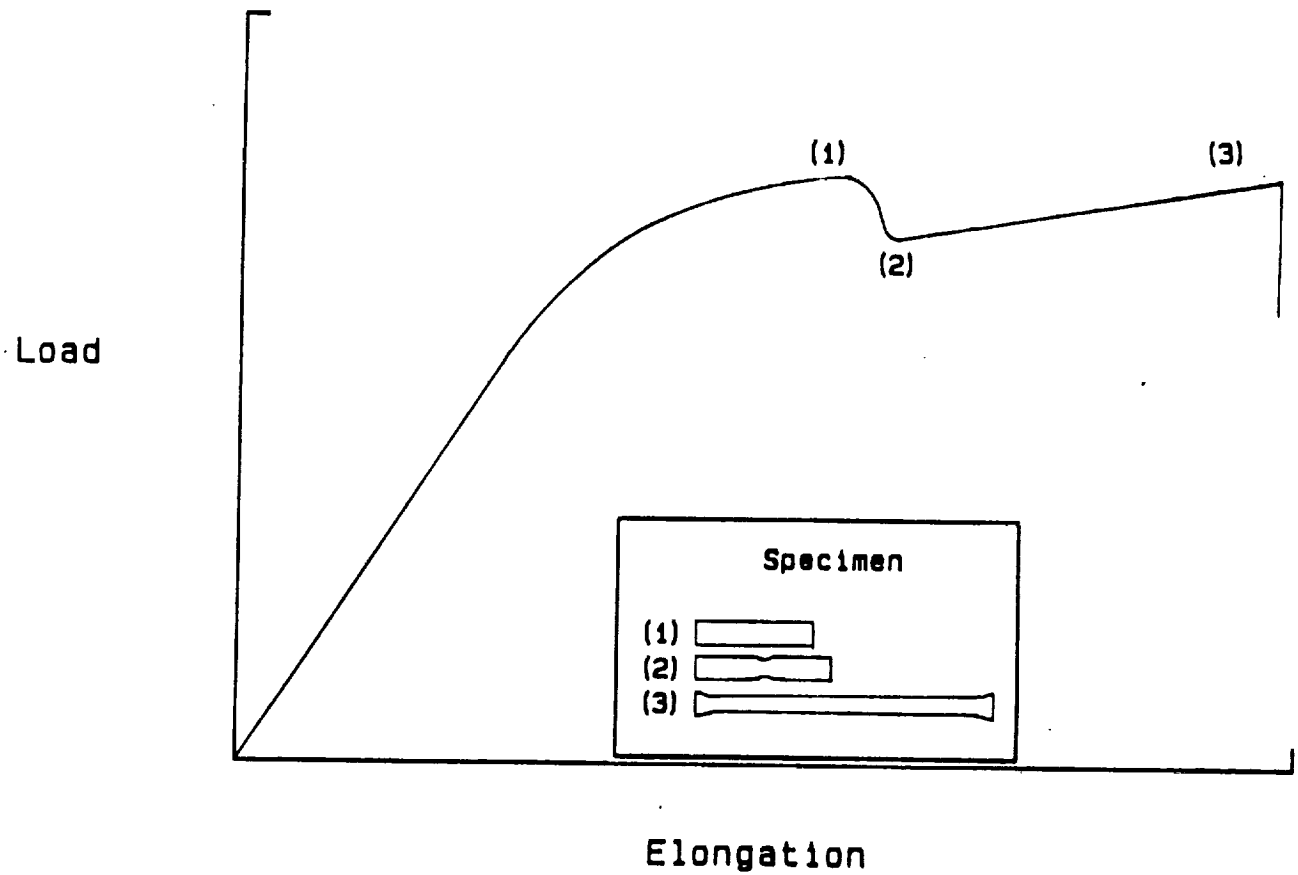
Figure 5. Relationship between load and elongation for nonirradiated polyetherimide. The shape of the gauge section of the specimen at three elongations is shown in the insert.
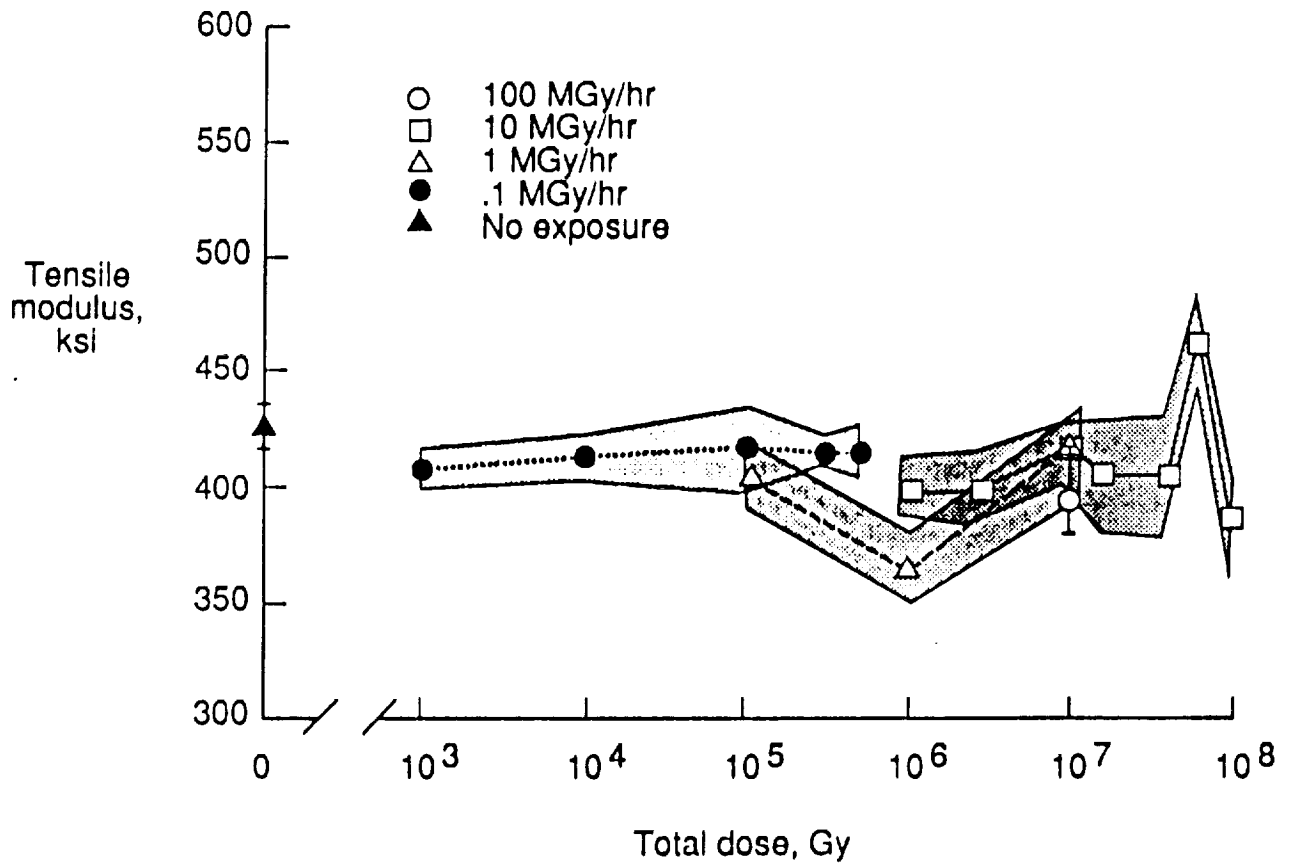
Figure 6. Elastic tensile modulus of electron-irradiated polyetherimide for four dose rates.
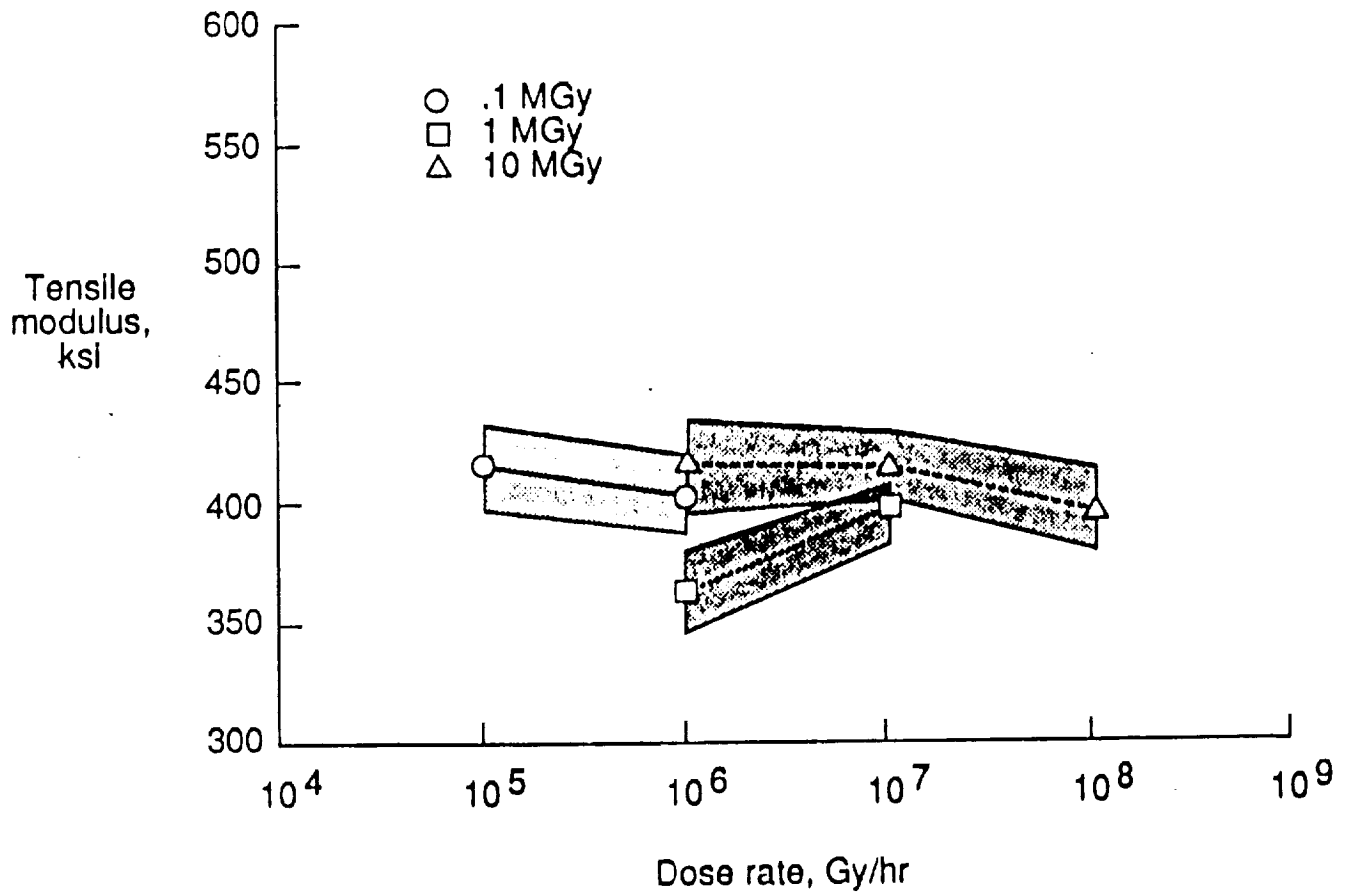
Figure 7. Elastic tensile modulus of electron-irradiated polyetherimide for three total absorbed doses.
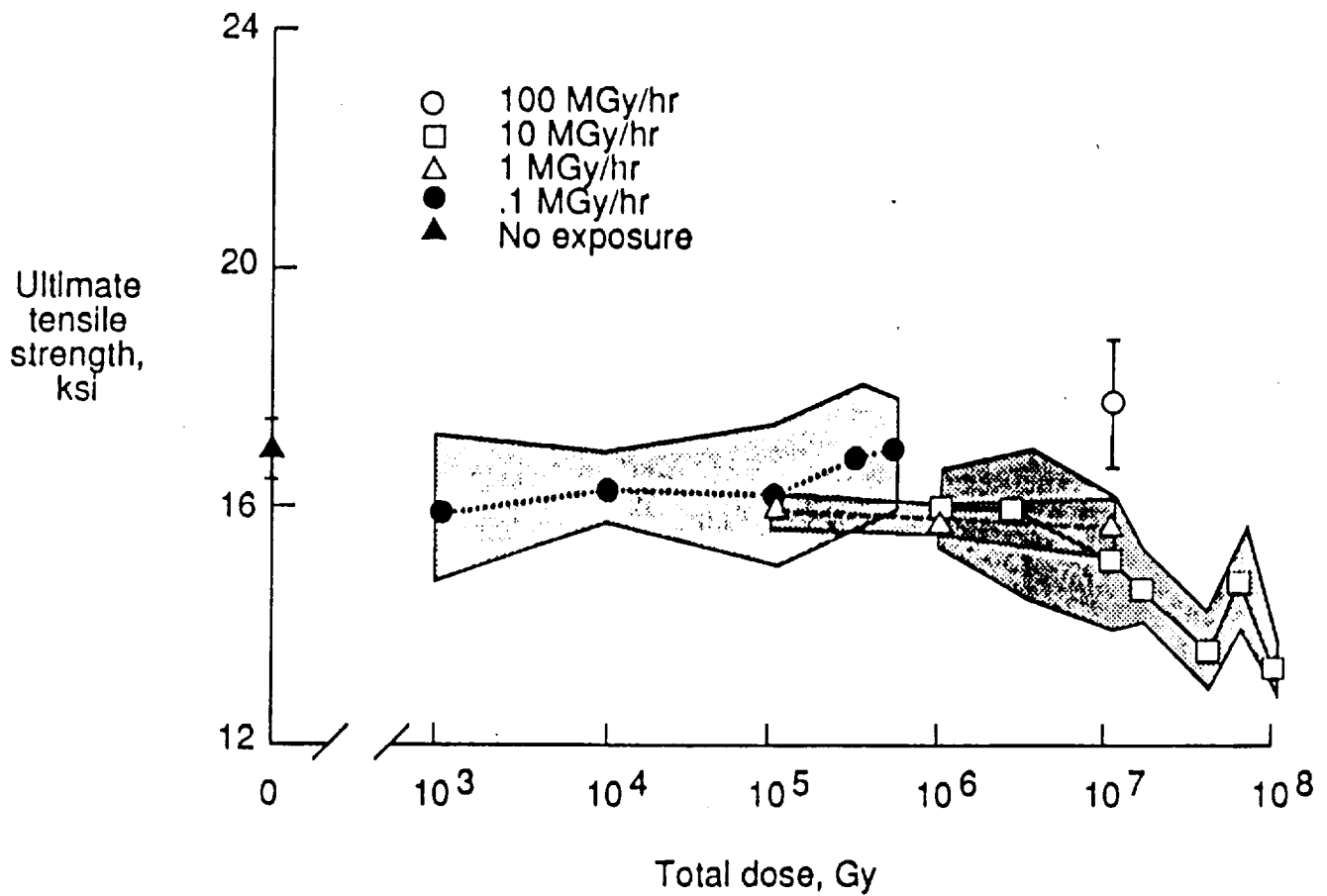
Figure 8. Ultimate tensile strength of electron-irradiated polyetherimide for four dose rates.
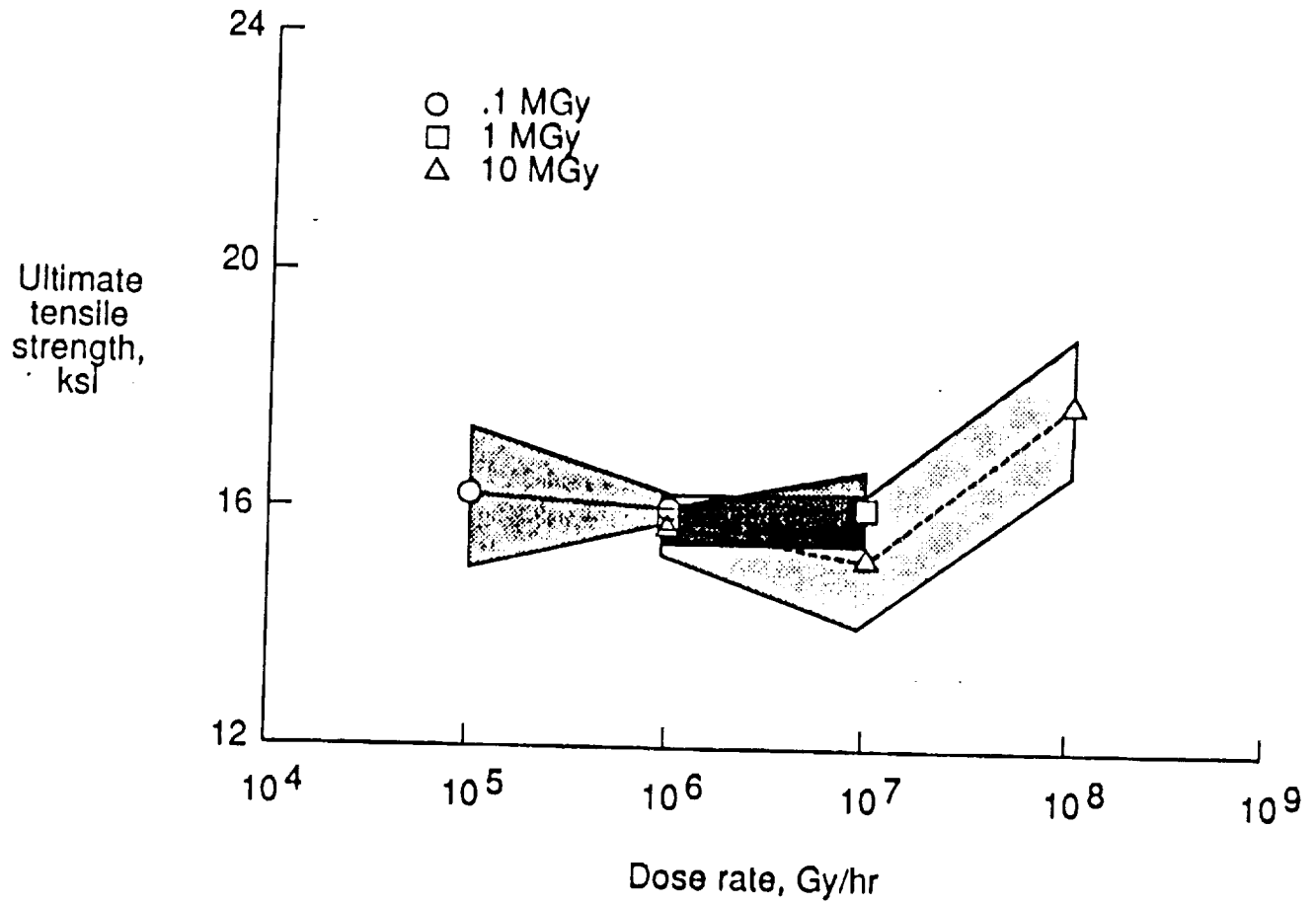
Figure 9. Ultimate tensile strength of electron-irradiated polyetherimide for three total absorbed doses.
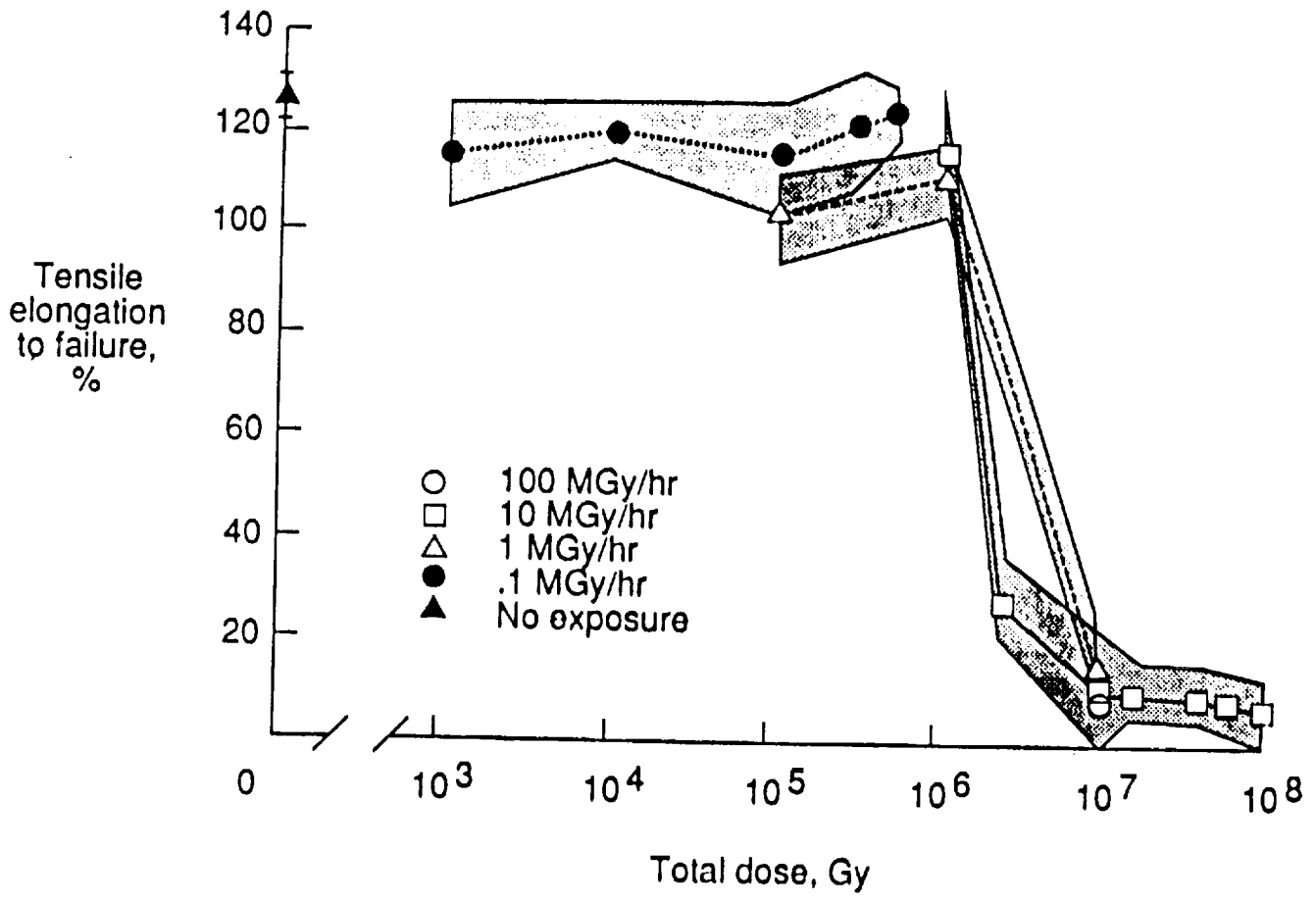
Figure 10. Elongation-to-failure of electron-irradiated polyetherimide for four dose rates.
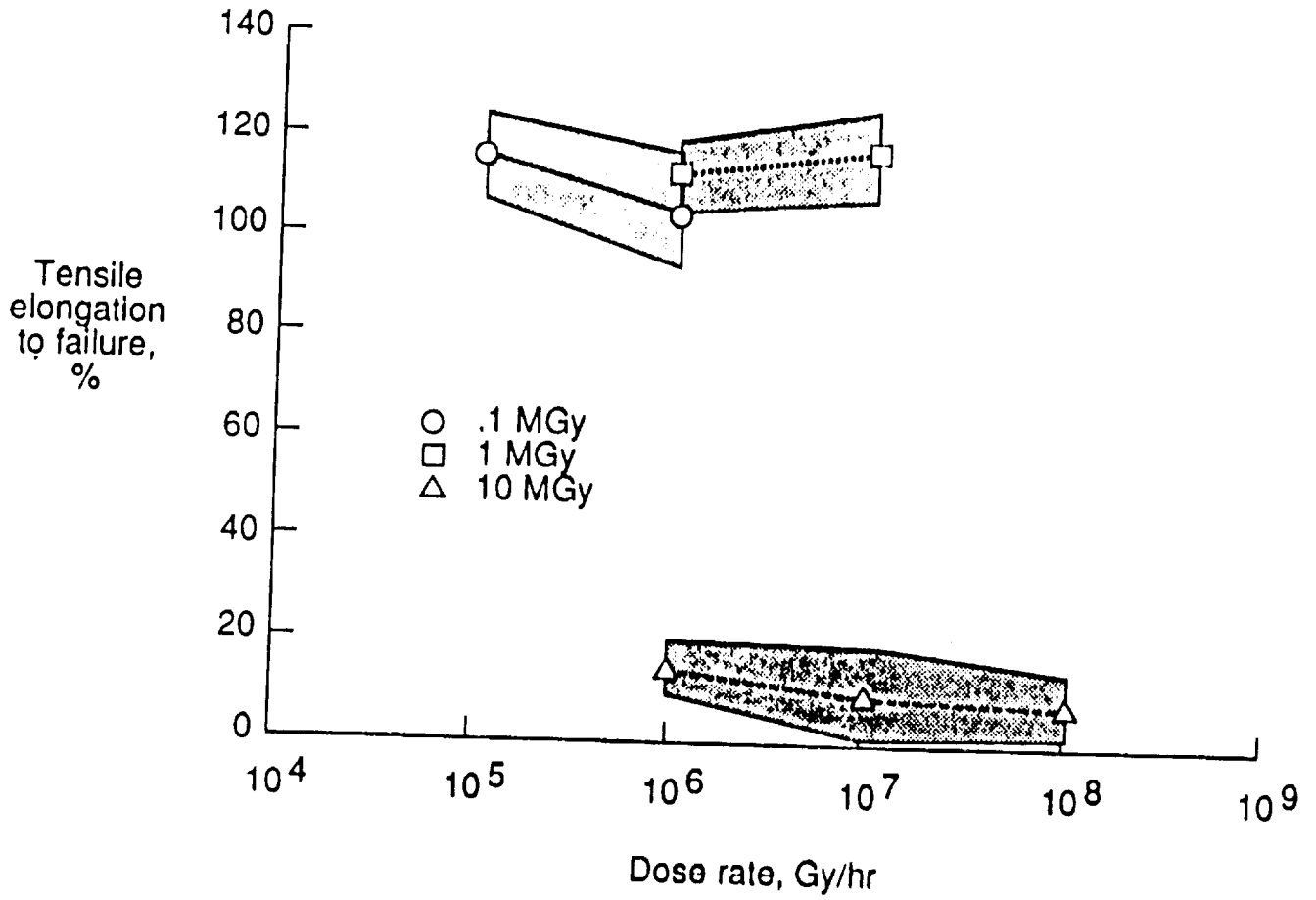
Figure 11. Elongation-to-failure of electron-irradiated polyetherimide for three total absorbed doses.

Figure 12. Unpaired electron density of electron-irradiated polyetherimide for five dose rates.

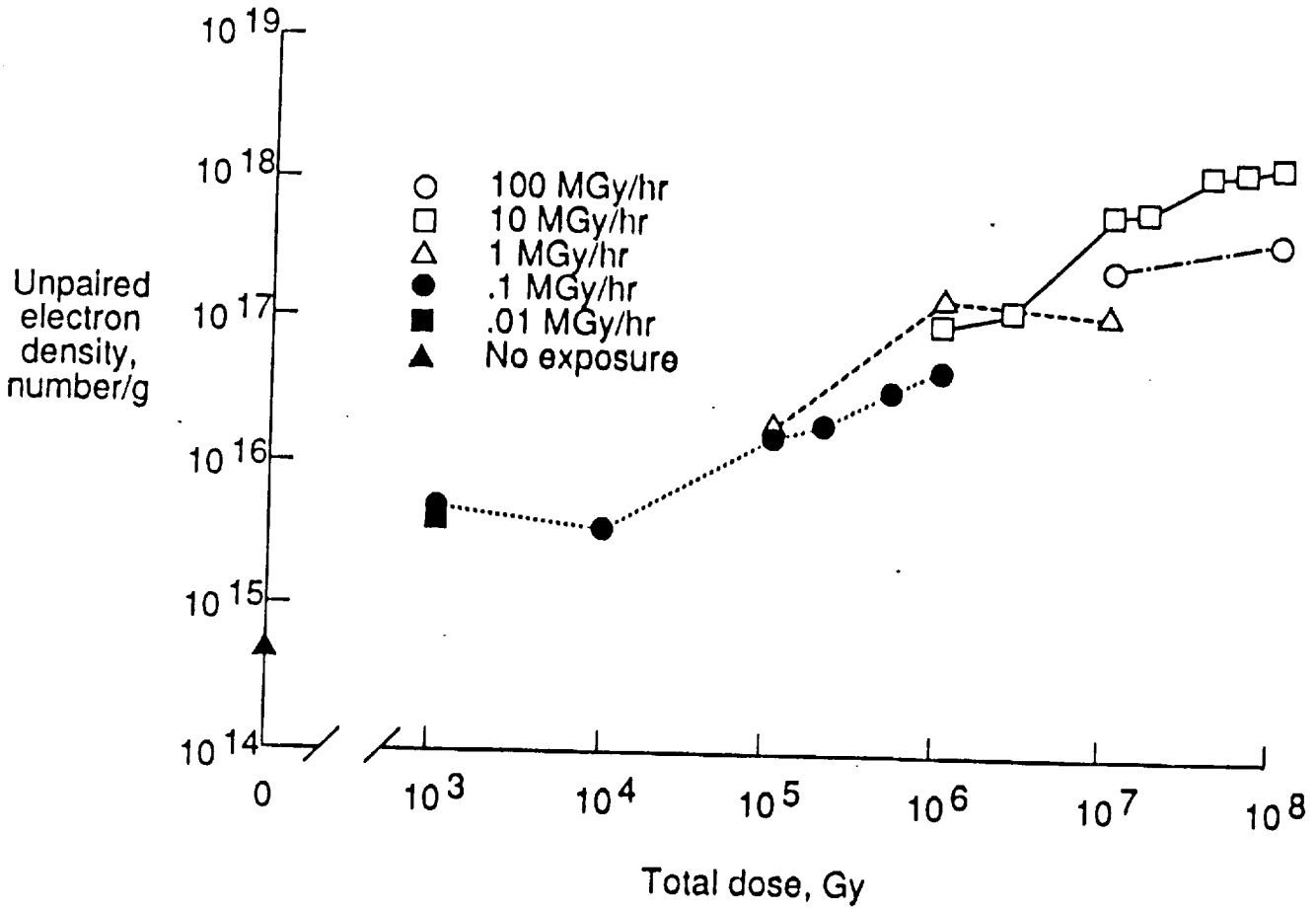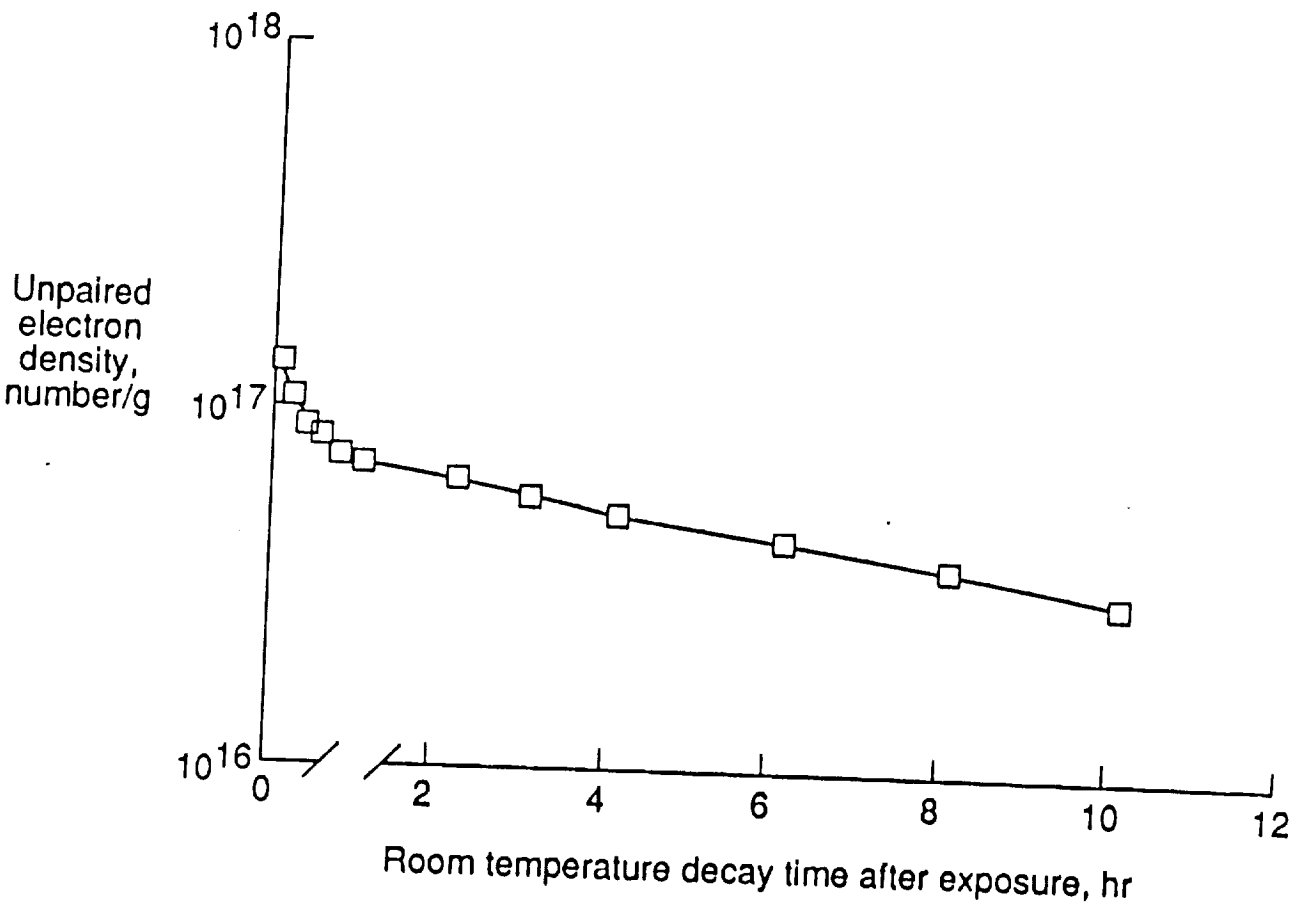Figure 13. Room temperature decay of unpaired electron density of electron-irradiated polyetherimide for 2.5-MGy total absorbed dose at a dose rate of 10 MGy/hr.
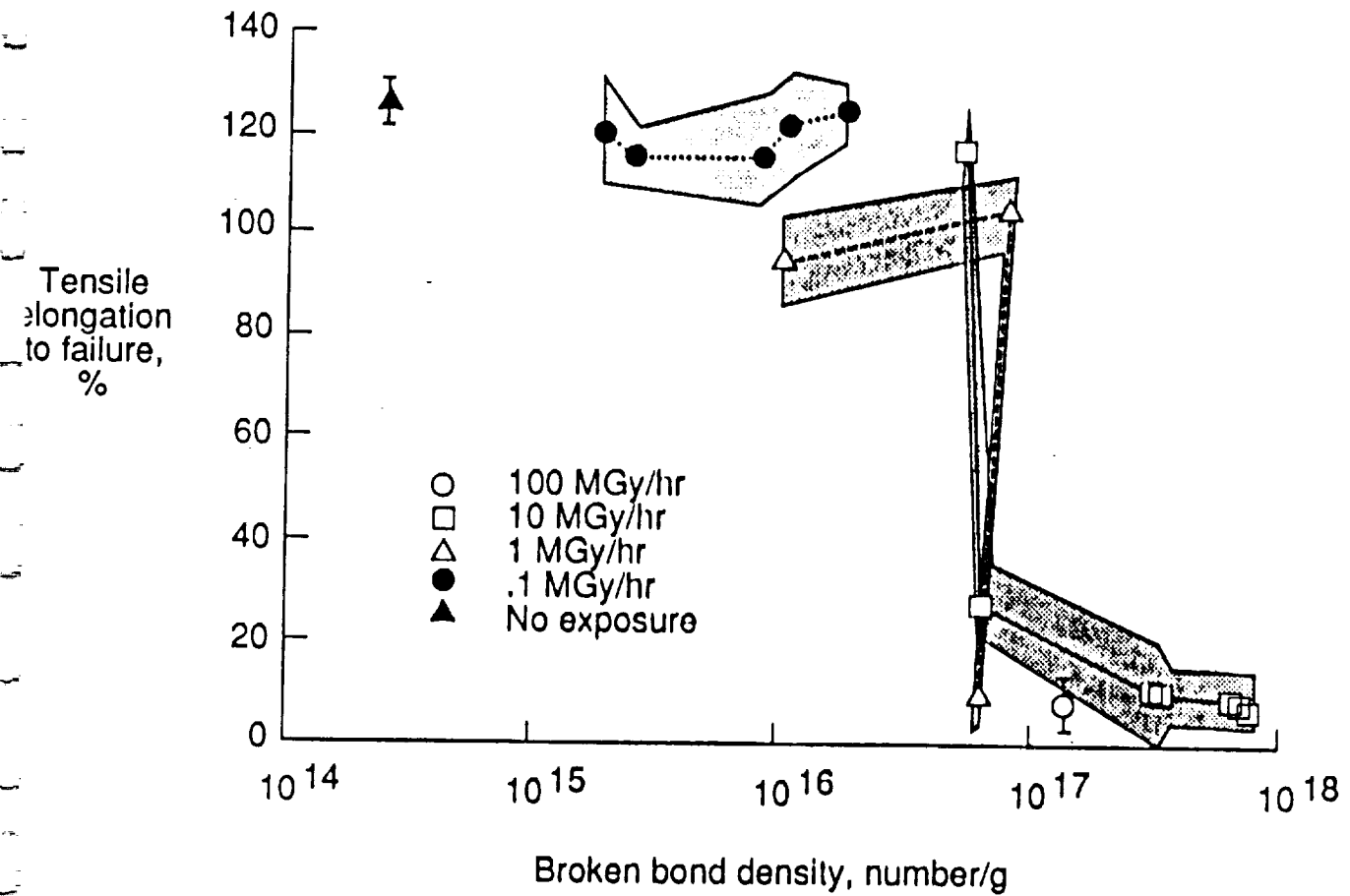
Figure 14. Relationship of elongation-to-failure with broken bond density for electron-irradiated polyetherimide.

Report Documentation Page

G-22

1. Report No. NASA TP-2928	2. Government Accession No.	3. Recipient's Catalog No.
4. Title and Subtitle Absorbed Dose Thresholds and Absorbed Dose Rate Limitations for Studies of Electron Radiation Effects on Polyetherimides		5. Report Date July 1989
		6. Performing Organization Code
7. Author(s) Edward R. Long, Jr., Sheila Ann T. Long, Stephanie L. Gray, and William D. Collins		8. Performing Organization Report No. L-16585
9. Performing Organization Name and Address NASA Langley Research Center Hampton, VA 23665-5225		10. Work Unit No. 506-43-21-04
		11. Contract or Grant No.
12. Sponsoring Agency Name and Address National Aeronautics and Space Administration Washington, DC 20546-0001		13. Type of Report and Period Covered Technical Paper
		14. Sponsoring Agency Code

15. Supplementary Notes

16. Abstract

The threshold values of total absorbed dose for causing changes in tensile properties of a polyetherimide film and the limitations of the absorbed dose rate for accelerated-exposure evaluation of the effects of electron radiation in geosynchronous orbit have been studied. Total absorbed doses from 1.0 kGy to 100 MGy and absorbed dose rates from 0.01 to 100 MGy/hr were investigated, where 1 Gy equals 100 rads. Total doses less than 2.5 MGy did not significantly change the tensile properties of the film, whereas doses higher than 2.5 MGy significantly reduced elongation-to-failure. There was no measurable effect of the dose rate on the tensile properties for accelerated electron exposures.

17. Key Words (Suggested by Authors(s)) Radiation Electron Dose Dose rate Polyetherimide	18. Distribution Statement Unclassified—Unlimited Subject Category 27		
19. Security Classif. (of this report) Unclassified	20. Security Classif. (of this page) Unclassified	21. No. of Pages 19	22. Price A03

APPENDIX H

MECHANISM OF ELECTRICAL CONDUCTIVITY IN AN IRRADIATED POLYIMIDE

H. R. Ries,†‡ W. L. Harries,† S. A. T. Long§ and E. R. Long, Jr§

†Department of Physics, Old Dominion University, Norfolk, VA 23529-0116, U.S.A.
§NASA Langley Research Center, Hampton, VA 23665-5225, U.S.A.

Abstract—A polyimide was exposed to 1.0 MeV electron radiation. The radiation-induced radical density and d.c. conductivity were measured at various post-irradiation times. The radiation-induced radical density was found to be correlated to the increased d.c. conductivity through a hopping model of conductivity. The post-irradiation radical species were identified.

INTRODUCTION

Currently, much effort is being directed towards development of comprehensive theories of conduction in polymers [1, 2]. The experimental effort has centered around conductivity changes caused by variations in the polymer structure [3–5], variations of the types and quantities of dopant molecules in the polymeric material [6–9], and variations of the types and quantities of polar groups incorporated in the polymer chain [10, 11]. Studies have also been made of the increased conductivities in polymers during irradiation of the polymers with various sources [12–14]. Other research efforts have suggested that the radical densities in polymers may be related to the d.c. conductivity [15–17]. Since radicals are produced during the irradiation of polymers, some of which remain after cessation of irradiation, studies of the post-irradiation radical densities and conductivities provide a unique opportunity to investigate a possible relationship between a polymer's conductivity and radical density.

To our knowledge, only one study of radiation-generated radicals and conductivity has been conducted previously. In that study, Monteith *et al.* found a correlation between the radiation-induced radical density and the post-irradiation conductivity in a polyethylene terephthalate, although no quantitative form was suggested for the relationship [17]. In the present experiments, a correlation is found to exist between the radiation-induced radical density and the radiation-induced conductivity in the polyimide. We investigate the use of the hopping model to explain the correlation, a model which has previously been applied to polymers with various dopants [8, 9], but not to the case of irradiated polymers.

---

‡ Presently at Norfolk State University.

EXPERIMENT

Three-mil Kapton®, a polyimide manufactured by du Pont de Nemours, Inc., was exposed to 1.0-MeV electron radiation provided by a Dynamitron electron accelerator to total absorbed doses of 1, 5, and 9.5×10^7 Gy. The absorbed dose rate was 5×10^5 Gy h^{-1}, and a cooling system was employed to ensure that the specimen temperatures did not exceed 30°C during irradiation. Typically, 0.5 h elapsed between the cessation of radiation and the immersion of the specimens in liquid nitrogen. The repeat unit for Kapton is:
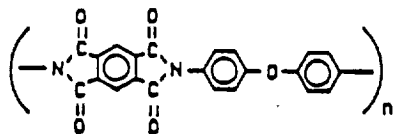
where *n* is the number of such units in a polymer chain.

The radical density was measured using a Varian E-Line Century Series Model E-109E electron paramagnetic resonance (EPR) spectrometer. The EPR specimens were maintained at a temperature of −186°C during EPR data collection. The reference standard used was a strong pitch standard provided by Varian.

The d.c. conductivity was measured at room temperature 60 s after application of 500 V across the specimen. Prior to irradiation, the d.c. conductivity specimens were sputter-coated with 7-cm diameter electrodes of approx. 5 nm chromium covered by 100 nm of palladium. The collection electrode was surrounded by a 0.16-cm gap and a guard ring. These electrodes provided reproducible contact with the material at various post-irradiation times, and were found to be unaffected by exposure to liquid nitrogen.
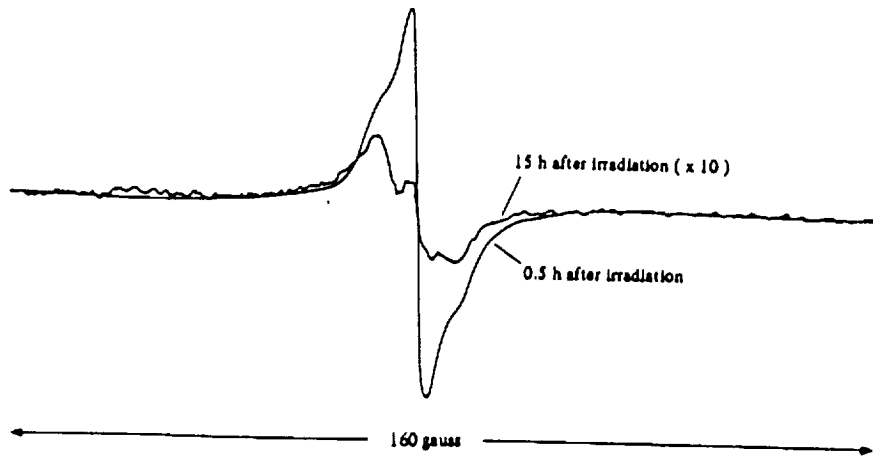
Fig. 1. EPR spectra of 3-mil standard-stock Kapton, 0.5 and 15 h after exposure to 1.0-MeV electron radiation. Absorbed dose rate $= 5 \times 10^5$ Gy h^{-1}, total absorbed dose $= 9.5 \times 10^7$ Gy.

EXPERIMENTAL RESULTS

The EPR spectra of the irradiated polyimide 0.5 and 15 h after exposure to electrons are shown in Fig. 1. The relative heights of the different peaks in the spectra are not the same at different post-irradiation times. Consequently, more than one radical is generated by the irradiation. Based upon computer simulations of the various post-irradiation spectra and consideration of the chemical structure of the polyimide, the radicals were tentatively identified to be a ketone radical, a phenyl radical, and a phenoxyl radical. These identifications are in agreement with the results of Long and Long [18], which were based upon infrared spectroscopy data as well as EPR data.

The total organic radical density in Kapton as a function of total absorbed dose is shown in Fig. 2(a), where it can be seen that the radical density increases
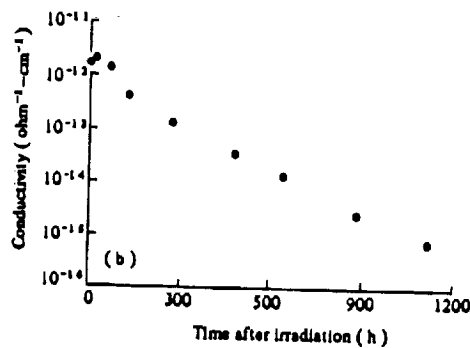
Fig. 2. Total organic radical density in 3-mil Kapton after exposure to 1.0-MeV electron radiation; (a) at various total absorbed doses; and (b) at various post-irradiation times. Absorbed dose rate $= 5 \times 10^5$ Gy h^{-1}, total absorbed dose $= 9.75 \times 10^7$ Gy.
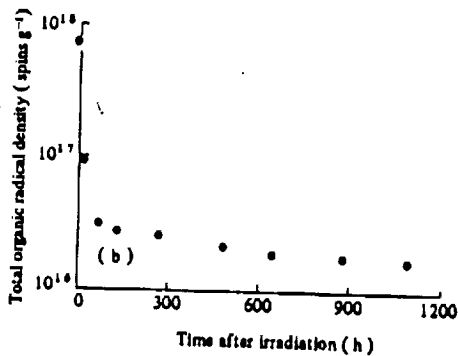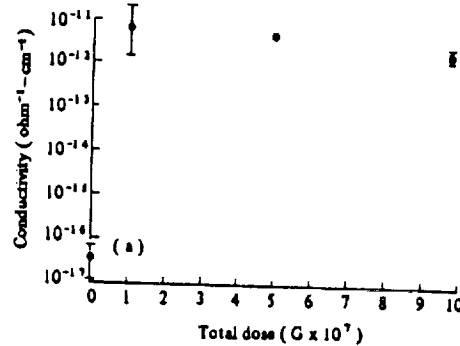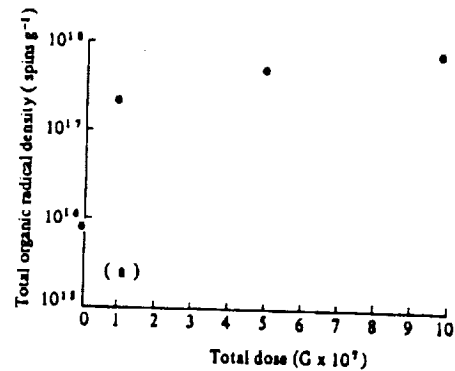

Fig. 3. Conductivity in 3-mil Kapton after exposure to 1.0-MeV electron radiation; (a) at various total absorbed doses; and (b) at various post-irradiation times. Absorbed dose rate $= 5 \times 10^5$ Gy h^{-1}, total absorbed dose $= 9.75 \times 10^7$ Gy.

from 8×10^{15} spins g^{-1} in the non-irradiated material to over 10^{17} spins g^{-1} in the irradiated Kapton. The post-irradiation radical density decay curve is shown in Fig. 2(b).

The conductivity as a function of total dose in Kapton is shown in Fig. 3(a). The non-irradiated Kapton conductivity is $4 \pm 3 \times 10^{-17}$ ohm^{-1}-cm^{-1}, whereas the irradiated conductivity values 0.5 h after irradiation are over 10^{-12} ohm^{-1}-cm^{-1}. As indicated in Fig 3(b), however, this conductivity increase is not permanent. Three months following irradiation, the conductivity had returned to its non-irradiated value in all of the specimens tested.

ANALYSIS

In experiments by Mort *et al.* [19], and Pfister [8], hopping conductivity processes were found to occur in molecularly-doped Lexan, with the dopant molecules acting as hopping sites. The mobility μ was found to be of the form:

$$\mu = Kd^2 \exp(-d/d_0), \qquad (1)$$

where d is the average separation distance between the dopant molecules, d_0 is a hopping parameter dependent upon the type of dopant molecules, and K is a constant of proportionality.

In our experiment, comparison of the post-irradiation radical density decay in Fig. 2(b) and conductivity decay in Fig. 3(b) suggests that the increase in Kapton's conductivity after irradiation is associated with its increase in radical density. We suggest that the conductivity dependence on the radical density in our experiment will be of the same form as the conductivity dependence on molecular dopant density in the experiments of Mort *et al.* [9] and Pfister [8].

In deriving the form of the hopping conductivity based on the spatial overlay of wavefunctions, Mott and Davis [2] found that the mobility obeyed:

$$\mu = k'd \exp(-d/d_0)\sinh(eEd/2kT), \qquad (2)$$

where k' is a proportionality constant and E is the applied electric field. When

$$\frac{eEd}{2kT} \ll 1 \qquad (3)$$

as in the work of Mort *et al.* and Pfister, eqn (2) reduces to eqn (1).

In our experiment, however, we assume the radicals provide hopping sites for the charge carriers (electrons) in the material. The average distance (d) between radicals is

$$d = \rho^{-1/3}, \qquad (4)$$

where ρ is the radical density in unpaired spins cm^{-3}. This distance was too large to satisfy the condition of

eqn (3), so the full form of eqn (2) was applied in this experiment. Since the conduction electrons in polymers may come from a variety of sources, we further assume that if the carrier density (n) is approximately constant, then the conductivity σ is given by

$$\sigma = K''d \exp(-d/d_0)\sinh(eEd/2kt), \qquad (5)$$

where K'' is a new proportionality constant. Combining and rearranging eqns (4) and (5) we obtain

$$\ln[\sigma\rho^{+1/3}/\sinh(eE\rho^{-1/3}/2kT)]$$
$$= -\rho^{-1/3}/d_0 + \ln K''. \qquad (6)$$

Figure 4 is a plot of expression (6), where σ, ρ, E, and T are measured, and presents data from all of the radiation exposures, and from the average of all of the non-irradiated data as well.

The linear correlation coefficient between the 26 data points in Fig. 4 is 0.94. This indicates that the hopping model of eqn (6) is close to the form through which the radiation-induced radical density and the radiation-induced conductivity are related.

The slope of the line in Fig. 4 is -5×10^8 m^{-1}, which corresponds to a value of 2.0 nm for d_0, the localization parameter. This value is comparable to the 2.4 nm measured by Rohl [6, 11] in polyethylene with varying concentrations of carbonyl sites.

As stated earlier, three different radical species were identified in the irradiated polyimide. All three types of radical species are expected to contribute unequally to the hopping conductivity, and variations in their relative densities with dose may account for the lack of a perfect fit in Fig. 4. Attempts were made to analyze the EPR spectrum and hence establish the association of a specific radical with the conductivity increase, but separation of the effects of the different radical densities has not yet been achieved.
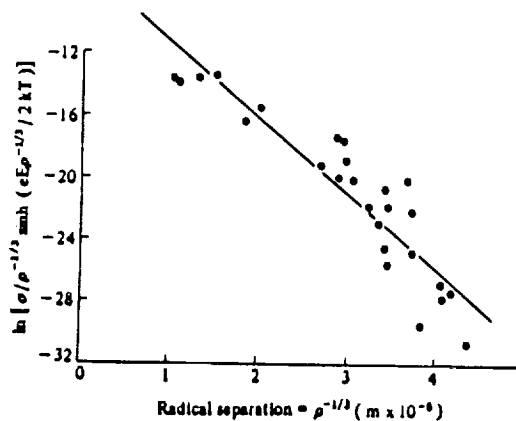

Fig. 4. A plot of the Kapton conductivity data and radical density data for all total absorbed doses, assuming a relationship of the form of eqn (6), $\ln[\sigma\rho^{+1/3}/\sinh(eE\rho^{-1/3}/2kT] = -\rho^{-1/3}/d_0 + \ln K''$ where $\rho^{-1/3}$ is the average radical separation. The line represents a straight line fit to the data points, with slope $= -5 \times 10^8$ m^{-1}.

PCS 30/7—F

738 H. R. Ries *et al.*

SUMMARY

Increased electrical conduction together with an increased radical density were found to occur in Kapton after exposure to 1.0-MeV electrons in doses greater that 10^7 Gy. Phenyl, phenoxyl, and ketone radicals were identified in the EPR spectrum of irradiated Kapton. The conductivity and the radical density were found to be related by a hopping model. Additional studies of the conductivity and radical density in Kapton after various doses and types of irradiation, as well as studies of Kapton with molecular dopants, would be of interest to further clarify the conduction processes in Kapton.

REFERENCES

1. Bottger H. and Bryskin V.V., *Phys. Status Solidi* (*b*) 113, 9 (1982).
2. Mott N.F. and Davis E.A., *Electronic Processes in Non-Crystalline Materials*, second edn. Clarendon Press, Oxford (1979).
3. Brom H.B., Tomkiewicz Y., Aviram A., Broers A. and Sunners B., *Solid St. Commun.* 35, 135 (1980).
4. Amborski L.E., *J. polym. Sci.* 62, 331 (1962).
5. Bruck S.D., *Polymer* 6, 319 (1965).
6. Rohl P., Electronic Hopping Transport Mechanism in Polyethylene, *Conference Rec. 1984 IEEE International Symposium on Electrical Insulators*, pp. 186–189 (1984).
7. Limburg W., Pai D.M., Pearson J.M., Renfer D., Stolka M., Turner R. and Yanus J., *Organ. coat. plast. Chem.* 38, 5(1978).
8. Pfister G., *Phys. Rev.* B16, 3676 (1977).
9. Mort J., Pfister G. and Grammatica S., *Solid St. Commun.* 18, 693 (1976).
10. Suzuoki Y., Muto H., Cai G., Mizutani T. and Ieda M., *Jap. J. appl. Phys.* 23, 91 (1984).
11. Rohl P., Dispersive Hopping Transport in Polyethylene, *Proceedings of the 1st International Conference on Conduction and Breakdown in Solid Dielectrics*, pp. 50–55 (1983).
12. Tyutnev A.P., Mingaleev G.S., Saenko V.S. and Vannikov A.V., *Phys. Status Solidi* (*a*) 79, 651 (1983).
13. Martin E.H. and Hirsch J., *Solid St. Commun.* 7, 279 (1969).
14. Gross B., Seggern H. von and Berkley D.A., Rate Theory of Radiation-Induced Conductivity of Fluoroethylene Propylene (FEP), *Annual Report of the Conference on Electrical Insulating Dielectric Phenomena*, p. 206. National Academy of Sciences, Washington D.C. (1982).
15. Bruck S.D., *J. polym. Sci.* C17, 169 (1967).
16. Ehrlich P., *Electrical Properties of Polymers* (Edited by K.C. Frisch and A.V. Patsis), pp. 26–36. Technomic, Westport, Connecticut (1972).
17. Monteith L.K., Turner D.T. and Ballard L.F., *Correlation of Electrical Conductivity and Radiation-Induced Free Radical Concentration in Poly(Ethylene Terephthalate) and Related Compounds*. NASA CR-66743 (1969).
18. Long S.A.T. and Long E.R., Jr, *Bull. Am. phys. Soc.* 30, 498 (1985).

APPENDIX I

DYNAMIC MECHANICAL ANALYSIS OF POLYMERIC MATERIALS

Kristen T. Kern and Wynford L. Harries
Old Dominion University
Department of Physics
Norfolk, Virginia 23529

and

Sheila Ann T. Long
NASA Langley Research Center
Mail Stop 229
Hampton, Virginia 23665-5225

ABSTRACT

Polymeric materials exhibit mechanical behavior which is dependant on temperature. Dynamic mechanical analysis measures the mechanical damping and resonant frequency of a material over a temperature range. Values of the dynamic loss modulus, storage modulus, and loss tangent can be calculated from these data. The glass transition temperature and onset temperature are obtained from curves of the dynamic moduli versus temperature.

INTRODUCTION

Polymeric materials do not deform easily at low temperatures. This is referred to as the glassy state. At high temperatures, the same material will be rubbery and will deform easily. The temperature at which this change in behavior occurs is called the glass transition temperature, T_g. The transition usually occurs over a temperature range, called the glass transition region. Materials are structurally sound at temperatures below the onset to the glass transition region, hence the importance of determining the glass transition temperature and the onset temperature.

The response, or strain, of a polymeric material to a sinusoidal stress is characterized by a modulus. The modulus, the ratio of stress to strain, is composed of the storage modulus and the loss modulus. The storage modulus is related to the amount of energy stored in the material as a deformation and returned to the oscillation, while the loss modulus is related to the amount of energy lost through friction.

When the temperature is low (glassy state), the loss modulus is small and the storage modulus is large. As the temperature increases, the intermolecular friction changes and the loss modulus increases (transition region) to a maximum (T_g). At still higher temperatures, the loss modulus decreases (rubbery state), and the storage modulus is also small.

Dynamic mechanical analysis of polymeric materials is analogous to the simplified, linear model shown in Figure 1. The equation of motion for this damped, driven harmonic oscillator is

$$M \, d^2x/dt^2 + B \, dx/dt + Kx = F_0 \sin wt$$

where M is the mass of the oscillating body, B is the coefficient of friction, K is the spring constant, x is the displacement of the mass from its equilibrium position, and F_O is the magnitude of the applied sinusoidal force. For oscillation at resonant frequency, the position of the mass is 90° out of phase with the applied force, and can be written

$$x = x_O \cos wt$$

where x_O is the maximum displacement. Substituting this expression with its first and second derivatives into the differential equation of motion and comparing the coefficients of the sine and cosine terms, we obtain the equalities

$$K = Mw^2$$

and

$$wB = -F_O/x_O$$

The first of these equations shows that the spring constant, which represents the ability of the oscillation mechanism to store energy, is proportional to the square of the resonant frequency. This is analogous to the storage modulus of a material. The second equation shows that the damping term, representing the loss of energy from the system, is proportional to the applied force and inversely proportional to the magnitude of the oscillation. This is analogous to the loss modulus of a material.

EXPERIMENTAL

The DuPont[1] 982 Dynamic Mechanical Analyzer (DMA) is used to measure the mechanical damping and resonant frequency of a sample of material. The sample is clamped between the ends of two rigid arms, each of which are free to oscillate around a pivot point. See Figure 2. The arms are driven to oscillate at the resonant frequency of the material. The energy lost from the oscillation during each cycle, the damping, is measured and a feedback signal is returned to the driving mechanism to maintain a constant oscillation amplitude. This feedback signal, in millivolts, is recorded as a measure of the damping due to the specimen.

The 982 DMA is accompanied by the 1090 Thermal Analyzer (see Figure 3) which is used for data acquisition, data analysis, and temperature control. With the use of liquid nitrogen, the system can record the resonant frequency and damping of a material from -150°C to 500°C. See Figure 4.

ANALYSIS

Data analysis programs provided by DuPont for use on the 1090 TA calculate the loss and storage moduli from damping and frequency values stored by the 1090 TA. An example of the resulting curves for a sample of T300/934 graphite/epoxy composite is shown in Figure 5. The transition onset temperature is found by drawing tangents to the loss modulus curve before the transition region and during the increasing part inside the transition region, as shown in Figure 5. The intersection of these two tangents is considered to occur at the onset temperature. The glass transition temperature is taken to be the temperature at which the loss modulus reaches a peak.

CONCLUSION

The data shows that the glass transition temperature is 240°C (±5°C) for T300/934 graphite/epoxy composite. The onset temperature is 218°C (±5°C), below which the material would be structurally sound.

---

[1] The use of trademarks or manufacturers' names in this publication does not constitute endorsement, either expressed or implied, by the National Aeronautics and Space Administration.

Figure Captions

Figure 1. The simplified linear model of dynamic mechanical analysis. A mass M attached to a spring of elasticity, K, is driven by an applied sinusoidal force, F. Energy is lost from the oscillation by friction.

Figure 2. The dynamic mechanical analyzer. A. The oscillation mechanism consists of two arms with a driving mechanism. The sample is clamped at the ends of the arms. B. The sample is flexed in the manner shown (exaggerated here).

Figure 3. The DuPont 1090 Thermal Analyzer, right, and 982 DMA with heating chamber in place. At the left is the liquid nitrogen tank.

Figure 4. Frequency and damping signal over temperature for a sample of T300/934 graphite/epoxy composite. The resonant frequency decreases in the glass transition region as the stiffness of the sample decreases.

Figure 5. Plots of the dynamic moduli and loss tangent versus temperature calculated from the data in Figure 4. The glassy region is at lower temperatures. The glass transition region begins at the onset temperature, 218°C. The rubbery region is at the highest temperatures. The loss tangent, tan δ, is the ratio of the loss modulus to the storage modulus.
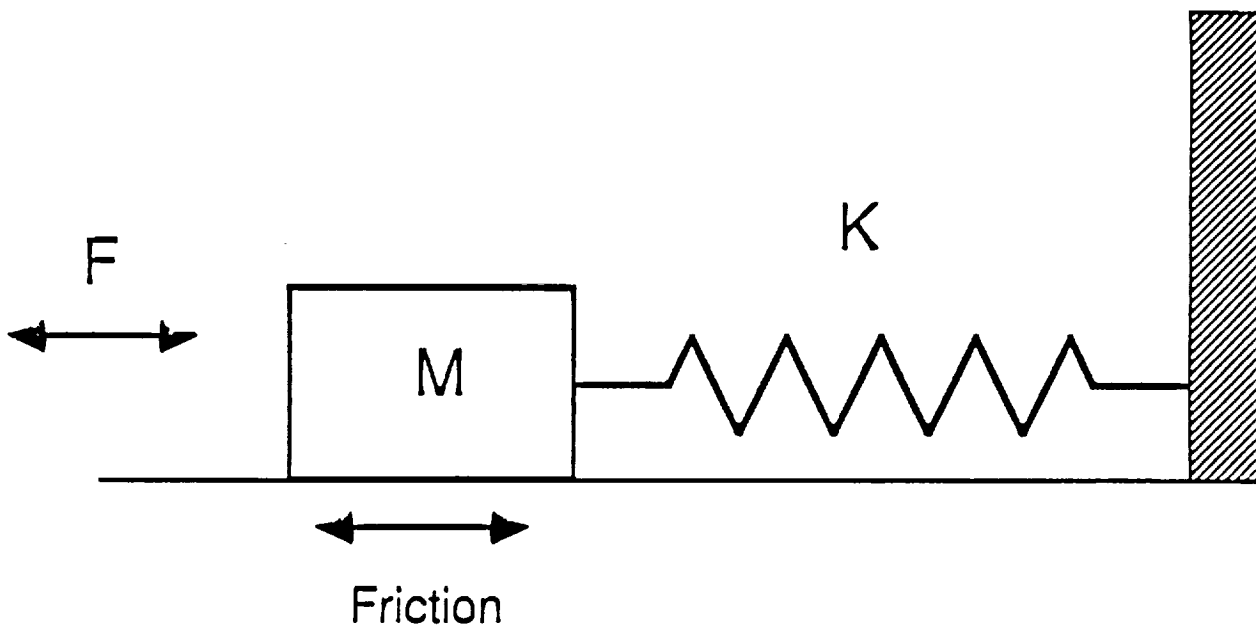
$$M\, d^2x/dt^2 + B\, dx/dt + Kx = F_O \sin wt$$

For oscillation at resonant frequency,

$$x = x_O \cos wt$$

$$K = Mw^2$$

$$wB = -F_O/x_O$$

A.

Sample

A

B

A'

B'

Driven

B.

A

A'

B'

B

Tan δ

Flexural loss modulus (GPa)

Flexural storage modulus (GPa)

Temperature (°C)

$T_g = 240°C$

$T_{onset} = 218°C$

Flexural storage modulus
Flexural loss modulus
Tan δ
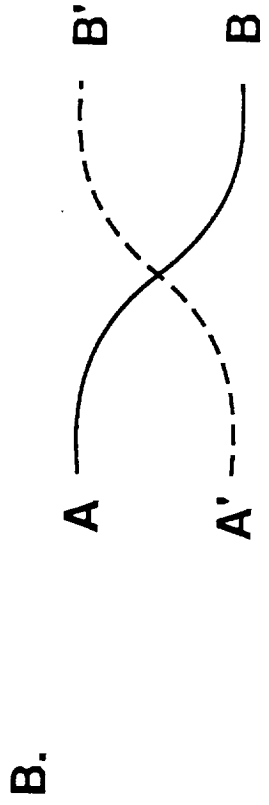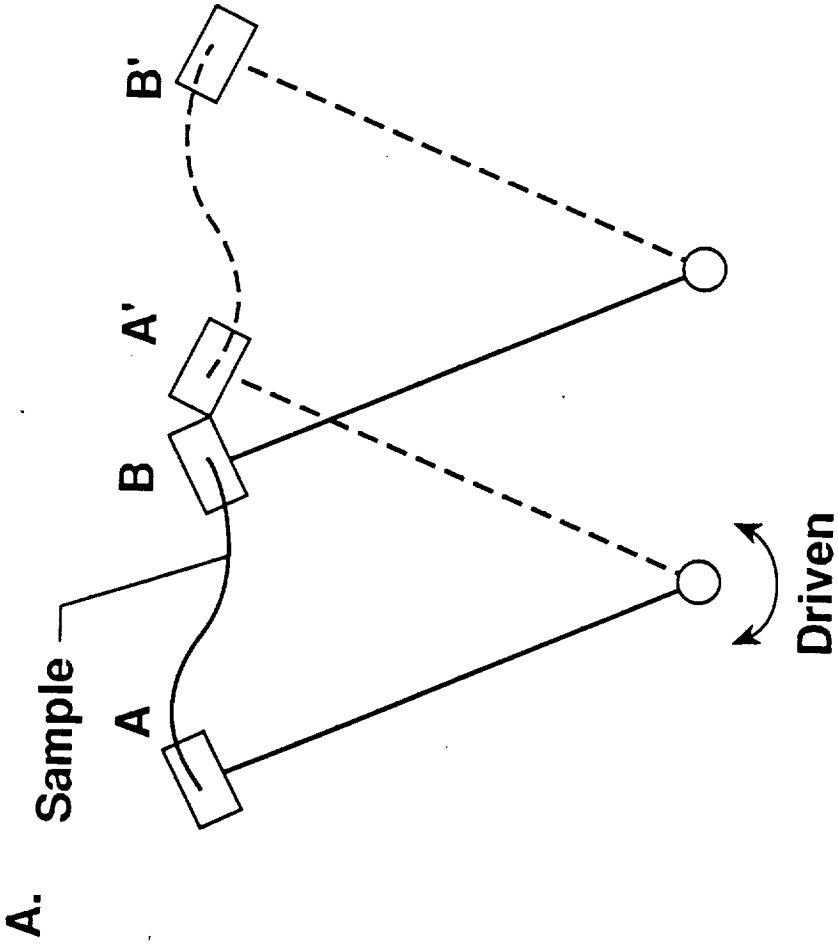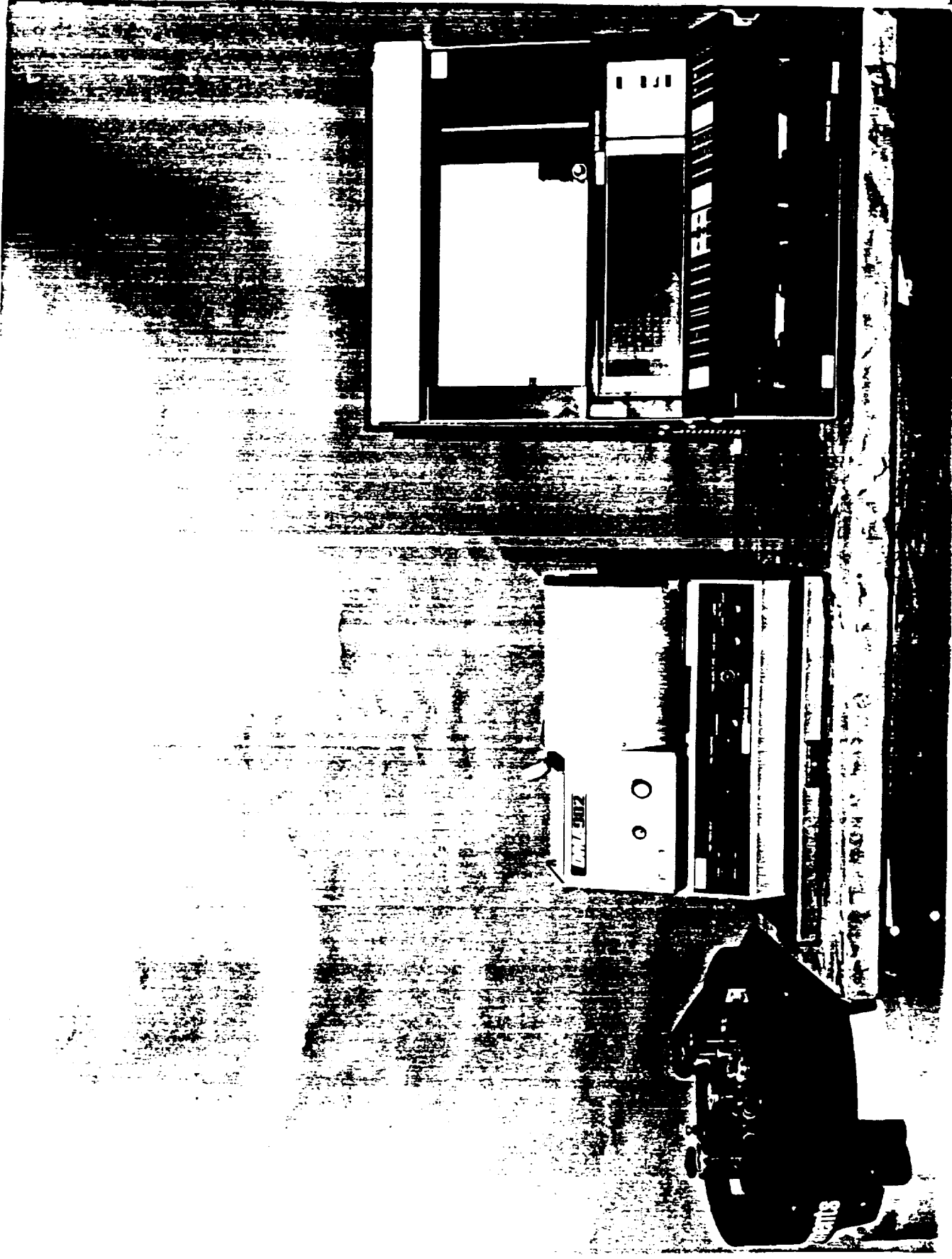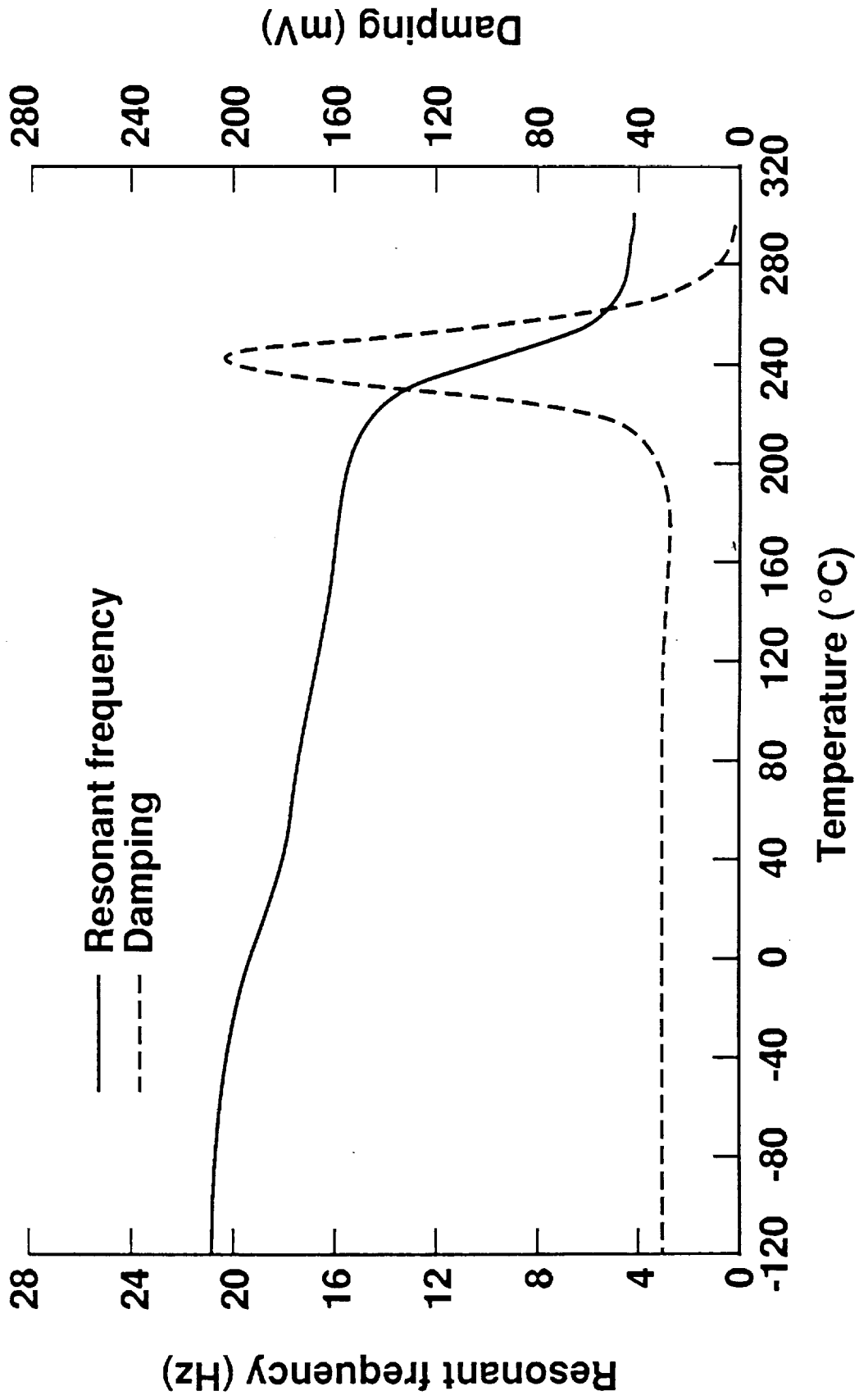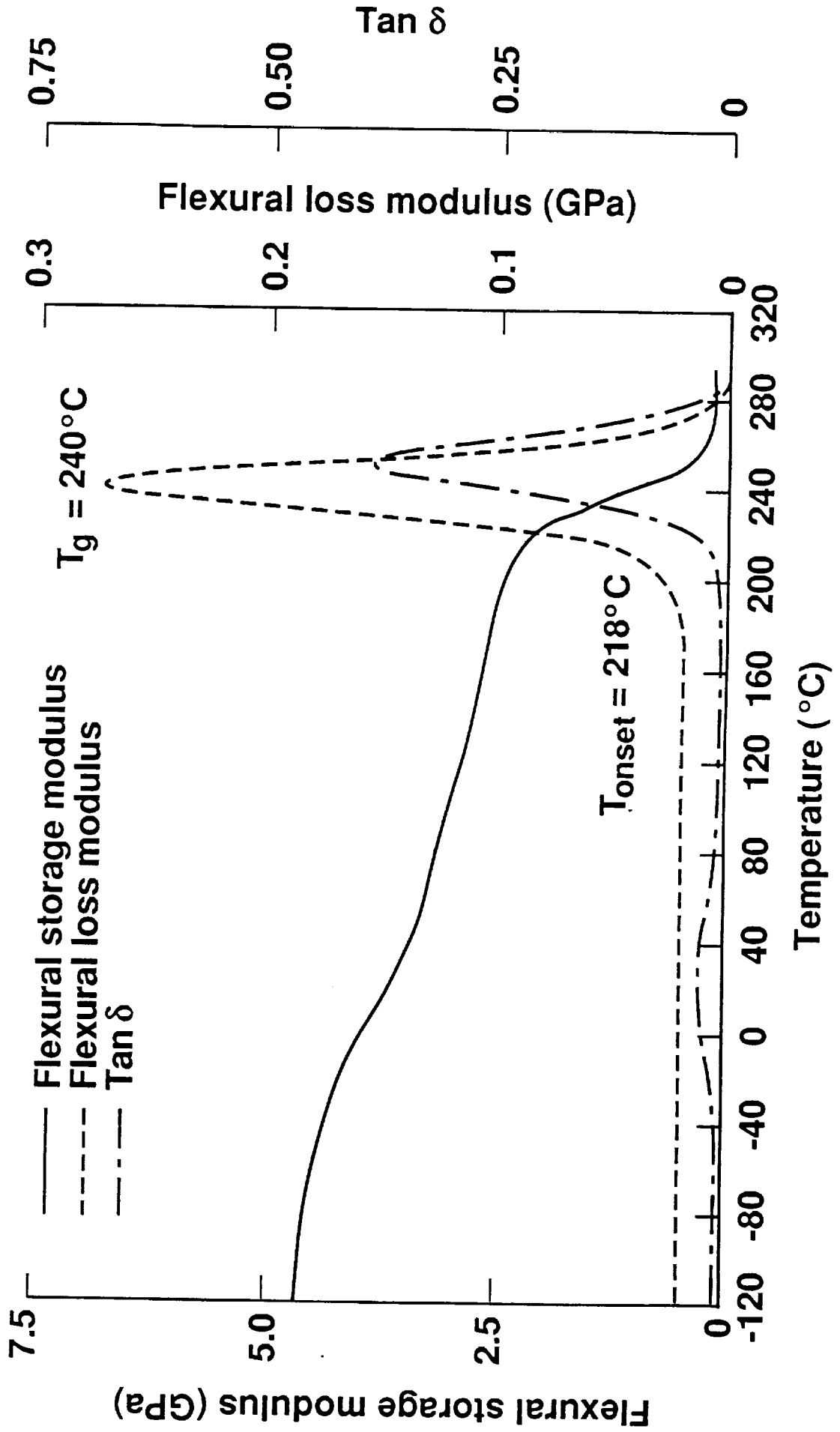
APPENDIX J

Effects of Electron Radiation and Thermal Cycling on Sized and Unsized Carbon Fiber - Polyetherimide Composites.

Kristen T. Kern*, Edward. R. Long, Jr**., Sheila Ann T. Long**, and Wynford L. Harries*.

*Old Dominion University, Norfolk, Virginia 23529
**NASA Langley Research Center, Hampton, Virginia 23665

INTRODUCTION.

The mechanical performance of a composite material depends on the quality of the interface between the fibers and matrix. A good interface allows the transfer of stress between the fibers. During the manufacturing of composite materials, a sizing is often applied to the fibers to protect them during processing and to improve the adhesion of the matrix material to the fibers.

The effects of the space environment on the mechanical properties of a material must be investigated before the material may be used with confidence in space applications. Conditions in geosynchronous Earth orbit (GEO) include exposure to energetic electron radiation and temperature extremes. During a thirty year mission, a structure in GEO is expected to receive a total dose as high as 100 kilograys (kGy) from trapped electron and proton radiation. The temperature of a structure is expected to vary between -150 degrees Fahrenheit (^{O}F) and +150 ^{O}F as it is exposed to, and hidden from solar heating.

Carbon fiber-polyetherimide composite materials are being investigated for use in space applications. Polyetherimides are thermoplastics and thus have temperature stability that is superior to that of epoxies. This study is an investigation of how the mechanical properties of a carbon fiber-polyetherimide composite are affected by the use of fiber sizing and exposure to electron radiation and thermal cycling.

EXPERIMENTAL.

Two unidirectional, 4-ply composite materials were manufactured, one using sized Celion 6000 fibers and one using unsized Celion 6000 fibers. Both composites were made with Ultem 1000 as the matrix material. The sizing was a 2 percent epoxy wash. the mechanical properties of the fibers and resin materials are shown in Table 1. The composite was cured at 650 ^{O}F for 15 minutes under a pressure of 300 pounds per square inch (psi). The thickness and fiber volume fraction of both materials are shown in Table 2. The completed composite panels were cut into one-half inch wide strips, some with the fiber direction parallel to the long dimension and some with the fiber direction transverse to the long dimension. The strips were then cut to sample length.

Samples were exposed to no exposure, electron radiation, thermal cycling, and electron radiation followed by thermal cycling. Exposures to 1-MeV electron radiation were performed under vacuum with a Radiation Dynamics, Inc. Dynamitron. The total dose was 100 kGy absorbed at a rate of 0.5 kGy per hour. Thermal cycling exposures were performed under a vacuum with heating by electric coils and cooling by a liquid nitrogen manifold. The temperature range was -150 ^{O}F to +150 ^{O}F for 1000 cycles. The sequential radiation followed by thermal cycling exposures were to the same conditions as the individual exposures. Samples were stored in a vacuum at room temperature between exposure and testing.

Mechanical performance was evaluated by using the three-point flex test and dynamic mechanical analysis (DMA). The three-point flex test is a flexural strain-to-failure test using American Society of Testing and Materials (ASTM) standard D790-84a, method 1. The rate of strain was 0.02 inches per minute. The specimens were supported by two 0.25 inch diameter supports while a loading nose applied the strain to the mid-point of the sample. The specimens were 0.5 inch wide and one inch long. The specimen support span was 0.547 inches, giving a span to depth ratio of 19.5 for the sized material and 22.8 for the unsized material. Eight specimens of each composite material were tested with each fiber direction, longitudinal and transverse, after each of the four exposures for a total of 128 specimens. DMA were performed using a DuPont 982 DMA in conjunction with a 1090 Thermal Analyser. Specimens were subject to constant amplitude, flexural deformation at resonant frequency. Mechanical damping and frequency were recorded for temperatures between -184 $^\circ$F and 608 $^\circ$F. Dynamic loss and storage moduli were calculated for each sample along with the dissipation factors. The glass transition temperature T_g was taken to be the temperature at which the dynamic loss modulus reached a maximum. DMA specimens were one half inch wide and two inches long. For each material, three specimens were analyzed with each fiber orientation after each of the four exposures for a total of 48 specimens.

RESULTS AND DISCUSSION.

Figure 1-A shows the average ultimate stress for the unexposed sized and unsized material determined from the three-point flex test data. For longitudinally oriented fibers, the sized material had an ultimate stress that was 16 percent less than that of the unsized material. For the transverse fiber orientation, the ultimate stress of the sized material was 24 percent greater than that of the unsized material. The value of the ultimate stress is dominated by the fibers in the longitudinal aspect and by the matrix material in the transverse case.

The average ultimate strain of each material in the unexposed condition is shown in Figure 1-B. No signifigant difference between the materials appears for either the longitudinal or the transverse fiber orientation. The ultimate strain is also dominated by the fibers in the longitudinal case and by the matrix in the transverse case. The three-point flex test does not involve large strains throughout the material, and thus is not sensitive to small differences in brittleness.

The modulus of each material, shown in Figure 1-C for both fiber orientations, was lower for the sized material by 21 percent for the longitudinal fiber direction and by 11 percent for the transverse case. The one standard deviation error margins overlapped in the transverse case. The modulus of a composite with longitudinal fiber direction is dependent on the ability of the matrix material to transfer load between the fibers. The modulus of material with transverse fiber orientation is similarly dependent but to a lesser extent. Thus, the data indicate that the sizing applied to the fibers in this study inhibits the transfer of stress between the fibers.

The results of the three-point flex test for the exposed material are shown in Figures 2 thru 5. A comparison of the ultimate stress of the radiated unsized material with transverse fiber orientation in Figure 2-A to that of unexposed material shows a 30 percent increase after the exposure. However, as may be seen in Figures 3-A, 4-A and 5-A, there were no changes in the ultimate stress of the longitudinal unsized material or in the ultimate stresses of the longitudinal and transverse sized material. Similarly as may be seen in part B of Figures 2 thru 5 the ultimate strain only changed for the unsized material with transverse fibers. But in the case of the modulus, the material with unsized longitudinal fibers

showed the only change as may be seen in part C of Figures 2 thru 5. The change in tensile properties do not occur for more than one material and fiber direction, and thus do not suggest any change in material properties. The DMA results shown in table 3, display an increase in the T_g of each material by 13 °F to 33 °F after radiation exposure.

Radiation doses similar to those used in this study have been shown to cause large decreases in the strain to failure[4] and as much as a 36 °F increase in the T_g[5] of neat resin Ultem films. The strain to failure of the film was much larger than that which occurred in the three-point flex testing of the composite. Thus the strain effects reported in Reference 4 are not seen in this study. The increase in the T_g of Ultem film was shown to be caused by radiation induced crosslinking. The change in T_g after radiation exposure for the composite agrees with that found for the film and thus suggests that the increase in T_g of the composite is due to crosslinking in the matrix material.

Thermal cycling had no effect on the ultimate stress of either material, regardless of fiber orientation, as seen in part A of Figures 2 thru 5. the ultimate strain, shown in part B of Figures 2 thru 5, decreased after thermal cycling for the sized material with both fiber directions and for the unsized material with longitudinal fiber orientation. the modulus of each material shown in part C of Figures 2 thru 5 increased after thermal cycling for both fiber orientations. The T_g, shown in Table 3, was unaltered by thermal cycling for both materials. The temperature range during thermal cycling was not high enough to cause further curing or break bonds in the matrix material. The thermal cycling could, however, act to relieve internal stresses associated with the cure cycle.

The sequential exposures, radiation followed by thermal cycling, showed the same effects on the T_g and modulus as separate radiation and thermal cycling exposures. The T_g increased after the sequential exposures approximately the same amount it increased after the radiation exposures. The modulus of each material increased approximately the same amount after the sequential exposures as it increased for the thermal cycling exposures. Thus there is no indication that radiation and thermal cycling exposures act synergistically when exposures are performed sequentially.

CONCLUSIONS.

The modulus of Celion 6000-Ultem 1000 composite made with 2 percent epoxy wash sizing was found to be lower than the modulus of similar material made with no fiber sizing, indicating that the sizing may inhibit the transfer of load between the fibers and the matrix material. Electron radiation exposure to a dose of 100 kGy raises the T_g of both sized and unsized material. Comparison to studies of Ultem films suggests that the increase is due to crosslinking in the matrix material. Mechanical properties as investigated with the three-point flex test are unchanged by the radiation. Conversely, thermal cycling increases the modulus of the composites, possibly by relieving internal stresses, but has no effect on the T_g.

REFERENCES.

1. D.R. Tenny, G.F. Sykes, Jr., and D.E. Bowles, AGARD Conference Proceedings, 1983. AGARD-CP-327, June 1983.
2. S.S. Tomkins, G.F. Sykes,Jr., and D.E. Bowles, The Thermal and Mechanical Stability of Composite Materials for Space Structures. IEEE/ASM/ASME/SME Space Technical Conference, Anaheim, CA, Sept. 1985. Technical Paper No. EM 85-979.
3. ASTM Standard D790-84a. American Society for Testing and Materials, Philadelphia, PA, 1984.

4. E.R. Long, Jr., and S.A.T. Long, Spectroscopic Analysis of Radiation-Generated changes of a Polyetherimide Film. NASA Technical Paper 2429, May, 1985.

5. S.A.T. Long, E.R. Long, Jr., H.R. Ries, and W.L. Harries, Electron-Radiation Effects on the AC and DC Electrical Properties and Unpaired Electron Densities of Three Aerospace Polymers. IEEE Transactions on Nuclear Science, NS-33, 6, 1390 (1986).

Table 1. The mechanical properties of neat Ultem resin film and Celion 6000 fibers.

	Ultem 1000	Celion 6000
Modulus (PSI)	4.0×10^5	3.3×10^7
Ultimate Stress (PSI)	1.5×10^4	5.5×10^5
Elongation to Failure (%)	60	1.64

Table 2. Material Properties.

	Unsized	Sized
Thickness (Inches)	0.024	0.028
Fiber Volume Fraction (%)	56.9	55.8

Table 3. T_g (°F) of sized and unsized C6000-Ultem 1000 composite. (Average difference from mean is 6.7 °F)

	Unsized		Sized	
	Long.	Trans.	Long.	Trans.
Unexposed	483	469	487	451
100 kGy	516	486	500	471
1000 Thermal Cycles	481	466	484	444
100 kGy followed by 1000 thermal cycles	509	495	502	477

Figure 1. Unexposed sized and unsized C6000 - Ultem 1000 composite flexural properties.

(a) Ultimate stress, PSI

(b) Ultimate strain, in./in.

(c) Modulus, PSI

Unsized
Sized

Longitudinal Transverse

Figure 2. Transverse, unsized C6000 - Ultem 1000 composite flexural properties.
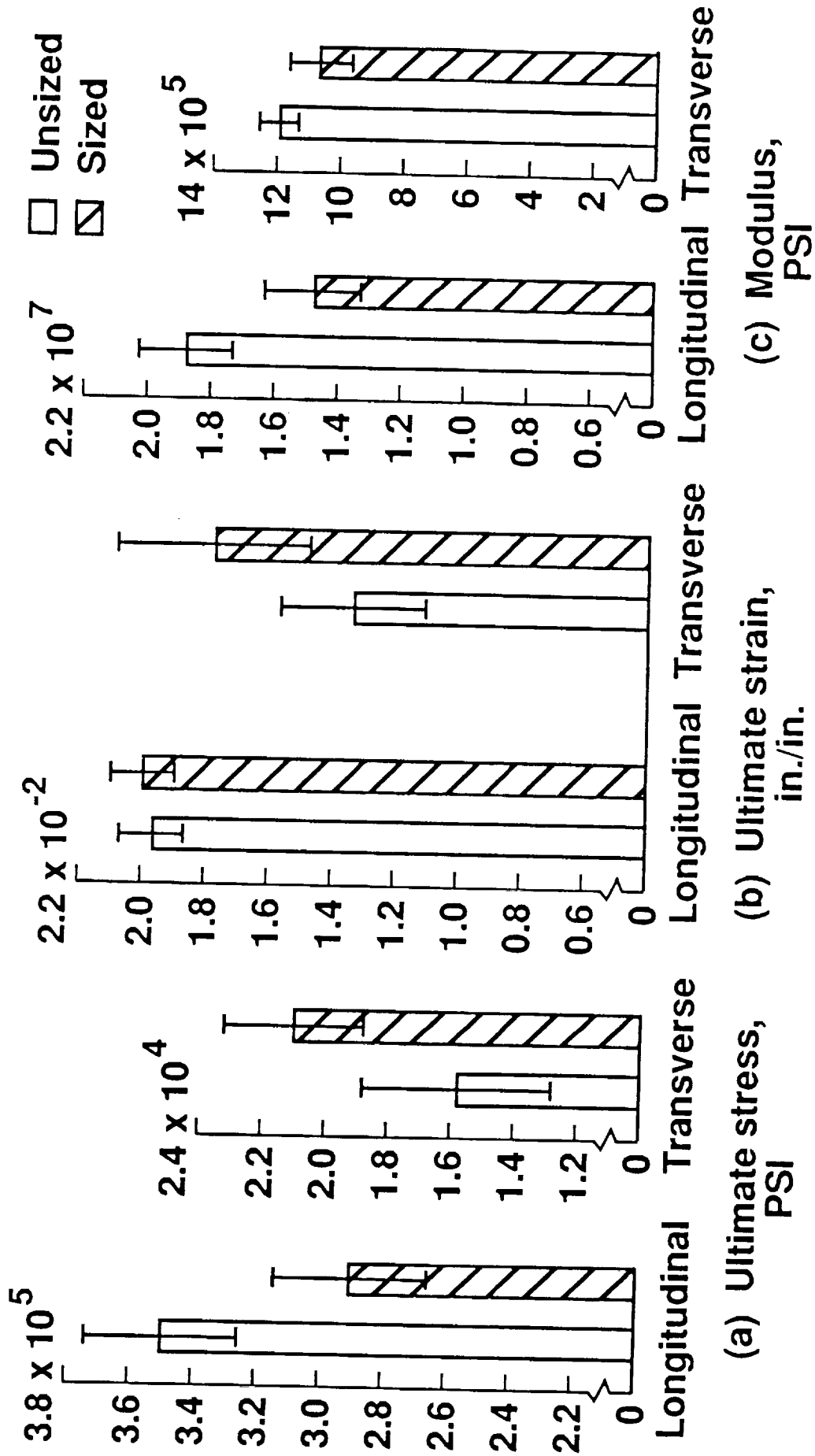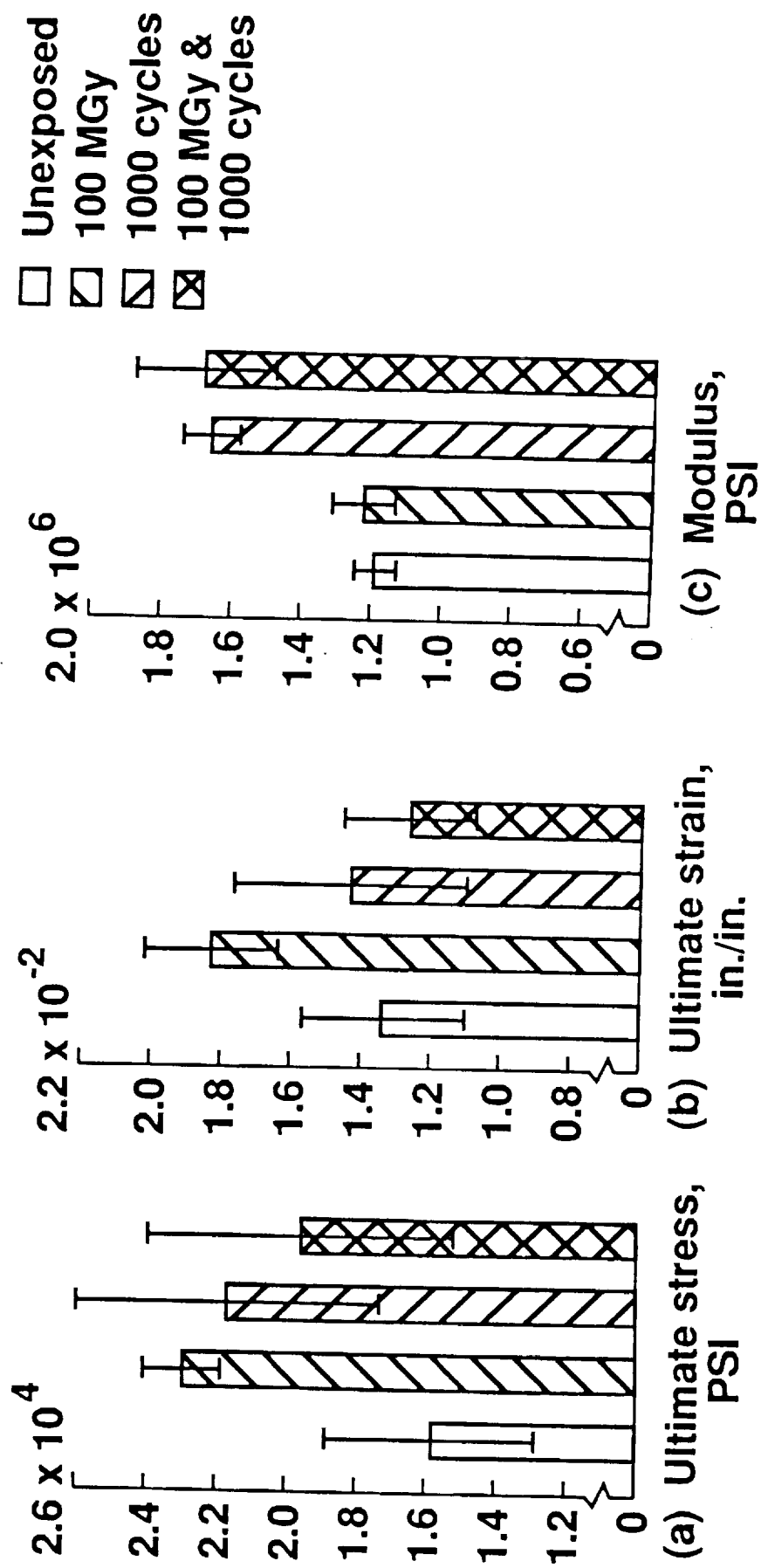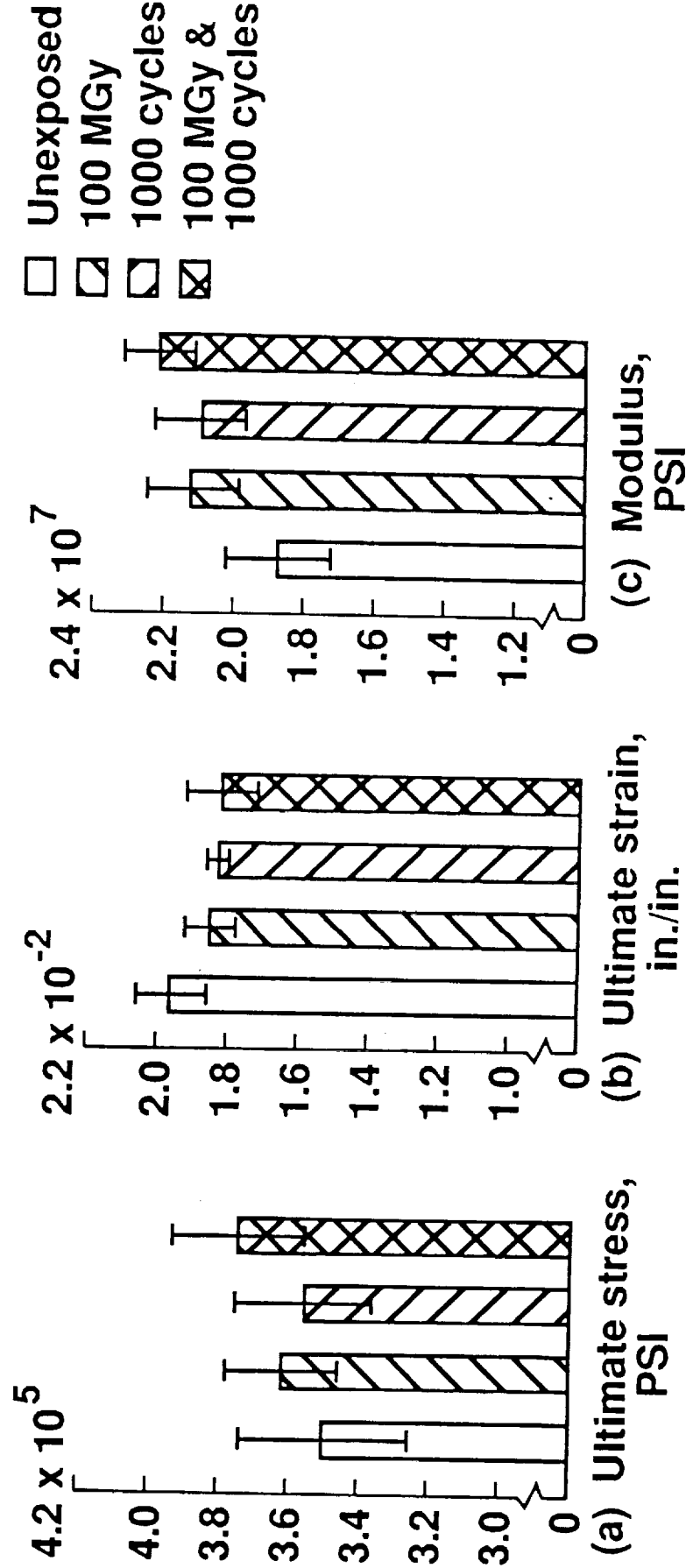
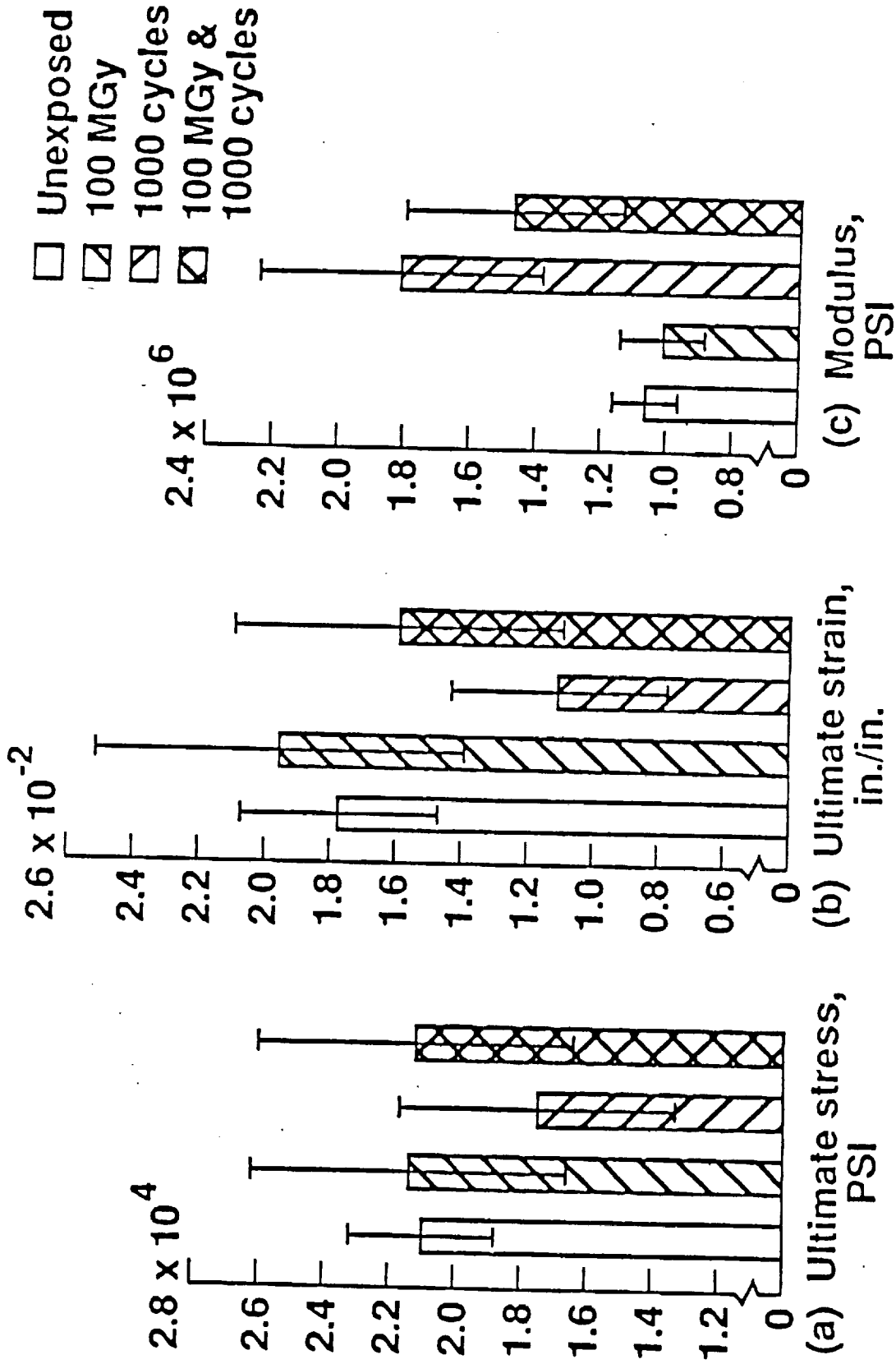Figure 3. Longitudinal, unsized C6000 - Ultem 1000 composite flexural properties.

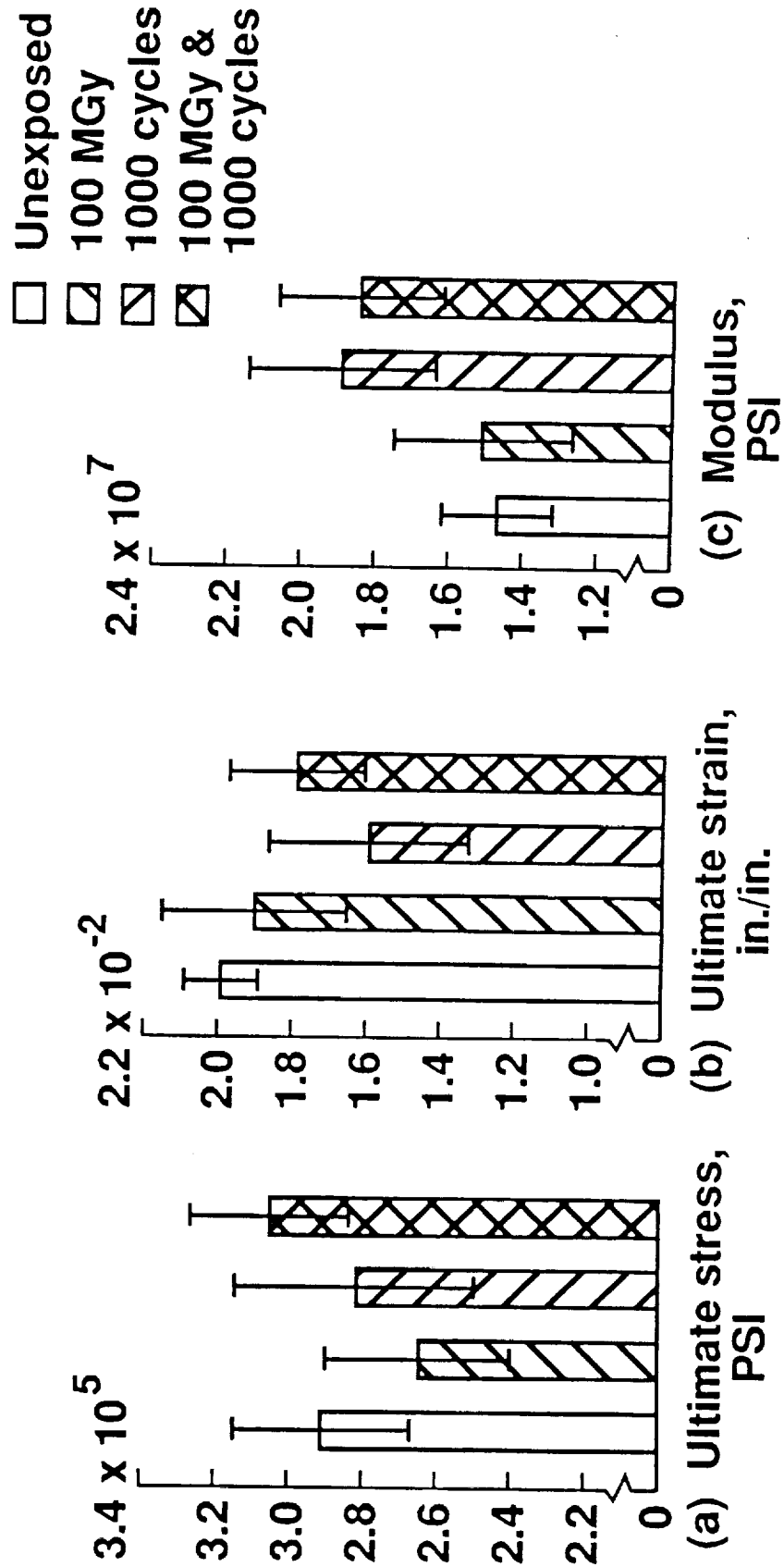Figure 4. Transverse, sized C6000 - Ultem 1000 composite flexural properties.

Figure 5. Longitudinal, sized C6000 - Ultem 1000 composite flexural properties.

APPENDIX K

Spectroscopic Techniques to Study Polymer-Atomic Oxygen Reactions for Low-Earth Orbit Simulations

P.C. Stancil,* S.A.T. Long,† E.R. Long, JR.,† and W.L. Harries†
*Department of Physics, Old Dominion University
Norfolk, Virginia 23529
†NASA Langley Research Center
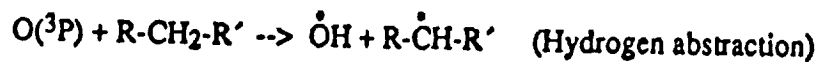Hampton, Virginia 23665-5225

INTRODUCTION

An important consideration for structures in low-Earth orbit (LEO) is the effect of atomic oxygen (AO) on materials. LEO, between 200 and 500 kilometers, consists predominately of AO in the neutral triplet ground state, $O(^3P)$.[1] AO is highly reactive with many polymers currently used and intended for future use in space applications and is considered to be the major cause of material deterioration on Shuttle flight experiments.[2] The development of adequate Earth-based LEO simulation facilities and the understanding of polymer-AO reactions is therefore important for future space endeavors.

This paper examines the use of a radio-frequency glow-discharge (RFGD) generated oxygen plasma as a viable LEO simulator. The plasma environment is evaluated through emission and infrared spectroscopic techniques. The same emission techniques are further used to determine polymer-AO reaction products from polymeric materials exposed to the RFGD generated AO, with results presented for polyetherimide (PEI) and fluoroethylenepropylene-polytetrafluoroethylene (FEP-PTFE).

EXPERIMENTAL

For many years oxygen RFGD's have been used to study AO reactions with organic compounds, but little has been known about the particle composition of the discharge plasma. For instance, does the AO exist primarily in the $O(^3P)$ state or do significant quantities of $O(^1D)$, $O(^1S)$, and higher excited states or other reactive species exist for substantial lifetimes long enough to play a role in the reaction process? If so, it is possible that these states may react differently than $O(^3P)$, thereby obscuring the effects of $O(^3P)$. To address this question, an emission spectrum of the discharge glow was obtained. By identifying the various atomic lines and molecular bands, the constituents of the plasma can be determined.[3,4] If local thermodynamic equilibrium is assumed, the plasma temperature can be estimated from the relative intensities of atomic lines.[5] The relative densities of the constituents can be calculated from the relative line/band intensities, transition oscillator strengths, state statistical weights, and state energies.[6]

To determine whether the weakly excited state, $O(^1D)$, exists in the discharge, the following known quantum-state selective reactions with polyethylene (PE) were investigated:[7]

$$O(^3P) + R\text{-}CH_2\text{-}R' \rightarrow \overset{\bullet}{O}H + R\text{-}\overset{\bullet}{C}H\text{-}R' \quad \text{(Hydrogen abstraction)}$$

$$O(^1D) + R\text{-}CH_2\text{-}R' \rightarrow R\text{-}HCOH\text{-}R' \quad \text{(Oxygen insertion)}$$

Infrared spectra of unexposed and exposed PE resin were recorded to determine which reaction(s) occurred. A decrease in C-H absorbance bands after exposure indicates a loss of H (abstraction) and therefore reactions by $O(^3P)$, while an appearance of O-H bands would indicate that O is being inserted and therefore reactions by $O(^1D)$.

Exposure of polymeric materials in the discharge also results in an emission spectrum characteristic of the particles in the plasma. In this case, the plasma consists not only of the ambient AO environment, but also of volatile particles resulting from polymer-AO reactions. As above, these reaction products can be determined from spectra line identification. Also, the total integrated area of the spectrum can give a measure of the reactivity of the polymer.

The emission spectra were obtained with an Oriel** monochromator system consisting of a fused-silica fiber-optic cable, a 1/8-meter grating monochromator (MC) with a 50-Å bandpass, a photomultiplier tube (PMT), and associated electronics for MC control and data acquisition. The current investigation window is limited to between 3000 and 8000 Å. The infrared spectra were obtained with a Perkin-Elmer 599 Spectrophotometer.

AO is produced in an RFGD consisting of capacitance-coupled electrodes driven by a 13.56 MHz power supply with an impedance matching network (Structural Probe, Inc., Plasma Prep II). The reaction vessel consists of a 15-cm long by 10.5-cm diameter cylindrical quartz chamber. The discharge is operated at a chamber pressure of 200 millitorr, RF power supply of 100 W, and a flowrate of 0.011 SLPM of 99.5% pure O_2. Specimens are placed on a blown-glass holder with their surface normal to the incident AO flux. Specimens are typically thin resin disks 7/8" in diameter by 3 mils thick. The PEI was manufactured by General Electric Co.; FEP-PTFE, by E.I. du Pont de Nemours & Co.; and PE, by Union Carbide Corp.

RESULTS AND DISCUSSION

The spectrum of the oxygen RFGD is given in Figure 1 with corresponding line assignments. The plasma is determined to consist of OI (neutral atomic oxygen), HI (neutral atomic hydrogen), N_2, and O_2^+ from the line identification. After correcting for the fiber-optics, grating, and PMT efficiencies, the relative density of each constituent was calculated from the parameters described above. These values are displayed in Table 1 and compared with the LEO composition. The presence of O_2 is assumed because at 200 millitorr it is known not to yield an emission spectrum[8] and 100% dissociation is highly improbable.[9] The amount of O_2 is estimated from comparison with results obtained in reference 9. In addition, the forbidden transitions $O(^1S)$ to $O(^1D)$ and $O(^1D)$ to $O(^3P)$ do not appear in the spectrum, indicating that the low-lying excited states $O(^1D)$ and $O(^1S)$ do not exist in the discharge. The plasma temperature is calculated to be 4700 K (0.4 eV).

_____

**The use of trademarks or manufacturers' names in this paper is for accurate reporting and does not constitute an official endorsement, expressed or implied, of such products or manufacturers by the NASA.

Figure 2 displays an infrared difference spectrum between an unexposed and 2-hr AO-exposed PE resin. The spectrum shows a decrease in C-H bands (increased transmittance) with no appearance of O-H bands, suggesting H abstraction by $O(^3P)$. This further substantiates that $O(^1D)$ is not present and that $O(^3P)$ is the primary reactive state of AO in the discharge.

Figure 3 gives the molecular structures of PEI and FEP-PTFE. Their AO-exposed emission spectra are given in Figures 4 and 5, respectively. For PEI, the source lines, OI and O_2^+, and impurity lines, HI and N_2, are observed, as in Figure 1. The remaining lines are attributed to the reaction products from the PEI-AO reaction. The products are CO, CO^+, CO_2^+, C_2, and possibly NO, NH, N_2^+, CH^+, H_2O, OH, and OH^+. These are expected, since PEI contains only the elements C, H, O, and N. The reaction products are mostly diatomic molecules - no large chains or polymer fragments. This is reasonable, since the long polymer chains are interwoven and removal of them is physically hindered. This suggests that initially the AO attacks primarily the dangling pendant components - the CH_3 in the isopropylidine group. Additionally, it is noted that the spectrum was taken after a relatively short exposure of less than 1-hr; the corresponding mass loss was less than 0.2%. It is, therefore, possible that a time-dependent effect might be seen for longer exposures. After the pendant groups at the surface of the material are exhausted, attack on the polymer backbone may occur, giving larger polyatomic reaction products.

The spectrum for FEP-PTFE is similar, but with a pronounced decrease in intensity. The lines OI, HI, N_2, and O_2^+ are all observed again, as well as the reaction products CO, CO^+, CO_2^+, and C_2. The presence of the other reaction products seen in the PEI spectrum and F_2, NF, and CHF is questionable. We might also expect to see CF, CF_2, CHOF, and NF_2, but their emissions are beyond the observation window into either the UV or IR regions, so conclusions cannot be drawn to their presence. The observed products are as expected, since FEP-PTFE contains only the elements C and F. O and F do not combine, since F has an electronegativity greater than O. This also suggests that only the CF_3 in the FEP group is attacked, resulting in mainly diatomic reaction products. The backbone of the chain can then be attacked in the location of the absent CF_3, resulting in chain shortening. The short chains, however, would still be physically hindered from escape. Again, the spectrum was recorded after less than a 1-hr exposure; the mass loss was less than 0.1%. Larger polymer products may be seen after longer exposure times.

From the emission spectra, it is seen that the intensity area of PEI is greater than FEP-PTFE, which is greater than the oxygen discharge. This corresponds to the mass losses of PEI and FEP-PTFE of 0.2% and 0.1%, respectively. Therefore, the integrated area of the spectrum can give a measure of the reactivity or durability of a material exposed to the oxygen RFGD.

CONCLUSIONS

The emission and infrared spectroscopy data of the oxygen RFGD indicate that $O(^3P)$ is the primary reactive constituent in the discharge, thus supporting the position that it can adequately simulate the LEO environment. The reactions of PEI and FEP-PTFE with AO are shown through emission spectroscopy to result in primarily diatomic reaction products.

ACKNOWLEDGEMENT

REFERENCES

1. A.E. Hedin, *J. Geophys. Res.* 88, 10710 (1983).
2. J.T. Visentine, L.J. Leger, J.F. Kuminecz and I.K. Spiker, *Proc. of AIAA 23rd Aerospace Sciences Meeting* (1985).
3. G.R. Harrison, *"MIT Wavelength Tables"*, MIT Press (1970).
4. R.W.B. Pearse and A.G. Gaydon, *"The Identification of Molecular Spectra"*, Chapman and Hall (1976).
5. G.V. Marr, *"Plasma Spectroscopy"*, Elsevier (1968).
6. W.L. Wiese, M.W. Smith and B.M. Glennon, *"Atomic Transition Probabilities - H through Ne"*, NSRDS-NBS4, Vol I (1966).
7. R.J. Cvetanovic, *Proc. of NASA Workshop on Atomic Oxygen Effects*, 47 (1986).
8. M.W. Feast, *Proc. Phys. Soc.* A 62, 114 (1949).
9. A.T. Bell and K. Kwong, *AIChe J.* 18, 990 (1972).
10. J. Yee, *Planet. Space Sci.* 36, 89 (1988).

Table 1. Comparison of Oxygen RFGD and LEO Constituents

Constituent	Polymer Interaction	Percent Composition, %	
		LEO[1,10]	Oxygen RFGD
$O(^3P)$	Yes	54 - 83	19 - 48
$O(^1D)$	Yes	2×10^{-6} - 3×10^{-4}	0
$O(^1S)$	Yes	10^{-7} - 10^{-5}	0
HI	Yes	4×10^{-3} - 1	0.9 - 2.2
O_2^+	Yes	5×10^{-7} - 7×10^{-5}	6×10^{-5} - 10^{-4}
O_2	No	0.2 - 3	50 - 80
N_2	No	1 - 50	3×10^{-3} - 9×10^{-3}
HeI	No	7×10^{-2} - 13	0
ArI	No	2×10^{-3} - 3×10^{-2}	0

Figure 1. Emission spectrum of oxygen RFGD.

Figure 2. Infrared difference spectrum of unexposed and AO (2-hr) exposed polyethylene.

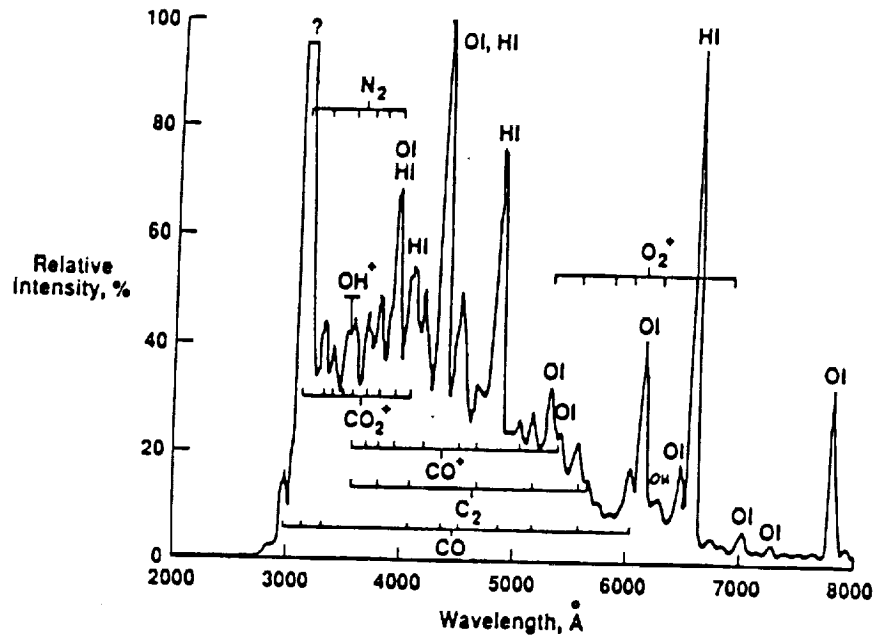Figure 3. The repeat units for polymers studied.

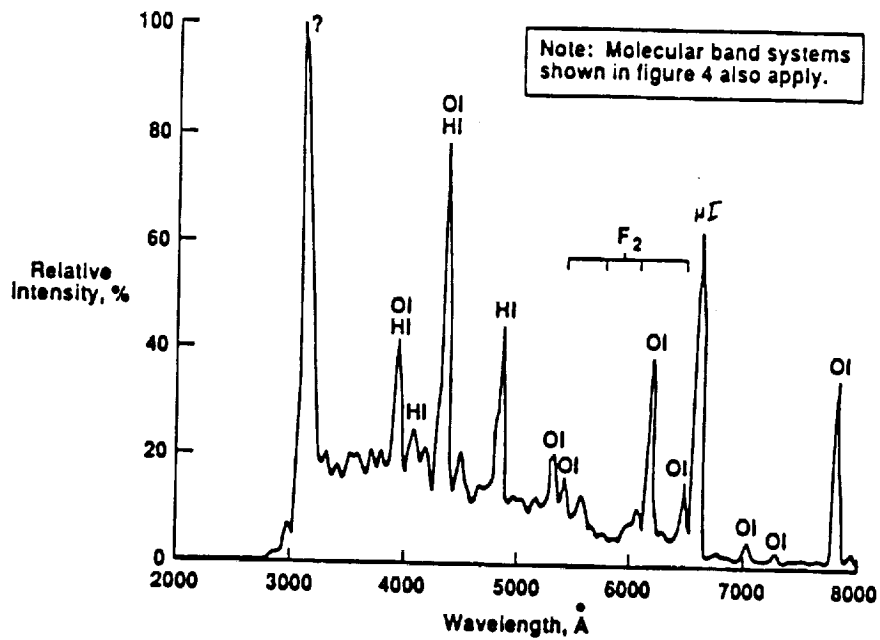Figure 4. Emission spectrum of polyetherimide in oxygen RFGD

Figure 5. Emission spectrum of fluoroethylenepropylene-
polytetrafluoroethylene in oxygen RFGD

APPENDIX L

APPENDIX L

ADHESIVES PROGRAM

Six commercial adhesives* have been identified for potential use in space applications. Four of these six are currently being evaluated under this cooperative agreement; FM300M, manufactured by American Cyanamid; EA9320 NA, EA934 NA, and EA9396, manufactured by Dexter Hysol.

Exposure Conditions

The environmental conditions to which the adhesives are being exposed are intended to simulate the conditions experienced by spacecraft Earth orbit. These conditions include 1 MeV electron radiation and temperature extremes due to solar heating. Test specimens receive radiation doses of 10^7 rads, the equivalent dosage of a 30-year mission in low Earth orbit, and 3×10^8 rads, the equivalent dosage of a 30-year mission in a polar Earth orbit. Temperature extremes in Earth orbit can be as high as 150 degrees Fahrenheit (°F) and as low as -150 degrees (°F). Test specimens are exposed to cycles over this temperature range to simulate time in orbit.

Mechanical Tests

The adhesive bonds are tested to determine tension lap shear (TLS) strength and molecular properties. The TLS strength is measured by bonding aluminum to graphite-epoxy composite with the adhesive in question. To simulate the geometry of the space station tube design, a thin aluminum shield is bonded to the composite at the bond area. The bonded material is then placed in tensile load parallel to the bond. The load is increased until the bond fails. The glass transition temperature of the adhesive is

---

*Reference to individual commercial products does not imply endorsement by NASA.

determined by introducing low amplitude, sinusoidal loading perpendicular to the bond and measuring the response of the adhesive as the temperature is increased. The energy lost in the oscillation is related to the friction between molecules in the adhesive and composite resin. The energy loss reaches a maximum at the glass transition temperature as the polymer changes from behaving like a glass to behaving like a rubber.

Test Program

Four adhesives have been tested for TLS strength. The exposure conditions under which testing has been performed are: no exposure, 1000 thermal cycles, 3 x 108 rads of electron radiation, and 1 x 10^7 rads of electron radiation followed by 2000 thermal cycles. The measurements are being continued.